SINGLE-CELL GENE-EXPRESSION ANALYSIS BY QUANTITATIVE RT-PCR

Thesis by

Luigi A. Warren

In Partial Fulfillment of the Requirements

For the Degree of

Doctor of Philosophy

California Institute of Technology

Pasadena, California

2008

(Defended July 17, 2007)

ACKNOWLEDGEMENTS

I would like to thank the members of my thesis committee, Ellen Rothenberg, Scott Fraser, Paul Sternberg, James R. Heath, and (above all) my advisor, Stephen Quake, for their advice and support. My scientific collaborators, David Bryder and Derrick Rossi, and their director, Irving Weissman, allowed me to apply novel single-cell analysis techniques to real biological problems. Stuart Kim and Jan Vijg were guiding influences for the aging study, and Geoffrey Schiebinger helped out tremendously with the experimental work. I extend my appreciation to the members of the Quake lab—most especially, to Joshua Weinstein, who worked out the analytic solution to the digital-PCR response-curve problem that appears in the appendix, and to Joshua Marcus, who gave freely of his time to get me started on microfluidics. I am also grateful to Eric Davidson for sharing his hard-won insights into the character of gene-regulatory networks, and Stuart Kauffman for stimulating conversations on the same subject. Both have written excellent books, which will shape our understanding for years to come.

ABSTRACT

The problem of development has long been one of the key issues in biology. With stem-cell therapies on the horizon, the "reverse engineering" of developmental programs promises to become a task of great practical significance. We now understand the general schemes by which transcriptional networks regulate cellular differentiation and morphogenesis. These genetic circuits function as complex state machines which, over the course of development, undergo sequenced transitions that bring cells to specific end states. A variety of different gene-expression assays can be used to follow these transitions. The sensitivity of the assays now in common use limits the resolution with which we can follow the activity of genetic-regulatory networks. This thesis describes two projects aimed at refining an established gene-profiling method, quantitative RT-PCR, so that it can be used to profile transcriptional-network states cross-sectionally within developing cell populations at single-cell resolution. Two advanced qRT-PCR protocols were developed to support these projects, one based on microfluidic "digital PCR," the other based on multiplexed "preamplification PCR." These protocols were used to measure transcription-factor expression in hematopoietic progenitor cells, and to evaluate the effects of aging on the stability of gene regulation. In their current form, the digital PCR and preamplification techniques will permit the analysis of perhaps a few hundred to a few thousand cells in a single-cell survey. By combining microfluidic-chip assays with the preamplification method, it will soon be possible to scale up to the analysis of many thousands of cells, while profiling many different transcription factors in each individual cell. This should facilitate the modeling of the transcriptional networks which control cellular differentiation as we press forward into the era of "tissue engineering."

TABLE OF CONTENTS

LIST OF FIGURES

Chapter 1

OVERVIEW

1.1 Introduction

Progress in stem-cell biology has raised hopes for a revolution in therapeutics, based on the application of tissue regeneration techniques to make up deficits arising from injury, disease, and old age. A more detailed understanding of the molecular mechanisms that govern development will be needed before the promise of regenerative medicine can be realized. The broad principles underlying the action of gene regulatory networks have already been elucidated, and it is no longer a mystery how a fixed DNA sequence can specify the dynamic, conditional processes involved in cellular differentiation and morphogenesis. Nevertheless, the genetic networks controlling development are highly complex, and their characterization remains difficult even with the most sensitive molecular assays available today. New techniques will be required to gather the data needed to model these circuits and rationally intervene in cellular differentiation programs for the purposes of "tissue engineering."

Self-renewing, multipotent stem cells were first identified in the hematopoietic system, and hematopoiesis remains the most tractable research model for investigating cell differentiation in mammals. Fluorescence-activated cell sorting (FACS) has been the principal enabling technology for hematopoietic studies. The power of FACS stems from its unique ability to analyze cell populations cross-sectionally with single-cell resolution. When applied to superficially homogeneous blood progenitor cells recovered from bone marrow, FACS reveals a diversity of cellular phenotypes, which present as natural clusters when cells are visualized in gene-expression space. On further inquiry, many of these subpopulations have

emerged as intermediates in the branching path by which hematopoietic stem cells (HSCs) develop into the specialized cell types of the blood. FACS has facilitated the progressive refinement of progenitor taxonomies, which has in turn allowed researchers to focus in on key molecular actors and decision points in the cellular-differentiation process.

FACS is limited in that it surveys only membrane-protein expression, and yet we know that cell-fate choice is directly controlled by transcription factors acting in the cell nucleus. The expression of these regulatory factors can be evaluated using a variety of standard mRNA assays, including qRT-PCR, SAGE, and microarray analysis, and such measurements have provided insight into the networks controlling hematopoiesis. Still, conventional assays only give us population-average expression profiles, based on mRNA derived from thousands of cells, so the data they provide is necessarily conditioned by preestablished cell taxonomies.

To analyze population structure at the transcriptional-network level, we need assays sensitive enough to quantitate multiple, low-abundance transcripts in single cells, and convenient enough to expedite the analysis of many individual cells. This thesis describes two projects undertaken to improve the sensitivity and throughput of single-cell gene profiling:

1. The first project sought to develop an assay with the sensitivity required to quantitate transcription factors in single cells. FACS was used to immunophenotype and sort blood progenitor cells into RT-PCR buffer, and the cell lysates were then reverse transcribed in a conventional thermocycler. The cDNA preps were quantitated in the Fluidigm Digital Array chip using a multiplexed TaqMan assay. Inside the chip, each cDNA sample is subdivided into 1200 isolated compartments immediately before the PCR. A scan of the fluorescence in the chip at the PCR end point gives a count of the number of template molecules in the sample. Absolute expression

levels of the housekeeping transcript GAPDH and the hematopoietic transcription factor PU.1 were measured in 116 cells using this methodology.

2. The second project measured the cell-to-cell variability of transcript levels in cells isolated from young and old mice, to evaluate the hypothesis that transcriptional regulation is destabilized with age. Again, FACS was used to prepare single-cell lysates for analysis. For this study, achieving high sample throughput was more important than maximizing assay sensitivity. This motivated a different technical approach to cDNA quantitation, based on "preamplification PCR." Reverse transcription was coupled with 15 cycles of multiplex PCR, and the "preamplified" cDNA was diluted and analyzed in six independent SYBR Green qPCR assays using a standard real-time PCR machine. Parallel reactions on RNA quantitation standards were used to convert qPCR threshold-cycle readouts into absolute mRNA copy numbers. A total of 324 cells were evaluated in the study (figure 1.1).

1.2 Organization

Chapter 2. Regulatory Coding of Lymphoid Lineage Choice by Hematopoietic Transcription Factors

This chapter reviews the literature on the transcriptional control of differentiation in the branch of hematopoiesis which gives rise to the adaptive immune system.

Chapter 3. Single-Cell Gene-Expression Analysis

This chapter summarizes current methods for analyzing gene expression at the protein and mRNA levels, with a particular emphasis on single-cell assays.

Chapter 4. Thesis Methods

This chapter explains the technical choices behind the two single-cell analysis protocols developed for the thesis work, and discusses their respective merits and potential.

Chapter 5. Transcription Factor Profiling in Individual Hematopoietic Progenitors by Digital RT-PCR

This chapter describes the hematopoiesis/digital PCR study.

Chapter 6. Transcriptional Instability is Not a Universal Attribute of Aging

This chapter describes the aging/preamp PCR study.

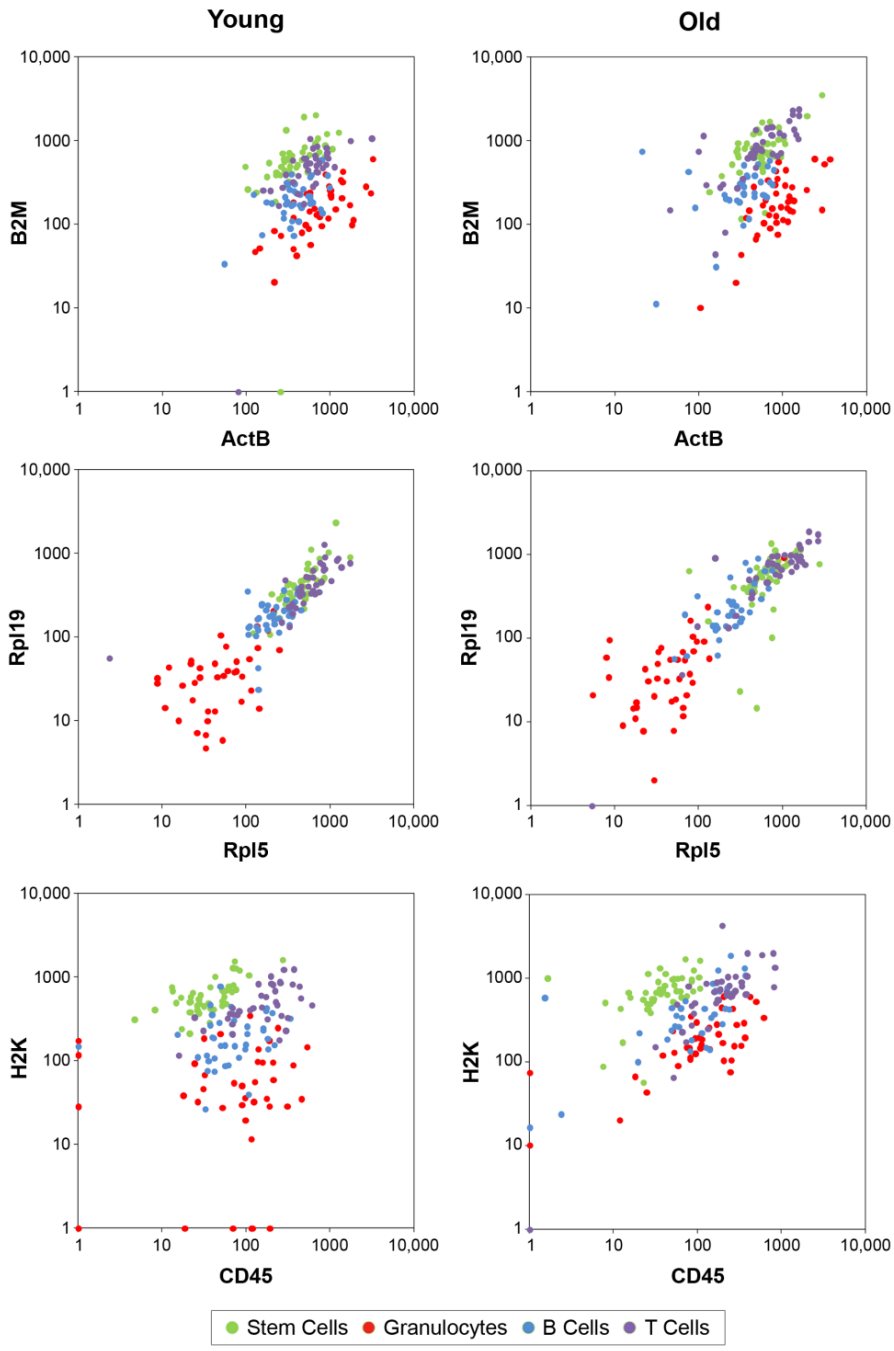

Figure 1.1. Single-cell gene-expression analysis. The 2D scatterplots summarize the mRNA copy-number data from the aging study. The levels of six mRNA species were measured in 324 individual hematopoietic cells. Four FACS-purified cell populations were evaluated in young and old mice: hematopoietic stem cells (HSCs), granulocytes, naïve B-2 B cells, and naïve CD8 T cells. Although the analysis targeted housekeeping and pan-hematopoietic genes, the four cell populations still show distinctive expression signatures. The levels of the coregulated ribosomal subunit genes Rpl5 and Rpl19 were strongly correlated within and across cell types.

Chapter 2

REGULATORY CODING OF LYMPHOID LINEAGE CHOICE BY HEMATOPOIETIC TRANSCRIPTION FACTORS*

Luigi A. Warren and Ellen V. Rothenberg

2.1 Summary

During lymphopoiesis, precursor cells negotiate a complex regulatory space, defined by the levels of several competing and cross-regulating transcription factors, before arriving at stable states of commitment to the B-, T- and NK-specific developmental programs. Recent perturbation experiments provide evidence that this space has three major axes, corresponding to the PU.1 versus GATA-1 balance, the intensity of Notch signaling through the CSL pathway, and the ratio of E-box transcription factors to their Id protein antagonists.

---

* This chapter was originally published in Current Opinion in Immunology, 15(2), 2003. The references for this chapter appear in the References and Recommended Reading section.

2.2 Abbreviations

bHLH	basic helix–loop–helix
CLP	common lymphoid progenitor
CMP	common myeloid progenitor
CSL	CBF1, Suppressor of Hairless, Lag-1
DC	dendritic cell
GM-CSF	granulocyte-macrophage colony-stimulating factor
HSC	hematopoietic stem cell
Id	inhibitor of differentiation
IL	interleukin
IL-7Rα	IL-7 receptor α
M-CSF	macrophage colony-stimulating factor
NK	natural killer
Notch-ICN	Notch intracellular domain
TCR	T-cell receptor

2.3 Introduction

Hematopoiesis offers us an unusually revealing picture of cellular differentiation, a process which underpins all metazoan development. In contrast to the situation in solid tissue, blood cells maintain, and to a lesser extent arrive at, their terminal phenotypes cell autonomously, without the influence of the fate choices of neighboring cells and without requiring stable association with the supporting matrix. This independence of a fixed tissue geometry makes hematopoietic differentiation relatively simple to adapt to *in vitro* conditions, thereby facilitating inquiry into the causative factors involved in lineage choice and developmental program progression. Furthermore, at least ten different hematopoietic cell types are generated continuously throughout life from a pool of multipotent stem cells. Neither multipotentiality nor the processes through which individual cells winnow their options down towards lineage commitment are dependent on any special conditions restricted to embryonic states. Thus, hematopoiesis affords us our best hope of answering the fundamental questions of vertebrate cellular differentiation: What are the origins of

symmetry breaking and diversity in development? How is homeostatic control over specific cell-type populations achieved? How do transcription factor expression profiles encode lineage decisions and divide up the multitude of possible cell fates? How do differentiation programs unfold? What stabilizes the end states of development?

This review focuses on the elements of the hematopoietic program that generate lymphocytes; that is, B cells, T cells and natural killer (NK) cells. Our concern here is with the early branch points leading to the three basic lymphoid career choices, and not the later decisions that fine-tune morphologically similar cells to highly specific immunological roles, such as the $CD4^+$ versus $CD8^+$ choice in late T-cell development. Much is known about how these choices activate the downstream gene expression cascades that implement B-lineage differentiation [1–3, 4**, 5–7], but these causal relationships are far less clear for the NK and T-cell lineage programs. Therefore, differentiation genes will be touched on only briefly and our principal interest will be the generation of developmental diversity itself.

2.4 Developmental Choices are Defined by Combinations of Essential Functions

Definitive lymphopoiesis—that is to say, production of lymphocytes in the adult organism—begins with self-renewing, pluripotent hematopoietic stem cells (HSCs) in the bone marrow. These cells can differentiate into any of the cell types found in blood. One major pathway for lymphocyte development passes through an intermediate cell type called the common lymphoid progenitor (CLP), an HSC-derived cell in which the potential for development along the competing myeloid and erythroid pathways is shut off [8, 9]. It is controversial whether this is the only pathway for lymphocyte development; as reviewed elsewhere [10*], there is evidence for lymphoid differentiation from precursors with various combinations of

potentials. It could be that stochastic variation of gene expression in HSCs, either within a population or within an individual cell over time, correlates with future differentiation potential without defining a canonical series of intermediate types. Each "destination" in the differentiation process is defined by its own unique set of regulatory functions, but the path that leads to that destination may not be uniquely prescribed [11**].

The debate over the pathways involving "CLPs" or other mooted early lymphoid precursors can be sidestepped by focusing on patterns of gene expression needed for arrival at each destination, rather than the perhaps tendentious naming of intermediate cell types. Given our current ignorance of the principles governing regulatory network architecture, we should be wary of overcommitting ourselves to a strictly hierarchical model of development. If we think of a gene expression profile as a vector that defines cellular state as a point in a high-dimensional space, we can conceptualize differentiation as the tracing of a path through space from a stable start point to a stable end point. As the points along the way correspond to relatively unstable states, it is perfectly feasible that diverse trajectories link the same start and end. Moreover, if the regulatory network comprises subnets that are weakly coupled, so that they can collapse into stable patterns of gene expression more or less independently, we could well have a situation in which multiple quasi-stable intermediates can converge at the same end state (figure 2.1).

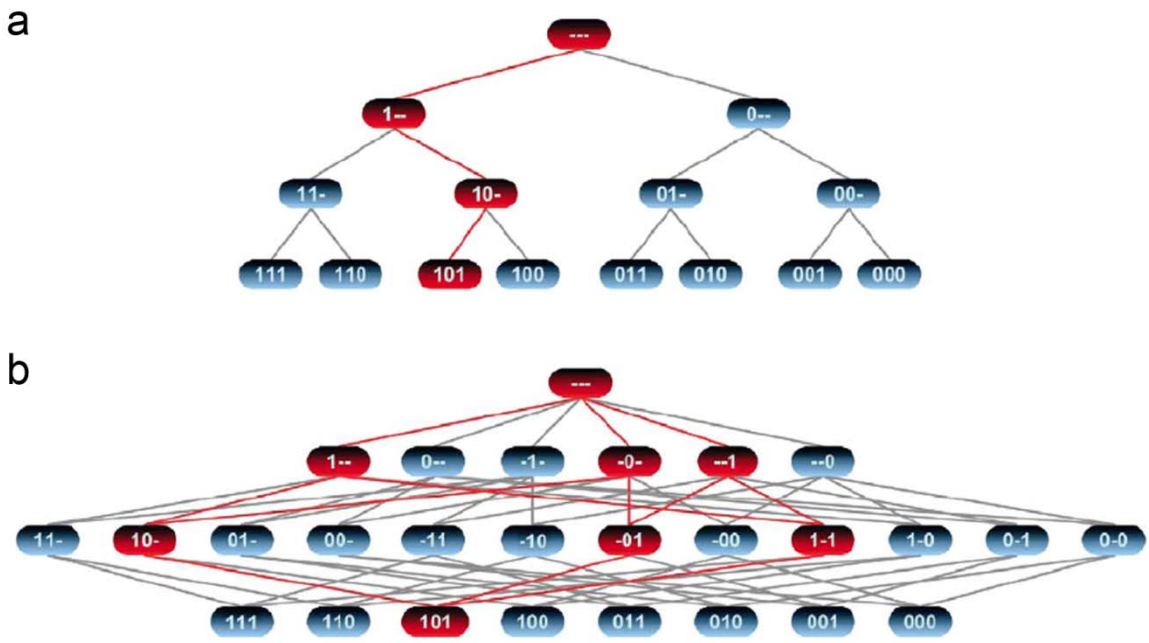

Figure 2.1. Alternative models for the regulatory network architecture responsible for encoding lineage assignment. Modularity is a prerequisite for an evolvable system. Thus, both (a) and (b) postulate that the network incorporates smaller "subnets" of highly coupled, cross-regulating transcription factors, which can assume self-stabilizing states (0,1) more or less independently. The figure shows the progressive commitment of three bistable subnets, starting from a completely uncommitted progenitor network. (a) In the sequenced subnet commitment model, the subnets stabilize in a predetermined order during development, constrained by genetic linkages that function as "enable" signals, subdividing developmental space in a stepwise fashion in the process. This picture corresponds to our traditional notion of hierarchical lineage commitment. (b) In the autonomous subnet commitment model, subnets can stabilize independently and asynchronously, generating a much more diverse population of intermediates. The attainable end states are the same for both models, but the number of permissible trajectories and intermediates is greater in the second scenario, as the highlighted transitions from the uncommitted initial state to the arbitrarily chosen end state "101" exemplify. These models depict idealized extreme cases, of course. Real lineage-choice networks probably exploit both design principles.

It is particularly important to consider this model because stem cells and immature precursor cells actively express genes that could serve any of several developmental fates, before they make absolute lineage decisions. Stem cells and multilineage precursors coexpress lymphoid and myeloerythroid genes in the same cells [12, 13*, 14]. Populations of CLPs and their myeloid counterparts (common myeloid progenitors; CMPs) still express combinations of genes associated with all of their potential descendents [13*, 15**–17**]. Few, if any, "differentiation genes" in this system are true markers of lineage commitment. Furthermore, the uncommitted progenitors simultaneously express many of the transcription factors that serve later in the differentiation pathway as specific regulators of divergent differentiation. A vivid precedent for the ways in which such a system can give rise to diverse cell types is provided by the gene regulatory networks that have been developed in detail for some embryonic tissues [18, 19**, 20, 21].

In light of these considerations, we will resist the temptation to taxonomize intermediates and instead concentrate on identifying the transcription factors and regulatory subnets that play decisive roles in channeling HSC development towards the three lymphoid fates. With respect to each lineage option, we can ask the following questions: What is the proximate causative factor determining the choice to pursue that option? How does this factor push development in a particular direction? What is the ultimate source of the diversity in the fate decision?

2.5 PU.1- and GATA-Family Transcription Factor Levels Jointly Encode Lymphoid, Myeloid and Erythroid Lineage Choice

When expressed at a high level, the Ets transcription factor PU.1 induces several characteristic myeloid genes, including Mac-1 (CD11b), F4/80, GM-CSF receptor and M-

CSF receptor (CD115) [22, 23, 24**, 25]. Lack of PU.1 completely blocks macrophage development and impairs other myeloid development [26, 27]. However, PU.1 is also required for the generation of lymphoid lineages, albeit at a lower level. PU.1 knockouts lack B cells and are deficient in fetal thymocytes [27, 28]. At low levels—but not at high levels—PU.1 directly induces the receptor for the canonical lymphoid cytokine, IL-7 [4**, 29]. IL-7 receptor α (IL-7Rα) promotes both survival and proliferation of pro-B cells and pro-T cells, with a continuing role in mature T cells. This is likely to be a major function, if not the only one, for which PU.1 is needed in B-cell development, because retroviral transduction with IL-7Rα can rescue PU.1$^{-/-}$ B-cell precursors, albeit at low efficiency [4**, 29]. At least some of the effects of IL-7 are mediated by inhibition of apoptosis through the caspase inhibitor Bcl2, but there is evidence that this cytokine is more than just a survival factor [30]. PU.1 knockouts also show defects in natural killer (NK) cell development, although these are less severe than the defects in the B or T lineages [31], which may be explained by their reduced dependency on IL-7Rα. Whether IL-7Rα is the only PU.1 target gene that is needed for T-lineage precursors still remains to be tested. GATA-1 is a positive regulator of erythroid and megakaryocytic genes and is essential for erythroid development.

When expressed at high levels, GATA-1 can participate in a mutually antagonistic relationship with PU.1 to influence cell fate [32–34]. PU.1 and GATA-1 can associate in the nucleoplasm; GATA-1 loses its DNA-binding ability andPU.1 loses its transactivation capacity in the resulting dimer. PU.1 can also antagonize GATA proteins through competitive interactions with the coactivator CBP [35*, 36]. Both PU.1 and GATA-1 are suspected to be positively autoregulating [37–39], and there is substantial evidence that they can activate the expression of transcription factors that collaborate with them in the myeloid and erythroid programs, respectively [38, 40, 41].

It is a plausible working hypothesis that the subdivision of hematopoietic precursor potential into lymphoid, myeloid and erythroid compartments is governed by the mutual antagonism of PU.1 and GATA-1, a coupling which may be said to constitute a simple regulatory subnet. In this hypothesis, cells with GATA-1 in a self-sustaining high-activity state turn on erythroid gene batteries, while repressing the gene batteries required for the competing myeloid and lymphoid programs by antagonizing PU.1. When GATA-1 is in the "off" condition, the choice between myeloid and lymphoid programs is determined by the PU.1 expression regime. High PU.1 expression, stabilized by positive feedback, activates the myeloid batteries, including myeloid cytokine receptors, while turning off IL-7Rα expression and disabling lymphoid program progression. Low levels of PU.1 activity could promote the lymphoid programs through IL-7-mediated pathways and through the absence of competing myeloid and erythroid gene expression. Figure 2.2 shows the proposed division of developmental space on the basis of PU.1 levels.

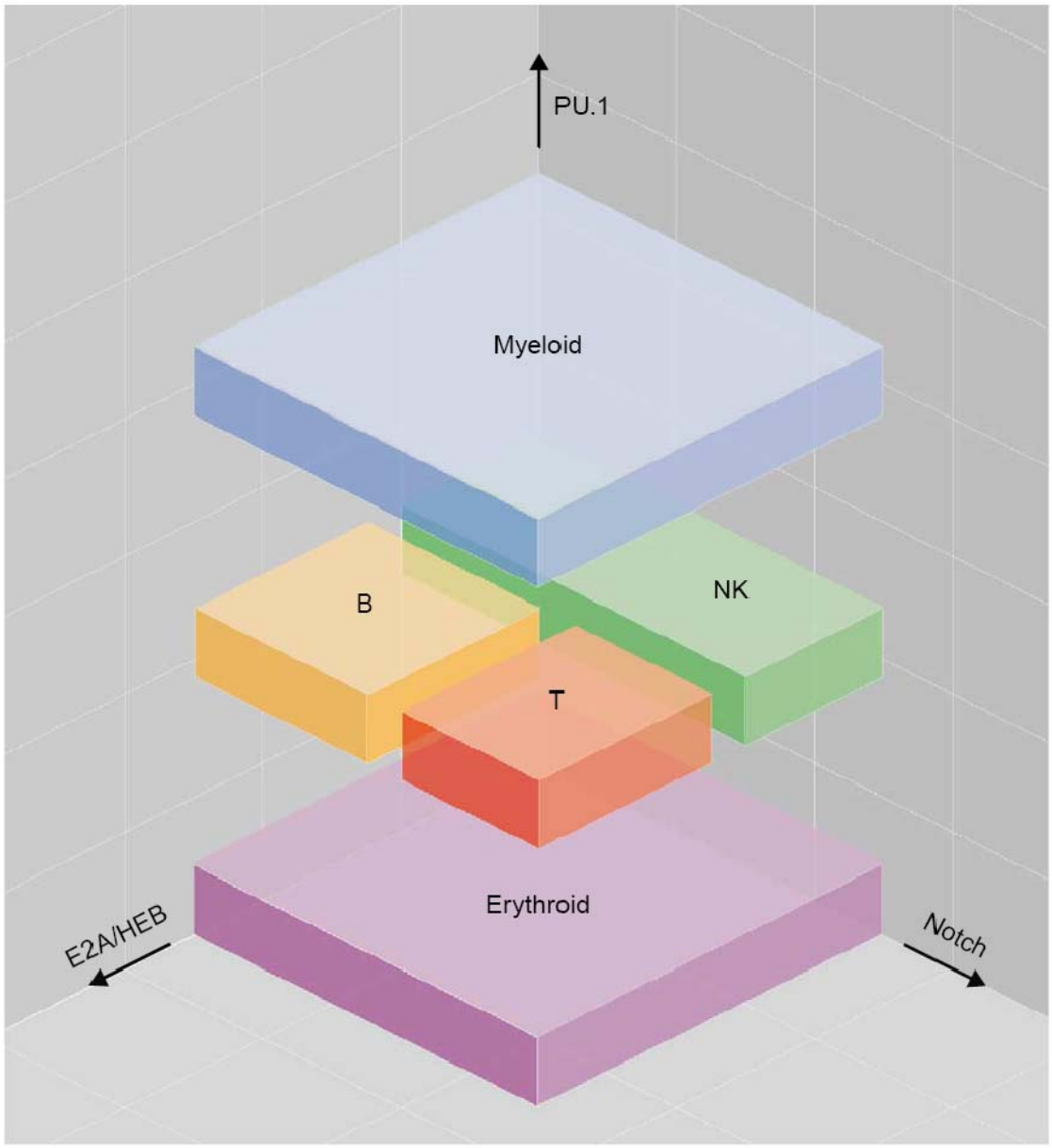

Figure 2.2. Hypothetical subdivision of early hematopoietic regulatory space by three transcription factors: PU.1, E2A/HEB and Notch. According to the model, assignment to the erythroid, lymphoid or myeloid compartment is encoded by the expression level of PU.1: in the absence of PU.1, precursors progress down the erythroid/megakaryocytic path, in the presence of high levels of PU.1 they take on myeloid fates, and between these two extremes, they follow lymphoid pathways. Within the lymphoid compartment, antagonism of the E proteins E2A and HEB by Id factors directs cells toward the NK-lineage program. When the E proteins are unopposed, differentiation proceeds down the B-lineage pathway, unless the T-lineage program is engaged by high levels of Notch activation.

2.6 The Origin of Diversity in Primary Hematopoietic Lineage Choice is Unknown

If this model is correct it raises a question: what is the source of the diversity in the expression levels of the primary fate-determining genes? Given the apparent absence of any instructive signals from neighboring cells, the null hypothesis for the source of diversity in gene expression must be stochastic variation. Single-cell assays show significant heterogeneity in gene expression among hematopoietic progenitors within the same apparent class, including even the precocious low-level expression of terminal differentiation genes [15**]. This suggests that multipotent cells may operate in a loosely regulated regime in which random fluctuations in gene expression are exploited for symmetry breaking and the generation of developmental diversity.

A gene expression "free for all" could supply the feedstock for a production line that turns out multiple differentiated cell types, but there must also be some mechanism for channeling individual differentiating precursors toward circumscribed functional roles. The thresholding implied by the winner-takes-all, dichotomous logic of the GATA-1/PU.1 subnet seems a plausible mechanism for effecting such a transition, but poses the problem of how a presumably less than stable state of intermediate PU.1 expression could funnel into a major lineage pathway such as lymphopoiesis. In reality, the subnet governing this choice is likely to be bigger than just GATA-1 and PU.1. We know that both proteins occur in small families and that some of their relatives, specifically GATA-2, GATA-3 and the Ets factor Spi-B, play overlapping and partially redundant roles in at least some of the same regulatory pathways [42*, 43, 44]. The net result might be a more rugged stability landscape than the precipice-like terrain implied by a simple GATA-1/PU.1 titration relationship. For example, at lower levels of expression, the combination of PU.1 and GATA-2 is stable enough to give

rise to the additional cell fate choice of mast cells [45], and low levels of both PU.1 and GATA-3 are essential for early T-cell development, although high levels of either disrupt it [46**]. Alternatively, complexity might reside in other transcription factors whose roles have yet to be characterized.

This general model may suggest new possible explanations for the roles of some apparently unrelated factors. For example, the transcription factor Ikaros has long been known to be essential for most lymphocyte development [47], but there has been some controversy over its precise function. Ikaros has no definite positive regulatory targets and is suspected of regulating the packaging of multiple genes into open or closed chromatin states [48]. Loss of function of this factor has little effect on erythroid or myeloid cells but blocks lymphocyte development specifically in a pattern resembling loss of function of PU.1 [47]. It would be interesting to investigate, therefore, whether a major role of Ikaros is to stabilize the precarious low-PU.1 expression state that lymphocyte development depends upon.

Finally, it is conceivable that the statistical distributions and kinetics of the fate decision mechanism obviate the need for a stable lymphoid progenitor expression code. Instead, a delay before commitment to alternative lineage programs might be sufficient. For example, if the average dwell time before excursions into positive feedback-stabilized GATA-1^{hi} and PU.1^{hi} regimes is long enough, a significant fraction of unstable PU.1^{lo} precursors could be swept into the lymphoid program first. This diversion could be rendered irreversible by downstream "lockdown" in the lineage-specific programs. It is not clear whether the CLP intermediate itself has such lockdown mechanisms; however, in the case of B-cell development, Pax-5 expression clearly plays this stabilizing role [49*, 50]. In the case of T-cell development, stabilization is linked to the shutoff of erythroid differentiation cofactors,

such as SCL/Tal-1, LMO-1 and LMO-2, and eventually of PU.1 (and Spi-B) itself [24**, 51, 52].

2.7 The Thymus Promotes the T-Lineage Fate Choice via Notch Signaling

The regulatory space that is permissive for lymphocyte development is subdivided along axes on the basis of Notch activity and on the balance of E-box-binding transcription factors with Id (for "inhibitor of differentiation") proteins (figure 2.2).

The regulation of differentiation and morphogenesis through Notch signaling is a recurring theme in a wide range of organisms and tissues. Even within hematopoiesis, Notch has diverse, context-dependent functions. For example, Notch signaling in the bone marrow can keep HSCs self-renewing [53], and the pathway also has important roles in the later, immunological stages of lymphocyte development [54, 55]. A large transmembrane protein, Notch is found in four forms in mammals, encoded by paralogous genes expressed in distinctive but overlapping patterns. Notch has multiple activating ligands, antagonists and downstream pathways. The integration of a complex set of signaling inputs with a developmentally specific transcription factor context underlies the multivalent character of Notch as a regulator.

Despite these poorly understood nuances, it does seem clear that activation of Notch by ligands produced in the thymus is the determining factor in channeling lymphoid development away from the B-cell program and towards the T-cell program [55, 56]. We cannot exclude the possibility that the starting population of HSCs or multipotent progenitors includes subpopulations that are predisposed to thymic homing and subsequent T-lineage development, for example, through the expression of the appropriate adhesion

molecules. However, transgenically induced Notch signaling is sufficient by itself to produce T-lineage committed precursors in the bone marrow [57, 58*, 59, 60], whereas conditional knockout or inhibition of Notch1 signaling is sufficient to instigate B lymphopoiesis within the thymus [61–63].

The mechanisms by which Notch signaling induces the T-fate choice are still under investigation. Thymic stimulation of the Notch pathway is mediated by the binding of the Delta-like ligand to the Notch1 receptor. Notch signaling involves proteolytic cleavage that liberates the intracellular domain (Notch-ICN) as a consequence of ligand binding. Multiple downstream interactions are known or suspected to mediate the effects of Notch on gene expression, including the NF-kB pathway [64]. However, it appears that the impact of Notch on the T-fate choice is routed primarily through CSL (for CBF1, Suppressor of Hairless, Lag-1), also called recombination signal binding protein J (RBP-J), the mammalian ortholog of *Drosophila* Su(H). A ubiquitous transcriptional repressor, CSL binds to Notch-ICN, which incorporates a transcriptional activation domain. The CSL-Notch-ICN complex becomes an activator of the same genes that CSL alone would otherwise repress, creating a sharp binary switch in the regulatory state. Conditional knockout of CSL is sufficient to arrest T-cell development and divert progenitors to B-lineage fates in the thymus, while leaving myeloid and B development in the bone marrow untouched [65**].

At minimum, the Notch-ICN–CSL complex promotes T-lineage fates by initiating transcription of pTα [66*] and upregulating expression of the basic helix–loop–helix (bHLH) transcription factor, HES-1. The pTα protein helps form a "trial" T-cell receptor (pre-TCR) to validate TCRb chain rearrangement, and is essential for the development of mature TCRαβ T cells [67]. Interestingly, pTα is usually expressed in γδ T-cell development, even

though it has no essential functional role there. Nevertheless, although pTα plays an important part in advancing the T-cell development program, it seems improbable that its downstream effects can be felt early enough to block the B-lineage program.

HES-1, which is also upregulated by Notch-ICN–CSL, is a bHLH protein related to *Drosophila* hairy and enhancer-of-split. It seems to function as an early T-lineage survival factor. It is critical for the expansion of T-lineage precursors during the first phase of TCR gene rearrangement [68]. However, the block to T-cell differentiation in HES-$1^{-/-}$ mice does not prevent T-lineage specification, in contrast to the situation in Notch$1^{-/-}$ mice. Overexpression of HES-1 or the related gene HES-5 in bone marrow progenitors partially blocks B-cell development, albeit much more weakly than Notch-ICN itself [69*]. Thus, it seems that HES family gene induction mediates only a subset of the effects of Notch on the T/B lineage choice.

It has also been proposed that Notch signaling blocks the B-lineage differentiation program by antagonizing E47, an E-box transcription factor transcribed from the E2A locus [56]. E47 is centrally involved in B-cell commitment [3]: it participates in the regulation of virtually all B-cell genes, and activates EBF and in turn Pax5, the factor responsible for locking down the B lineage choice. However, E47 and its splice variant E12 also play important early roles in T commitment. The waters are muddied here by the redundancy that seems to exist between E2A splice variants and the closely related HEB factor, which is more highly expressed in T-lineage cells than in B-lineage cells [70]. A simplistic hypothesis along the lines that Notch disables the B-lineage program by suppressing E47 activity is certainly inadequate. An inhibitory effect of Notch signaling on EBF or Pax5 would make sense, but has not yet been reported.

2.8 Id2 Titration of E Proteins Shunts Lymphoid-Inclined Progenitors Towards the NK Fate

As effectors of innate immunity, NK cells resemble T cells morphologically, but forego the somatic gene rearrangements needed to generate the TCR. In contrast to B and T cells, NK cells can emerge from either the bone marrow or the thymus. Accordingly, they are neither inhibited by nor dependent upon Notch1 signaling [58*, 59, 71]. It appears that the decisive factor in the NK fate choice is an early, sustained inhibition of E protein function mediated by high levels of Id protein expression [72, 73**].

Both E proteins and Id proteins belong to the class of bHLH transcription factors. The E proteins bind E-box sites as dimers. Id proteins lack the basic regions needed for DNA binding, but can still dimerize with E proteins. The resulting E–Id heterodimers cannot bind DNA. Thus, Id proteins act as "dominant negative" stoichiometric antagonists, titrating the activity of the E factors. There is evidence that the Id proteins often act as buffers, sequestering E proteins before they are needed to engage developmental programs.

As we have mentioned, the E47 protein is crucial to the initiation of the B-lineage program. E proteins also play a part in T-cell survival at early stages of commitment, including pTα activation [74*, 75]. They have additional roles in the downstream gene-rearrangement steps of both B- and T-cell development [3]. It appears that E proteins are uniquely dispensable to the development of NK cells, at least after the earliest progenitor stage [72], and indeed the early-onset activation of an E protein antagonist, Id2, seems to be the causative factor in pushing progenitors toward the NK-cell fate. High Id2 expression has been found in thymic progenitor subpopulations that express NK markers (MK Anderson, G Hernandez-Hoyos and EV Rothenberg, unpublished data; [72, 73**]) as well as in "committed NK progenitors"

in the bone marrow [76]. Id2 knockouts give rise to T cells but not NK cells, whereas forced expression of the related Id3 protein pushes thymocytes towards the NK-cell fate [72, 77].

2.9 Lymphoid/Dendritic Cell Relationships: A Legacy of PU.1 Dependence?

The role we propose for PU.1 in the generation of lymphoid precursors could explain the close relationship between these cells and dendritic cells (DCs). DCs, similar to macrophages, express PU.1 and depend upon PU.1 for their development *in vivo* [78, 79], and overexpression either of PU.1 or of its close relative, Spi-B, can cause preferential DC development [80*, 81]. Lymphoid precursors remain capable of differentiating into DCs, or in some cases into macrophages, until after the T- and B-lymphoid specification pathways have diverged [82–87]. In T-cell differentiation, PU.1 downregulation, shortly followed by Spi-B downregulation, coincides with the end of the period in which DC or macrophage differentiation can occur [28, 52, 86, 87, 88**]. In B cells, PU.1 and Spi-B continue to be expressed throughout maturation. This might underlie the susceptibility of some B-lineage cell types to conversion into macrophage-like cells, even after immunoglobulin gene rearrangement [82–84].

The other conditions that divide up the developmental potential space of lymphoid precursors are all permissive for at least some classes of DCs. Notch signaling is not required for DC development, but equally, it is not inhibitory [71, 89]. In fact, Notch signaling can induce preferential DC-like differentiation from monocytes while blocking their differentiation into macrophages. A variety of Id:E protein ratios are also permissive for DCs in the broadest sense, although particular subsets are sensitive to high or low ratios [90]. This broad tolerance for Notch/bHLH conditions suggests that DC (and sometimes

macrophage) development can result from an increase in the activity of PU.1 (or possibly Spi-B) across the whole plane of lymphoid-permissive conditions shown in figure 2.2.

2.10 Conclusions

In this discussion, we have reviewed evidence suggesting that the crucial conditions for initiating lymphoid development and specifying distinct lymphoid types are the balances established among different transcription factors, including PU.1, GATA-1, Notch-ICN–CSL, and E proteins versus Id proteins. In our model, the transcriptional subnet state $PU.1^{lo}$ $GATA\text{-}1^{-}$ "encodes" the lymphoid choice in a hematopoietic stem cell or an early, multipotent progenitor. The $Id2^{hi}$ state shunts these progenitors towards the NK-lineage pathway, whereas CSL-mediated Notch signaling in response to an instructive Delta signal forces thymically localized cells towards the T-lineage pathway. The remainder of the lymphoid-tagged cells activate the B-cell program.

This model prompts us to classify the B-cell fate as the default pathway for lymphoid development, in as much as it pinpoints two agents, Notch and Id2, whose intervention appears to be required to promote the alternative T- and NK-lineage fates. Given our ignorance of the antecedents that establish the all-important E:Id protein expression profiles of lymphoid precursors, we should probably resist such a leap of logic. An evolutionary argument can be made for the NK cell as the founder member of the lymphoid class, and there is at least a suggestion of this in the way that E proteins play key roles both in B- and T-lineage fate commitment and in the downstream engagement of adaptive immunity-specific differentiation genes.

Even if we believe that we have identified the key factors driving the lineage decisions in this system, we find ourselves on shakier ground when we turn to the question of how these

factors engage the selected developmental programs. The best-understood case, that of B cells, prominently features two additional transcription factors activated only within the B-cell pathway: EBF and Pax5. It is not known what factors might play corresponding roles in the T- or NK-lineage pathways. The most problematic part of the story is the means by which Notch signaling promotes the T-lineage fate at the expense of the B-lineage fate. We know that E proteins are critical in the early development of both lineages, but it remains obscure how the E protein-triggered cascade that leads to Pax5 expression and B-lineage commitment is disabled in Notch-activated thymic progenitors.

The biggest open question remaining, however, is the most interesting, and the most general in its implications: where does the diversity in the lineage-choice-directing factors come from? In lymphopoiesis, we have a partial answer for T cells, as we know that the T-lineage fate choice is directed by at least one instructive signal from the microenvironment, even if some of the details are uncertain. We can only speculate on the basis of the variety in expression levels of what we might term the "internal" signals used here: the PU.1, GATA-1 and Id2 levels that subdivide developmental space. The problem reduces to one of finding stable modes in a stochastically agitated gene regulatory network. New expression assays, such as gene chips and single-cell PCR, hold much promise for addressing the fundamental question of how natural heterogeneity in gene expression is converted into the ordered diversity of functionally specialized cell types.

2.11 References and Recommended Reading

Papers of particular interest, published within the annual period of review, have been highlighted as follows: * of special interest; ** of outstanding interest.

1. Schebesta M, Pfeffer PL, Busslinger M: Control of pre-BCR signaling by Pax5-dependent activation of the BLNK gene. Immunity 2002, 17:473-485.

2. Schebesta M, Heavey B, Busslinger M: Transcriptional control of B-cell development. Curr Opin Immunol 2002, 14:216-223.

3. Quong MW, Romanow WJ, Murre C: E protein function in lymphocyte development. Annu Rev Immunol 2002, 20:301-322.

4.** DeKoter RP, Lee H-J, Singh H: PU.1 regulates expression of the interleukin-7 receptor in lymphoid progenitors. Immunity 2002, 16:297-309.

Hematopoietic progenitors recovered from PU.1-null mutant embryos do not express the lymphoid cytokine receptor gene IL-7Rα. Both PU.1 and IL-7Rα transgenes rescue B-lineage differentiation, which is normally abrogated in these mutants, PU.1 being more effective in this regard than IL-7Rα. Chromatin immunoprecipitation (ChIP) assays revealed that PU.1 binds directly to the IL-7Rα promoter. It therefore appears that PU.1 promotes early B-lineage development in large part by facilitating IL-7 signal transduction.

5. Gisler R, Sigvardsson M: The human V-preB promoter is a target for coordinated activation by early B cell factor and E47. J Immunol 2002, 168:5130-5138.

6. Sigvardsson M, O'Riordan M, Grosschedl R: EBF and E47 collaborate to induce expression of the endogenous immunoglobulin surrogate light chain genes. Immunity 1997, 7:25-36.

7. Garvie CW, Hagman J, Wolberger C: Structural studies of Ets-1/Pax5 complex formation on DNA. Mol Cell 2001, 8:1267-1276.

8. Akashi K, Traver D, Miyamoto T, Weissman IL: A clonogenic common myeloid progenitor that gives rise to all myeloid lineages. Nature 2000, 404:193-197.

9. Kondo M, Weissman IL, Akashi K: Identification of clonogenic common lymphoid progenitors in mouse bone marrow. Cell 1997, 91:661-672.

10.* Rothenberg EV, Dionne CJ: Lineage plasticity and commitment in T-cell development. Immunol Rev 2002, 187:96-115.

This is an interpretive review that argues for a regulatory gene-based understanding of lymphoid lineage choices. Lymphoid developmental choices are characterized as more consistent with a "window of opportunity" model, based on the overlap of transcriptional regulators than with a particular mandated succession of binary choices. Also discussed is evidence that discrete lockdown functions are used to terminate developmental plasticity in T-cell development (see also [24**, 46**]).

11.** Rothenberg EV, Anderson MK: Elements of transcription factor network design for T-lineage specification. Devel Biol 2002, 246:29-44.

This is an interpretive review that presents the case for the essential combinatoriality of lineage specification functions in lymphoid development. This review also presents the first

draft assembly of genetic regulatory network elements for T-cell specification and discusses the interpretation of the linkages in developmental terms (see also [24**, 46**]).

12. Hu M, Krause D, Greaves M, Sharkis S, Dexter M, Heyworth C, Enver T: Multilineage gene expression precedes commitment in the hemopoietic system. Genes Dev 1997, 11:774-785.

13.* Akashi K, He X, Chen J, Iwasaki H, Niu C, Steenhard B, Zhang J, Haug J, Li L: Transcriptional accessibility for multi-tissue and multi-hematopoietic lineage genes is hierarchically controlled during early hematopoiesis. Blood 2003, 101:383-389.

This paper presents the first systematic microarray hybridization analysis to compare gene expression patterns in hematopoietic stem cells with those of partially restricted CLPs and CMPs. The results emphasize the developmental breadth of gene expression pattern among primitive stem cells, and the role of negative as well as positive gene regulation in lineage commitment. The authors propose that stem cells start with a characteristically open chromatin conformation spanning many loci, giving rise to promiscuous, low-level expression of lineage-specific transcripts. In this model, lineage restriction involves the progressive closing of chromatin domains with the concomitant loss of promiscuous gene expression (see also [15**–17**]).

14. Delassus S, Titley I, Enver T: Functional and molecular analysis of hematopoietic progenitors derived from the aorta-gonadmesonephros region of the mouse embryo. Blood 1999, 94:1495-1503.

15.** Miyamoto T, Iwasaki H, Reizis B, Ye M, Graf T, Weissman IL, Akashi K: Myeloid or lymphoid promiscuity as a critical step in hematopoietic lineage commitment. Dev Cell 2002, 3:137-147.

Inspired by the approach of [12], this paper uses powerful single-cell gene-expression analyses to prove that individual cells of the CLP and CMP classes are generally lymphoid- or myeloid-restricted in their gene expression profiles, respectively. The authors also show that individual cells of the CLP and CMP classes simultaneously express sets of genes that are normally associated with mutually exclusive developmental fates in their descendants, albeit at levels approximately an order of magnitude below those characteristic of legitimate expression in committed cell types. CLPs coexpress genes that are both T- and B-cell specific, and CMPs coexpress genes that are both myeloid and erythroid specific. However, although HSCs promiscuously express a broad spectrum of hematopoietic lineage genes, they are largely devoid of lymphoid expression, perhaps reflecting the late emergence of lymphopoiesis in evolution. Considerable heterogeneity in gene expression profiles was also noted within each class of cells. Given the snapshot-like nature of the assay, these variations could represent either fluctuating levels in individual cells or a distribution of stable expression patterns. The findings suggest that multipotency is sometimes mediated by coexpression of competing lineage programs at intermediate or "floating" levels as a prelude to exclusive, winner-takes-all commitment.

16.** Igarashi H, Gregory SC, Yokota T, Sakaguchi N, Kincade PW: Transcription from the RAG1 locus marks the earliest lymphocyte progenitors in bone marrow. Immunity 2002, 17:117-130. See annotation to [17**].

17.** Gounari F, Aifantis I, Martin C, Fehling HJ, Hoeflinger S, Leder P, von Boehmer H, Reizis B: Tracing lymphopoiesis with the aid of a pTα-controlled reporter gene. Nat Immunol 2002, 3:489-496.

These two papers, [16**, 17**], show that a practical implication of the multilineage gene activation in precursors is that lymphoid precursors can be recognized and isolated at an extremely early stage, by their expression of stable reporter genes under the control of early lymphoid regulatory elements. Cells expressing RAG1 [16**] or pTα [17**] are capable of differentiating into T, B, or NK cells, although in each case repression as well as activation of genes is seen with particular cell fates. This body of work emphasizes the regulatory instability of the intermediate states between hematopoietic stem cells and committed lymphoid precursors.

18. Davidson EH, Rast JP, Oliveri P, Ransick A, Calestani C, Yuh C-H, Minokawa T, Amore G, Hinman V, Arenas-Mena C et al.: A provisional regulatory gene network for specification of endomesoderm in the sea urchin embryo. Devel Biol 2002, 246:162-190.

19.** Davidson EH, Rast JP, Oliveri P, Ransick A, Calestani C, Yuh CH, Minokawa T, Amore G, Hinman V, Arenas-Mena C et al.: A genomic regulatory network for development. Science 2002, 295:1669-1678.

This is the first multilineage developmental system to be solved by genomic regulatory network analysis based on empirical perturbation studies, and is a potential model for approaches to analysis of hematopoietic developmental choices. This is the most accessible presentation of this work to a general audience.

20. Tumpel S, Maconochie M, Wiedemann LM, Krumlauf R: Conservation and diversity in the cis-regulatory networks that integrate information controlling expression of Hoxa2 in hindbrain and cranial neural crest cells in vertebrates. Dev Biol 2002, 246:45-56.

21. Dasen JS, Rosenfeld MG: Combinatorial codes in signaling and synergy: lessons from pituitary development. Curr Opin Genet Dev 1999, 9:566-574.

22. Lloberas J, Soler C, Celada A: The key role of PU.1/SPI-1 in B cells, myeloid cells and macrophages. Immunol Today 1999, 20:184-189.

23. Fisher RC, Scott EW: Role of PU.1 in hematopoiesis. Stem Cells 1998, 16:25-37.

24.** Anderson MK, Weiss A, Hernandez-Hoyos G, Dionne CJ, Rothenberg EV: Constitutive expression of PU.1 in fetal hematopoietic progenitors blocks T-cell development at the pro-T stage. Immunity 2002, 16:285-296.

This work uses the approach pioneered in [77] to demonstrate an upper limit for PU.1 expression levels in T-cell precursors, similar to the dose-dependence of PU.1 activity in B-cell development [4**, 29]. The definition of the developmental window for PU.1 effects here correlates with *in vivo* regulation of PU.1 in normal pro-T cells, and links the perturbation to *in vivo* developmental plasticity. The effects of PU.1 misexpression on the pattern of gene expression in a pro-T-like cell line are shown to be governed by bistable switchlike behavior that implicates additional network functions in the response.

25. Yamada T, Abe M, Higashi T, Yamamoto H, Kihara-Negishi F, Sakurai T, Shirai T, Oikawa T: Lineage switch induced by overexpression of Ets family transcription factor PU.1 in murine erythroleukemia cells. Blood 2001, 97:2300-2307.

26. Scott EW, Simon MC, Anastasi J, Singh H: Requirement of transcription factor PU.1 in the development of multiple hematopoietic lineages. Science 1994, 265:1573-1577.

27. McKercher SR, Torbett BE, Anderson KL, Henkel GW, Vestal DJ, Baribault H, Klemsz M, Feeney AJ, Wu GE, Paige CJ, Maki RA: Targeted disruption of the PU.1 gene results in multiple hematopoietic abnormalities. EMBO J 1996, 15:5647-5658.

28. Spain LM, Guerriero A, Kunjibettu S, Scott EW: T cell development in PU.1-deficient mice. J Immunol 1999, 163:2681-2687.

29. DeKoter RP, Singh H: Regulation of B lymphocyte and macrophage development by graded expression of PU.1. Science 2000, 288:1439-1441.

30. Berg LJ, Kang J: Molecular determinants of TCR expression and selection. Curr Opin Immunol 2001, 13:232-241.

31. Colucci F, Samson SI, DeKoter RP, Lantz O, Singh H, Di Santo JP: Differential requirement for the transcription factor PU.1 in the generation of natural killer cells versus B and T cells. Blood 2001, 97:2625-2632.

32. Cantor AB, Orkin SH: Hematopoietic development: a balancing act. Curr Opin Genet Dev 2001, 11:513-519.

33. Graf T: Transcription factors that induce commitment of multipotent hematopoietic progenitors: lessons from the MEP system. In Hematopoiesis: a Developmental Approach. Edited by Zon LI. New York: Oxford University Press; 2001:355-362.

34. Nerlov C, Tenen DG, Graf T: Regulatory interactions between transcription factors and their role in hematopoietic lineage determination. In Hematopoiesis: a Developmental Approach. Edited by Zon LI. New York: Oxford University Press; 2001:363-367.

35.* Hong W, Kim AY, Ky S, Rakowski C, Seo S-B, Chakravarti D, Atchison M, Blobel GA: Inhibition of CBP-mediated protein acetylation by the Ets family oncoprotein PU.1. Mol Cell Biol 2002, 22:3729-3743.

This paper describes a mechanism through which PU.1 can antagonize GATA-1 activity by interference with its acetylation. Even if this should not turn out to be the major mechanism for PU.1/GATA antagonism, it could be significant as a way for PU.1 to selectively antagonize acetylationdependent functions of GATA factors while permitting their acetylation-independent functions [36]. This mechanism could contribute to the combinatorial regulatory potential for intermediate states in which both PU.1 and GATA factors are expressed.

36. Yamagata T, Mitani K, Oda H, Suzuki T, Honda H, Asai T, Maki K, Nakamoto T, Hirai H: Acetylation of GATA-3 affects T-cell survival and homing to secondary lymphoid organs. EMBO J 2000, 19:4676-4687.

37. Chen H, Ray-Gallet D, Zhang P, Hetherington CJ, Gonzalez DA, Zhang DE, Moreau-Gachelin F, Tenen DG: PU.1 (Spi-1) autoregulates its expression in myeloid cells. Oncogene 1995, 11:1549-1560.

38. Seshasayee D, Gaines P, Wojchowski DM: GATA-1 dominantly activates a program of erythroid gene expression in factor-dependent myeloid FDCW2 cells. Mol Cell Biol 1998, 18:3278-3288.

39. Tsai SF, Strauss E, Orkin SH: Functional analysis and *in vivo* footprinting implicate the erythroid transcription factor GATA-1 as a positive regulator of its own promoter. Genes Dev 1991, 5:919-931.

40. Anderson KP, Crable SC, Lingrel JB: The GATA-E box-GATA motif in the EKLF promoter is required for *in vivo* expression. Blood 2000, 95:1652-1655.

41. Nerlov C, Graf T: PU.1 induces myeloid lineage commitment in multipotent hematopoietic progenitors. Genes Dev 1998, 12:2403-2412.

42.* Dahl R, Ramirez-Bergeron DL, Rao S, Simon MC: Spi-B can functionally replace PU.1 in myeloid but not lymphoid development. EMBO J 2002, 21:2220-2230.

This paper uses a knock-in system to test the interchangeability of Spi-B and PU.1. The results emphasize the key role of PU.1 and/or the perfect regulation of PU.1 levels to generate lymphoid lineages.

43. Chen D, Zhang G: Enforced expression of the GATA-3 transcription factor affects cell fate decisions in hematopoiesis. Exp Hematol 2001, 29:971-980.

44. Weiss MJ, Keller G, Orkin SH: Novel insights into erythroid development revealed through *in vitro* differentiation of GATA-1-embryonic stem cells. Genes Dev 1994, 8:1184-1197.

45. Walsh JC, DeKoter RP, Lee HJ, Smith ED, Lancki DW, Gurish MF, Friend DS, Stevens RL, Anastasi J, Singh H: Cooperative and antagonistic interplay between PU.1 and GATA-2 in the specification of myeloid cell fates. Immunity 2002, 17:665-676.

46.** Anderson MK, Hernandez-Hoyos G, Dionne CJ, Arias A, Chen D, Rothenberg EV: Definition of regulatory network elements for T-cell development by perturbation analysis with PU.1 and GATA-3. Devel Biol 2002, 246:103-121.

This paper presents evidence that T-cell specification depends on low levels, but not high levels, of GATA-3, just as it depends on low, but not high, levels of PU.1. This demonstrates the distinction between T-lymphoid regulatory requirements and the regulatory requirements of erythromegakaryocytic development, as emphasized in the accompanying review [11**]. An extensive analysis of gene-expression alterations in T-cell precursors under perturbation with GATA-3 and PU.1 leads to the assembly of the first draft assembly of regulatory network elements for T-cell specification.

47. Georgopoulos K: Transcription factors required for lymphoid lineage commitment. Curr Opin Immunol 1997, 9:222-227.

48. Brown KE, Guest SS, Smale ST, Hahm K, Merkenschlager M, Fisher AG: Association of transcriptionally silent genes with Ikaros complexes at centromeric heterochromatin. Cell 1997, 91:845-854.

49.* Mikkola I, Heavey B, Horcher M, Busslinger M: Reversion of B cell commitment upon loss of Pax5 expression. Science 2002, 297:110-113.

This paper formally proves that normal precursors undergoing B-cell specification cannot become committed without sustained expression of the lockdown functions provided by Pax5.

50. Busslinger M, Nutt SL, Rolink AG: Lineage commitment in lymphopoiesis. Curr Opin Immunol 2000, 12:151-158.

51. Herblot S, Steff AM, Hugo P, Aplan PD, Hoang T: SCL and LMO1 alter thymocyte differentiation: inhibition of E2A-HEB function and pre-Tα chain expression. Nat Immunol 2000, 1:138-144.

52. Anderson MK, Hernandez-Hoyos G, Diamond RA, Rothenberg EV: Precise developmental regulation of Ets family transcription factors during specification and commitment to the T cell lineage. Development 1999, 126:3131-3148.

53. Varnum-Finney B, Xu L, Brashem-Stein C, Nourigat C, Flowers D, Bakkour S, Pear WS, Bernstein ID: Pluripotent, cytokine-dependent, hematopoietic stem cells are immortalized by constitutive Notch1 signaling. Nat Med 2000, 6:1278-1281.

54. Allman D, Punt JA, Izon DJ, Aster JC, Pear WS: An invitation to T and more: notch signaling in lymphopoiesis. Cell 2002, 109(Suppl):S1-S11.

55. Borowski C, Martin C, Gounari F, Haughn L, Aifantis I, Grassi F, von Boehmer H: On the brink of becoming a T cell. Curr Opin Immunol 2002, 14:200-206.

56. MacDonald HR, Wilson A, Radtke F: Notch1 and T-cell development: insights from conditional knockout mice. Trends Immunol 2001, 22:155-160.

57. Allman D, Karnell FG, Punt JA, Bakkour S, Xu L, Myung P, Koretzky GA, Pui JC, Aster JC, Pear WS: Separation of Notch1 promoted lineage commitment and expansion/transformation in developing T cells. J Exp Med 2001, 194:99-106.

58.* De Smedt M, Reynvoet K, Kerre T, Taghon T, Verhasselt B, Vandekerckhove B, Leclercq G, Plum J: Active form of Notch imposes T cell fate in human progenitor cells. J Immunol 2002, 169:3021-3029.

This reference presents an *in vitro* culture system in which hematopoietic precursors can be isolated and shown to differentiate into T/NK precursors when transduced with activated Notch, losing B-cell differentiation activity. This confirms and extends earlier results from whole animal studies and culture systems that do not permit the direct determination of T-lineage potential [59–63].

59. Jaleco AC, Neves H, Hooijberg E, Gameiro P, Clode N, Haury M, Henrique D, Parreira L: Differential effects of Notch ligands Delta-1 and Jagged-1 in human lymphoid differentiation. J Exp Med 2001, 194:991-1002.

60. Pui JC, Allman D, Xu L, DeRocco S, Karnell FG, Bakkour S, Lee JY, Kadesch T, Hardy RR, Aster JC, Pear WS: Notch1 expression in early lymphopoiesis influences B versus T lineage determination. Immunity 1999, 11:299-308.

61. Koch U, Lacombe TA, Holland D, Bowman JL, Cohen BL, Egan SE, Guidos CJ: Subversion of the T/B lineage decision in the thymus by lunatic fringe-mediated inhibition of Notch-1. Immunity 2001, 15:225-236.

62. Radtke F, Wilson A, Stark G, Bauer M, van Meerwijk J, MacDonald HR, Aguet M: Deficient T cell fate specification in mice with an induced inactivation of Notch1. Immunity 1999, 10:547-558.

63. Wilson A, MacDonald HR, Radtke F: Notch 1-deficient common lymphoid precursors adopt a B cell fate in the thymus. J Exp Med 2001, 194:1003-1012.

64. Cheng P, Zlobin A, Volgina V, Gottipati S, Osborne B, Simel EJ, Miele L, Gabrilovich DI: Notch-1 regulates NF-kB activity in hemopoietic progenitor cells. J Immunol 2001, 167:4458-4467.

65.** Han H, Tanigaki K, Yamamoto N, Kuroda K, Yoshimoto M, Nakahata T, Ikuta K, Honjo T: Inducible gene knockout of transcription factor recombination signal binding protein-J reveals its essential role in T versus B lineage decision. Int Immunol 2002, 14:637-645.

Using a conditional knockout, the authors showed that CSL is essential for early T-cell differentiation in the thymus. The knockout also had the effect of inducing B lymphopoiesis in the thymus, again recapitulating the effects of a Notch knockout and supporting the central role of the CSL–Notch-ICN complex in regulating the B versus T lineage choice.

66.* Reizis B, Leder P: Direct induction of T lymphocyte-specific gene expression by the mammalian Notch signaling pathway. Genes Dev 2002, 16:295-300.

The first demonstration of a pathway through which a T-lineage-associated gene is directly regulated by Notch–CSL in the earliest stages of T-lineage specification. The initial onset of pTα expression is shown to depend on the CSL site in its cis-regulatory region for correct timing.

67. von Boehmer H, Aifantis I, Feinberg J, Lechner O, Saint-Ruf C, Walter U, Buer J, Azogui O: Pleiotropic changes controlled by the pre-T-cell receptor. Curr Opin Immunol 1999, 11:135-142.

68. Tomita K, Hattori M, Nakamura E, Nakanishi S, Minato N, Kageyama R: The bHLH gene Hes1 is essential for expansion of early T cell precursors. Genes Dev 1999, 13:1203-1210.

69.* Kawamata S, Du C, Li K, Lavau C: Overexpression of the Notch target genes Hes *in vivo* induces lymphoid and myeloid alterations. Oncogene 2002, 21:3855-3863.

HES genes encode bHLH transcription factors that can act as repressors. HES-1 and HES-5 are directly upregulated by Notch via the CSL (here called CBF1) pathway. Transplantation of transgenic mouse bone-marrow tissue expressing either Hes family genes or Notch-ICN showed that, although constitutive Notch signaling leads to a complete block in B-lineage development, overexpression of HES-1 or HES-5 can produce a partial block. In a reporter gene assay, NotchIC, HES-1 and HES-5 (but not HES-2 or HES-3) were found to inhibit the transactivation potential of E2A, an E protein that plays a key role in B-lineage commitment. These experiments suggest that Notch could suppress the B-lineage fate in part through HES-mediated repression of the E2A gene.

70. Zhuang Y, Barndt RJ, Pan L, Kelley R, Dai M: Functional replacement of the mouse E2A gene with a human HEB cDNA. Mol Cell Biol 1998, 18:3340-3349.

71. Radtke F, Ferrero I, Wilson A, Lees R, Aguet M, MacDonald HR: Notch1 deficiency dissociates the intrathymic development of dendritic cells and T cells. J Exp Med 2000, 191:1085-1094.

72. Yokota Y, Mansouri A, Mori S, Sugawara S, Adachi S, Nishikawa S, Gruss P: Development of peripheral lymphoid organs and natural killer cells depends on the helix-loop-helix inhibitor Id2. Nature 1999, 397:702-706.

73.** Ikawa T, Fujimoto S, Kawamoto H, Katsura Y, Yokota Y: Commitment to natural killer cells requires the helix-loop-helix inhibitor Id2. Proc Natl Acad Sci USA 2001, 98:5164-5169.

This paper presents a comparison of hematopoietic cells recovered from the fetal thymus of wild-type and Id2-null mice, which revealed a sharp reduction in the number of cells

expressing the NK cell marker CD122 (IL-2R) in the mutants. Overall thymocyte cellularity was about the same for mutant and wild type, which suggests that thymically localized hematopoietic progenitors simply follow the T-lineage program in the absence of Id2. Buttressing this inference, Id2-null fetal thymic organ culture (FTOC) failed to produce mature NK cells but exhibited normal T-cell development, whereas RT–PCR analysis of wild-type progenitors fractionated on the basis of CD122 expression revealed a strong correlation between Id2 levels and NK-lineage commitment.

74.* Kee BL, Bain G,Murre C: IL-7Rα and E47: independent pathways required for development of multipotent lymphoid progenitors. EMBO J 2002, 21:103-113.

This paper shows that the pathways regulating IL-7Rα expression and the pathways dependent on E47 are not redundant but complementary in promoting the survival of T-lymphoid progenitors through the earliest stages of their development.

75. Petersson K, Ivars F, Sigvardsson M: The pTα promoter and enhancer are direct targets for transactivation by E box-binding proteins. Eur J Immunol 2002, 32:911-920.

76. Rosmaraki EE, Douagi I, Roth C, Colucci F, Cumano A, Di Santo JP: Identification of committed NK cell progenitors in adult murine bone marrow. Eur J Immunol 2001, 31:1900-1909.

77. Heemskerk MHM, Blom B, Nolan G, Stegmann APA, Bakker AQ, Weijer K, Res PCM, Spits H: Inhibition of T cell and promotion ofnatural killer cell development by the dominant negative helix loop helix factor Id3. J Exp Med 1997, 186:1597-1602.

78. Anderson KL, Perkin H, Surh CD, Venturini S, Maki RA, Torbett BE: Transcription factor PU.1 is necessary for development of thymic and myeloid progenitor-derived dendritic cells. J Immunol 2000, 164:1855-1861.

79. Guerriero A, Langmuir PB, Spain LM, Scott EW: PU.1 is required for myeloid-derived but not lymphoid-derived dendritic cells. Blood 2000, 95:879-885.

80.* Schotte R, Rissoan MC, Bendriss-Vermare N, Bridon JM, Duhen T, Weijer K, Briere F, Spits H: The transcription factor Spi-B is expressed in plasmacytoid DC precursors and inhibits T, B, and NK cell development. Blood 2003, 101:1015-1023.

The PU.1 relative Spi-B has been shown to have similar effects to PU.1 itself when it is overexpressed in lymphoid precursors [24**]. Here, Spi-B is also shown to be expressed normally in the plasmacytoid class of DCs, and its overexpression enhances the generation of these cells from hematopoietic precursors in a permissive culture system. These observations strengthen the link between the normal expression of Spi-B and PU.1, which continues through the early stages of T-cell development, and the ability of these early T-cell precursors to differentiate along the DC pathway.

81. Iwama A, Osawa M, Hirasawa R, Uchiyama N, Kaneko S, Onodera M, Shibuya K, Shibuya A, Vinson C, Tenen DG, Nakauchi H: Reciprocal roles for CCAAT/enhancer binding protein (C/EBP) and PU.1 transcription factors in Langerhans cell commitment. J Exp Med 2002, 195:547-558.

82. Bauer SR, Holmes KL, Morse HC III, Potter M: Clonal relationship of the lymphoblastic cell line P388 to the macrophage cell line P388D1 as evidenced by immunoglobulin gene rearrangements and expression of cell surface antigens. J Immunol 1986, 136:4695-4699.

83. Principato M, Cleveland JL, Rapp UR, Holmes KL, Pierce JH, Morse HC III, Klinken SP: Transformation of murine bone marrow cells with combined v-raf-v- myc oncogenes yields clonally related mature B cells and macrophages. Mol Cell Biol 1990, 10:3562-3568.

84. Borrello MA, Phipps RP: The B/macrophage cell: an elusive link between $CD5^+$ B lymphocytes and macrophages. Immunol Today 1996, 17:471-475.

85. Res PCM, Couwenberg F, Vyth-Dreese FA, Spits H: Expression of a pTα mRNA in a committed dendritic cell precursor in the human thymus. Blood 1999, 94:2647-2657.

86. Lee C-K, Kim K, Geiman TM, Murphy WJ, Muegge K, Durum SK: Cloning thymic precursor cells: demonstration that individual pro-T1 cells have dual T-NK potential and individual pro-T2 cells have dual αβ-γδ T cell potential. Cell Immunol 1999, 191:139-144.

87. Shortman K, Vremec D, Corcoran LM, Georgopoulos K, Lucas K, Wu L: The linkage between T-cell and dendritic cell development in the mouse thymus. Immunol Rev 1998, 165:39-46.

88.** King AG, Kondo M, Scherer DC, Weissman IL: Lineage infidelity in myeloid cells with TCR gene rearrangement: a latent developmental potential of pro-T cells revealed by ectopic cytokine receptor signaling. Proc Natl Acad Sci USA 2002, 99:4508-4513.

Ectopic expression of the CD122 (IL-2Rβ) cytokine receptor in CLPs, followed by addition of ligand, generates signals that can cause these lymphoid-restricted precursors to shift their differentiation program to a completely myeloid one. This paper shows that the ability of cells to be trans-differentiated by ectopic receptor signaling is under tight developmental regulation. This responsiveness persists through the first two stages of T-cell precursor development in the thymus and then terminates at the same time that normal T-cell

precursors are found to be fully committed. As discussed in [10*], the loss of responsiveness coincides with the timing of endogenous PU.1 downregulation. These results emphasize the regulatory instability of precursors during the first stages of lymphoid differentiation, even while the cells are initiating expression of T-cell genes such as pTα.

89. Ohishi K, Varnum-Finney B, Serda RE, Anasetti C, Bernstein ID: The Notch ligand, Delta-1, inhibits the differentiation of monocytes into macrophages but permits their differentiation into dendritic cells. Blood 2001, 98:1402-1407.

90. Spits H, Couwenberg F, Bakker AQ, Weijer K, Uittenbogaart CH: Id2 and Id3 inhibit development of $CD34^+$ stem cells into predendritic cell (Pre-DC)2 but not into Pre-DC1: evidence for a lymphoid origin of Pre-DC2. J Exp Med 2000, 192:1775-1783.

Chapter 3

SINGLE-CELL GENE-EXPRESSION ANALYSIS

3.1 Gene-Expression Assays

The "central dogma" of developmental biology holds that development is underwritten by regulated changes in gene expression. In order to study this process, we need techniques for measuring how gene activity patterns vary within the developing organism. Since most genes encode messenger RNAs which are translated into proteins, expression can be assessed at either the RNA or the protein level. In principle, protein quantitation is more informative, because only a gene's peptide end product directly affects cell function. As translation and protein degradation can be loci for gene-specific regulation, RNA assays cannot capture all the expression changes which attend development. This is mitigated by the fact that post-transcriptional control is often effected by transcriptional modulation of regulatory genes. Moreover, it has been discovered recently that eukaryotic genomes harbor large, previously unrecognized classes of untranslated genes, such as microRNAs and shRNAs [1-3]. These genes encode short RNAs which modulate translation, mRNA degradation, epigenetic silencing, and perhaps still other processes; many seem to be involved in developmental processes. It seems likely, then, that most of the gene-expression changes involved in development are associated with measurable changes in the level of cellular RNAs.

3.1.1 *In Vivo* Assays

Ideally, we would like to monitor genetic activity *in vivo*, to follow exactly how genes are regulated in time and space. Over the past few years, transgenic reporter methods have made this feasible. In the reporter-gene approach, a synthetic gene coding either a fluorescent

protein (e.g., Green Fluorescent Protein, or GFP), or an enzyme which catalyzes the production of a visualizable product (e.g., β-galactosidase or luciferase), is introduced into a living organism. The transgene may be expressed under the control of a promoter sequence derived from a gene of interest, so that its spatiotemporal expression recapitulates that of the natural gene. Alternatively, the endogenous gene is replaced with one encoding a fusion protein which incorporates a reporter peptide sequence into the natural product. Reporter genes can provide unprecedented insight into developmental processes, and have also been used to study the basic mechanisms of gene regulation. Advanced microscopy techniques allow reporter expression to be evaluated at the single-cell level—in some cases, even at the single-molecule level. Reporter-based experiments have been used to investigate the sources of noise in gene expression [4, 5]; to characterize a stochastic genetic switch [6, 7]; to evaluate the "gene regulation function" of a gene [4, 8]; to analyze the behavior of natural and artificial transcriptional circuits [7, 9, 10]; to demonstrate the bursty nature of translation [11]; and, to quantitate the kinetics of transcription factor induction, binding, and facilitated (1D/3D) diffusion [12]. Of course, the experimental procedures involved in reporter-based studies are difficult and time consuming. Another important limitation is that these analyses are generally limited to evaluating a single gene, or at most a very few genes, at one time.

3.1.2 *In Situ* Assays

For developmental studies, the next best thing to looking at the dynamic regulation of gene expression *in vivo* is to visualize the spatial patterning of expression *in situ*, in preserved tissue samples. Histological staining has been applied for decades to examine the distribution of specific proteins within fixed, permeabilized tissue. Originally, staining was performed using small-molecule dyes which had been shown by trial and error to bind particular proteins or

other cellular macromolecules with some degree of specificity. The generality and selectivity of the histological staining approach has been greatly enhanced by the development of immunological methods, and it is now possible to make dye-conjugated antibodies to label almost any protein of interest. *In situ* staining of RNA targets can be achieved with oligonucleotide hybridization probes. In traditional *in situ* hybridization (ISH) protocols, a radioactive probe is used to label the RNA of interest. This approach is being supplanted by fluorescence *in situ* hybridization (FISH), which employs dye-conjugated probes.

Techniques like confocal microscopy have made it possible to look at the subcellular localization of protein or RNA targets with fluorophore-tagged antibodies or oligo probes. Advanced FISH protocols have been used to take snapshots of transcriptionally active genes, and to count RNA transcripts in the nuclei and cytoplasm of individual mammalian cells; these studies have revealed the bursty character of transcription, and suggest that gene expression in eukaryotes involves the stochastic decondensation of large chromatin domains [13-15]. Fluorescence-based assays can be multiplexed through the use of multiple dye colors in the same assay. Generally, spectral overlap between dyes severely limits the number of targets that can be assayed in the same *in situ* experiment; however, simultaneous evaluation of ten different genes has been demonstrated using a bar-coding strategy in which different fluorophore combinations are assigned to each RNA target [13].

3.1.3 *In Vitro* Assays

As valuable as *in vivo* and *in situ* techniques are, their applicability is restricted to highly focused studies targeting one or, at most, a handful of genes. These methods do not permit the profiling of a large panel of genes, nor are they suited to high-throughput surveys involving many individual samples. Although there are exceptions, the expression data

yielded by *in vivo* and *in situ* methods tend to be non-quantitative, and generally do not lend themselves to statistical analysis, collation in public databases, or systematic data mining. *In vitro* protein and RNA assays were originally developed to facilitate detection of rare molecular species in homogenized samples using specialized chemistries. Improvements in the sensitivity of these molecular assays, and in the technology for reading out the results, have yielded methods which can rapidly and inexpensively generate masses of quantitative gene-expression data. In consequence, the term *gene profiling* is now almost synonymous with the use of *in vitro* techniques such as quantitative RT-PCR (qRT-PCR) and "gene chip" arrays.

3.1.3.1 Protein Assays

Antibody-based protein assays such as western blot, chromatin immunoprecipitation (ChIP), and Enzyme-Linked Immunosorbent Assay (ELISA) are widely used to isolate, detect and quantitate specific proteins within homogenized samples. However, the production of an antibody against a novel protein target is a lengthy and expensive process. Moreover, the specificity of protein-antibody binding in any given experimental context is unpredictable, so immunological assays frequently require considerable optimization. These techniques are incompatible with high-order multiplexing and, since proteins cannot be amplified, relatively large amounts of analyte are required to perform even a single assay.

3.1.3.1.1 Immuno-PCR

In the last few years, the sensitivity of *in vitro* protein quantification has been improved by combining antibody labeling with PCR amplification and detection [16, 17]. In "immuno-PCR," the antibody probes used to label a target are linked to oligonucleotides; the binding

of two antibodies to the same molecule brings these "tails" into proximity, establishing a substrate for ligation and qPCR-based quantification. Immuno-PCR is at least a hundred times as sensitive as ELISA, the traditional "gold standard" for *in vitro* protein detection. In principle, the method can detect a single protein molecule. This level of sensitivity is rarely approached in practice owing to the relatively poor specificity of antibody-target binding.

3.1.3.1.2 Protein Microarrays

Highly multiplexed protein microarray assays have recently become available [18]. In a protein microarray, antibody probes for thousands of different targets are arrayed on a solid substrate. A sample of protein extract is incubated on the array, and the probes capture and segregate their specific targets. The array is imaged after the incubation to obtain the abundance profile of the probed species. The antigens bound to the antibody array can be detected using a variety of different labeling techniques—for example, covalent coupling of fluorophores to the sample proteins prior to the incubation step. Typically, the intensities of equivalent spots in assays run on distinct biological samples are compared to read out fold differences in the expression of the associated species; absolute quantitation and interspecies abundance comparisons are generally not supported.

3.1.3.1.3 FACS

One well-established protein assay which lends itself to a survey approach is fluorescence-activated cell sorting (FACS). This technique allows the expression of plasma membrane proteins to be quantitated in living cells *ex vivo*; it therefore straddles the divide between *in vivo* and *in vitro* methods. In FACS, a suspension of cells is stained with dye-conjugated antibodies against cell-surface proteins, and the sample is aspirated into a cell sorter for

analysis. Within the instrument, cells are pressure-fed through a narrow channel in single file. Each cell is individually illuminated by a laser and photodetectors measure the light output, thus affording a quantitative readout of protein expression. The more sophisticated instruments incorporate a programmable electrostatic cell-deflection mechanism which permits the selective recovery of cells based on surface phenotype. FACS is therefore a powerful tool for sorting and purifying cells, as well as for protein expression analysis.

The latest generation of cell sorters can analyze thousands of cells per second. Advances in optics and dye chemistry are constantly increasing the number of different cell-surface markers which can be evaluated simultaneously [19-21]. Four- or five-way multiplexing is now common practice. High-end systems can support the quantification of ten or more proteins at once, although exploiting their full potential remains challenging given the unpredictable specificity of antibody labeling. While FACS is normally used to analyze surface-protein expression, intracellular protein levels can be evaluated *in situ* in fixed, permeabilized cells. This is still relatively uncommon, owing to the limited availability of antibodies against intracellular proteins and the complexity of the sample preparation protocol. Intracellular fluorescent reporters such as GFP can be assayed without the need for permeabilization and staining [22, 23].

Bacteria and hematopoietic cells make ideal targets for FACS analysis. Certain solid-tissue cell types can be evaluated after disaggregation, the difficulty involved varying with the size and morphology of the cells of interest. Our understanding of the cellular differentiation process in mammals is to a large extent based on studies of hematopoiesis enabled by FACS. The analytical power of flow cytometry is tied to the fact that it measures gene expression at the single-cell level. Most *in vitro* gene profiling techniques provide ensemble-average

expression measurements on samples derived from thousands or even millions of individual cells. For developmental studies, the significance of the data they produce is limited by the phenotypic purity of the cells contributing to the analyte. In contrast, FACS can be used to explore the population structure of a biological sample. By revealing how morphologically similar cells cluster into subpopulations when viewed in gene-expression space, FACS has spurred the stepwise refinement of cell taxonomies. As the classification of developmental progenitors gets more fine grained, it becomes more practical to pinpoint the regulatory events which move differentiation forward. From this standpoint, the main limitation of FACS is that it does not let us follow these events directly, since the key actors involved are predominantly transcription factors which operate within the cell nucleus.

3.1.3.2 RNA Assays

Generally, available *in vitro* RNA assays outperform protein assays with respect to ease of use, sensitivity, quantitative accuracy, and potential for multiplexing. This can be attributed to the relative simplicity of nucleic-acid chemistry; the specific and predictable character of strand hybridization can be exploited for RNA amplification and detection, but peptides offer no such convenient "handle" for analysis. Of the many RNA assays now available, the most prevalent are serial analysis of gene expression (SAGE), microarray analysis, and quantitative reverse-transcription PCR (qRT-PCR). A sequencing-based method, SAGE can be used to profile an entire mRNA transcriptome based on a single RNA sample, without requiring any prior knowledge of the transcripts to be assayed. Microarray experiments can evaluate tens of thousands of preselected mRNA targets at a time, at a considerably lower cost than SAGE. qRT-PCR offers much higher sensitivity than the other two methods, and can be applied to tiny amounts of starting material—even the RNA isolated from a single

cell. It can also provide more accurate quantification of specific transcripts, and is the most flexible and cost-effective assay for focused studies targeting from one to a few dozen genes.

3.1.3.2.1 SAGE

In SAGE, the messenger RNA fraction of an RNA isolate is reverse transcribed into cDNA using oligo(dT) primers that bind the transcripts' poly(A) tails. Special restriction enzymes are used to clip short (10–14 bp) fragments from the transcripts; these "tags" are amplified by PCR and the products are ligated together to form long "concatamers" which are cloned and sequenced. The resulting sequence data is parsed to determine the relative frequencies of recovered tags in the cDNA pool. These "expressed sequence tags" (ESTs) can be matched against cDNA and genomic sequence databases to profile the abundance of known mRNAs, individual exons, and previously unknown transcripts in the original sample. As with all techniques which rely on global reverse transcription of mRNA, SAGE incurs the risk of underrepresenting hard-to-transcribe sequences. In addition, while the tag-sampling approach may give fairly accurate profiling of particular exons, it cannot accurately measure the abundance of specific mRNA splice forms.

Other sequencing-based profiling strategies can provide the coverage of SAGE while offering more robust quantitation—for example, the "brute-force" sequencing of a library of full-length cDNA clones. As a typical mammalian cell contains 10^5–10^6 mRNA transcripts, with most species expressed at below 10 copies [24-26], on the order of a million sequencing reactions might be required to comprehensively profile even a single cell type. This is not yet a practical proposition, but the availability of low-cost, high-throughput sequencing technologies may change this situation within the next decade.

3.1.3.2.2 Microarray Analysis

In microarray analysis, polyadenylated RNA is globally reverse transcribed into cDNA using oligo(dT) primers, fluorescently labeled, and hybridized to immobilized oligonucleotide or cDNA probes arrayed on a glass slide or a "gene chip." In some protocols, the cDNA pool is used to template runoff RNA transcription reactions, in which case complementary RNA (cRNA) rather than cDNA is hybridized to the array. Dye labels are incorporated into the transcripts using fluorophore-tagged primers or by means of covalent-coupling chemistries. Following hybridization of the analyte, the microarray is imaged to obtain a readout of the mRNA expression profile in the original sample. Typically, microarray analyses are run in parallel on at least two biologically distinct samples; after normalization to allow for global variations in signal level, relative spot intensities are used to estimate fold expression changes in differentially regulated genes.

3.1.3.2.3 Quantitative RT-PCR

Quantitative RT-PCR is currently the "gold standard" for mRNA analysis, offering the best sensitivity, dynamic range, and reproducibility of any standard technique [27]. In qRT-PCR, mRNA transcripts are first reverse transcribed into cDNA using oligo(dT), random oligomer, or gene-specific primers; the cDNAs of interest are then exponentially amplified by PCR using gene-specific primers. The concentration of amplicon in the reaction is monitored with fluorophore-conjugated hybridization probes or DNA-intercalating dyes. Template quantitation is based on the number of PCR cycles required for fluorescence to reach an arbitrary threshold. Low-order multiplexing (2–5 targets) is feasible using multiple primer pairs and different-colored probes, but tends to be problematic due to formation of "primer dimer" side products and competition between assay targets [28, 29]. Moreover,

since very small amounts of template are required, evaluation of multiple targets can usually be achieved more easily by aliquoting sample to parallel simplex qPCR reactions.

3.2 Single-Cell Analysis

With the exception of FACS, *in vitro* protein assays are generally insufficiently sensitive to carry out expression analysis on individual cells. RNA assays are more readily adapted to this task, but single-cell mRNA profiling is still uncommon. The first studies were reported about twenty years ago, and several dozen more have since appeared in the literature. The main obstacle that must be overcome is the tiny quantity of RNA recoverable from an individual cell. Most mammalian cells contain about 10–40 pg of RNA, of which about 0.1–1 pg is mRNA, corresponding to 10^5–10^6 messages [30-32]. The mRNA population of these cells includes ~10^4 transcript species, mostly present at below ten copies. Housekeeping and effector genes tend to be expressed at medium-to-high levels (10^2–10^4 copies). Transcription factors, which are among the most interesting targets for developmental studies, are usually expressed at low abundance (<100 copies) even when the genes are fully active.

3.2.1 Technical Approaches

Standard SAGE and microarray protocols call for microgram quantities of input material, corresponding to on the order of 10^6 cells' worth of RNA. The sample requirement can be reduced by two orders of magnitude in advanced versions of these assays [33, 34]. Global mRNA amplification methods have been developed which can generate sufficient analyte from much smaller amounts of RNA; the most popular approaches are runoff transcription from cDNA templates, and PCR amplification of cDNA using generic primers. Both techniques have been applied to facilitate broad-spectrum single-cell transcript profiling with microarrays or (as in early studies) "slot-blotted" cDNA arrays. There has been little interest

in applying SAGE to single cell analysis, presumably because of the labor and expense that would be entailed in the processing of each individual sample.

In principle, qRT-PCR can detect a single molecule of messenger RNA. With efficient reverse transcription, detection of one mRNA copy using standard qPCR dye chemistries requires about forty cycles of PCR; a typical housekeeping transcript in a single cell might be detected after around thirty cycles of amplification. However, the RNA input for gene profiling experiments is routinely scaled to support detection after around 15–25 PCR cycles, as this is considered the most trustworthy regime for quantitation. qRT-PCR-based expression profiling is therefore usually performed on homogenized samples derived from hundreds or thousands of cells. While conventional protocols have occasionally been applied to quantitate mRNA transcripts in single-cell lysates, such assays have been limited to the evaluation of a few, relatively highly expressed genes.

The difficulty of achieving reliable qRT-PCR quantitation from a single cell is compounded when multiple genes or rare transcripts are targeted in the analysis. Global mRNA amplification has been used in conjunction with PCR to allow profiling of multiple targets in a single cell. Increasingly, though, qRT-PCR studies have turned to sequence-specific preamplification for the profiling of panels of genes. In this strategy, a short round of multiplex PCR is used to make enough analyte for independent, simplex qPCR analyses on all genes of interest. For studies based on limiting amounts of RNA, this "preamp" approach establishes a middle ground between conventional, simplex or low-order multiplexed qRT-PCR assays and broad-spectrum microarray analysis based on global mRNA amplification.

3.2.2 Sample Preparation

Most of the single-cell gene profiling work reported to date involves the use of intrinsically low-throughput techniques for harvesting cell samples, such as patch-clamp aspiration of the cytosol [30, 35], or the picking of individual cells in a micropipette, sometimes with the aid of a micromanipulator stage [36-48]. Laser Capture Microdissection (LCM) supports a more automated approach to single-cell recovery. In this technique, an acetate film is placed on top of a tissue slice and fused to operator-designated targets with a laser; cells of interest are recovered by peeling away the film [31, 32]. Flow sorting can be used to isolate single immunophenotyped cells at high throughput, but so far only a few studies have employed this method [49-51]. Single-cell lysis, mRNA isolation, and cDNA synthesis have been combined on a microfluidic chip [52]. It may soon be possible to integrate cell culture, phenotypic characterization, and nucleic acid analysis in a lab-on-a-chip approach [53-63].

Traditional RNA isolation protocols involve multiple materials transfer steps, which is laborious when many samples have to be processed in parallel, and may risk sample loss and inconsistent recovery when applied to tiny amounts of RNA. These methods typically entail the use of chaotropic salts or proteases to inactivate RNases released by cell lysis; as these reagents are incompatible with enzymatic reactions, an RNA purification step is almost always required. An optimized chaotropic-salt strategy designed for single-cell applications has been described [64]. However, in most single-cell studies the need for RNA purification has been obviated through the use of freeze-thaw, heat, detergent or hypotonic cell lysis in the presence of a peptide RNase inhibitor [36-38, 41-46, 50, 65-68]. More elaborate protocols allow nuclear and cytoplasmic material to be fractionated through the application

of mild detergents which disrupt the plasma but not the nuclear membrane, followed by centrifugal separation of the cell nuclei [69].

Most of the single-cell RT-PCR studies published to date have employed a traditional, two-step approach to RT-PCR, in which mRNA is first reverse transcribed into cDNA, and then all or part of the reaction product is transferred into a separate PCR reaction. A more streamlined single-cell protocol has been described in which the RT and PCR steps are performed in the same reaction buffer using a blend of reverse transcriptase and *Taq* polymerase, a simplification which reportedly also improves the sensitivity of the assay [70].

3.2.3 Global mRNA Amplification

Much effort has gone into the development of global mRNA amplification methods to reduce the sample requirement for broad-spectrum gene profiling assays. The two most widely-used methods are linear amplification based on *in vitro* transcription (IVT), and exponential amplification by Sequence-Independent RT-PCR (SIP RT-PCR):

1. The most common IVT strategy is the "antisense RNA" (aRNA) method described by Eberwine et al in 1990. In this approach, mRNA is globally reverse transcribed using a "heeled" oligo(dT) primer which incorporates a promoter sequence for T7 phage RNA polymerase on its 5' end. After second-strand synthesis, T7 polymerase is used to make runoff RNA transcripts from the double-stranded cDNA. Typically, runoff transcription permits a thousandfold amplification of the original template. Million-fold amplification can be achieved by adding a second round of cDNA synthesis and runoff transcription. Expression profiling on the RNA amplification product can be performed using any of a number of standard assays, including RT-PCR, Northern Blot, slot-blot cDNA arrays, and microarray analysis [30, 71, 72].

2. SIP RT-PCR involves PCR amplification of cDNA based on generic primers. The most widely-used version approach was originally presented in 1993 by Brady and Iscove [73]: oligo(dT)-primed first-strand cDNAs are homomerically tailed with adenosine (dA) using terminal transferase, and the resulting products are amplified by PCR using oligo(dT) primers. Because PCR efficiency is sensitive to amplicon length, the duration of the RT step or the reverse transcriptase concentration is typically limited to keep all the transcripts short. In the related Three-Prime End Amplification (TPEA) approach, the tailing reaction is eschewed in favor of the use of a generic upstream primer designed to anneal to a random sequence that occurs every few hundred bases of mRNA sequence [34, 35, 37, 74].

Many commercial IVT kits are now available for preamplifying small mRNA samples for microarray analysis [34]. However, as the aRNA protocol is laborious and lengthy, two-round amplification is rarely applied, and single-cell microarray analysis using IVT is not a routine procedure [34, 44]. The amplification factor attainable with SIP RT-PCR is much higher than for IVT—up to 10^{11}-fold amplification has been claimed with high-fidelity representation [75]—and the protocol is much simpler and quicker. Modified versions of the Brady-Iscove technique have largely superseded aRNA as the method of choice for broad-spectrum profiling of single cells [31, 34, 37, 40, 41, 43-46, 48, 68, 74-76].

Global amplification is not without drawbacks. Most of the available methods exhibit so-called 3' bias because the RT step is based on oligo(dT) priming, and therefore only mRNA sequences near the poly(A) tail are recovered [31]. While this may be viewed as an acceptable limitation when collecting data on thousands of different targets, in more focused studies it is desirable to have the option of looking at any preferred region of a target, e.g.,

because only certain splice variants are of interest, or because sensitivity is limited for targets whose 3' sequence is inefficiently reverse transcribed or amplified [68]. The uniformity of both linear and exponential amplification across different transcripts is also subject to some uncertainty, especially when amplifying very small samples [34, 68].

3.2.4 RT-PCR Techniques

Microarrays evaluate thousands of genes in a single assay, but the data they produce may not always be reliable with respect to particular mRNAs, owing to the diversity of species involved in the hybridization process. High-quality expression data on a small set of genes are often preferred, and qRT-PCR therefore remains popular as a gene-profiling tool. For single-cell work, microarray analysis has the additional drawback that analysis of each RNA sample involves a relatively lengthy and costly experiment. Typically, single-cell analysis is used to survey cell-to-cell heterogeneity or population structure. Currently, qRT-PCR is the highest-throughput method for evaluating single-cell gene expression at the RNA level.

3.2.4.1 Transcript Quantification

While PCR has long set the standard for sensitivity in nucleic acid detection, the technique has only recently become highly quantitative, due to the development and commercialization of qPCR (or "real-time PCR"). In the PCR-based single-cell studies published in the nineties, amplified cDNA was evaluated on a gel at the PCR end point using ethidium bromide staining or autoradiography. PCR end-point analysis usually gives only a "positive/negative" call or, at best, a semiquantitative readout of template abundance. Now that real-time PCR instruments are widely available, qPCR is increasingly being applied to quantitative profiling of gene expression in individual cells [36, 47, 52, 66, 68, 77].

While qPCR "threshold cycle" (Ct) readouts can be used to profile single-cell transcript levels cross-sectionally within a given study, they do not facilitate the comparison of data from independent researchers. The traditional approach to this problem is to normalize gene-expression measurements to an internal standard, such as the readout for a housekeeping gene. This approach has significant weaknesses even when applied to population-level measurements [78-84]. Relative expression data becomes almost meaningless at the single-cell level, because the copy numbers of all transcripts vary widely and to a large extent independently from cell to cell [14, 36, 48, 51, 68]. However, the move to single-cell analysis raises the possibility of putting gene profiling data on an absolute basis, i.e., transcript copies per cell. One early single-cell study demonstrated the possibility of transcript counting in individual cells by applying Poisson analysis to PCR reactions conducted on limiting dilutions of cDNA prep [69]. As will be described in the next chapter, single-cell transcript counting can be automated through the use of "digital PCR" [51, 85].

Some single-cell studies have used DNA or RNA quantitation standards to permit absolute transcript quantitation. In this strategy, the copy number of an endogenous transcript is estimated based on the gel band intensity or qPCR threshold-cycle readout relative to standards-based reactions [52, 66, 68]. The reference templates can be spiked into lysate reactions, if they are distinguishable from the natural targets, in a technique called "competitive PCR." Alternatively, diluted PCR products or runoff-transcribed copies of the natural RNA template can be analyzed in separate reactions run alongside cell-based samples. Since the efficiency of cDNA synthesis can vary significantly based on the specific RT enzyme, priming strategy, and other reaction conditions [86, 87], the use of RNA standards is the most robust approach to absolute quantification of mRNA copy number.

3.2.4.2 Multiplexing Strategies

RT-PCR analysis of multiple genes in single cells is hindered by the very limited amount of RNA in each sample. Four main options are available to tackle this problem:

1. *Subdivision of the analyte*. In this approach, the single-cell RNA isolate or cDNA prep is aliquoted to independent, gene-specific RT-PCR or PCR assays for amplification and analysis. This strategy has been used to evaluate a few genes per cell in several published studies [36, 40, 42, 66, 69]. As the quantitation of even a single mRNA in a cell lysate pushes the limits of conventional qPCR, the subdivision method is not scalable to the profiling of panels involving dozens of genes. Further, the reduction in dynamic range and the sampling noise associated with aliquoting inevitably compromise quantitation of low-abundance transcripts.

2. *Single-tube multiplexing*. The entire RNA or cDNA sample is amplified in a single-tube multiplexed RT-PCR or PCR, and the different amplicons are size-separated and visualized on a gel, or analyzed *in situ* with color-coded probes in a multichannel qPCR machine. While this avoids the loss of sensitivity incurred by subdividing the analyte, the design and validation of multiplex PCR assays is complicated by increased potential for primer-dimer side reactions, and the possibility of competitive inhibition of rare targets by abundant targets [28, 29]. These problems increase with the level of multiplexing and the number of PCR cycles needed to detect product. Four- and five-channel qPCR instruments are now relatively affordable, but their full potential is rarely exploited even in conventional gene profiling work, and single-tube multiplexed analysis has not found favor for single-cell studies.

3. *Global mRNA amplification.* SIP RT-PCR or IVT is applied to the cDNA prep to amplify polyadenylated transcripts, and the product is aliquoted to gene-specific PCR or RT-PCR reactions for analysis. This method offers great flexibility in the choice of analyzed genes, and has found application in a number of single-cell studies [40, 48, 68, 76]. The main disadvantages to global mRNA amplification have already been mentioned in the context of microarray studies: (1) the restriction that the gene-specific assays must target the 3' end of transcripts, and (2) the concern that the amplification may distort transcript representation. These weigh more heavily in the RT-PCR context as alternative strategies are available; when the genes of interest are known beforehand, more reliable quantification can be achieved by using sequence-specific reverse transcription and amplification. Global amplification also adds complexity to the assay protocol, particularly in the case of the IVT approach.

4. *Sequence-specific preamplification.* Multiple cDNA targets are initially amplified together in a single-tube multiplexed reaction, using a limited number of PCR cycles so that the uniformity of amplification is uncompromised by reagent depletion effects; the product is then aliquoted to gene-specific PCRs for analysis. Some early single-cell studies employed low-order single-tube multiplexing and aliquoted the product to simplex PCRs, often using nested primers to increase specificity and avoid amplification of primer-dimer products carried over from the multiplexed reaction; second-round products were subjected to gel analysis [38, 50, 88]. The potential of the staged PCR approach has been further explored in the last few years, both in the context of single-cell studies and more generally for applications involving limiting amounts of RNA [77, 89, 90]. Refined protocols have been developed which permit multiplexing of dozens of assays, in some cases using primer sets originally designed

for simplex PCR; the analysis phase has also been rendered fully quantitative through the use of SYBR Green or TaqMan qPCR. Recently, the approach has been applied to profiling microRNA expression in single cells, using special looped primers for the RT step, allowing 220 targets to be quantitated within the same sample [47, 67].

Currently, sequence-specific preamplification (also referred to as "multiplexed tandem PCR," or "preamp") looks like the most promising strategy for increasing the breadth of single-cell qRT-PCR analysis. The technique leverages the experience already gained in the design of highly specific qRT-PCR assays. Validated primers and probes are available off the shelf for thousands of different human and rodent mRNA targets, including splice variants, and it should be feasible to apply these as is to highly multiplexed single-cell studies using standard assay chemistries. The main obstacle to the full exploitation of "preamp" to single-cell studies is the number of individual qPCR analyses that will have to be performed on each cell lysate. However, lab-on-a-chip solutions that automate the subdivision and parallel analysis of preamplified reactions have recently become available, and this difficulty should be considerably alleviated in the near future.

3.2.5 Applications

An early motivation for the development of single-cell gene profiling was to evaluate cell types which are found in highly heterogeneous tissues—particularly specialized classes of neuron [30, 39, 42, 66, 72, 88]. Gene expression in such cells cannot be evaluated by analysis of homogenized tissue samples, nor is it generally practical to recover and pool many phenotypically similar cells by microdissection. Cell types which are by their very nature rare, such oocytes, stem cells, and certain neoplastic cells, also represent obvious targets for single-cell analysis [31, 76, 91].

Owing to the difficulty of current protocols, the scale of the single-cell gene profiling studies performed to date has been small, encompassing dozens or at most hundreds of cells per survey. However, this has already been sufficient to offer some insights into the population structure of morphologically similar cells, such as early hematopoietic progenitors [40, 50, 51], cells of the developing and mature pancreas [36, 43], embryonic stem cells [47], stem cells and downstream progenitors of the skin [45] and muscle [38], and activated T cells [77].

Quantitative profiling of mRNA expression in single cells has revealed that, even among phenotypically similar cells, the heterogeneity of transcript levels is substantial [14, 36, 51]. These studies have shown that cellular transcript abundance typically exhibits a longtailed distribution, with a small fraction of the cell population expressing much higher-than-average level of transcript. Recently, the possibility that gene-expression "noise" or regulatory instability increases with age has been raised by quantitation of cell-to-cell variability in cardiomyocytes harvested from young and old animals [48].

Chapter 4

THESIS METHODS

4.1 Overview

Research conducted during the nineties demonstrated the technical feasibility of single-cell transcript profiling, opening up the possibility of analyzing gene-regulatory states cross-sectionally in differentiating cell populations. Early single-cell studies were limited with respect to their ability to quantitate transcript abundance, evaluate multiple genes per cell, detect rare messages, and survey many individual cells. The high-throughput, multiparametric single-cell profiling FACS enables at the surface-protein level remains beyond the capabilities of RNA methods. In spite of the restrictions of the technique, FACS has transformed the study of cellular differentiation. It seems likely that cross-sectional studies of intracellular gene expression will eventually offer a similar boost to developmental studies, especially once the assays become sensitive enough to characterize the networks controlling fate commitment and phenotypic specification. The experimental work described here was undertaken with the aim of bringing this goal within reach.

The thesis work encompassed single-cell assay development and two research studies, described in detail in the following chapters. The first study focused on the early steps of hematopoietic cell differentiation. From a technical standpoint, the main objective was to demonstrate that transcription factors, which are typically expressed at mRNA levels of $\ll$100 copies per cell, can be profiled quantitatively in single cells. The second study sought to evaluate the recently advanced hypothesis that gene regulation is destabilized in aging

animals; the analysis involved absolute quantitation of six different transcripts within hundreds of individual hematopoietic cells.

A common strategy was applied in both research projects for mRNA recovery and reverse transcription. High-throughput sample preparation was enabled by flow-cytometric sorting of individual, immunophenotyped cells directly into RT-PCR buffer. Using this approach, hundreds of single-cell lysates can be prepared in 96-well plates in the course of a single FACS session. The recovered cells undergo hypotonic lysis after being dispensed to reaction buffer, eliminating the need for an RNA isolation step; ribonuclease inhibitors were used to protect transcripts from degradation by RNases released on cell lysis. To maximize the efficiency and specificity of cDNA synthesis, samples were reverse transcribed using a thermostable RT enzyme and gene-specific primers. To simplify sample processing and increase RNA recovery, DNase digestion of genomic DNA was eschewed in favor of the use of exon-straddling primers, where possible, and No-RT controls were used to check the genomic-background signal. Use of an RT-*Taq* enzyme blend obviated any need for dilution or aliquoting between the RT and PCR steps of the analysis.

Different technical strategies were employed for cDNA quantitation in the two research studies. Since the hematopoiesis work focused on transcription factor expression, an assay method which was quantitative down to a few cDNA copies per cell was essential. To meet this requirement, single-cell cDNA preps were analyzed by "digital PCR" in a microfluidic chip. In digital PCR, a sample is subdivided into many compartments before amplification, and a count of positive reactions at the PCR end point provides a direct readout of template copy number. Within the chip, a duplex TaqMan assay was used to measure the levels of a transcription factor (PU.1) and a housekeeping gene (GAPDH) in each single-cell prep. The

aging study presented less of a challenge from a sensitivity standpoint, as rare transcripts were not evaluated. On the other hand, there was a greater premium on achieving a high level of multiplexing and surveying many cells. For this work, the analysis of cDNA began with a round of multiplexed PCR, which was coupled with the RT step in a single-tube protocol; the "preamplified" products were then analyzed in a conventional real-time PCR machine using SYBR Green qPCR assays. Absolute quantification of transcript copy number was facilitated by running parallel reactions on runoff-transcribed RNA standards.

4.2 Sample Preparation

4.2.1 Cell Isolation

In most published single-cell protocols, samples are collected by manual recovery of cells from a suspension using a micropipette. This is labor intensive, but not excessively burdensome in the context of studies which, at this point, still require extensive assay development and validation, and involve multistep protocols for the analysis of each sample. However, faster, more automated cell-isolation strategies will be required if single-cell profiling studies are ever to be scaled up to evaluate thousands of cells. The only available single-cell isolation technique which can support high-throughput recovery is cell sorting by flow cytometry, so this was clearly the method of choice for the thesis work.

Cell sorting can be applied to cultured cell lines or primary cells recovered from laboratory animals. In general, primary cells cannot be maintained in culture for long periods, so the exploratory work on single-cell analysis was facilitated by the use of a cell line, SCID.adh. These immortalized cells, derived from a murine T-cell lymphoma, are phenotypically similar to thymocytes. SCID.adh suspension cultures are easily maintained in a 37 °C incubator; they grow vigorously, requiring replating to fresh medium daily. The cell concentration in

the SCID.adh cultures was typically $>10^5$ cells/mL, so an ample supply of cells was always on hand for early experiments.

FACS sessions generally have to be scheduled well in advance, so the early cell-based experiments were done using homogenized lysates made up from cells recovered directly from culture plates. For this purpose, the cell concentration of the SCID.adh culture was first estimated using a hemocytometer. An aliquot of cells was then collected and centrifuged, and the pelleted cells were brought up in lysis buffer. The lysates were diluted as necessary and analyzed by qRT-PCR to evaluate different mRNA recovery methods.

Experiments on FACS-sorted cells began once the general outlines of a lysate-analysis protocol had been defined. These trials focused on refinement of the cell-lysis method, strategies to contain RNA degradation, and standardization of post-sample collection handling and storage. For these experiments, all the reagents required for cell lysis and one-step qRT-PCR were combined in a master mix, including primers, probes and enzyme. 20 μL aliquots of this solution were dispensed to the wells of a 96-well PCR plate. Cultured SCID.adh cells were pelleted, washed, and brought up at a concentration of $\sim 10^5$ cells/mL in Phosphate-Buffered Saline (PBS) supplemented with 2% FCS and 2 mM EDTA to maintain viability. Since these experiments involved an homogeneous cell population, antibody staining against surface markers was not required for the FACS sort; live cells were gated based on Forward Scatter/Side Scatter and 7-Amino-Actinomycin D (7-AAD) staining.

The process of FACS-sorting individual cells to the wells of a 96-well plate ("clone sorting") is highly automated. A motorized X-Y stage repositions the plate to permit dispensing to each well. For the FACS operator, setting up a sort involves the definition of sort gates to

isolate the populations of interest, some testing and adjustment to maximize the accuracy of cell dispensing, and entry of the plate layout for the sort in a spreadsheet. The plate layout specifies the number of cells to dispense and the gating to apply at each well position. For the early trials, these layouts were very simple, the machine being set to dispense a single live-gated cell to most of the wells in the plate—the remaining wells were left blank, to serve as No Template Controls (NTCs) during the subsequent qRT-PCR analysis.

In early trials, as soon as the sorter had completed dispensing cells to a 96-well plate, the plate was chilled on ice and transferred to a qPCR machine for mRNA analysis. For the purposes of optimizing the assay protocol, all these trials were done using an off-the-shelf TaqMan assay for GAPDH, a housekeeping gene expressed at 10^2–10^3 copies in mammalian cells. The output of each experimental run comprised a set of Ct readouts which could be used to evaluate the efficiency and reproducibility of the single-cell assay, and the effects of differing lysis conditions, cell concentrations, additives, etc., on these parameters.

The prototyping experiments confirmed that the FACS-based isolation approach is rapid, convenient, and effective. Once appropriate sort criteria have been defined, a cell sorter can set up a 96-well plate of single-cell lysates in a matter of minutes; 1000–2000 samples can be prepared in the course of a single FACS session with minimal operator intervention.

The cell-isolation strategy formulated during the assay-development phase was elaborated and modified in several respects for the later research studies:

1. The cells recovered in the hematopoiesis and aging studies were primary cells, necessitating a more complex sample prep. Hematopoietic stem cells (HSCs) and early lineage progenitors were recovered from the bone marrow of dissected mice; lymphocytes and granulocytes were obtained by tail bleeding live mice. Red blood

cells were removed from all isolates using ACK lysis buffer. Progenitor cells were purified from bone marrow-derived cell suspensions using beads coated with antibodies against c-kit (a membrane receptor expressed in these populations). The beads were recovered by magnetic-column separation. Enriched cell isolates were incubated with fluorescently-labeled antibodies against a variety of cell-type-specific surface markers to permit immunophenotyping during the FACS sort.

2. Complex, hierarchical sort gates had to be defined to support the recovery of different cell types from the heterogeneous primary-cell isolates. A portion of each isolate was analyzed by FACS to calibrate the gating. Single-cell isolation can be performed in one pass, or the isolate can be fractionated into phenotypically purified populations which are then clone sorted separately. In the "single-sort" approach, used in the hematopoiesis study, the heterogeneous isolate is clone sorted directly to 96-well plates, and the FACS operator revises the plate layout to specify the appropriate gating for each collection plate. In the double-sort strategy, used in the aging study, the isolate is first sorted by cell type into a series of collection tubes, and these samples are then resorted to single-cell collection plates. The single-sort method is quicker and reduces the time cells have to be maintained *ex vivo* on ice, while double sorting increases the phenotypic purity of the collected cells.

3. In the research work, multiple collection plates were prepared during each FACS session; the plates were transferred to a -20 °C freezer immediately after cell recovery and analyzed over a period of days or weeks. Tests showed that the qRT-PCR readout level and consistency were at least as good from plates subject to a single freeze-thaw cycle as from directly-analyzed plates. (A trial with -80 °C storage

indicated that this may compromise assay performance, perhaps because the RT, *Taq*, or RNase inhibitors in the lysate preps are not fully refractory to freezing; however, the data were very limited, and this option was not further investigated.)

4. For the research studies, primers and enzymes were left out of the collection-plate master mix, and added to the samples only at the start of the reverse transcription reaction. This approach adds a step to the protocol, but brings two benefits: (1) it decouples the selection of assay targets from sample preparation, and (2) it reduces the potential for RT-mediated primer-dimer product formation, which is especially a concern for multiplexed assays.

5. While assay development was carried out using a FACSVantage cell sorter (BD Biosciences, San Jose, CA), cell sorting for the research studies was done using the more advanced, 13-color FACSAria system. Clone sorts were done into 12, 20, or 50 μL buffer volumes in early trials; based on the qRT-PCR readouts from the lysates, the FACSVantage had no problem reliably sorting cells into any of these volumes. A 10 μL volume was used in the research work. The single-cell recovery efficiency was high in the hematopoiesis study, confirming that it is feasible to reliably dispense cells to this sample volume. The FACSAria system used in the aging study had a persistent problem reliably hitting the wells, which was not resolved. The missed wells (~40%, on average) were randomly distributed in each plate, which suggests an issue with the stability of the sort stream on this particular machine.

A potential added benefit of the FACS isolation strategy is that surface-protein expression measurements are made on each cell that passes through the sorter. Thus, in principle, the

data collected on recovered cells could include both transcript and protein levels, increasing the dimensionality of the analysis. The "index sort" function required to retrieve fluorescence data for clone-sorted cells had not been implemented in the FACSAria software at the time the research was carried out, so there was no opportunity to exploit this possibility.

4.2.2 Cell Lysis

The plasma membrane of mammalian cells can be lysed using a variety of relatively gentle methods, including the application of detergents, freeze-thaw cycles, heating, and osmotic stress. Initial trials focused on detergent lysis, taking a cue from an early study which used flow cytometry to recover mRNA from lymphocytes sorted into a buffer containing 0.05% NP-40 [49]. First, qRT-PCR experiments were done with NP-40 spiked into the reaction mix, to see if assay performance would be compromised using a single-tube lysis/RT-PCR buffer. (A similar non-ionic detergent, Triton X-100, has been identified as a potential PCR inhibitor [92].) These trials indicated that PCR efficiency was unaffected by NP-40, although at high concentrations (≥1%), perturbations in the fluorescence signal were noted. The effect of different detergent concentrations was then evaluated in cell-based reactions, using FACS to sort single cells into the reaction buffer. Table 4.1 summarizes the GAPDH data from one of these experiments. This and subsequent trials showed that there was no benefit to adding detergent to the lysis buffer. Other workers have observed that efficient lysis of mammalian cells can be achieved by directly transferring cells to RT-PCR buffer [36]. Most likely, the cells swell and rupture due to the hypotonicity of the reaction buffer.

Table 4.1. Effect of NP-40 concentration on single-cell GAPDH readouts

Samples	[NP-40]	Average Ct	Ct s.d.	Min Ct	Max Ct
21	0%	28.5	0.5	27.3	29.7
21	0.005%	28.6	0.5	27.5	29.5
21	0.05%	28.5	0.4	27.8	29.4
21	0.5%	28.5	1.8	23.8	30.7

NP-40 was omitted from the buffer for the research work, but another non-ionic detergent, Tween 20, was used at a final concentration of 0.15% in the digital PCR project, to facilitate loading reverse-transcribed lysates into the microfluidic chip. The practice of adding Tween 20 was carried over to the aging study, even though the qPCR analysis was performed in a conventional instrument. Judging from the results of the NP-40 trials, the inclusion of detergent in the lysis buffer is probably redundant, at least for hematopoietic cells.

4.2.3 RNA Recovery

The main obstacle to the efficient recovery of mRNA from a cell lysate is that ruptured cells release potent ribonuclease activity into the lysis buffer. Inside an intact cell, the half-life of messenger transcripts is typically on the order of hours or days, despite the presence of endogenous ribonucleases [93-95]. The intracellular rate of mRNA degradation is slowed by several factors: (1) many cellular RNases are sequestered in lysosomes, (2) natural RNase-inhibitor (RI) proteins titrate the activity of some RNase species by binding the enzymes' functional sites, and (3) the folding of ribonucleases requires formation of internal disulfide bridges, which is disfavored in the reducing environment of the cytosol. These protections are lost once the cell membrane is disrupted. Unchecked, the RNase liberated on cell lysis can degrade much of the released mRNA before it can be reverse transcribed into cDNA.

A number of strategies are available for countering RNase activity during mRNA recovery:

1. High temperatures can be used to temporarily denature RNase.
2. Chaotropic salts can be used to non-specifically denature protein.
3. Proteases can be used to non-specifically degrade protein.
4. High lysate volumes can be used to slow degradation kinetics.
5. Natural or synthetic RIs can be used to block RNase activity.

Heat-inactivation of RNase is hindered by the rugged character of these proteins, whose tertiary structure is stabilized by disulfide cross-links. The exploratory phase of assay development included a few experiments with the Cells-to-cDNA II kit (Ambion, Austin, TX), which uses a 10 minute, 75 °C heat treatment to inactivate RNases. The GAPDH Ct readouts from analyses of SCID.adh lysates processed with the kit were several cycles higher than expected, which suggested that the RNA recovery efficiency was low. RNA is heat-labile, so isolation techniques which involve heat treatment may incur sample loss due to spontaneous hydrolysis. The poor results of the initial trials, the proprietary, "black-box" nature of the Cells-to-cDNA buffer, and the concern that RNA hydrolysis might reduce assay sensitivity discouraged further evaluation of this technical approach.

More traditional RNA isolation kits use chaotropic salts or enzymatic proteases to inactivate RNases. Since these reagents also inactivate reverse transcriptase, an RNA purification step is typically included in the protocols, making them ill suited to high-throughput applications. Proteolytic digestion of RNases can be followed up with thermal-inactivation to irreversibly denature the protease, obviating RNA purification. However, this method again introduces the possibility of inefficient recovery owing to RNA hydrolysis during the heat treatment.

At the outset of assay development, simple dilution looked like a promising strategy for RNase containment. The volume of a typical hematopoietic cell is on the order of 1 pL, so endogenous RNases should be diluted 10^7-fold when one cell is lysed in 10 μL of buffer. It therefore seemed possible that the need for chemical ribonuclease inhibitors would be obviated in single-cell analysis. This was attractive because the preferred RT-PCR strategy involved performing cDNA synthesis at temperatures (50–70 °C) outside the recommended operating range of most RI products.

Many early trials focused on establishing a safe cell concentration range for mRNA recovery in the absence of ribonuclease inhibitors. Experiments using homogenized SCID.adh lysates gave an early indication that dilution would not be the hoped-for cure-all. Serial dilutions of lysate were allowed to stand for a several minutes and then analyzed by qRT-PCR. Ideally, the resulting Ct values would be expected to go down by one cycle with each doubling of the lysate concentration, in a classic qPCR standard-curve relationship. In practice, while this relationship was observed for the most dilute samples, the Ct values fell more slowly than expected going to higher concentrations, and then started increasing. Analysis of the data from these trials indicated that, in the absence of RIs, lysate concentrations of >0.1 cells/μL might entail a significant loss of mRNA before cDNA synthesis, with a steep falloff in recovery going to higher concentrations. Thus, while efficient recovery of mRNA from one cell dispensed into 10 μL of buffer might be borderline feasible, there would be no leeway for analyzing lysates made from higher number of cells in the same volume.

FACS-based trials provided insight into the relation between cell concentration and mRNA recovery under more realistic assay conditions. For these experiments, the cell sorter was set to dispense a ramped number of cells to wells containing a fixed volume of RT-PCR buffer.

After qRT-PCR analysis of the lysates, the Ct values were plotted against cell count. Similar trends emerged to those seen in the trials with homogenized lysates, with the qPCR signal falling off at high cell concentrations (figure 4.1).

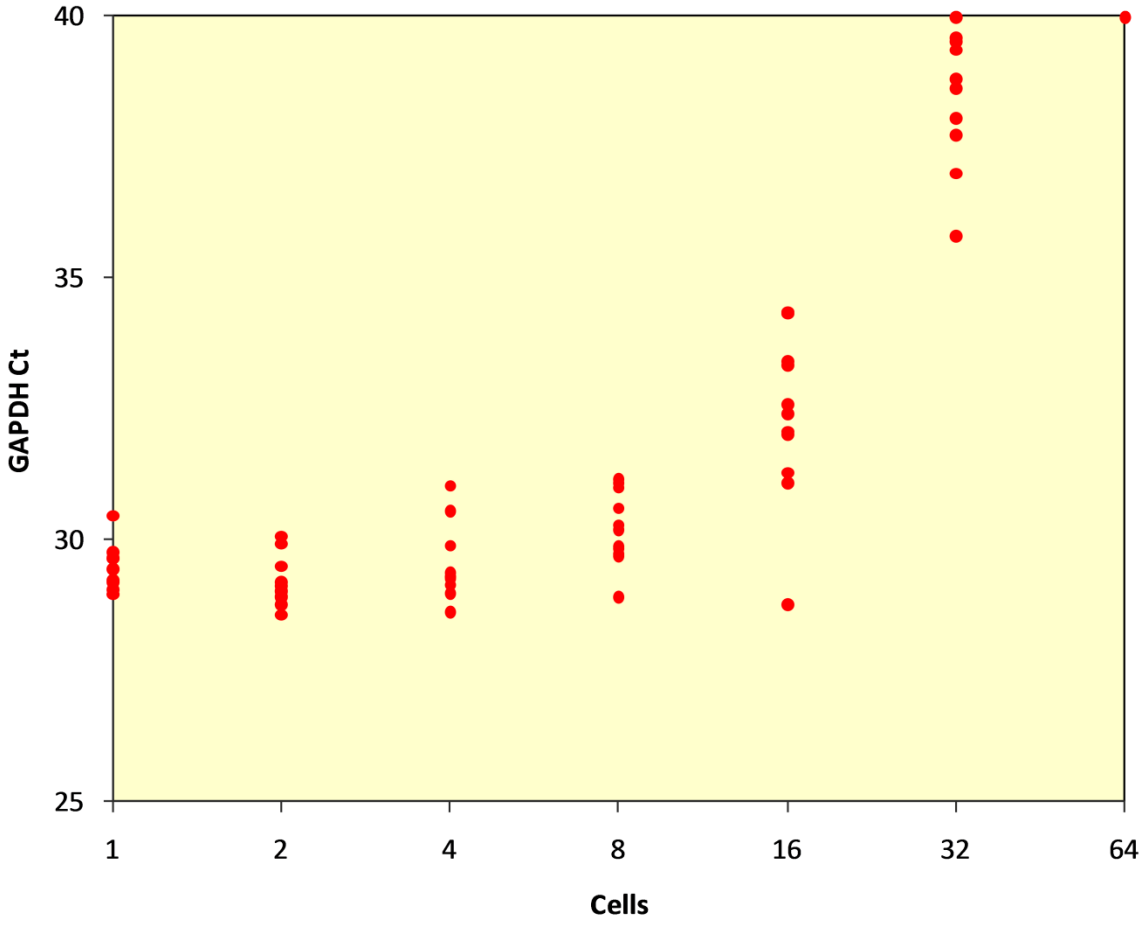

Figure 4.1. Cell-concentration ramp analysis. FACS was used to sort a binary ramp of 1–64 SCID.adh cells into 20 µL of qRT-PCR buffer. The GAPDH Ct values for single-cell samples were around 30, which is reasonable for this target. The Cts for two-cell samples were slightly lower, but at higher cell concentrations the Ct actually increases, indicating significant degradation of mRNA before the RT step.

The data from the "cell ramp" experiments were fit to a mathematical model to estimate the safe cell-concentration range for mRNA recovery. The model assumes that (1) endogenous RNase activity is the main factor in the cell-concentration-dependent RNA losses, and (2) RNases quickly and freely diffuse away from the cell on lysis. On this model, mRNA levels should undergo exponential decay with a half-life inversely proportional to the RNase concentration (and therefore the cell concentration) in the lysate. If N cells are dispensed to V μL of buffer, the fraction, F, of mRNAs recovered into the RT step is given as follows:

$$F = e^{-kN/V}.$$

Here, *k* is a proportionality constant whose value depends on a number of factors which should be (approximately) invariant within a given set of experimental conditions, including the number of RNases per cell, the kinetic rate constant governing the degradation reaction, and the time interval between lysis and cDNA synthesis. Once the model is fitted to the data, *k* can be estimated and the efficiency of mRNA recovery can be calculated relative to the ideal case where no RNases are present (F = 1).

To fit the model to the data, we need to convert between Ct readouts and relative amounts of cDNA. We start by computing a "delta Ct" value for each sample relative to the average single-cell readout, Ct_{sc}:

$$\Delta Ct = Ct - Ct_{sc}.$$

The ratio of the concentration of cDNA in a sample to that in an average single-cell sample can be calculated from the ΔCt value given the efficiency of PCR amplification, E_{pcr}:

$$\frac{[cDNA]}{[cDNA_{sc}]} = \left(1 + E_{pcr}\right)^{-\Delta Ct}.$$

With a good set of primers, E_{pcr} should be close to 100%, i.e., the amplicon doubles every cycle, so we will introduce the following simplification:

$$\frac{[\mathrm{cDNA}]}{[\mathrm{cDNA_{sc}}]} = 2^{-\Delta \mathrm{Ct}}.$$

From the recovery model, we expect this ratio to depend on the number of cells in the lysate and the attendant loss factor due to RNase activity:

$$\frac{[\mathrm{cDNA}]}{[\mathrm{cDNA_{sc}}]} = \frac{\mathrm{N} \cdot e^{-kN/V}}{e^{-k/V}} = \mathrm{N} \cdot e^{-k(N-1)/V} = 2^{-\Delta \mathrm{Ct}}.$$

Therefore:

$$\ln\left(\mathrm{N} \cdot e^{-k(N-1)/V}\right) = \ln(\mathrm{N}) - k \cdot (\mathrm{N}-1)/\mathrm{V} = -\Delta \mathrm{Ct} \cdot \ln(2).$$

Rearranging:

$$\ln(\mathrm{N} \cdot 2^{\Delta \mathrm{Ct}}) = k \cdot (\mathrm{N}-1)/\mathrm{V} \;\; \therefore \;\; k = \frac{\ln(\mathrm{N} \cdot 2^{\Delta \mathrm{Ct}})}{(\mathrm{N}-1)/\mathrm{V}}.$$

The value of k can therefore be estimated from a least-squares linear fit of the appropriately-transformed data (figure 4.2). For the 20 μL ramp data, we get an estimate of k = 6.4 μL.

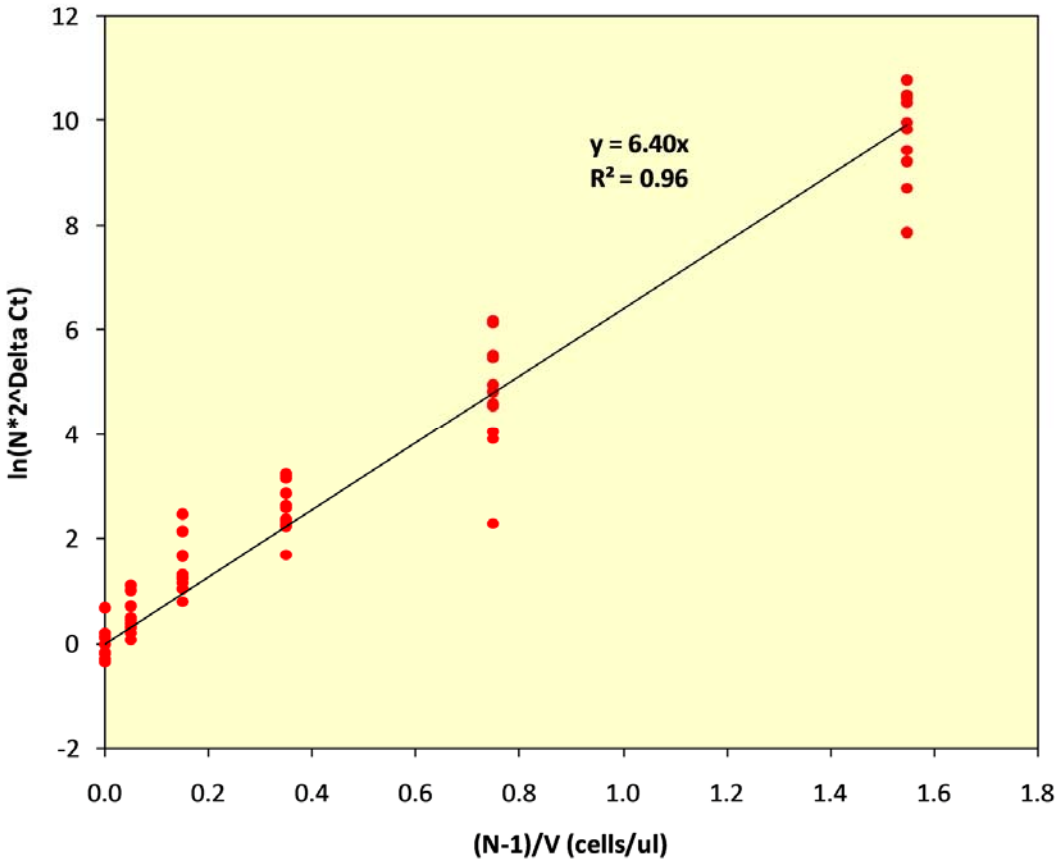

Figure 4.2. Least-squares fit to mRNA-loss model. From the slope of the line, we get an estimate of k = 6.4 μL.

The Ct data from the cell-ramp trials gave a good fit to the model, and the values obtained for k from trials using 20 μL and 50 μL lysate volumes were within 10% of each other. For the single-cell case, we have: $F_{sc} = e^{-k/V}$. We can substitute the estimate of k into this formula to compute the mRNA recovery efficiencies for single-cell samples prepared in different lysate volumes (table 4.2).

Table 4.2. Projected single-cell mRNA recovery (k = 6.4 μL)

Lysate Volume (μL)	mRNA Recovery
10	53%
20	73%
50	88%
100	94%

The data from the SCID.adh ramp trials indicated that a high lysate volume (≥50 μL) would be needed to recover ≥90% of the mRNA from a single cell without the use of ribonuclease inhibitors. This was particularly problematic for the digital PCR study, as the sample volume in the microfluidic chip was only 7.5 μL. In addition, it seemed likely that the actual "safe" dilution would be sensitive to cell type and cell-to-cell heterogeneity.

It may seem surprising that the RNase burden of one cell could have such potent activity after ~10^7-fold dilution. A simple order-of-magnitude calculation gives an idea of how this is possible. The rate constants for diffusion-limited reactions involving small molecules are usually on the order of 10^8 L·mol^{-1}·sec^{-1}, but rates of 10^{10}–10^{11} L·mol^{-1}·sec^{-1} have been reported for protein-nucleic acid interactions, even in the absence of facilitated diffusion [96]. Assume that the cellular RNase burden is ~10^6 molecules (equivalent to ~0.1% of the 10^{-10} g of protein in a cell), and take a rate constant for the RNase-mediated degradation

reaction of 10^{10} L·mol^{-1}·sec^{-1}. Within a 10 μL volume, the reaction rate per mRNA molecule is then:

$$10^{10}\ \text{L·mol}^{-1}\text{·sec}^{-1} \cdot (10^{6} / N_A)\ \text{mol} / 10^{-5}\ \text{L} = 0.002\ \text{sec}^{-1}.$$

In this scenario, the half-life of mRNA in lysis buffer is on the order of minutes. It is not clear when most of the RNase-mediated losses occur—whether during the preparation of the lysate, or during the RT step itself—but RNases probably do have a window of several minutes to attack their targets in between cell lysis and reverse transcription.

After it became clear that RIs would have to be included in the reaction buffer, experiments focused on evaluating different products and measuring the range of cell concentrations over which they restored normal standard-curve relationships. SUPERase-In (Ambion) emerged as a promising RI for the single-cell application. According to the manufacturer's datasheet, SUPERase-In is active in the range of 37–65 °C, making it compatible with high-temperature reverse transcription. FACS trials showed that the addition of this RI to the RT-PCR buffer effectively inhibited RNase activity in the cell-concentration range of interest (figure 4.3).

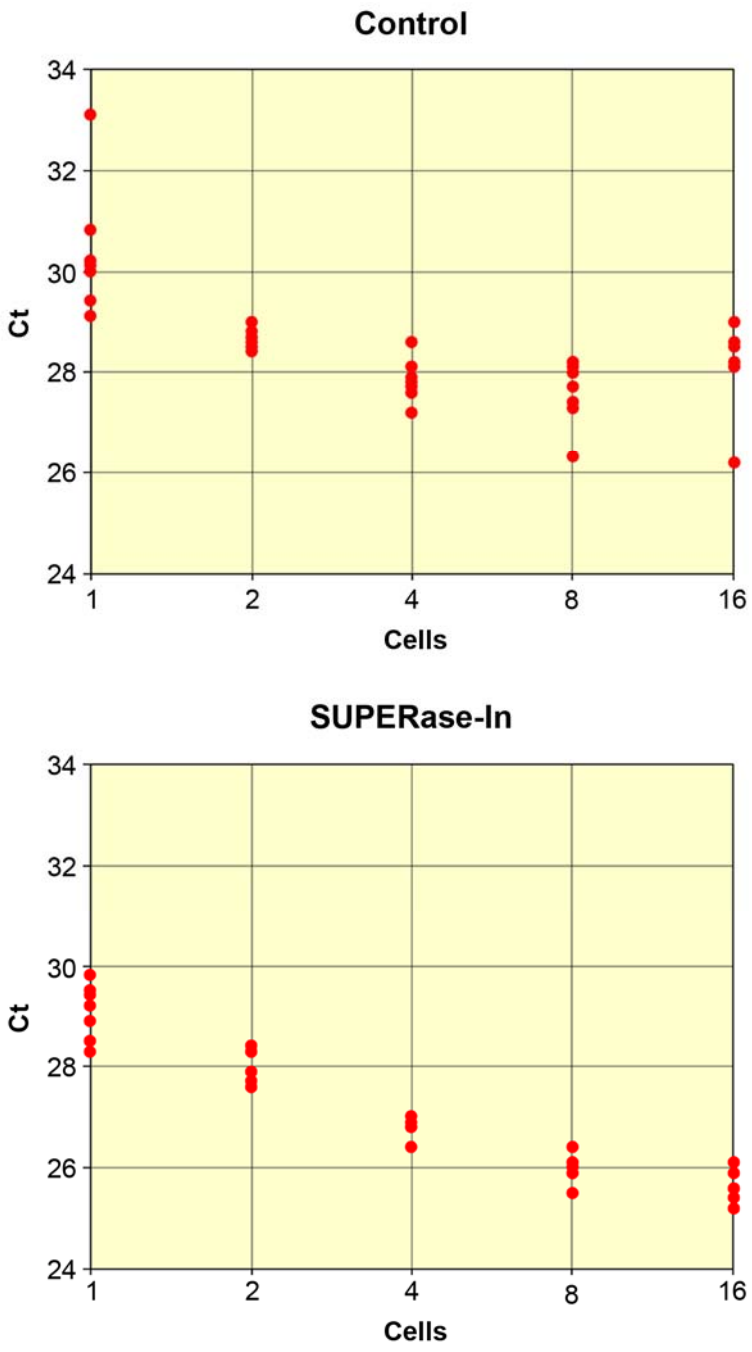

Figure 4.3. Effect of SUPERase-In on mRNA recovery. The charts show the GAPDH Cts obtained from 12 μL qRT-PCR reactions based on FACS-dispensed binary ramps of 1–16 SCID.adh cells per reaction. Addition of SUPERase-In to the buffer restores normal PCR standard-curve relationships, at least up to the 8-cell case.

In cell-ramp trials conducted using a 12 µL volume, the standard-curve relationships looked good for 1–5 cells per reaction, but the recovery efficiency and consistency dropped off at cell concentrations of ≥0.5 cells/µL. Since this cannot be taken as a general result, applicable to all cell types, cell-ramp controls were used during the research work to check that the single-cell samples were in the "safe zone" for RNase activity (figure 4.4).

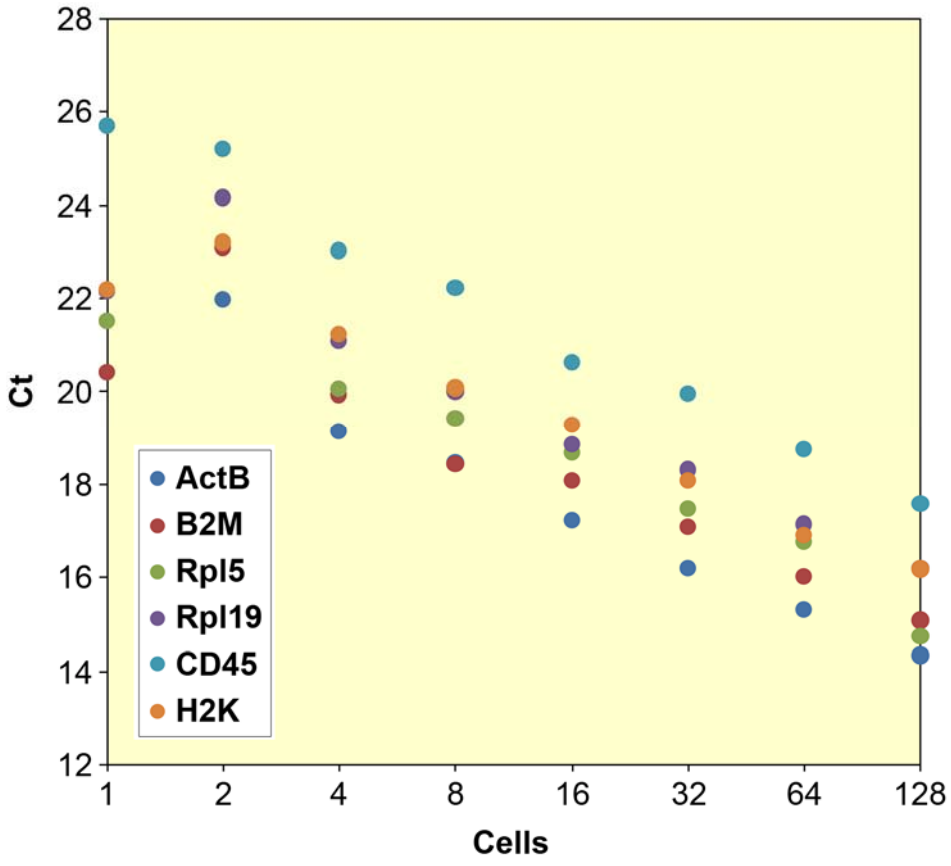

Figure 4.4. Cell-concentration ramp control from the aging study. Analysis of 8-tube strips containing from 1 to 128 cells FACS-dispensed to 10 µL of buffer showed that normal standard-curve relationships were preserved even at cell concentrations well above those used to evaluate single cells, indicating that RNase-mediated RNA loss was contained under the assay conditions applied.

The fit between the cell-ramp data and the exponential-decay model and the observation that RI rescued standard-curve relationships supported the theory that the falloff in qRT-PCR signal at high cell concentrations was due to freely diffusing endogenous RNases. Still, it remained possible that other RNA losses were incurred in the hypotonic-lysis protocol; for example, transcripts might be degraded before the plasma membrane ruptures or become entrapped in cellular debris and made unavailable for reverse transcription. To check that hypotonic lysis was efficient at recovering mRNA into the RT step, experiments were performed to compare this strategy to traditional RNA isolation methods. RNeasy (Qiagen, Valencia, CA), a popular, GITC-based RNA isolation kit, was used to lyse 10,000 viable cells sorted into CB buffer by FACS, and a qRT-PCR standard curve was run on serial dilutions of RNA purified from the cell prep. The results were compared to a standard-curve analysis on an isolation-free cell-ramp trial (figure 4.5). The comparison showed that the efficiency and consistency of recovery with the isolation-free protocol was, if anything, superior to that achieved with the conventional, multistep chaotropic prep. Later experiments compared hypotonic lysis to RNA isolation using PicoPure (Molecular Devices, Sunnyvale, CA), a GITC-based kit optimized for processing very small samples. In these experiments, low numbers of cells were sorted directly into the PicoPure extraction buffer. Again, the results gave an edge to the isolation-free protocol.

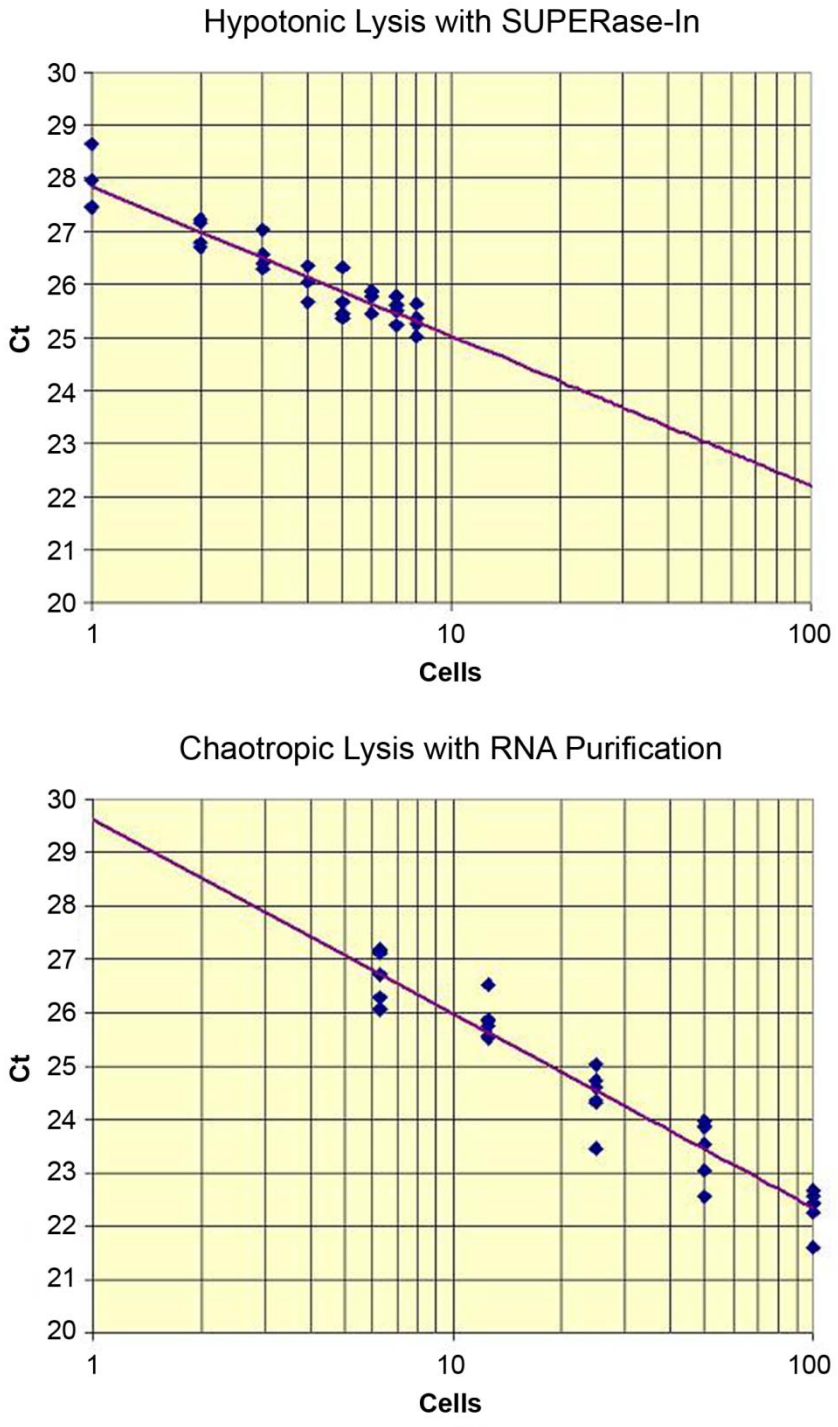

Figure 4.5. Hypotonic lysis versus chaotropic mRNA isolation. The charts show GAPDH Cts from 12 μL qRT-PCRs conducted on cellular mRNA prepared using the isolation-free, hypotonic-lysis method or Qiagen's RNeasy RNA isolation kit. The results indicate that the isolation-free protocol recovers at least as much mRNA as the chaotropic lysis prep.

4.2.4 Genomic Background

Most RNA isolation protocols incorporate an optional DNase treatment step to digest contaminating genomic DNA (gDNA). Since DNase activity is incompatible with cDNA synthesis, inclusion of this step generally mandates either RNA purification or thermal inactivation of the DNase enzyme. Digestion of gDNA therefore complicates sample processing, and may compromise assay sensitivity due to losses incurred during RNA purification or heat-induced RNA hydrolysis [64]. These considerations argued against the inclusion of a DNase step in the single-cell assay protocol, but the issue of genomic background had to be addressed nonetheless.

At first sight, gDNA carryover might not appear to be a major concern for mRNA quantitation, as the cellular copy number of all but the rarest transcripts well exceeds the two copies of the encoding gene present in a diploid genome. To some extent, the inclusion of a DNase step in standard RNA isolation protocols may reflect low mRNA-to-cDNA conversion efficiency in early RT protocols. However, genomic background can still be a problem, even given efficient reverse transcription. Many genes have multiple homologues within the genome, including both related, functional genes and untranscribed pseudogenes; this is particularly true of highly conserved genes involved in basic cellular processes [97]. Non-specific amplification of these homologous gDNA sequences may produce a non-trivial background signal during qRT-PCR [98].

To keep the protocol streamlined and maximize RNA recovery, DNase treatment was not included in the single-cell analysis protocol, and the problem of genomic background was instead addressed at the level of assay design and validation. For most of the targets analyzed in the research studies, the qPCR assay design included an exon-straddling primer or probe,

increasing specificity for cDNA over gDNA templates. "No RT" controls using *Taq* rather than an RT/*Taq* enzyme blend were performed to verify that the genomic background signal from lysate preps was well below that typical of RT+ reactions. In the aging study, which employed SYBR Green qPCR, melt-curve analysis was also applied to check if the predominant amplification product had a melting temperature (T_m) characteristic of the expected cDNA transcript (figure 4.6).

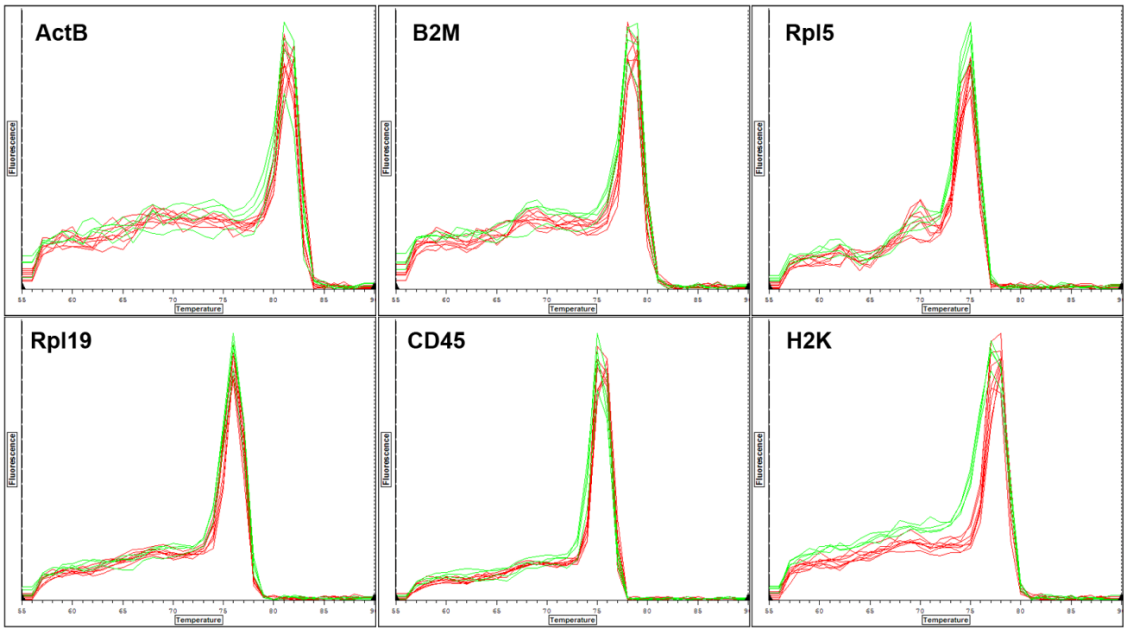

Figure 4.6. Melt-curve analysis of qRT-PCR products. In the aging study, melt curves were performed at the end of SYBR Green qPCRs to check for primer-dimer or non-specific product formation. These are plots of dI/dT from one qPCR run; the peaks indicate the T_m of the amplification products. The red curves correspond to cell-lysate reactions, and the green curves to parallel reactions on runoff-transcribed RNA standards. In these analyses, Rpl5 and Rpl19 sometimes gave significant secondary peaks around 70 °C, a few degrees below the T_m of the standards. These peaks probably came from non-specific amplification of homologous transcripts or genomic DNA; the ribosomal-subunit genes are evolutionarily ancient and have many homologues. The non-specific product peaks were only significant in granulocytes, which had low levels of Rpl5/Rpl19 expression.

4.3 Transcript Quantitation

4.3.1 RT Priming Strategy

Reverse transcription can be primed using gene-specific primers (GSPs), so that only particular mRNA targets are transcribed into cDNA; alternatively, non-specific oligo(dT) or random-hexamer primers can be used to synthesize a cDNA pool representing the entire population of messages in the RNA sample. Non-specific priming is mandatory for broad-spectrum evaluation of cDNA by microarray or SAGE, and affords total flexibility in the choice of assay targets in the qPCR context. However, the two common non-specific priming methods both have significant drawbacks:

1. Since reverse transcriptase is inefficient at producing full-length transcripts, cDNA made using oligo(dT) primers usually only gives good representation of the 3' ends of messages; qPCR assays designed for use on these preps must be targeted accordingly. The 3' bias effect can make it difficult to design an efficient or selective qRT-PCR assay for some targets.

2. If random-primed RT is applied directly to total RNA, the resulting cDNA prep will contain a superabundance of ribosomal RNA sequence, which can compromise the performance of downstream quantitation assays. Preisolation of poly(A) mRNA using oligo(dT)-coated columns or beads can be used to address this problem, but complicates sample processing and may impact mRNA recovery efficiency.

For qRT-PCR studies targeting a few, preselected genes, there is evidence that assay sensitivity and accuracy can be improved through the use of gene-specific RT primers [86, 92]. This might also be expected on theoretical grounds:

1. The sensitivity of qRT-PCR assays is strongly dependent on the efficiency of reverse transcription. It is fairly easy to achieve almost 100% transcription efficiency from DNA templates using *Taq* polymerase, but robust, efficient reverse transcription from RNA templates remains problematic [86]. The reasons for this are not fully understood, but there is a consensus that RT enzymes have difficulty transcribing through regions of RNA secondary structure [92, 99, 100].

2. Random priming has to be performed at low temperatures (~25 °C) because of the low affinity of short oligomers for their templates. The RT incubation temperature can be ramped up once nascent transcripts are formed, to disrupt RNA secondary structure and allow more complete transcript extension. Even so, any regions of template which were highly folded at the initial priming temperature may be underrepresented at the end of cDNA synthesis.

3. While oligo(dT) priming can be performed at temperatures similar to those used for gene-specific priming (~50 °C), mRNAs which are GC-rich and high in secondary structure at the 3' end may not be efficiently converted to cDNA. In contrast, gene-specific RT primers can be designed to target template regions with low predicted secondary structure, increasing the likelihood of efficient reverse transcription.

4. Global reverse transcription may reduce the specificity and therefore the accuracy of transcript quantitation because a large, heterogeneous population of cDNA transcripts is carried forward into the qPCR analysis, increasing the probability that non-specific priming of homologous sequences will affect the Ct readout.

Since sensitivity, specificity and quantitative accuracy were priorities for the single-cell analysis work, gene-specific priming was preferred from the outset, and no attempt was made to evaluate global reverse-transcription strategies during assay development.

4.3.2 RT Chemistry

In traditional "two-step" qRT-PCR protocols, reverse transcription and qPCR analysis are performed in separate buffers optimized for the different enzymatic reactions involved. In the last few years, more convenient "one-step" qRT-PCR kits have become increasingly popular. In one-step qRT-PCR, reverse transcriptase and *Taq* polymerase are included in the same reaction buffer; after RT incubation, the cDNA product is immediately analyzed by qPCR without opening the reaction vessel. Two-step RT-PCR protocols are compatible with GSP, oligo(dT), and random priming strategies. In a single-tube reaction, carryover of undiluted random hexamers or oligo(dT) primers and primer extension products into PCR may result in competitive inhibition of the target reaction. For this reason, gene-specific RT priming is almost always preferred for single-tube RT-PCR; typically, the reverse PCR primer serves as the GSP for the reverse-transcription reaction.

One-step RT-PCR kits are still fairly new on the market, and most of the single-cell studies reported in the literature have applied conventional, two-step RT-PCR protocols. Benefits of the single-tube approach include streamlined sample processing and reduced opportunities for sample loss and contamination [70]. Traditional two-step protocols call for a substantial dilution of the RT reaction product going into the PCR step, which can be problematic for single-cell work. For example, the manual for the SuperScript III First-Strand cDNA Synthesis kit (Invitrogen, Carlsbad, CA) suggests that a maximum of 10 µL of a 20 µL RT reaction be taken forward into a 50 µL qPCR; however, the use of only 2 µL of product is

preferred. The recommended volume for qPCR reactions in a standard thermocycler is 10–100 μL, while the sample-panel volume in the digital PCR chip used for the hematopoiesis study was only 7.5 μL. Given that the practical volume for recovering single cells by FACS is about 10 μL, a 10×-to-250× dilution of RT product would hard to reconcile with qPCR analysis of the entire mRNA content of a cell. Dilution going into the qPCR step can be obviated by purifying the cDNA away from the reaction buffer [101], but this approach significantly complicates sample processing.

From the outset, then, one-step RT-PCR chemistries looked promising for high-throughput single-cell analysis. Two-step RT-PCR is often cited as the more sensitive approach, but the reasons why this should be so are rarely explored. Two issues are probably involved:

1. Usually, the limiting factor in the sensitivity of qPCR assays is competitive inhibition due to the amplification of primer-dimer (PD) products. Today, most commercial *Taq* enzymes incorporate "hot start" protection mechanisms which virtually eliminate formation of PD products during reaction setup. In general, though, RT enzymes are not hot-start protected. These enzymes are active at low temperatures, and have DNA-dependent as well as RNA-dependent polymerase activity. Consequently, significant amounts of PD product may be present in cDNA preps [102]. Two-step GSP-based reactions may be less affected because the forward PCR primers are excluded from the RT buffer [103]. PD-related inhibition is probably not a significant issue in two-step qRT-PCR protocols based on oligo(dT) or random-hexamer priming, because (1) the RT primers are highly diluted in the qPCR, and (2) primer-extension products carried over from the RT step cannot be efficiently amplified by the gene-specific primers used in the PCR.

2. Although the mechanism is not understood, reverse transcriptases can inhibit PCR at the concentrations used in traditional RT protocols [101, 102, 104-107]. This effect can lead to poor qPCR assay performance in single-tube reactions, unless the RT-to-*Taq* ratio and other aspects of the buffer chemistry are carefully optimized. Evaluation of a variety of single-tube kits, attempts to "home brew" a single-tube chemistry using a preferred combination of RT and *Taq* products, and discussions with vendors' technical staff all indicate that this is a non-trivial and, to some extent, unresolved problem.

Given the compelling advantages of single-tube RT-PCR chemistries for the single-cell application, the sensitivity question was addressed by systematic validation of assays using standard-curve trials. About half a dozen different one-step reaction kits were evaluated during assay development, including products based on AMV, MMLV and proprietary RT enzymes and two-enzyme blends. Invitrogen's CellsDirect SuperScript III/*Taq* gave the most consistent sensitivity and reproducibility of all the products evaluated (figure 4.7).

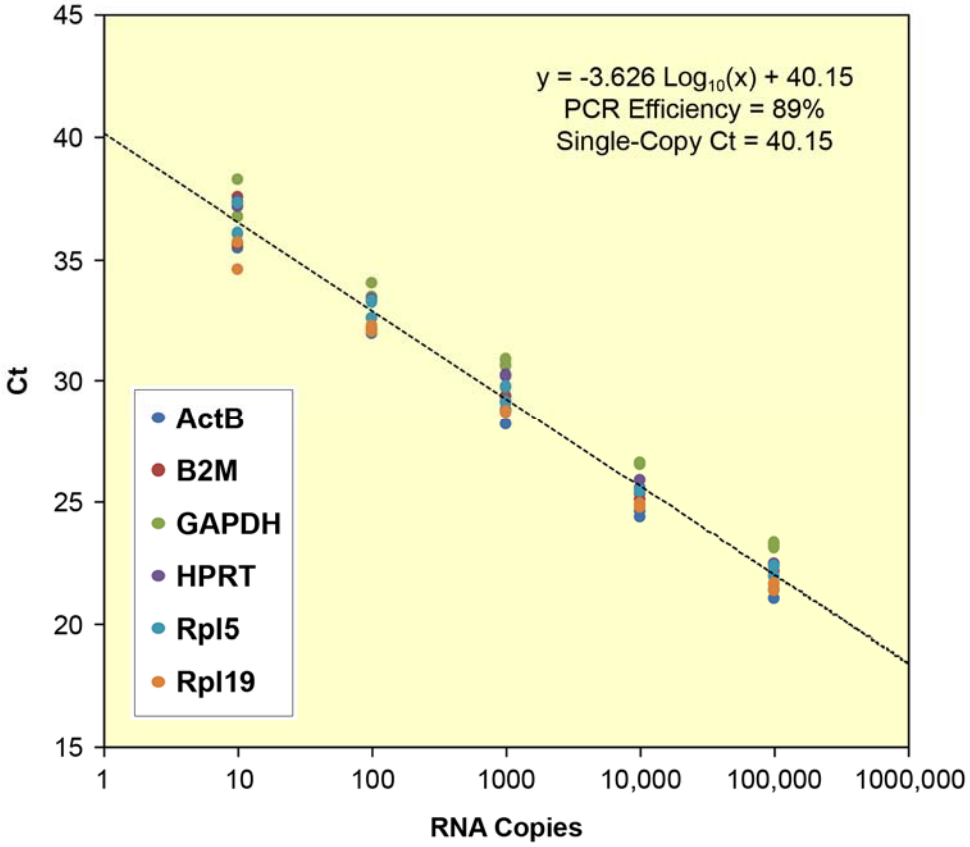

Figure 4.7. Six-plex qRT-PCR standard curve with SSIII/*Taq*. Aggregated results from 5-point standard-curve analyses on six different targets by simplex TaqMan qRT-PCR using CellsDirect SuperScript III/*Taq* enzyme blend. The templates were runoff-transcribed RNA; the *x*-axis gives the RNA copy number per 20 µL reaction. The PCR efficiency and single-copy Ct intercept is based on the data for all six assay targets.

4.3.3 Assay Design

4.3.3.1 Template Analysis

The first step in designing a qRT-PCR assay involves retrieving the sequence of the target transcript from public databases. Two databases were referenced for the single-cell studies:

1. NCBI Entrez Nucleotide (www.ncbi.nlm.nih.gov/sites/entrez?db=Nucleotide)
2. Ensembl *Mus musculus* (www.ensembl.org/Mus_musculus)

Differences were often found in the sequences recovered from Entrez and Ensembl, especially near the beginning and end of the transcripts. For this reason, all the finalized assay designs were checked for compatibility with sequences from both databases.

RNA-folding prediction software was used to identify secondary structure-free stretches of the mRNA template long enough to accommodate a qPCR assay (figure 4.8). While no systematic attempt was made to evaluate the impact of secondary structure on RT efficiency, some evidence for its significance emerged during assay development. Substandard Ct readouts were noted in standard-curve trials with a PU.1 assay whose amplicon overlapped predicted RNA secondary structure. A new assay was designed which completely avoided secondary structure. The revised assay gave a 2.5-fold improvement in RT efficiency relative to the original design, as assessed by digital PCR.

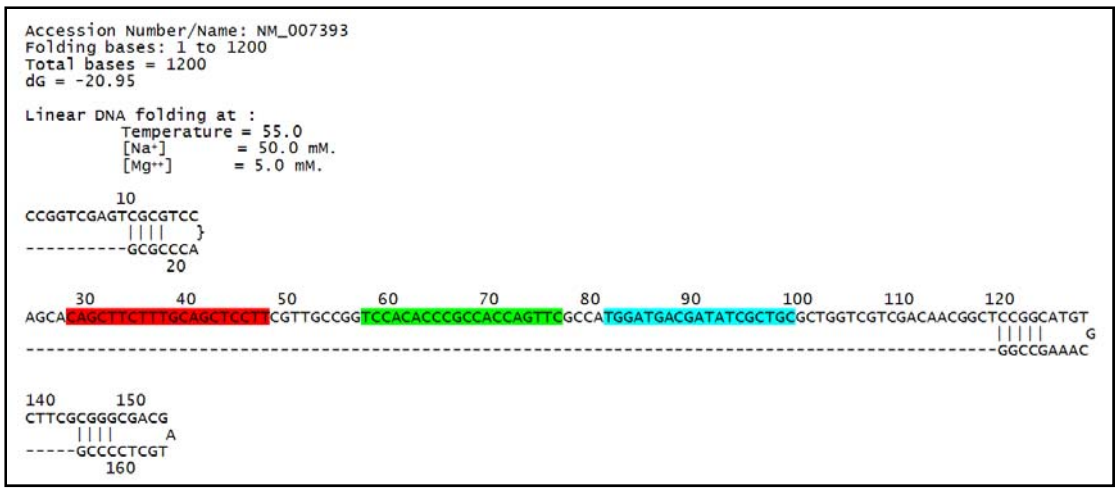

Figure 4.8. Secondary structure prediction. Part of the output obtained using the "Template Structure Search" feature of Premier Biosoft's Beacon Designer, showing the predicted folding of the first ~160 bases of the ActB transcript. The program uses the Quickfold server to predict the self-hybridization of PCR templates. The primer and probe sequences of the ActB assay designed for the aging study are highlighted. To maximize RT efficiency, the primers were designed to fall within a region that is completely free of secondary structure.

To minimize amplification from genomic templates, assays were designed to be cDNA-specific whenever possible. Specificity was achieved by including exon-straddling primers or probes in the assays. The Ensembl database gives the exon structure of mRNA transcripts. Figure 4.9 shows the first few hundred bases of the ActB mRNA sequence retrieved from Ensembl, with the exon structure indicated by alternating black and blue text; the primer and probe sequences for the ActB assay used in the aging study are underlined. Here, the TaqMan hybridization probe straddles a splice junction. In each of the other five assays used in the study, at least one of the selected primers straddles an exon boundary.[*]

[*] SYBR Green qPCR chemistry was ultimately preferred for the aging study, so the cDNA-specificity afforded by the probe in the ActB assay design was unavailed. Even so, the fact that the primers bracket an intron gives this assay some specificity toward cDNA.

Assay designs were also checked for specificity by running BLAST searches using the entire predicted amplicon sequence against genomic and cDNA databases. High-scoring matches were reviewed to see if the primer sets were likely to coamplify homologous transcripts or genes along with the primary mRNA target.

Figure 4.9. Design of a cDNA-specific assay. Part of the ActB mRNA sequence retrieved from the Ensembl database is shown, with the exon structure indicated by alternating black and blue text. Underlining indicates the positions of the ActB assay primers and probe. The probe sequence straddles an exon boundary and is therefore highly specific for the cDNA template. In addition, the primers target different exons, which are separated by a 959 bp intron in the ActB gene; 1031 bp amplicons derived from the genomic template will amplify less efficiently than the 72 bp cDNA-templated amplicons, adding to the specificity of the assay.

4.3.3.2 Primer/Probe Selection

Most of the assay design for the hematopoiesis study was done using a commercial software package, Beacon Designer Version 4 (Premier Biosoft, Palo Alto, CA). At the time of purchase, this product was unusual and possibly unique in supporting the automated design of multiplexed TaqMan assays. However, the program also had important limitations: it was not "exon aware," and the algorithm for qualifying multiplex primer combinations seemed excessively conservative, treating all high-affinity PD interactions, and not just 3' end

interactions, as equally problematic. As the single-cell work progressed, this fully automated solution was set aside in favor a semiautomated, iterative design approach.

All the assay design for the aging study was performed using Primer3 (frodo.wi.mit.edu), a free, web-based program (figure 4.10). First, regions of transcript long enough to accommodate a TaqMan assay (≥75 bases) were qualified based on the absence of RNA secondary structure and presence of exon-splice junctions. Each candidate region was evaluated separately as a template for Primer3 assay design. The program was set to pick forward and reverse primers with T_ms around 60 °C (the program default), and a hybridization probe with a T_m of 70 °C; the desired product size was set to 75–150 bases. Default settings were used for all other parameters. Primer3 was usually able to find multiple, high-scoring assay designs for each candidate region. Designs lacking an exon-straddling primer or probe were eliminated from further consideration.

```
PRIMER PICKING RESULTS FOR gi|6671508|ref|NM_007393.1| Mus musculus actin, beta, cytoplasmic (Actb), mRNA

No mispriming library specified
No hyb oligo mishyb library specified
Using 1-based sequence positions
OLIGO            start  len      tm     gc%   any   3'  seq
LEFT PRIMER         29   20   59.90   50.00  5.00  0.00 CAGCTTCTTTGCAGCTCCTT
RIGHT PRIMER       100   19   60.76   52.63  8.00  0.00 GCAGCGATATCGTCATCCA
HYB OLIGO           58   20   68.90   65.00  2.00  0.00 TCCACACCCGCCACCAGTTC
SEQUENCE SIZE: 1892
INCLUDED REGION SIZE: 1892

PRODUCT SIZE: 72, PAIR ANY COMPL: 3.00, PAIR 3' COMPL: 1.00

    1 CCGGTCGAGTCGCGTCCACCCGCGAGCACAGCTTCTTTGCAGCTCCTTCGTTGCCGGTCC
                               >>>>>>>>>>>>>>>>>>>>          ^^^

   61 ACACCCGCCACCAGTTCGCCATGGATGACGATATCGCTGCGCTGGTCGTCGACAACGGCT
      ^^^^^^^^^^^^^^^^^    <<<<<<<<<<<<<<<<<<<<
```

Figure 4.10. Primer design using Primer3. Part of the listing produced by Primer3 for the ActB assay, showing the predicted T_m for the primers and probe (approximately 60 °C and 70 °C, respectively) and the size of the PCR amplicon (72 bases). The program also highlights the positions of the primers and probe in the template.

Candidate primers were checked against assays previously qualified for use in multiplexed reactions using FastPCR (www.biocenter.helsinki.fi/bi/Programs/fastpcr.htm), a freeware application (figure 4.11). Primer picks which showed significant potential for 3' PD interactions were disqualified.

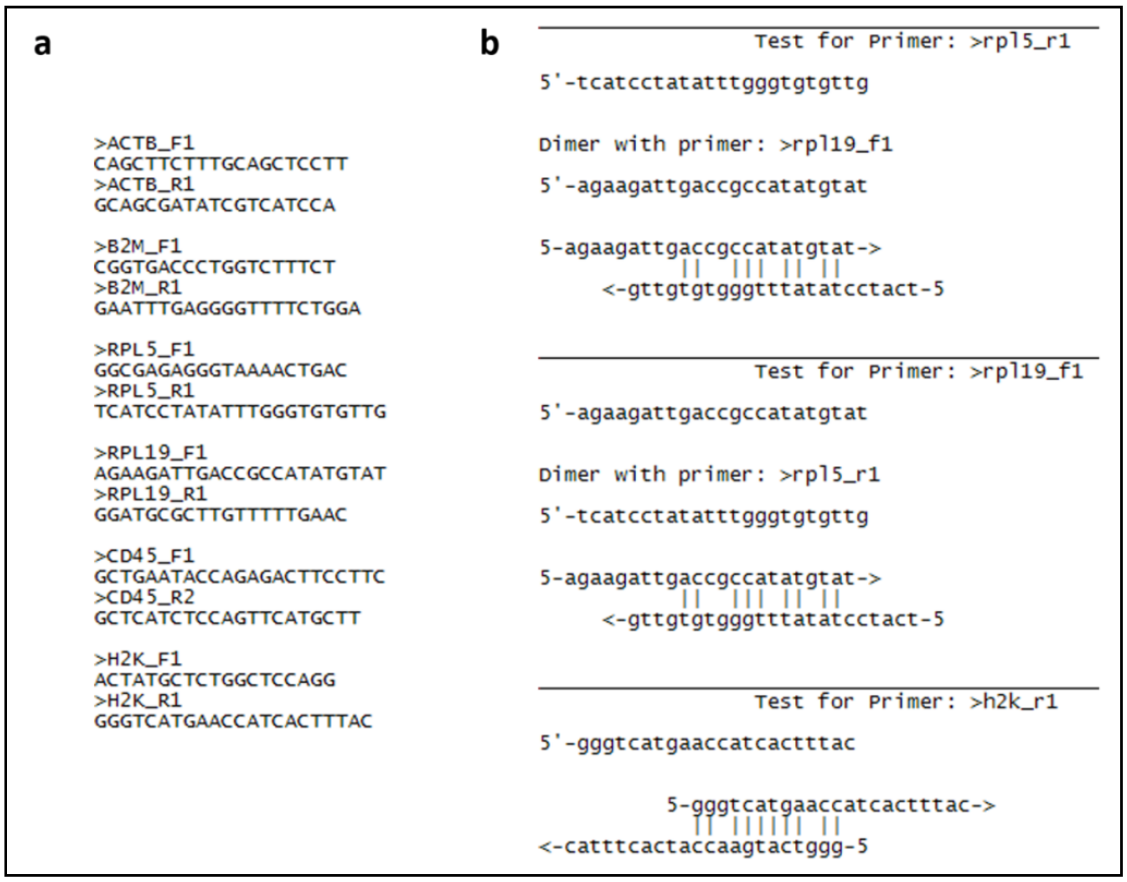

Figure 4.11. FastPCR analysis of primer-dimer interactions. (a) The six primer pairs used in the aging study were entered into the FastPCR program. (b) The program identified two significant base-pairing interactions for the input primer set. (The first two entries in the listing refer to the same interaction.) Neither of these interactions involves 3'-end complementarity, so it is unlikely that the identified primer dimers will template the production of efficiently-amplified secondary products. The primer set therefore passes *in silico* screening.

For some targets, the multiplicity of design criteria made it difficult to find a suitable assay in a single pass, and multiple rounds of Primer3 design and FastPCR analysis were required before a satisfactory solution was identified. In such cases, a larger pool of candidate assays could be generated by relaxing Primer3's design parameters, e.g., widening the acceptable range of primer T_m values, or reducing the minimum permitted probe T_m. Most of the primers designed using Primer3 and FastPCR performed well in empirical qualification trials, and it rarely proved necessary to redesign assays.

4.3.4 Assay Validation

4.3.4.1 PCR Efficiency

Programs like Primer3 apply well-established design rules to identify primer sequences that should give highly efficient PCR amplification. However, the *in silico* screening of primers is still imperfect, and some automated primer picks give low PCR efficiency in practice. In principle, high PCR efficiency is not a prerequisite for accurate cDNA quantitation:

1. Within the digital PCR chip used for the hematopoiesis study, a perfect assay might give a "callable," above-background TaqMan signal after about 25 cycles of amplification. An assay with 70% amplification efficiency would give the same fluorescence readout after around 33 cycles ($25 \times \log(2.0) \div \log(1.7) = 32.7$). In theory, then, both assays should give the same digital readout if the end-point analysis is conducted after 40 cycles of PCR.

2. In the real-time PCR assays used in the aging study, transcript copy number was computed based on the ΔCt between a cell-lysate sample and reference reactions bearing 1000 copies of runoff-transcribed RNA. The ΔCt calculation is as follows:

$$N_{mRNA} = 1000 \cdot \left(1 + E_{pcr}\right)^{(Ct_{std} - Ct)}.$$

So long as the value of E_{pcr} is known for a given assay, this formula can be used to calculate transcript abundance regardless of PCR amplification efficiency.

Nevertheless, low-efficiency assays are more vulnerable to competitive inhibition by non-specific side reactions. Suppose a short primer-dimer extension product amplifies with 100% efficiency. After 30 PCR cycles, its abundance relative to the target amplicon will be over a hundred times higher in a 70% efficient assay than in a 100% efficient assay ($2.0^{30} \div 1.7^{30} = 131$). Since it is relatively easy to find primers which give near-optimal PCR efficiency, all candidate assays were evaluated in simplex qPCR standard-curve trials to ensure that they gave efficient amplification. In standard-curve analysis, qPCR is performed on a dilution series of templates, and the efficiency of amplification is calculated from a plot of Ct versus the log of template concentration. The Ct readouts for samples with 1 unit of template and N units of template are related as follows:

$$N = \left(1 + E_{pcr}\right)^{(Ct_1 - Ct)}.$$

Taking the log of both sides:

$$\log(N) = (Ct_1 - Ct) \cdot \log\left(1 + E_{pcr}\right).$$

Rearranging, we derive an expression with the form $y = mx + c$:

$$Ct = -\frac{1}{\log(1+E_{pcr})} \cdot \log(N) + Ct_1.$$

Therefore, given a plot of Ct versus log(N), the PCR efficiency of an assay is computed from the slope of the best-fit line as follows:

$$E_{pcr} = 10^{-1/slope} - 1.$$

The intercept of the plot on the *y*-axis gives the value of Ct_1; if the template is quantitated in copies per reaction, this is the projected single-copy Ct for the assay.

The E_{pcr} estimates derived from standard-curve analysis are approximate; typically, adjusting the fluorescence threshold or baseline normalization used in calling Ct values can easily alter the calculated value by several percentage points. There is no absolute cutoff for what constitutes an acceptable assay, but primers which have ≥90% PCR efficiency may be considered near optimal, while an E_{pcr} value below 80% indicates a substandard assay.

Sometimes, a low-efficiency assay can be rescued by increasing the primer concentration of one or both primers in the pair, raising their effective T_m in the reaction. This kind of optimization was explored early on in assay development, but the use of high primer concentrations was eventually rejected because it promotes primer-dimer formation. All primers were empirically qualified at a relatively low, fixed reaction concentration (100 nM); assays which failed to give satisfactory PCR efficiency under these conditions were eliminated or redesigned.

In addition to providing an estimate of priming efficiency, qPCR standard-curve trials can provide clues to other problems. A standard curve which gives a near-optimal E_{pcr} value but an unexpectedly high Ct_1 intercept may signal poor TaqMan probe performance or, in RNA-based reactions, low RT efficiency. Non-linearity in the standard curve at the low end of the template-concentration range, with increasing ΔCt between successive template dilutions, may indicate that the primers have significant PD-forming potential even in the context of simplex PCR. Primer-dimer formation can be investigated by using SYBR Green assays to

visualize the accumulation of low-T_m products in no-template reactions; increased primer concentrations can be used to exaggerate the problem in debug assays.

4.3.4.2 Multiplex Compatibility

Transient base-pairing between primers with 3'-end complementarity can produce substrates for polymerization by reverse transcriptase and *Taq* (figure 4.12). Often, the resulting short primer-dimer extension products amplify very efficiently during PCR; they can give rise to spurious signals in SYBR Green reactions, and compete with target amplicons for reagents irrespective of dye chemistry. Competitive inhibition of the primary amplification reaction is most likely when the true PCR template is at low abundance. Under these conditions, the ratio of template to secondary product starts out low, and any advantage in amplification efficiency enjoyed by the latter is magnified by the many cycles of exponential amplification required to reach the detection threshold. The primer-dimer problem is exacerbated in multiplexed PCR, owing to the high overall primer concentration and diversity of primer sequences in the reaction. *In silico* evaluation of multiplex primer sets is not always effective at identifying problematic interactions; in any case, as the level of multiplexing increases, compromises usually have to be made to meet other design criteria.

Figure 4.12. Primer-dimer extension. When primers have significant complementarity, they can hybridize to form short-lived dimers, especially at low temperatures. In the presence of abundant polymerase, primer dimers can template the synthesis of primer-extension products. If the base pairing occurs at the 3' ends of the primers, the extension products will have T_ms close to the annealing temperatures used in the PCR reaction. Efficient amplification of these short secondary products may exhaust PCR reagents or saturate polymerase activity before legitimate assay targets can be amplified to detectable levels.

Multiplexed PCR was used throughout the single-cell work, so the primer-dimer-forming potential of combined assays was a major concern. The specialized PCR methods employed provided some margin of safety: (1) in the chip assay used for the hematopoiesis study, the sequestration of individual cDNA molecules into 6 nL subreactions raises the concentration of template relative to PD products; (2) the multiplexed preamplification PCR used in the aging study was limited to 15 cycles to minimize the effect of reagent depletion on PCR efficiency. Nonetheless, multiplexed assay sets were qualified empirically to ensure that PD-mediated PCR inhibition was contained. For the digital PCR work, combined assays were evaluated by running standard curves in a 4-channel qPCR system, the Chromo4 (Bio-Rad, Hercules, CA); the same TaqMan probes used in the multiplexed chip assay were employed in these desktop trials. In the aging study, 6-plex primer sets were tested for compatibility by running low-concentration standard curves using the full two-stage "preamp" protocol.

4.3.4.3 Reverse-Transcription Efficiency

Reverse-transcription efficiency is not as easily assessed as PCR efficiency, and values are still hard to come by in the literature. The most thorough study on this question yet published reports numbers ranging from 2% to 90%, depending on the assay target, RT enzyme, and priming strategy [86]. In the current state of the art, then, it is hard to set an expectation level for the RT efficiency attainable in qRT-PCR. For this reason, no formal qualification procedure was used to screen candidate assays for RT efficiency. During assay development for the hematopoiesis study, efficiency estimates were made based on digital PCR analysis of cDNA preps derived from quantitated RNA runoff transcript (figure 4.13). The estimates routinely varied over a ~3-fold range depending on the assay target. One early assay design which gave particularly low efficiency was successfully redesigned based on this analysis.

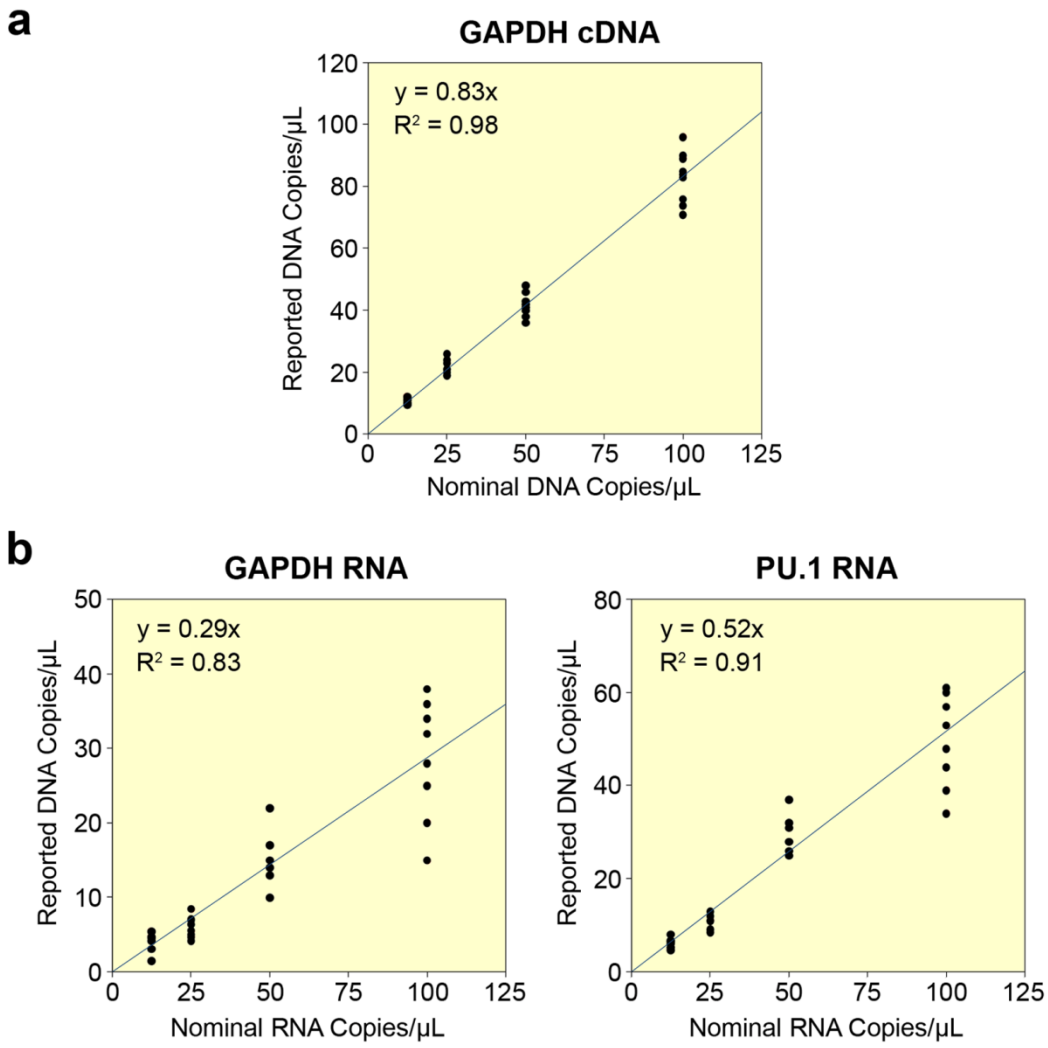

Figure 4.13. On-chip standard-curve assays. (a) Combined results from a series of three on-chip standard-curve trials performed on purified DNA template (Ambion GAPDH DECAprobe cDNA) using Bio-Rad iQ *Taq* polymerase supermix. Four template concentrations were analyzed: 12.5, 25, 50 and 100 copies/µL. Each concentration was evaluated in triplicate in every chip. The standard-curve fit was near-optimal ($R^2 \geq 0.99$) in the individual chips, and the interreplicate variation was within the expected Poisson sampling error. The slightly higher variability in the combined results probably reflects differences in final loaded sample volume between chips. (b) Combined results from three on-chip standard curve trials based on pooled GAPDH and PU.1 runoff RNA. Reaction mixes were made up with SSIII/*Taq*. The RT step was performed off chip in a conventional thermocycler. On-chip cDNA analysis was done using a duplex TaqMan assay. The RNA-based analyses displayed higher technical variability than seen in the trials based on purified DNA: the CV for the RT efficiency estimates derived from each panel was 20% for PU.1 and 29% for GAPDH.

No attempt was made to assess mRNA-to-cDNA conversion efficiency in the aging study. Since the transcript copy number quantitation was based on RNA references, RT efficiency was only a concern from a sensitivity standpoint in this case. The assays all gave reasonably high single-cell readouts on the six medium-to-high abundance transcripts evaluated in the study, so the efficiency of the RT step did not emerge as a major concern. The Ct values for 1000-copy RNA standards reactions were surprisingly tightly clustered across all six targets (figure 4.14), typically giving a standard deviation of less than one cycle after ~35 cycles of PCR amplification (15 cycles of "preamp" plus ~20 cycles of qPCR). At least some of the spread in Cts must have come from variations in PCR amplification efficiency between the different assays. This observation suggests that the RT efficiency was at least roughly similar for all six targets, with none of the individual assays performing substantially "below par."

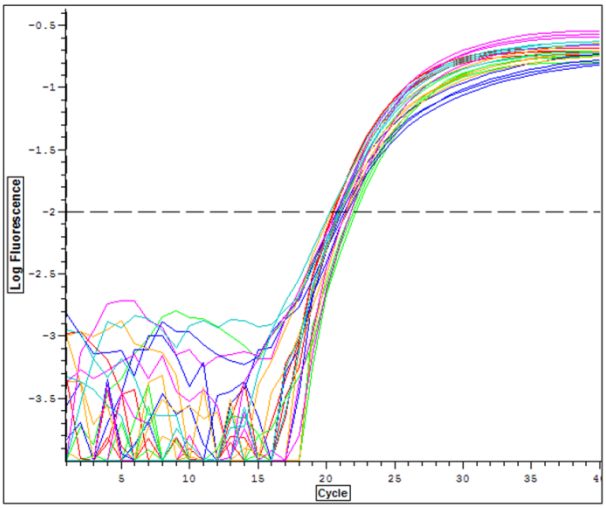

Assay	N	Ct S.D.
ActB	4	0.20
B2M	4	0.59
Rpl5	4	0.32
Rpl19	4	0.51
H2K	4	0.48
CD45	4	0.32
All	24	0.50

Figure 4.14. Clustering of RNA standards Cts. Quadruplicate RT/preamplification reactions were templated with a mixture of six different runoff-transcribed RNA standards. Each template was present at 1000 copies per reaction. Preamplification products were analyzed in 24 (4 × 6) SYBR Green qPCRs. The graph shows the amplification curves from the qPCR analysis; each assay target is represented by a different color. The six targets gave tightly clustered readouts, indicating that the RT and qPCR efficiencies were similar for all assays.

4.3.4.4 Experimental Templates

Much of the early assay validation work was done using mouse thymus cDNA and Poly(A) RNA preps purchased from Ambion. As a rule of thumb, 1 pg of either of these products is approximately equivalent to the transcript content of a single cell. However, the abundance of individual transcript species in the preps is unknown. This was not an issue for PCR efficiency calculations, but single-copy Cts could not be computed from standard curves based on these templates, nor could they be used for RT efficiency measurements.

Use of DECAprobe GAPDH cDNA template (Ambion) and homemade DNA standards made from UV-absorbance quantified, purified PCR products enabled a more quantitative approach to qPCR assay characterization. As the work progressed, though, the need for RNA standards became more pressing. This was addressed by using an *in vitro* transcription kit to make runoff RNA transcripts corresponding to all assay targets. The steps involved in producing these RNA standards were as follows:

1. PCR primers were designed against each target transcript, bracketing the amplicon regions of the qRT-PCR assays. A T7 phage promoter sequence was prepended to the upstream primers.

2. The primers were used to make templates for the *in vitro* transcription reactions, with Ambion's thymus cDNA prep serving as the PCR template. PCR products were cleaned up with the QIAquick kit (Qiagen) and checked for size and purity on a gel.

3. The MEGAscript T7 kit (Ambion) was used to make runoff transcripts from the PCR templates. Template DNA was removed from the preps in a DNase digestion step, and the RNA was column purified with Ambion's MEGAclear kit.

4. The purity and size of the runoff-transcribed RNA was evaluated using Novex gels (Invitrogen) or the Experion gel electrophoresis system (Bio-Rad).

5. RNA was quantitated by UV absorbance. The RNA concentration was converted to copies per μL after using Mongo Oligo (library.med.utah.edu/masspec/mongo.htm) to calculate the molecular weight of the transcripts.

6. A high-concentration stock comprising equimolar amounts of all target transcripts was prepared in TE pH 7.0; serial 10-fold dilutions were made from the stock. RNA reference dilutions were kept at -20 °C, and the master stock was archived at -80 °C.

4.3.5 Digital PCR

4.3.5.1 Background

Before the invention of real-time PCR, PCR was considered primarily a non-quantitative assay—visualization of reaction products on a gel at the PCR end point signaled if the target was present or absent, but usually little more than that. End-point PCR analysis can be made quantitative by performing reactions on serial dilutions of template; the dilution factor which causes PCR failure gives a rough estimate of DNA concentration. The limiting-dilution approach can also be used for highly accurate DNA quantitation, if the analyte is subdivided into many parallel PCRs so that each has a fractional probability of receiving a molecule of template. Then, the number of positive reactions provides a count of the input of template molecules [69]. This methodology was systematized and formally presented as "digital PCR" in a 1999 paper by Vogelstein and Kinzler [85]. Here, the technique was applied to determine the frequencies of wild-type and mutant alleles for a gene of interest. Genomic DNA harvested from normal and cancerous tissue was aliquoted to 7 μL PCR reactions arrayed in a 96-well plate. The DNA was quantitated and diluted before the analysis to

ensure that each well had a 50% chance of receiving template. After PCR, most of the positive reactions contained only wild-type or mutant amplicons; molecular beacons targeting these variants were added to the reactions to call the frequencies of each allele.

Digital PCR is a laborious technique when performed in multiwell plates, and the dynamic range of the readout is limited. Subdivision of analyte can be automated by dispersing samples into lipid micro-droplets ("emulsion PCR") [108, 109], or by using microfluidic valves to partition a sample in a "lab-on-a-chip" reactor. In the early 2000s, researchers at Fluidigm Corporation (South San Francisco, CA) demonstrated TaqMan-based digital PCR in a chip fabricated in PDMS (polydimethylsiloxane) silicone rubber using multilayer soft lithography [61, 110, 111]. A 2 μL sample was compartmentalized into 21,000 separate PCR reactions within the chip. Pneumatic pressure was applied to force the analyte into an array of parallel channels connected to the sample port by a crossbar channel. A comb-shaped valve with teeth perpendicular to these channels was incorporated into an adjacent layer of PDMS; hydraulic actuation of the valve pinched off the sample channels, forming a grid of 90 pL compartments (figure 4.15). Hydraulic pressure was maintained during thermocycling, both to keep the reaction compartments isolated, and to ensure that they remained hydrated despite thermally induced outgassing through the PDMS.

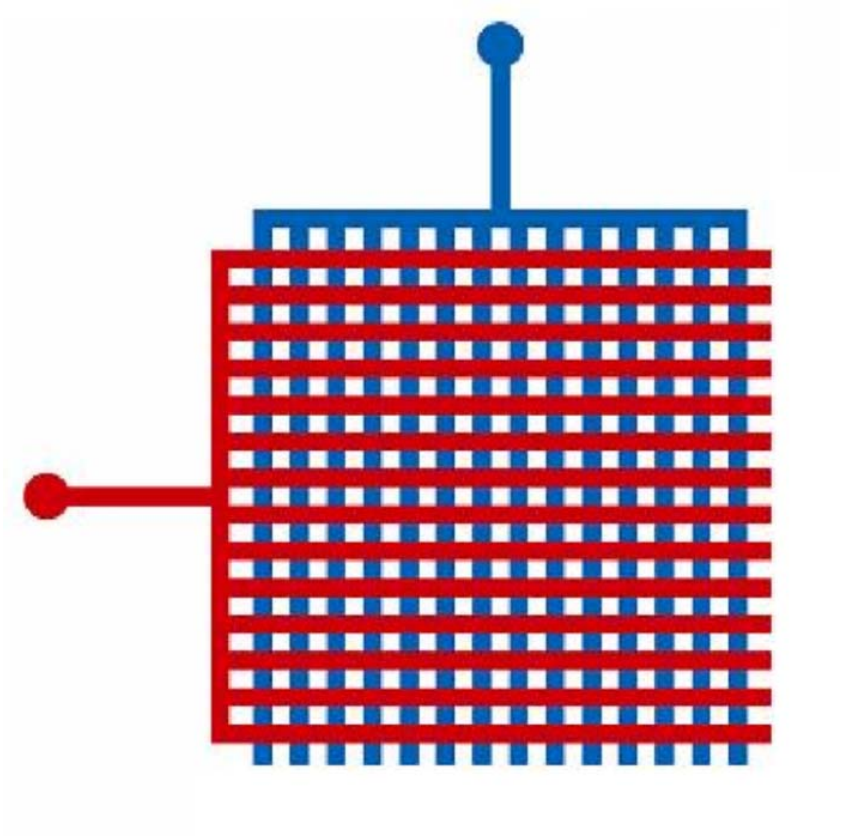

Figure 4.15. Analyte subdivision in an elastomeric chip. Sample is loaded into an array of channels connected to the input port via a crossbar (blue). A comb-shaped valve in an adjacent layer of the chip (red) is hydraulically actuated to pinch off the sample channels, partitioning the reaction within a grid of sealed compartments.

The early work for the thesis project focused on designing and building PDMS chips based on Fluidigm's original prototype. A few months into this effort, Fluidigm decided to pursue production of a commercial digital PCR chip. Efforts to manufacture a chip in-house were discontinued, and preproduction prototypes of what became known as the "Digital Array" chip served as the enabling technology for the hematopoiesis study.

The prototype Digital Array has a 25 mm square active area which contains an array of 14,400 6.25 nL PCR reaction chambers or "wells." The array is organized into twelve isolated sample panels, each with its own dedicated input port. There are 1200 wells in each panel, giving a loaded sample volume of 7.5 μL.* The number of reaction chambers determines the dynamic range of the digital PCR assay. If the template copy number is well below 1200, almost all chambers capture 0 or 1 molecules, and the number of positive reactions corresponds closely to the number of template molecules in the panel. At higher DNA concentrations, a significant fraction of chambers capture more than one molecule. Using the appropriate statistical correction, it should be possible to accurately estimate template abundance with as many as 2000 copies per panel (see appendix).

The reaction chambers in the original, experimental Fluidigm PCR chip were simply short stretches of sample channel pinched off by the teeth of the comb valve. In the Digital Array, each sample channel passes through fifty "high-hat" chambers molded into the PDMS; the

---

* For the production version of the Digital Array, the spacing between sample channels has been increased to improve chip yields; in this chip, there are 765 chambers per panel, and the loaded sample volume is approximately 5 μL.

comb valve is aligned so that its teeth pass between the chambers. This design increases the volume of analyte that can be loaded into a given amount of chip "real estate." The well dimensions in the prototype chips were approximately 150 × 150 × 250 microns. The loaded volume per chamber is slightly higher than the dry volume since (1) the chambers swell under pressure and (2) the PDMS is somewhat water permeable.

Prototype chips were available mounted on silicon wafers or 75 × 50 mm glass slides. Silicon wafers provide better thermal contact to the thermocycler block during PCR. However, only slide-mounted chips were compatible with end-point fluorescence imaging using the ArrayWoRx scanner at our disposal. Fluidigm supplied an optimized thermocycling profile which incorporated "overshoot" in the temperature ramps to make up for the inferior conductivity of the slide base.

To set up an experiment, samples were drawn into gel tips and spiked directly into the input ports of the chip. Plastic adaptors were used to connect the gel tips to a house air supply for sample loading. It took about 30 minutes to force the air in the sample channels out through the gas-permeable PDMS. This manually controlled loading method was cumbersome and trouble-prone. Also, based on PCR analyses conducted using the same analyte in different chips, the actual loaded sample volume routinely varied by ~10% between experiments.[*]

---

[*] The production version of the Digital Array is mounted in a plastic carrier the size of a microtiter plate; reactions are pipetted into wells molded into the carriers during the PCR setup, and then pressure loaded into the chips in an automated priming station.

4.3.5.2 Reaction Kinetics

In a digital PCR using the Fluidigm chip, each template molecule is confined within a reaction volume of 6.25 nL. This is 1/3200 the volume of the 20 µL reactions used for desktop standard-curve qPCRs. The single-copy Ct intercepts for TaqMan-based qPCR standard curves clustered around 40 cycles, with some variation depending on assay efficiency and the use of RNA or DNA template. To a first approximation, the 3200-fold increase in template concentration in the chip should reduce the number of cycles needed for single-copy detection by about 12 cycles ($\log(3200) \div \log(2) = 11.6$). On this basis, we might expect to detect positive reactions in the chip after around 25–30 cycles of PCR.

We can derive similar estimates from a consideration of PCR kinetics. The signal to noise (SNR) of TaqMan probes is on the order of 10, i.e., a cleaved, unquenched probe produces around ten times the fluorescence of a quenched probe [112]. Therefore, after 10% of the probes have been hydrolyzed, the fluorescence should be roughly double the background signal produced before PCR ($0.9 + 0.1 \times 10 = 1.9$). Whether a 2× increase in fluorescence is sufficient or more than sufficient to call a positive PCR reaction will depend on the SNR of the entire detection system. However, given that the above-background signal will double with every PCR cycle, the number of cycles required to cleave 10% of the probes should be close to that needed to reach the threshold of detection.

Given efficient probe binding and cleavage, the number of unquenched probes in a TaqMan PCR will be almost the same as the number of double-stranded amplicons. Starting from a single molecule of first-strand cDNA, the abundance of dsDNA amplicons will grow with the PCR cycle number as follows:

$$N_{dsDNA} = (1 + E_{pcr})^{(cycle-1)}.$$

If the TaqMan concentration in the PCR reaction is 50 nM, each chamber of the chip starts out with about 2×10^8 probe molecules (50×10^{-9} mol·L^{-1} • 6.25×10^{-9} L • N_A). The number of PCR cycles required to hydrolyze 10% of the probes can be calculated as follows:

$$(1 + E_{pcr})^{(cycle-1)} = 2 \times 10^7 \;\; \therefore \text{cycle} = \frac{\log(2\times10^7)}{\log(1+E_{pcr})} + 1.$$

This gives us estimates for the single-copy Ct in the digital PCR assay:

Ct = 29.6 (assumes E_{pcr} = 80%);

Ct = 25.2 (assumes E_{pcr} = 100%).

A clear distinction between the fluorescence in background and PCR-positive reaction chambers was seen in several experiments in which chips were imaged after 30–32 cycles. The finalized digital PCR protocol included a full 40 cycles of amplification, to provide a margin of safety in case any primer sets gave lower-than-expected efficiency on chip.

4.3.5.3 Primer Dimer Containment

Early multiplexed digital-PCR trials based on Ambion's thymus cDNA preps produced encouraging results. A triplex analysis targeting one high-abundance transcript (GAPDH) and two low-abundance transcripts (PU.1 and GATA-3) gave well-separated positive and negative reaction fluorescence, good interreplicate consistency, and plausible copy-number readouts for all three targets (figure 4.16). However, initial tests based on RNA templates produced much less satisfactory results. In these trials, Ambion Poly(A) RNA or quantitated runoff transcript was reverse transcribed off chip using Invitrogen's one-step SSIII/*Taq* chemistry, and the completed RT reactions were loaded into the Digital Array for cDNA quantitation. The chip assays displayed a variety of problems: (1) weak or highly variable

fluorescence in PCR-positive reaction chambers, (2) high interpanel and chip-to-chip variation, and (3) very low cDNA copy-number readouts from some reactions.

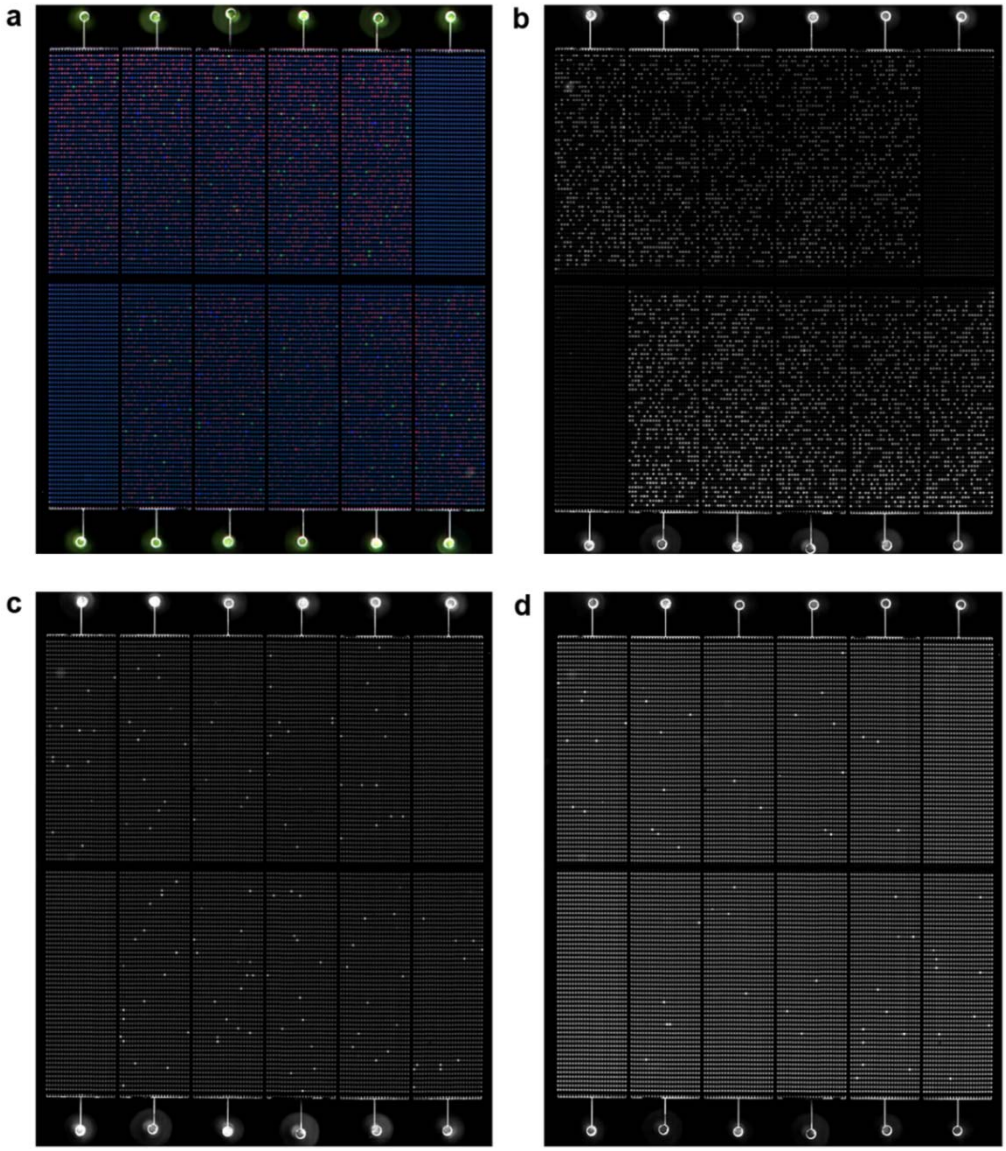

Figure 4.16. Triplex digital PCR on purified cDNA. Ambion Mouse Thymus cDNA was analyzed in the Digital Array using Bio-Rad's iTaq polymerase and TaqMan assays targeting a housekeeping gene (GAPDH) and two transcription factors (GATA-3 and PU.1). Ten panels received 3 pg each of cDNA (~3 cells equivalent); two corner panels received no template. The chip was imaged after 30 cycles of PCR. (a) False-color image showing all three assay channels. (b) Cy5/GAPDH channel. (c) Cy3/GATA-3 channel. (d) FAM/PU.1 channel.

Investigation into the poor performance of the RNA-based assays highlighted several issues:

1. SuperScript III is a fast-acting polymerase. The Ct values from qRT-PCRs done using a 1 minute RT step were very similar to those obtained using the 15 minute incubation recommended by the manufacturer.

2. SuperScript III has high activity at temperatures well below its recommended operating range (42–60 °C). In trials using the Chromo4, only a slight falloff in specific product formation was seen when the RT reactions were done at room temperature. Less than a tenfold reduction in product was seen when the RT temperature was lowered to 4 °C. Thus, either the enzyme retained much of its activity at 4 °C, or it was able to make substantial amounts of product during the brief temperature ramp between the RT step and the PCR hot start.

3. SuperScript III can make substantial quantities of PD product during reaction setup (figure 4.17). This might be expected in light of the enzyme's strong activity at low temperature; the amount of PD available for extension should also be much greater at the temperatures experienced during reaction setup than during the RT itself.

4. SuperScript III is much more thermostable than traditional MMLV RTs, with a half-life of 2.5 minutes at 60 °C [113]. A relatively harsh heat treatment is required to fully inactivate the enzyme. In one-step reactions performed in a conventional qPCR system, this is not a problem: (1) the enzyme is killed by the 95 °C hot start used to activate the *Taq* between the RT and PCR steps, and (2) the temperature never falls below the primer-annealing temperature during the subsequent qPCR analysis.

5. Heat inactivation of SuperScript III at the end of the RT is essential in the chip protocol because the completed reactions undergo ~30 minutes exposure to low temperatures during the sample-load step. The Platinum *Taq* polymerase included in Invitrogen's enzyme blend uses antibody-based hot-start protection. Although the standard qRT-PCR protocol calls for a 95 °C, 2 minute hot start, the manufacturers' literature indicates that the antibody can be released at lower temperatures (≥58 °C), albeit more slowly [114]. It was therefore difficult to define an SSIII heat-inactivation step which avoided the risk of liberating *Taq* activity before the chip load.

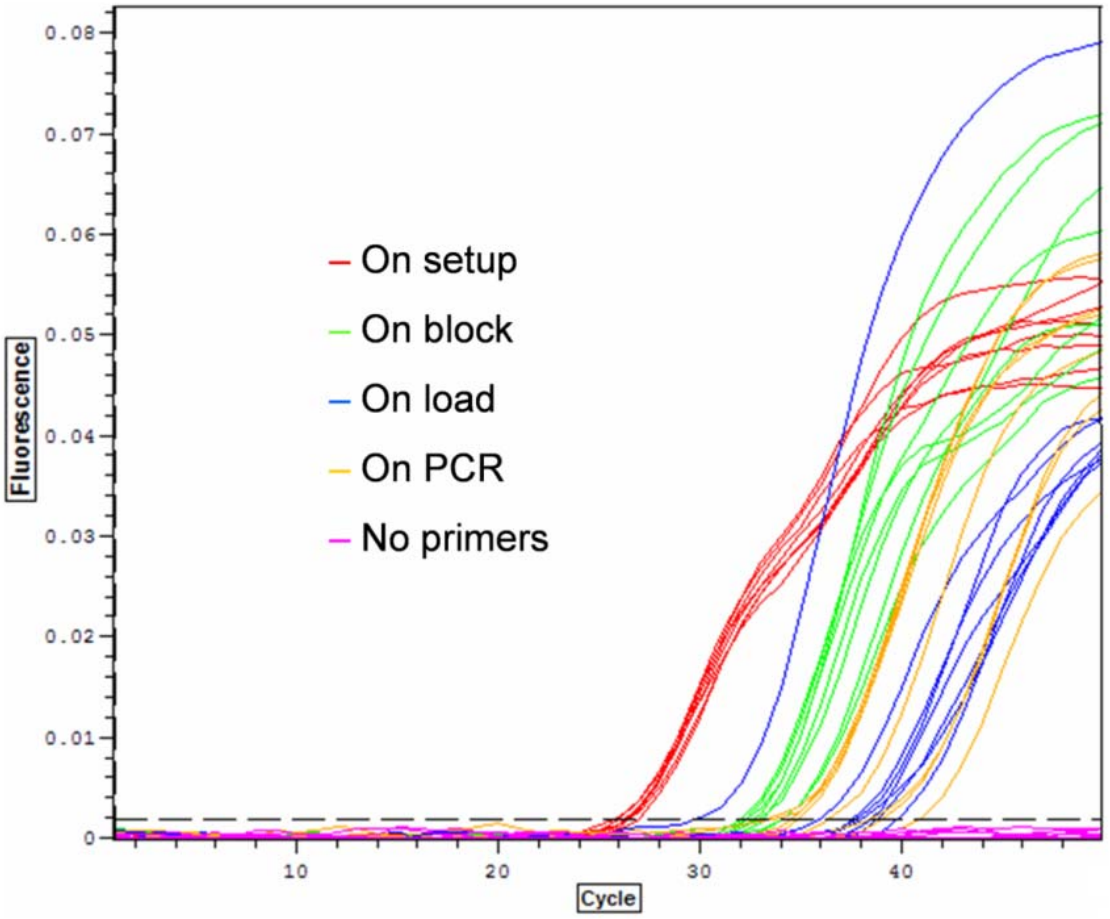

Figure 4.17. Primer-dimer product formation by reverse transcriptase. PD-product accumulation was evaluated by SYBR Green qPCR on no-template SSIII/*Taq* reactions. The thermal profile used included an RT heat inactivation followed by a 30 minute chilldown to 4 °C before qPCR to simulate the chip load step. Triplex primers were added to the samples at several different points: during the reaction setup; on the preheated thermocycler block at the start of the RT; immediately after RT heat-inactivation (the beginning of the simulated chip load); or just before the qPCR hot start. The Cts seen when primers were added during setup were several cycles lower than those seen when primers were added in later steps, indicating that most of the PD product was being formed by the reverse transcriptase during reaction assembly.

A variety of options were explored to contain the problem of PD-product formation during reaction setup and chip load:

1. One-tube chemistries were tested based on less thermostable MMLV RTs, including SuperScript II (Invitrogen) and Stratascript (Stratagene, San Diego, CA), with the idea that this would facilitate RT heat-inactivation without *Taq* activation. In qRT-PCR trials conducted in the Chromo4, the reverse-transcription efficiency of these enzymes appeared to be significantly below that of SuperScript III.

2. QuantiTect (Qiagen), a one-step system incorporating a chemically modified *Taq* with a long hot-start requirement (10 minutes at 95 °C), was investigated as another approach to the heat-inactivation problem. Again, Chromo4 trials gave SSIII/*Taq* a performance edge—although, in this case, the difference was slight.

3. Attempts to synthesize a one-tube chemistry combining the standalone version of SuperScript III with a chemically protected *Taq* initially gave very poor results, apparently due to RT inhibition of *Taq* [101, 102, 104-107]; even after optimization, the performance of this blend was never as consistent as that achieved with Invitrogen's one-step chemistry.

4. AccuRT (Applied Biosystems, Sunnyvale, CA), a single-enzyme RT-PCR solution with an aptamer-based, reversible hot-start mechanism, gave promising results, but was not qualified by the manufacturer for TaqMan-based qPCR. Tests were done to evaluate the possibility of using AccuRT with LUX primers (Invitrogen), but the initial results were unsatisfactory, and the superior specificity offered by TaqMan chemistry was in any case preferred.

The technical approach ultimately adopted for the hematopoiesis work involved the use of several PD-containment strategies:

1. The reaction concentration of all primers was reduced from 400 nM in early trials to 100 nM in working assays. Standard-curve analysis was used to check that high PCR amplification efficiency was maintained at the lowered primer concentration.

2. The assays which contributed most strongly to PD formation were identified by desktop qPCR analysis and disqualified, and the original goal of performing triplex PCR in the chip was scaled back to duplex PCR.

3. In the RT step, samples were loaded into a thermocycler after preheating the block to the RT incubation temperature (55 °C), and the SSIII/*Taq* blend was added after allowing the samples 1–2 minutes to warm up.

4. A relatively mild, 70 °C, 5 minute heat-inactivation step was used at the end of the RT reaction to denature SSIII without fully activating the *Taq*.

5. The chip load step was performed in a cold room at 4 °C.

Although these measures eliminated the gross problems seen in the early RNA-based chip assays, the variation in the cDNA copy number readouts from replicate RT reactions was generally significantly higher than that observed in reactions based on purified DNA (figure 4.13). In the current state of the art, the reverse-transcription step of qRT-PCR appears to be the major source of technical noise in the assay [86].

4.3.5.4 Image Processing

The commercial Digital Array is designed for use with an integrated thermocycler-imaging system. The Fluidigm system incorporates a full-field CCD camera which permits real-time imaging of the chip during the PCR run. This system was not available at the time of the hematopoiesis study; instead, after thermocycling on a standard flat-block thermocycler, chips were imaged using an ArrayWoRx microarray scanner (Applied Precision, Issaquah, WA). The scanner was modified to accept a metal carrier designed for slide-mounted microfluidic chips. Valve pressure was maintained during imaging to ensure that the reactions remained compartmentalized. The imaging process took around ten minutes per channel at the preferred 13-micron resolution. The confocal optics of the scanner provide relatively even illumination across the entire image field, obviating the need for a reference dye such as ROX in the PCR reactions. All three fluorescence channels of the ArrayWoRx (FAM/Cy3/Cy5) were therefore available for TaqMan signal analysis.

A Microsoft Visual C++ application was written to process the ArrayWoRx scan files. After the user has "tie pointed" the four corners of the active area of the chip (figure 4.18), the pixel data is resampled to build normalized images of the twelve sample panels. The software isolates the reaction wells in each panel image and computes a fluorescence-intensity value for each one. The user can sweep out rectangles to designate regions that should be excluded from the analysis due to chip defects, debris, glare, etc. The wells in each panel are rank ordered by intensity. Wells whose brightness exceeds that of a "baseline" percentage of the lowest-ranked wells by a user-specified threshold are called as positive. The baseline and threshold settings can be adjusted for each fluorescence channel independently. The DNA concentration in each panel is computed based on the count of

positive reactions and the total number of non-excluded wells. The application can generate a variety of different reports summarizing the results of the chip analysis (figure 4.19).

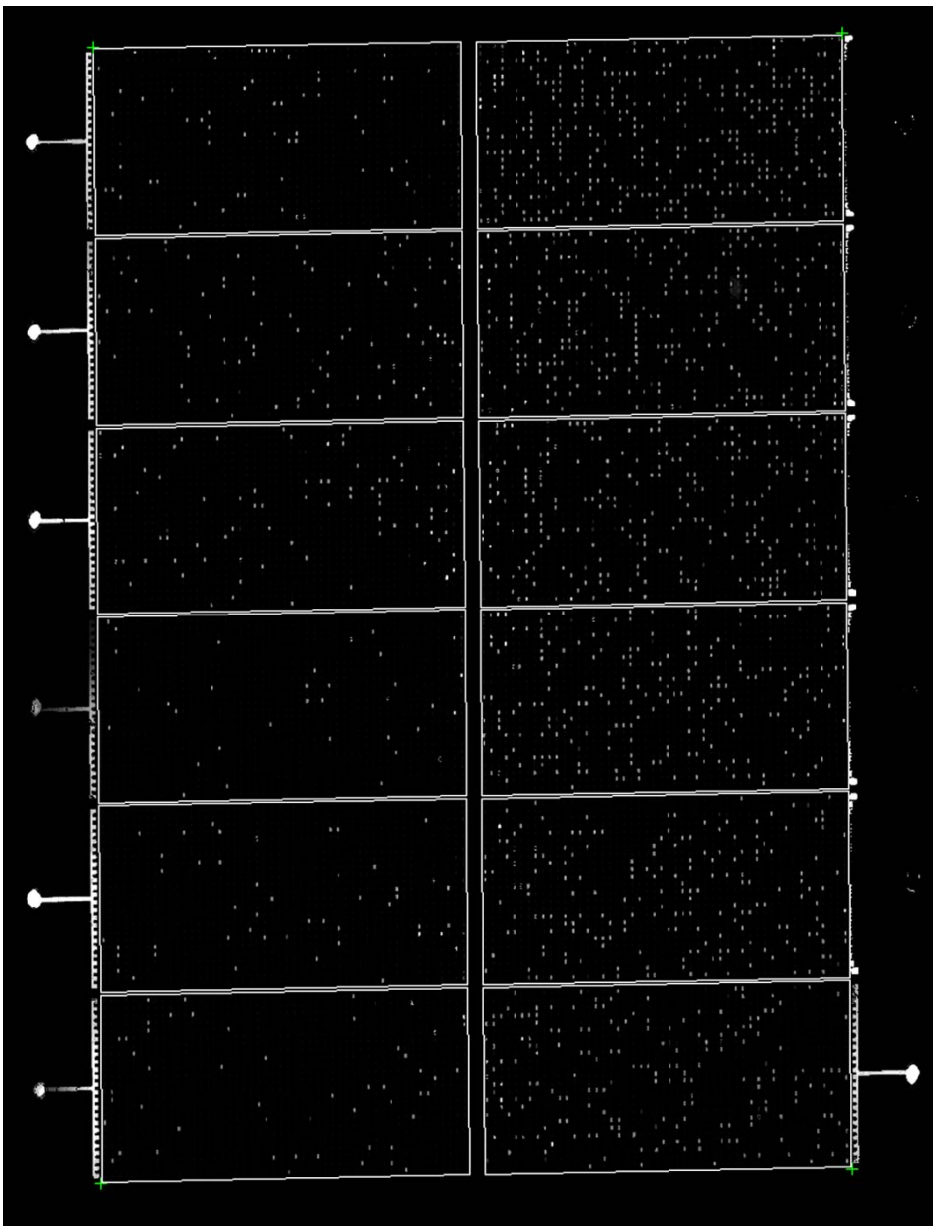

Figure 4.18. Identification of Digital Array panels. To permit automated assessment of the digital PCR readout, the scans produced by the ArrayWoRx are resampled and subimages corresponding to each chip panel are extracted from the normalized image data. The user must first designate the corners of the active area of the chip (green crosshairs); the software uses these "tie points" to resample the scan and extract the panel images.

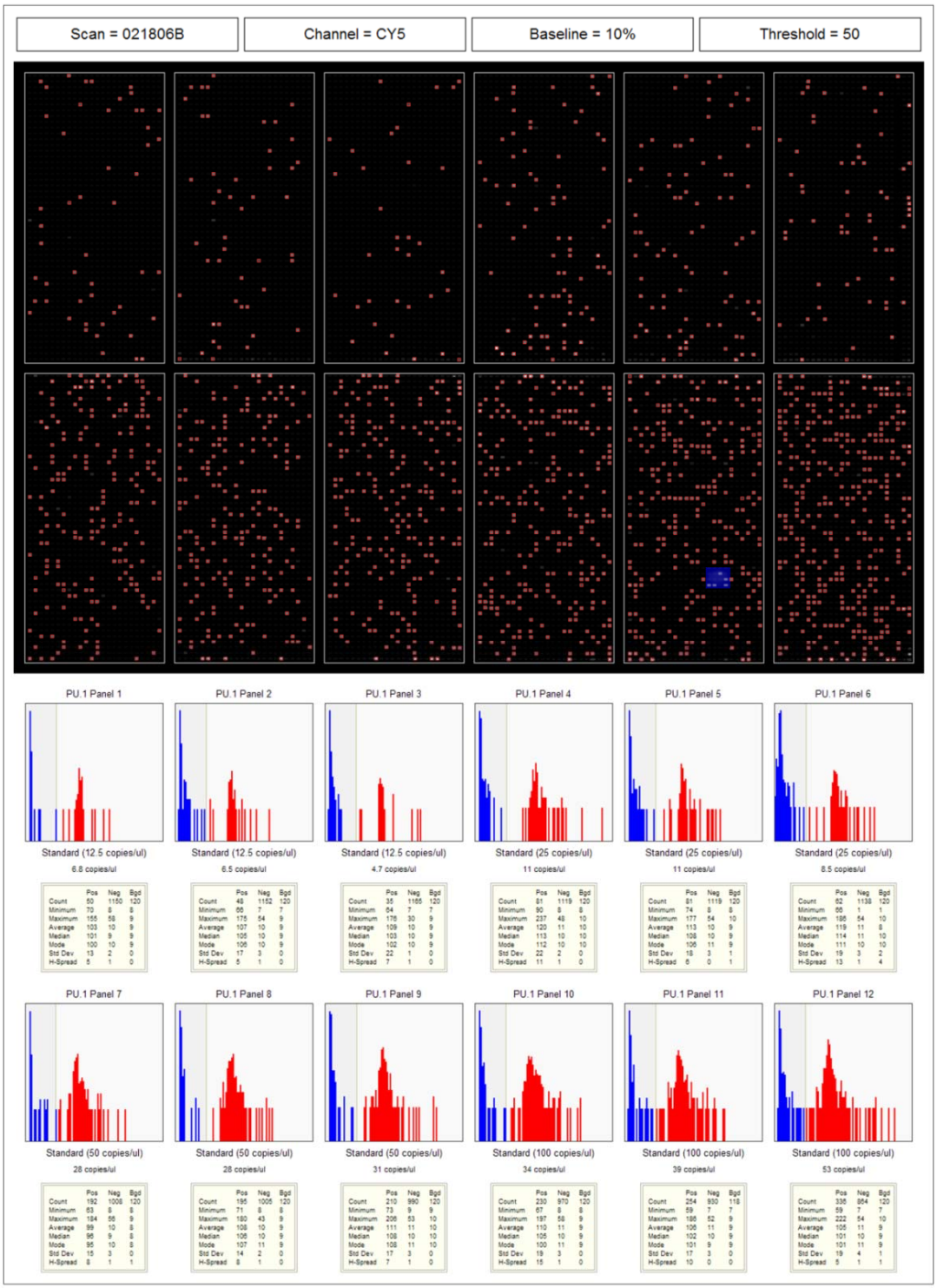

Figure 4.19. Digital PCR assay report. The report shows the normalized panel images, with positive well calls highlighted. User-excluded regions are indicated in blue. The calculated DNA concentration is shown for each sample, along with a statistical summary and a histogram giving the distribution of well intensities in the panel.

4.3.6 Preamplification PCR

4.3.6.1 Background

In a number of the single-cell studies published in the nineties, a round of multiplexed, sequence-specific PCR was applied to facilitate the evaluation of multiple genes in parallel, simplex PCRs. In the last few years, this strategy has been further developed and extensively characterized by at least three groups of researchers:

1. Peixoto et al published a study in *Genome Research* in 2004 [89] demonstrating 20-plex qRT-PCR analysis of single cells using multiplexed preamplification PCR. In the Peixoto work, cell lysates were first reverse transcribed using multiplexed, gene-specific RT primers. The cDNA was amplified ~30,000-fold in a 15-cycle multiplex PCR, and the amplification products were quantitated in parallel, independent SYBR Green qPCRs. The amplified templates were diluted 100-fold going into the qPCR round. A seminested priming strategy was employed, with only one of the primers in each simplex qPCR assay being shared with the preamplification PCR.

2. In a paper published in *Nucleic Acids Research* in 2005 [90], Stanley and Szewczuck described a similar methodology, which they entitled "Multiplexed Tandem PCR" (MT-PCR). In their protocol, a GSP-based RT reaction was coupled with 10–20 rounds of 72-plex PCR in the same tube; a short, 1 minute RT incubation and a low reverse-transcriptase concentration was used to minimize PD formation. SYBR Green qPCR analyses were done on 100-fold diluted preamplified cDNA. Seminested primers were used in the qPCR round, as in the Peixoto study. The MT-PCR protocol has since been commercialized by Corbett Research (Sydney, Australia).

3. Within the last year, Applied Biosystems (ABI) has introduced a commercial kit for preamplification PCR, the TaqMan PreAmp Master Mix Kit. ABI's protocol calls for 10–14 cycles of multiplexed "pre-PCR," followed by standard simplex TaqMan qPCR analysis of the product. A 20-fold dilution of the preamp product going into the qPCR is recommended with a 10-cycle pre-PCR, or an 80-fold dilution when using 14 cycles of pre-PCR. The kit is designed for use with the company's off-the-shelf TaqMan Gene Expression Assays, which combine primers and probes in the same mix. Up to a hundred assays may be pooled in the pre-PCR. The assays are used at their standard concentration (900 nM primers, 250 nM probes) for qPCR, but each individual assay is used at only 1/20 this concentration in the pre-PCR, to minimize primer-dimer formation. A 4 minute anneal-extend step is specified in the pre-PCR thermocycling profile, to give the primers time to bind their targets.[*] The ABI kit covers cDNA analysis only; an RT step is not included in the protocol.

4.3.6.2 Principle of the Method

The aim of preamplification is to take a limiting amount of cDNA and turn it into enough material to support the analysis of multiple target genes. For the method to be quantitative,

---

[*] The average time primers take to bind their templates is inversely proportional to their concentration in the reaction. At the primer concentrations normally used in PCR (around 0.1–1.0 μM), this time is on the order of seconds. The rate of primer-dimer formation scales with the product of the concentrations of the primers involved. Therefore, a 20× reduction in primer concentration should reduce PD product formation 400-fold, while increasing the required primer annealing time only 20-fold.

the PCR amplification efficiency of all targets must be maintained during both the pre-PCR and the qPCR steps of the protocol. In a multiplex PCR, amplification of high-abundance targets can lead to early depletion of reagents such as dNTPs or saturation of polymerase activity, compromising the amplification of less abundant targets and introducing bias into the quantitation. In both simplex and multiplex PCR reactions, highly efficient amplification of short PD products can competitively inhibit amplification of legitimate, low-abundance targets. Multiplexed reactions are especially prone to this effect because the diverse primer sequences used increase the possibility of primer-dimer formation. In preamplification protocols, these problems are contained by (1) limiting the number of cycles of multiplex PCR, and (2) by diluting the first-round products going into the qPCR.

In the context of single-cell analyses, few if any cDNA targets will exceed 10^4 copies. In a standard PCR, around 30 cycles of exponential amplification are required for a 10^4-copy template to significantly deplete a reaction. Thus, resource-competition between target amplicons should be trivial in 10–20 cycles of multiplexed PCR performed on single-cell preps. The amount of PD product produced during reaction setup and the pre-PCR itself will depend on the number and concentration of primers in the mix, their specific sequences and therefore PD-forming potential, and other reaction conditions (such as whether or not reverse transcriptase is present). Ultimately, the number of multiplex pre-PCR cycles which can be performed without incurring PD-mediated inhibition and amplification bias must be established empirically.

The dilution of the first-round reaction going into the qPCR step serves two purposes. A preliminary dilution, performed directly after the pre-PCR, quenches the reaction: the rapid dilution of *Taq*, dNTPs, magnesium ions, and primers prevents any significant PD-product

formation during the cooldown of the reaction. The pre-PCR product is further diluted in the assembly of the qPCR reactions. The net result is that the inherited multiplex primers will be at too low a concentration to find their targets efficiently in the qPCR. The dilution does not directly advantage the template relative to first-round PD products, since the concentration of both is reduced by the same factor. However, the only PD products which will be amplified efficiently during the qPCR step will be those derived from the specific assay primers during the pre-PCR (figure 4.20).

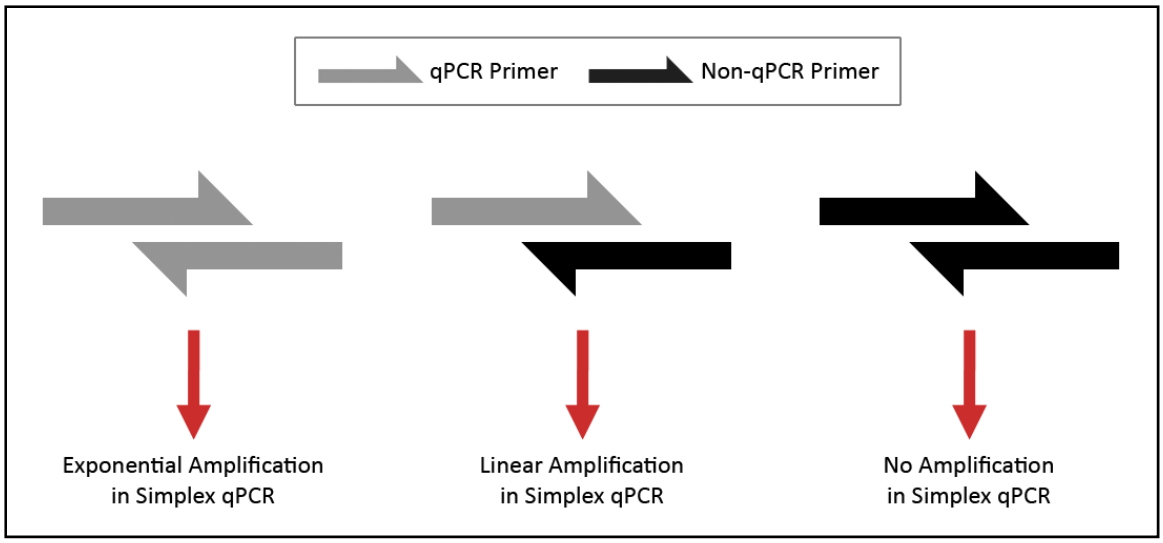

Figure 4.20. Pre-PCR secondary-product amplification in qPCR. Here, it is assumed that the primers used for the qPCR analysis are also used in the multiplexed pre-PCR, as in the ABI and aging-study protocols. Primer-extension products made from the simplex primer pair in the pre-PCR may be exponentially amplified on carryover to the qPCR round. If a qPCR primer and a primer from a different assay dimerize in the pre-PCR, the extension product from the non-qPCR primer may be transcribed efficiently in the qPCR phase; however, as the resulting transcripts will not themselves be efficiently primed, only linear amplification will result. PD products formed from two non-qPCR primers should not be efficiently transcribed during the qPCR phase.

Importantly, PD extension products derived from the qPCR primer pair during the pre-PCR round may amplify exponentially during the qPCR round, impacting assay performance. In fact, as more PCR cycles will be required overall to reach the threshold of detection (to make up for the dilution step) these PD products will have more opportunity to out-race the legitimate assay target than they would in a standard qPCR. The two-stage PCR approach only helps here if the assay primers are switched in the second round, as in the nested or seminested priming method preferred by Peixoto and Stanley.

4.3.6.3 Priming Strategy

The seminested priming approach adopted by Peixoto and Stanley adds a useful extra level of protection against primer-dimer effects in the qPCR round of analysis. However, nested priming was rejected for the aging study, for two reasons:

1. A requirement to use nested primers would have made it much harder to design assays which avoided RNA secondary structure.

2. Wide adoption of preamplification PCR will be encouraged if protocols can be defined which allow use of standard assay-design practices or off-the-shelf assays.

Traditionally, the design of multiplexed PCR assays involves qualification of compatible primer sets using software that identifies problematic 3' primer-dimer interactions. Peixoto et al used this approach for their 20-plex assay. The problem of *in silico* qualification becomes intractable as the desired level of multiplexing increases, because the number of possible pair-wise interactions between primers goes up with the square of the number of assays. The MT-PCR and ABI PreAmp protocols do not call for *in silico* primer qualification, relying instead on the built-in protections afforded by the method to limit the

impact of PD on assay performance. *In silico* qualification was applied in the aging study since (1) the work required the multiplexing of only six assays, and (2) the use of single-tube chemistry for RT/pre-PCR was expected to increase PD formation during the pre-PCR.

4.3.6.4 Preamp Parameters

A 10-cycle pre-PCR was used during initial assay prototyping, along with 100-fold template dilution going into the PCR step (40-fold during reaction quenching, and a further 2.5-fold during the qPCR setup). These conservative parameters gave good results in runoff RNA-based standard curve trials. A 10-cycle pre-PCR should provide ~1000-fold amplification of the cDNA template; after a 100-fold dilution, the template concentration in the qPCR step should therefore be ten times higher than in the original cell-lysate preps. A higher preamplification factor was preferred so that low-abundance targets would be detected well before the end of the 40-cycle qPCRs. Experiments showed no falloff in assay performance when the number of pre-PCR cycles was increased to 15, and this number was used for the working assays. Using these protocol parameters, the targets evaluated in the single-cell study generally gave Cts well below 30 during the qPCR analysis.

4.3.6.5 Real-Time PCR Chemistry

Since the aging study was designed to evaluate cell-to-cell heterogeneity, low intrinsic assay variability was particularly important. All the assays for the study were originally designed to incorporate TaqMan probes. Tests were done to compare the technique-related noise using TaqMan or SYBR Green chemistry in the qPCR step. Overall, SYBR Green gave slightly superior intrareplicate consistency (figure 4.21). This is probably because the early-cycle fluorescence in TaqMan reactions tends to fluctuate, impacting the baseline-subtraction process. Based on this analysis, SYBR Green chemistry was selected for the working assays.

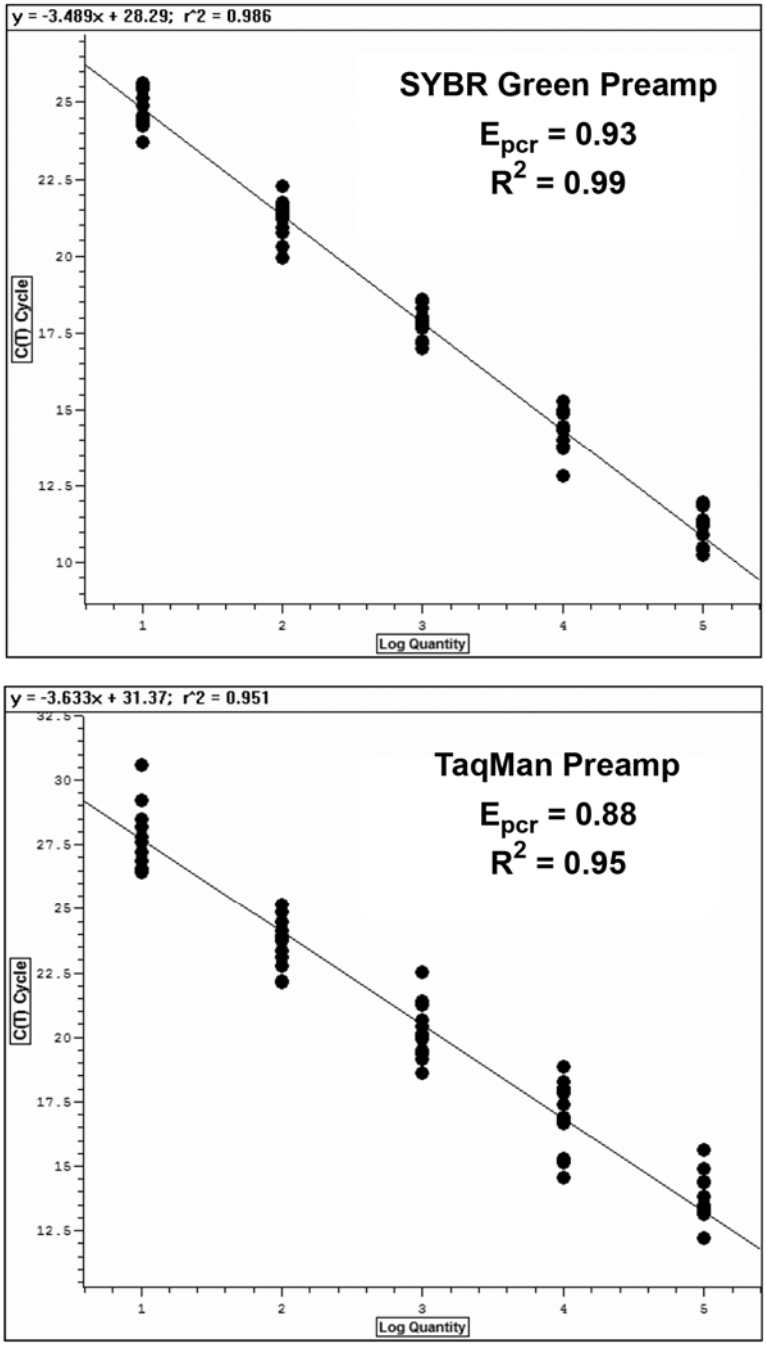

Figure 4.21. Technical noise in SYBR Green and TaqMan preamp assays. The plots show the results of qRT-PCR standard-curve trials based on a 6-plex RNA standards mix. The templates are at from 10 to 10^5 copies per reaction. RT/pre-PCR reactions were performed in duplicate for each point in the titration series. The qPCR standard curves here include the data for all six assay targets. SYBR Green chemistry gave more tightly clustered Cts, better calculated PCR efficiency, and lower single-copy Ct intercepts.

4.3.6.6 RNA Standards

Based on the digital PCR study, the cell-to-cell variation in transcript copy-number was expected to be fairly large, with a coefficient of variation (CV) of around 60%–100% (similar numbers emerged from aging study). Since the research was designed to evaluate whether this variation is different in young and old animals, it was important that the technique-related variation in mRNA quantitation be substantially less than the intrinsic biological variation. Trials conducted using runoff-transcribed RNA showed that the variation in the Ct readout between technical replicates analyzed in the same qPCR experiment was quite small—typically, under a half a cycle even at low template concentrations. However, the Ct values obtained for technical replicates evaluated in different qPCR runs routinely varied over a 2–3 cycle range. Thus, pooling raw Ct values from different experiments would have introduced unacceptable measurement noise into the aggregated data. This problem was addressed by converting the Ct readouts from cell lysates into absolute copy-number values, based on the readouts from RNA-standards reactions analyzed in the same experiment.

Four reactions containing 1000 runoff-transcribed copies of each of the six assay targets were processed alongside every strip of eight cell-lysate samples. The 1000-copy number was chosen to be close enough to the expected cell-based readouts to minimize the effects of variations in PCR efficiency on delta Ct calculations, but high enough that any Poisson sampling noise introduced during aliquoting of the RNA master mix would be insignificant.

A nominal 1000-copy Ct was first interpolated for each assay target based on the four Ct readouts from the standards reactions, as follows:

$$\mathrm{Ct}_{1000} = \log\left[\frac{4}{\sum_{i=1}^{i=4}(1+\mathrm{E_{pcr}})^{-\mathrm{Ct}_i}}\right] / \log(1+\mathrm{E_{pcr}}).$$

A nominal E_{pcr} value of 1.95 was used for all calculations. The absolute RNA copy number in the cell lysates was calculated by the ΔCt method:

$$N_{mRNA} = 1000 \cdot (1 + E_{pcr})^{(Ct_{1000} - Ct)}.$$

The interpolated standards Ct was also used to compute the estimated number of RNA copies in each technical replicate, again using the ΔCt method. The CV of the four estimates gives the well-to-well technical variability of the assay in terms of target copy number, rather than PCR cycles. This variation was ~25% for all six assays.

4.4 Conclusions

The following points emerge from the experimental work:

1. The qRT-PCR measurement error at low template copy number was similar using both digital PCR and preamplification PCR (20%–30%), and probably reflects tube-to-tube variability in the reverse transcription reaction. Given that the mechanism of transcription seems to introduce high levels of stochastic noise in cellular mRNA levels (CV > 60%), this accuracy should be adequate for most single-cell studies.

2. Although transcription-factor expression was only evaluated using the digital PCR method, it should also be possible to quantitate low-abundance transcripts with preamp PCR. In standard-curve trials using preamp, no falloff in assay linearity was discerned at 10–100 copies of RNA per reaction. With good primers, there is no reason in principle why qPCR should not be quantitative down to this level.

3. The limited sensitivity reported in some early single-cell qRT-PCR studies (10–20 mRNA copies limit of detection) may reflect aliquoting of cDNA following first-

strand synthesis or low RT efficiency using some of the older reverse transcription protocols. The RNA copy-number limit of detection for the protocols applied in the two single-cell studies is determined by the RT effiency of the individual assays and, in the case of the digital PCR method, the fraction of the total cDNA sample loaded into the active area of the chip (50%). Assuming 30%–50% RNA-to-cDNA conversion efficiency, this limit is ~2–3 copies using the preamp technique, and ~4–6 copies using the prototype chip assay.

4. The digital PCR work showed that primer dimer can be a significant issue in the chip assay, at least when using single-tube RT-PCR chemistries. A robust solution needs to be found before the potential of the chip for multiplexed single-cell analysis can be fully exploited. Use of a hot-start-protected reverse transcriptase is probably the best way to "end run" this problem. The options in this regard are still very limited, but vendors have indicated that this situation should improve in the near future.

5. High assay sensitivity and consistency were achieved with the multiplexing strategy developed for the aging study, despite the use of a coupled RT/pre-PCR step. It remains to be seen if this level of performance can be maintained if dozens of assays are combined in the pre-PCR. If this turns out to be problematic, changes could be made to the protocol to alleviate PD formation, e.g., adding forward PCR primers only after the reverse transcriptase has been inactivated, or incorporating a generic pre-PCR primer sequence into the RT primers. Use of a hot-start-protected reverse transcriptase might obviate any amendments to the protocol. AccuRT, evaluated in

the digital PCR work, may be worth revisiting for the pre-PCR application, since the enzyme's low 5'-exonuclease activity is only an issue for TaqMan qPCR.

6. The concept of normalizing expression measurements to an endogenous reference gene breaks down at the single-cell level. Use of RNA standards enables absolute transcript quantitation with the preamp protocol. Standards are not hard to make using *in vitro* transcription reactions, although this is still not a widespread practice. Digital PCR provides absolute copy-number readouts directly. Some of this advantage is lost due to the need to calibrate RNA-to-cDNA conversion efficiency for each assay target. This could change if future RT enzymes ever match the consistent, near-optimal transcription efficiency obtained with *Taq* polymerase.

7. Using flow cytometry and isolation-free mRNA recovery, a thousand single-cell mRNA samples can easily be prepared in the course of one FACS session. Even pipelining the RT/pre-PCR steps and performing five or six experiments a day, it would take weeks to process this number of cell lysates using the analysis protocols described here. In the near future, then, sample preparation should not be a bottleneck in single-cell studies targeted at hematopoietic cells.

8. Preamplification PCR is more scalable with respect to multiplexing than the chip assay, since the latter is limited by the number of TaqMan probe colors which can be discriminated in one reaction. With that being noted, the throughput of the methods is best compared in terms of expression measurements rather than cells analyzed. Fully pipelined, both protocols require about 2 hours per experiment. With preamp, up to 96 measurements can be taken in each experiment using a standard qPCR instrument. The number of data points yielded by each chip experiment depends on

the level of multiplexing. Using a duplex assay, 24 measurements can be made per PCR (12 samples × 2 channels). If primer dimer can be contained, it should be straightforward to do 5-plex analysis in the chip, to increase this to 60 data points.

9. The cost of the preamp assay is driven by qPCR reagent costs; a full 96-well plate of reactions runs less than $100. Reagent use is minimal in the digital PCR assay, but the microfluidic chips are still priced in the hundreds of dollars. Chip prices should decline substantially as the technology matures and production volumes increase.

Currently, the preamplification method looks more promising than digital PCR for single-cell gene profiling work, based on its low cost and scalability to high-order multiplexing. Efforts are underway to adapt the preamp protocol developed during the thesis work for use with a new Fluidigm chip, the "Dynamic Array." Using microfluidics to automate the qPCR-analysis phase of the protocol, a 100-fold improvement in throughput should be attainable with this approach. Preamplified cDNA and TaqMan assays are combined in the Dynamic Array to create a matrix of sample-assay combinations, which are then evaluated by real-time PCR using an integrated thermocycler-imaging system. In the production version of the chip, 48 samples can be combined with 48 assays, allowing 2304 qPCR measurements in the course of a single experiment. A 96 × 96 version of the chip is forthcoming. With the aid of this technology, it should soon become feasible to conduct gene-profiling studies encompassing thousands of individual cells and dozens of different assay targets.

Chapter 5

TRANSCRIPTION FACTOR PROFILING IN INDIVIDUAL HEMAPOIETIC PROGENITORS BY DIGITAL RT-PCR*

Luigi Warren, David Bryder, Irving L. Weissman, and Stephen R. Quake

5.1 Summary

We report here a systematic, quantitative population analysis of transcription factor expression within developmental progenitors, made possible by a microfluidic chip-based "digital RT-PCR" assay that can count template molecules in cDNA samples prepared from single cells. In a survey encompassing five classes of early hematopoietic precursor, we found markedly heterogeneous expression of the transcription factor PU.1 in hematopoietic stem cells and divergent patterns of PU.1 expression within $flk2^-$ and $flk2^+$ common myeloid progenitors. The survey also revealed significant differences in the level of the housekeeping transcript GAPDH across the surveyed populations, which demonstrates caveats of normalizing expression data to endogenous controls and underscores the need to put gene measurement on an absolute, copy per-cell basis.

---

* This chapter was originally published in Proceedings of the National Academy of Sciences, 103(47), 2006. The references for this chapter appear in the bibliography.

5.2 Introduction

Stem cells give rise to terminally differentiated cells of diverse types through a stepwise process involving the production of intermediates of progressively restricted lineage potential. This unfolding program is controlled by a transcriptional regulatory network: a chemical state machine with sequencing logic implemented by cross-regulating transcription factors, the states of the network realized in the abundance profile of these regulatory molecules. Transitions between preferred states are brought on by intrinsic metastability, stochastic fluctuation, and external signals [10, 115, 116]. Understanding the behavior of these networks is the key to understanding development itself. A prerequisite is the ability to characterize network states quantitatively, but the sensitivity of current gene profiling methods is not fully adequate to this task. Here we report on a study of hematopoietic stem cells (HSCs) and other early blood progenitors using an assay that overcomes the sensitivity problem.

Conventional gene-expression assays typically require thousands of cells' worth of RNA as analyte. Developmentally interesting cells, especially stem cells, are not always easily isolated in such quantities. More fundamentally, population-average expression data provide an incomplete picture, because functionally significant variations in regulatory-network state undoubtedly exist in cell types defined on the basis of a few phenotypic criteria. One consequence of this is that population-averaged experiments are subject to systematic errors in interpretation: although one can reliably infer qualitative trends from their results, it is difficult if not impossible to generate precise, quantitative results. Modern theories of systems biology are able to make quantitative predictions, and to test these theories quantitative data are required. Flow cytometry has transformed the study of cellular

differentiation by revealing diversity in the patterns of surface protein expression within populations of superficially similar cells. Similarly, one would like to survey transcriptional network states within populations cross-sectionally, which is possible only by measuring gene expression in individual cells.

In principle, RT-PCR has the sensitivity required for single-cell gene-expression analysis. However, the quantitation of rare messages, such as those for transcriptional regulators, pushes the limits of the art. Published single-cell protocols tend to be elaborate in terms of assay validation and practice [74]. To address this problem, we have developed a highly sensitive quantitative RT-PCR assay based on standard 5'-nuclease probe (TaqMan) chemistry and primer–probe design rules. The method uses a commercially available microfluidic chip to partition individual cDNA molecules into discrete reaction chambers before PCR amplification (figure 5.1). In effect, the chip performs a massively parallel limiting-dilution assay, a form of "digital PCR" [85]. In conventional quantitative PCR, quantitation is based on the number of amplification cycles required for dye fluorescence to reach a given threshold. Slight variations in amplification efficiency between reactions are magnified because of the exponential character of PCR; for this reason, interassay comparisons are only valid if gene-of-interest measurements are normalized to measurements on endogenous controls or synthetic standards [78]. In digital PCR, quantitation relies on binary, positive/negative calls for each subreaction within the partitioned analyte, affording an absolute readout of DNA copy number with single-molecule resolution. Applying the chip assay to cDNA generated from synthetic RNA standards, we have demonstrated that the sensitivity and linearity of quantitation is sufficient to address transcript measurements on single cells (see Materials and Methods).

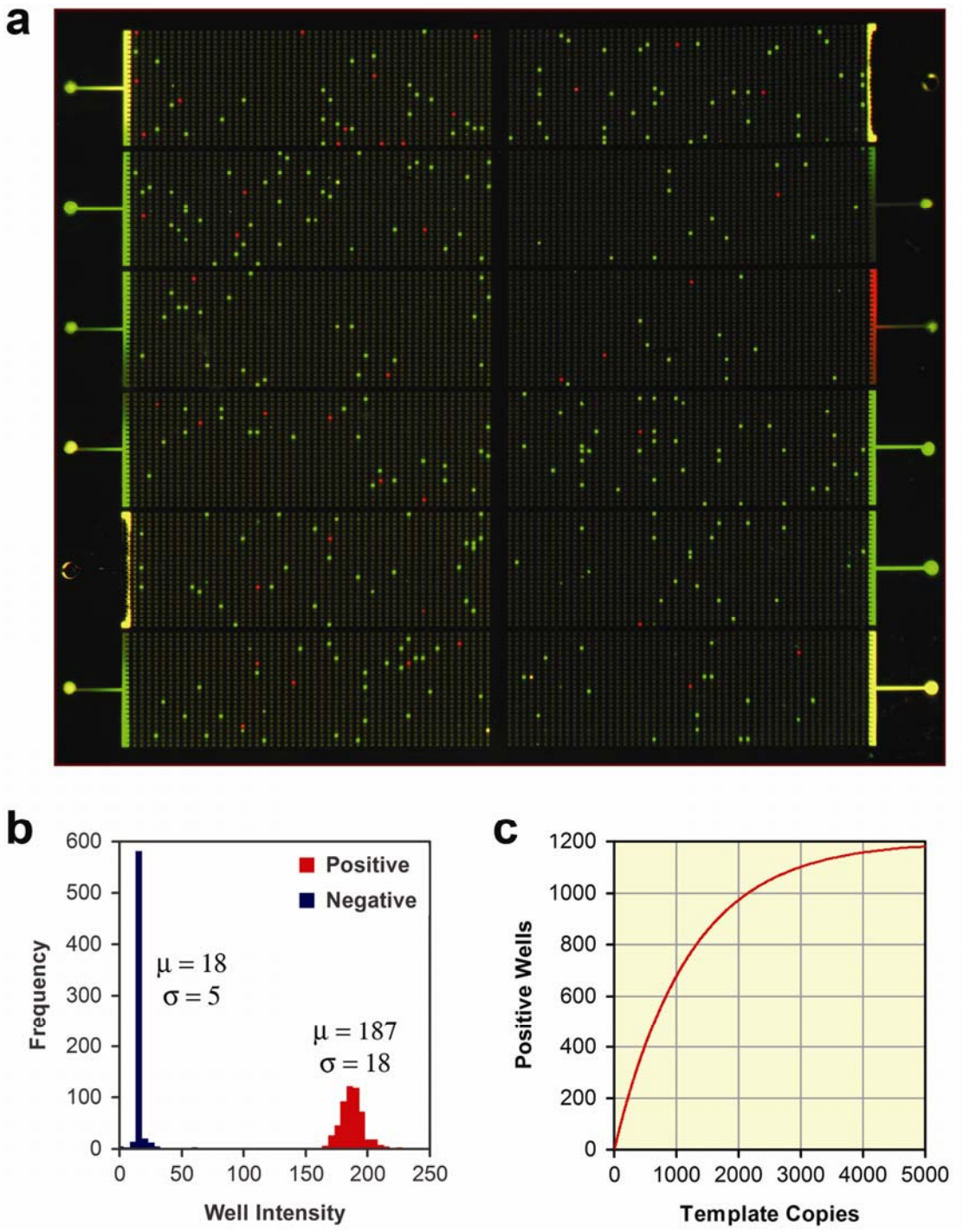

Figure 5.1. The Digital Array chip. (a) A PCR end-point scan of a chip. In this false-color image, the FAM signal (GAPDH) is shown in green and the Cy5 signal (PU.1) in red. The 12 samples analyzed here correspond to cDNA preparations derived from individual HSCs. Within a sample panel, 7.5 μl of analyte is partitioned into 1200 isolated reaction chambers ("wells") prior to PCR. At the cDNA concentrations encountered in the

single-cell survey, almost all wells capture either zero or one template molecules; after PCR, the count of high-intensity wells provides a readout of the number of template molecules in the original, unamplified sample. (b) Histogram of well intensities within a single Digital Array panel after 40 cycles of PCR. The analyte was cDNA reverse transcribed from PU.1 runoff transcript. Positive/negative calls are based on an operator-defined threshold. (c) Digital PCR response characteristic. In the digital assay, positive reactions signal compartments capturing one or more template molecules at the start of the PCR. At high template concentrations, a significant fraction of compartments start out with multiple template copies and the response curve becomes increasingly non-linear. For a panel with *n* compartments, the number of input molecules, *x*, can be computed from the readout of positive compartments, *y*, using the equation $x = \log(1 - y/n)/\log(1 - 1/n)$ (see Materials and Methods).

We applied the digital assay to a single-cell gene-expression survey focused on the early steps of hematopoiesis. After staining with fluorescent antibodies, flow cytometry can be used to fractionate blood progenitors based on membrane-protein expression. The lineage potential of many different subsets has been investigated by using clonal assays, resulting in schema for the prospective isolation of progenitors based on surface antigen profiles. Immunophenotyped cells are readily sorted into individual tubes for single-cell analysis [49]. In our experiments, cells were sorted directly into RT-PCR buffer; we subsequently added primers for the genes of interest, reverse transcribed the RNA, and quantitated the cDNA in the digital PCR chip (figure 5.2). The study encompassed murine blood progenitors belonging to the following canonical populations: HSCs, common lymphoid progenitors (CLPs), common myeloid progenitors (CMPs), and megakaryocyte–erythroid progenitors (MEPs) [117-122]. (Figure 5.3 positions these cell types within the classical model of the hematopoietic lineage tree.) Some recent work argues that the CMP subset is heterogeneous, functional diversity being correlated with differential expression of the cytokine receptor flk2 [23, 123]. We therefore decided to look at $flk2^+$ and $flk2^-$ CMP subsets, to see whether their gene-expression profiles were different. Our survey includes data from 116 individual cells, about two dozen from each of the five cell types of interest (HSC, CLP, CMP/$flk2^+$, CMP/$flk2^-$, and MEP).

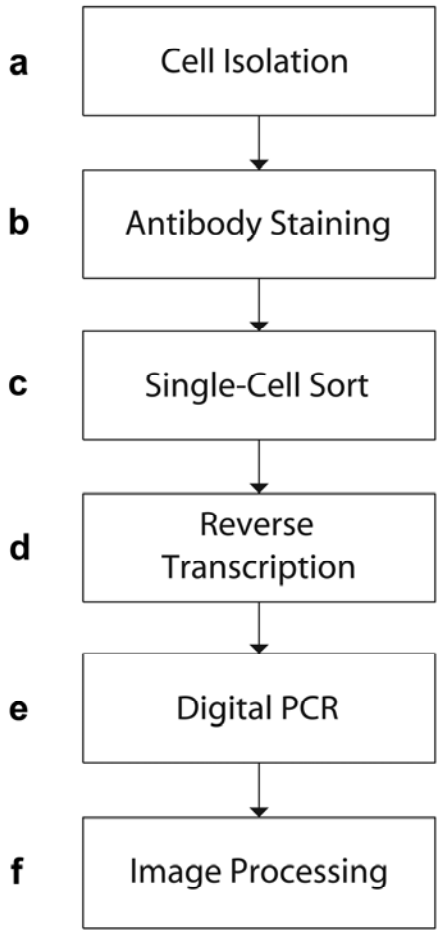

Figure 5.2. Experimental procedure used in the single-cell survey. (a) Cells are harvested from mouse bone marrow, then enriched for c-kit$^+$ early progenitors by immunomagnetic separation. (b) Purified cells are stained with a panel of fluorescent antibodies to surface proteins whose expression patterns define progenitor types of interest. (c) FACS is used to dispense individual immunophenotyped cells into RT-PCR buffer, where they undergo hypotonic/detergent lysis, releasing their mRNA. (d) Gene-specific primers and probes, reverse transcriptase, and DNA polymerase are added to the lysates, and the samples are reverse transcribed in a standard thermocycler. (e) Completed reactions are loaded into the digital PCR chip, which is pneumatically partitioned and thermocycled on a flat block. (f) End-point fluorescence images of the chip are processed to read out the levels of the transcripts targeted by the TaqMan assays.

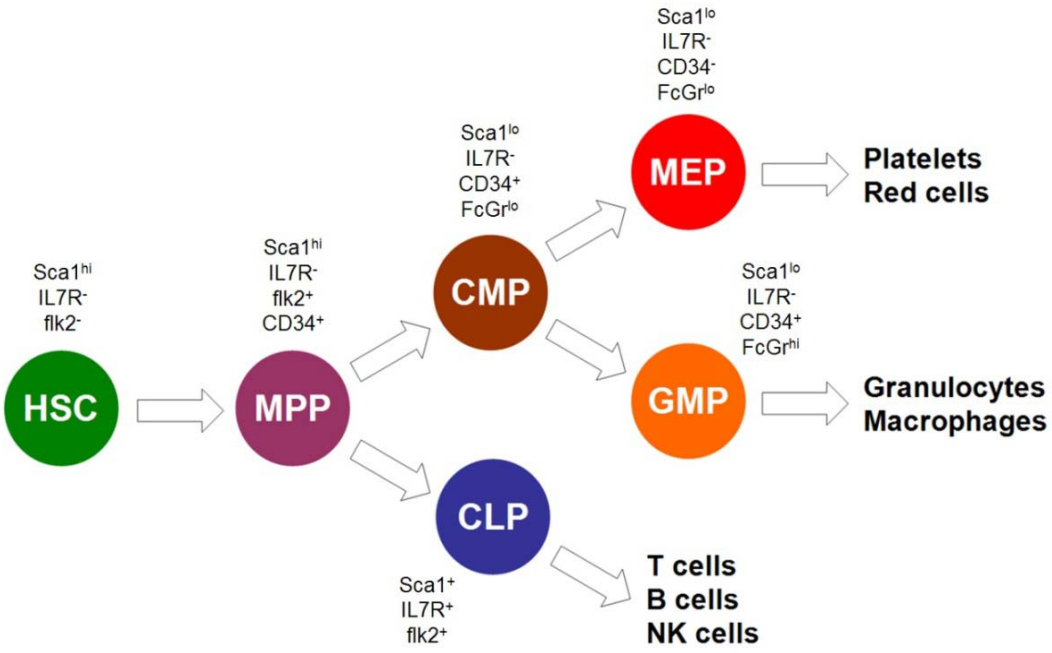

Figure 5.3. Early progenitors in the hematopoietic lineage tree, according to the classical model of blood differentiation. Upon activation, self-renewing hematopoietic stem cells (HSCs) give rise to a proliferating population of multipotent progenitors (MPPs). Two more restricted oligopotent precursors are derived from the MPP: the common myeloid progenitor (CMP), and the common lymphoid progenitor (CLP). The CMP population forks into still-more restricted oligopotent precursors: the megakaryocyte-erythroid progenitor (MEP), and the granulocyte-macrophage progenitor (GMP). The CLP develops into the unipotent precursors of B and T cells directly. Phenotypically, these early progenitors are all positive for the stem-cell factor receptor, c-kit, and negative for the lineage-specific markers which characterize more mature cells. The surface marker phenotypes which distinguish the different progenitor types within the Lineage$^-$ c-kit$^+$ compartment are indicated in the figure.

We measured the levels of two transcripts within every cell: a transcription factor, PU.1, and a housekeeping gene, GAPDH. PU.1 is known to be a major regulator of hematopoiesis. Its best understood role is the promotion of granulocyte–macrophage fate: expressed at high levels, PU.1 activates granulocyte–macrophage differentiation gene batteries, and PU.1 upregulation seems to be instrumental in funneling CMPs toward the granulocyte–macrophage progenitor (GMP) lineage [124, 125]. PU.1 is also thought to play other, context-dependent roles in blood differentiation at intermediate levels of expression [126, 127]. GAPDH encodes a glycolytic enzyme, glyceraldehyde-3-phosphate dehydrogenase. This gene commonly serves as an endogenous control in quantitative RT-PCR assays. In this practice, the readout for every gene of interest is normalized to the GAPDH signal, on the idealized assumption that GAPDH expression is uniform across cell types. Our assay reports absolute transcript levels, in copies per cell, so we did not need a reference for PU.1 quantification. However, we were interested in finding out to what extent GAPDH expression is truly independent of cell type. In addition, we expected levels of PU.1 to be so low that Poisson noise might obscure any clues our analysis would give to the general character of expression distributions. GAPDH is a high-abundance transcript, so we anticipated that its expression would be more informative in this regard.

5.3 Results and Discussion

We carried out on-chip assays using RNA runoff template to measure the efficiency and reproducibility of the digital RT-PCR assay. The estimated RNA-to-cDNA conversion efficiency was 0.50 ± 0.10 for PU.1 (CV = 20%) and 0.29 ± 0.09 for GAPDH (CV = 29%). We found an interassay CV of ~10% in similar trials using DNA standards, so some of the variability in the efficiency estimates came from the chip itself. Variation in the loaded

sample volume probably accounts for most of the chip-related technical noise. The limiting factor in the precision of the digital RT-PCR method is likely to remain the technical variability of reverse transcription [86].

The results of the single-cell survey are summarized in figure 5.4. All cell types gave mean readouts for GAPDH and PU.1 substantially exceeding the background of false positive signals detected in No Template and No RT control panels (table 5.1). PU.1 expression is highly elevated in the CMP/flk2^{+} subset, and strongly downregulated in the MEPs (table 5.2). The other three subsets show intermediate levels of expression, but the CMP/flk2^{-} resembles the MEP, with a less pronounced downshift. We used the Kolmogorov–Smirnov (K-S) test to measure the resemblance between the PU.1 data sets (table 5.3). The HSC distribution bears a strong resemblance to the distributions in the CLP and CMP/flk2^{-} cell types. The CMP/flk2^{+} stands alone: the P value for similarity was <0.01 in every comparison involving this set.

Table 5.1. False positives

	NTC (n=6)						No RT (n=3)		
GAPDH	2	1	1	4	3	1	3	2	2
PU.1	0	0	0	0	0	0	1	0	0

Counts of false-positive wells within NTC and single-cell No RT control panels. The equivalent copies-per-cell readouts would be double these values, as the loaded sample volume is half the RT reaction volume.

Table 5.2. Descriptive statistics (PU.1)

	HSC	CLP	CMP/flk2$^+$	CMP/flk2$^-$	MEP
Number of Samples	21	23	25	24	23
Median cDNAs/cell	6.0	4.1	14.1	3.0	2.0
Mean cDNAs/cell	8.5	5.5	21.7	6.5	3.7
Coefficient of Variation	95%	82%	120%	149%	180%
Geometric Mean cDNAs/cell	6.0	n/a	14.8	n/a	n/a
Geometric Standard Deviation	2.3	n/a	2.4	n/a	n/a

Descriptive statistics for the PU.1 expression single-cell data. The geometric mean and geometric standard deviation correspond to the back-transformed mean and standard deviation of the log-transformed data. These two statistics are more informative than the mean and standard deviation for lognormally distributed data. (Their values are mathematically undefined for data sets which include zero values, as was the case with the CLP, CMP/flk2$^-$ and MEP data sets here.)

Table 5.3. Subset comparisons (PU.1)

	HSC	CLP	CMP/flk2$^+$	CMP/flk2$^-$	MEP
HSC	1.00	0.89	0.00	0.37	0.03
CLP	0.89	1.00	0.00	0.89	0.20
CMP/flk2$^+$	0.00	0.00	1.00	0.00	0.00
CMP/flk2$^-$	0.37	0.89	0.00	1.00	0.67
MEP	0.03	0.20	0.00	0.67	1.00

Results of pairwise Kolmogorov-Smirnov comparison tests between PU.1 expression data sets. The tabulated values are the significance levels assigned by the test to the null hypothesis that the data from the two compared sets come from the same underlying distribution. A low P value (<0.05) is evidence that the distributions differ significantly.

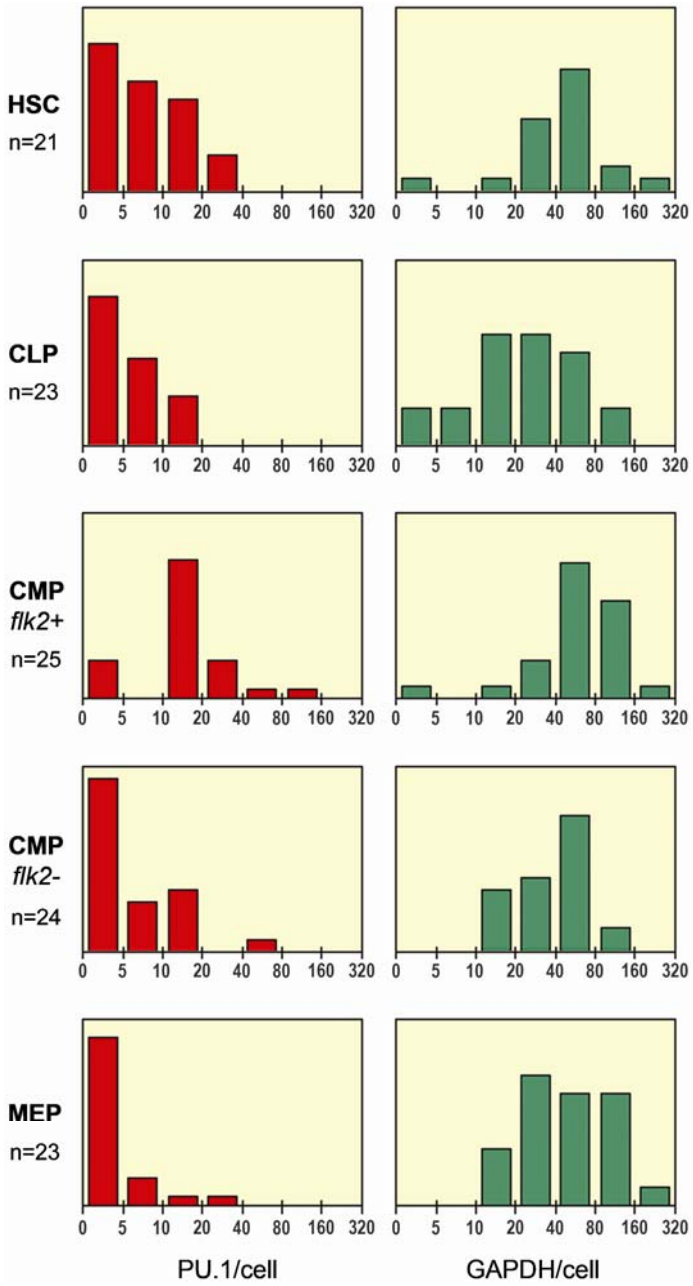

Figure 5.4. Gene expression in cDNA copies per cell, by cell type. The histograms show the number of individual cells in each subset that expressed PU.1 and GAPDH within the indicated bin ranges. PU.1 expression is heterogeneous in the stem cells, upregulated in the CMP/flk2$^+$ cells, downregulated in CMP/flk2$^-$ cells, and sharply downregulated in the MEPs. The similarity between PU.1 expression in CMP/flk2$^-$ and MEP cells is consistent with the possibility that flk2$^-$ CMPs are already biased towards the MEP lineage choice. GAPDH expression was significantly elevated in the CMP/flk2$^+$ cells, adding weight to the inference that the flk2$^-$ and flk2$^+$ CMP subpopulations are functionally distinct.

A previous, nonquantitative single-cell study of blood progenitors found that HSCs display variegated expression of transcripts normally associated with downstream lineages, including PU.1 [50]. This could represent nonproductive, "leaky" transcription, if the loci for downstream lineages are kept in a default, open chromatin state until fate commitment [128]. Alternatively, "noisy" transcription might be a mechanism for symmetry breaking, priming daughter cells toward diverse fates when the stem cell starts to proliferate and differentiate [129]. The distinction between leaky or noisy transcription and regulated transcription may be hard to draw; our data suggest that wide variations in message abundance between individual cells are the rule rather than the exception. However, the K-S comparison results and the relatively broad profile of the PU.1 distribution in the HSC subset argue that PU.1 expression is either loosely regulated or heterogeneously regulated within the stem-cell compartment.

A keystone of the classical model of hematopoietic differentiation is the division of progenitors into two major populations downstream of the multipotent progenitor (MPP): the lymphoid-restricted CLP, which gives rise to pro-B and pro-T cells, and the myeloerythroid-restricted CMP, which gives rise to granulocyte–macrophage progenitors and MEPs [130]. It has recently been claimed that the canonical CMP population is internally heterogeneous with respect to lineage potential [23]. According to this research, the expression level of the cytokine receptor flk2 is a marker for functional divergence: the $flk2^{+}$ CMP compartment is $PU.1^{hi}$, has lost MEP potential, and retains lymphoid as well as myeloid potential; $flk2^{-}$ CMPs comprise mostly $PU.1^{lo}$ cells with predominantly MEP potential. Our measurements reveal a sharp divergence in PU.1 expression within the $flk2^{-}$ and $flk2^{+}$ CMP subsets. The GAPDH results for these subsets, discussed below, add further evidence that they are nontrivially distinct, as the 2D gene-expression plot in figure 5.5

makes clear. The similarity between PU.1 expression in the CMP/flk2$^-$ cells and the MEPs meshes with the observation that the bulk of the flk2$^-$ CMP compartment is already megakaryocyte-erythroid-lineage restricted.

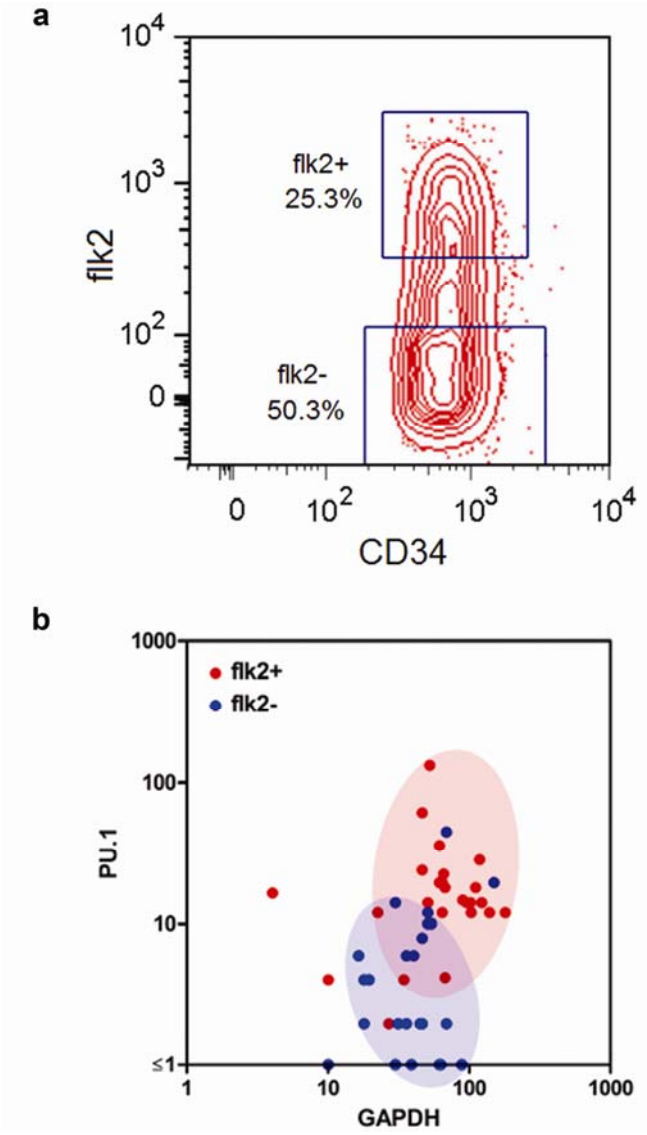

Figure 5.5. Resolution of flk2$^-$ and flk2$^+$ CMP populations based on gene expression. (a) The sort gates used to fractionate CMP cells into flk2$^+$ and flk2$^-$ subsets (biexponential plot). These gates were applied after first selecting Lineage$^-$ c-kit$^+$ Sca1^{lo} IL7R$^-$ CD34$^+$ FcGr^{lo} cells. (b) The distribution of GAPDH and PU.1 expression in the flk2$^+$ and flk2$^-$ CMP subsets, as determined by single-cell analysis. The shaded ellipsoids capture >85% of the observations within each set.

The expression of GAPDH was not constant across the six cell types examined, with the subset mean expression levels varying over a 2-fold range (table 5.4). K-S tests show that the differences are statistically significant (table 5.5). In 4 of 10 pairwise comparisons between subsets, the hypothesis that the data came from the same underlying distribution had a P value below 0.05. The CMP/flk2$^+$ subset had the highest GAPDH expression, and it was also the best resolved from the other subsets by the K-S measure. The variation in GAPDH level within these closely related subsets highlights a problem with the use of endogenous controls in RT-PCR quantitation. Normalization to the GAPDH signal reduces the apparent magnitude of PU.1 upregulation in the CMP/flk2$^+$ cell type, and equalizes the differences in mean expression between the HSC, CLP and CMP/flk2$^-$ types (table 5.6). It is impossible to say, at this level of analysis, whether such equalization is justified. Although normalized measurements are not necessarily less informative than absolute measurements, no two housekeeping genes can reasonably be expected to show the same dependence on cell type. No consensus exists as to the best choice of endogenous control and, indeed, no one gene is likely to be a good reference for every application [131]. Weighted normalization schemes based on multiple housekeeping genes have been proposed [83]. Still, it can be argued that this only makes the problem of standardization worse. The uncertainty which the practice of normalization introduces into gene measurement comparisons can only be resolved by a move to absolute quantitation, either through the use of quantitated synthetic controls (e.g., purified PCR product or RNA runoff transcript), or by the adoption of techniques which yield absolute measurements directly, such as the one described here.

Table 5.4. Descriptive statistics (GAPDH)

	HSC	CLP	CMP/flk2$^+$	CMP/flk2$^-$	MEP
Number of Samples	21	23	25	24	23
Median cDNAs/cell	45	26	65	43	45
Mean cDNAs/cell	58	37	72	47	61
Coefficient of Variation	86%	102%	58%	63%	78%
Geometric Mean cDNAs/cell	43	22	57	39	46
Geometric Standard Deviation	2.5	3.1	2.3	1.8	2.2

Descriptive statistics for the GAPDH single-cell expression data. The geometric mean and geometric standard deviation correspond to the back-transformed mean and standard deviation of the log-transformed data. These two statistics are more informative than the mean and standard deviation for lognormally distributed data.

Table 5.5. Subset comparisons (GAPDH)

	HSC	CLP	CMP/flk2$^+$	CMP/flk2$^-$	MEP
HSC	1.00	0.01	0.04	0.93	0.67
CLP	0.01	1.00	0.00	0.07	0.20
CMP/flk2$^+$	0.04	0.00	1.00	0.03	0.06
CMP/flk2$^-$	0.93	0.07	0.03	1.00	0.33
MEP	0.67	0.20	0.06	0.33	1.00

Results of pairwise Kolmogorov-Smirnov comparison tests between GAPDH expression data sets. The tabulated values are the significance levels assigned by the test to the null hypothesis that the data from the two compared sets come from the same underlying distribution. A low P value (<0.05) is evidence that the distributions differ significantly.

Table 5.6. Gene expression by subset

	HSC	CLP	CMP/flk2$^+$	CMP/flk2$^-$	MEP
Number of Samples	21	23	25	24	23
Mean PU.1 cDNAs/cell	8.5	5.5	21.7	6.5	3.7
Mean GAPDH cDNAs/cell	58	37	72	47	61
PU.1/GAPDH Ratio	0.15	0.15	0.30	0.14	0.06

It has recently been reported that the abundance of gene transcripts is lognormally distributed at the single-cell level [36]. We used several standard normality tests to ask whether the expression of GAPDH within each population was compatible with a normal or lognormal distribution (table 5.7). In all but the CMP/flk2$^+$ population, the lognormal model was clearly preferred. Lognormal distributions can arise when normally distributed variations compound multiplicatively, as might occur during the sequential steps of biochemical synthesis [132]. Intermittent, exponentially distributed bursts of biosynthesis can also give rise to similar, nonnormal, positively skewed distributions [11] which are also consistent with our observations. The geometric standard deviations for the GAPDH data sets are in the range of 1.8–3.1 (table 5.4), which indicates that transcript levels can routinely fluctuate over a full one-log range. It might seem surprising that robust behavior can be achieved by a system in which signal levels vary so widely. It must be remembered, however, that a snapshot of mRNA transcript level is not necessarily a true measure of the abundance of the corresponding protein. Messenger transcripts generally turn over much faster than the proteins they encode, which implies that protein expression may be buffered against stochastic fluctuations at the mRNA level. Redundancy and distributed control are additional strategies by which cells could make up for the inherent sloppiness of biochemical signaling [14]. If so, efforts to "reverse engineer" the transcriptional circuits controlling development

must ultimately address the synthesis of quantitative observations on multiple transcription factors within single cells. The power of flow cytometric population analysis has increased as the technology for multiplexing has improved; we expect the same to be true of single-cell surveys conducted at the transcriptional network level. In hematopoiesis, cell fate decisions depend on the coordinate activity of multiple transcription factors [133].

Table 5.7. Normality tests

		HSC	CLP	CMP/flk2$^+$	CMP/flk2$^-$	MEP
Raw Data	Shapiro-Wilk	0.00/0.00	0.00	0.49/0.35	0.00	0.00
	Anderson-Darling	0.00/0.00	0.00	0.42/0.27	0.02	0.01
	Lillefors	0.00/0.00	0.00	0.02/0.01	0.17	0.02
	Jacque-Bera	0.00/0.00	0.00	0.53/0.43	0.00	0.01
Log Data	Shapiro-Wilk	0.00/0.13	0.35	0.00/0.12	0.80	0.81
	Anderson-Darling	0.00/0.10	0.44	0.01/0.17	0.49	0.66
	Lillefors	0.02/0.08	0.53	0.01/0.23	0.55	0.52
	Jacque-Bera	0.00/0.21	0.58	0.00/0.13	0.91	0.65

Significance levels assigned by four different normality tests to the GAPDH expression data. Low P values (<0.05) favor rejection of the normality hypothesis. In the case of the HSC and CMP/flk2$^+$ data sets, tests were conducted on the complete data set (first tabulated value), and on the data set with a single, very low outlier data point removed (second value). The tests were applied to both raw and log-transformed expression data. With log-transformed input, the assigned significance levels pertain to the hypothesis of lognormality rather than normality. The normality hypothesis is strongly disfavored for all except the CMP/flk2$^+$ data set. The CLP, CMP/flk2$^-$ and MEP data sets were highly compatible with a lognormal distribution. Lognormality scores reached significance for the remaining HSC and CMP/flk2$^+$ data sets if their lowest outlier data points were excluded from the analysis.

When the targets for quantification are present at of the order of ten copies, a subdivision of the sample to permit independent single-plex assays introduces substantial measurement noise. For several reasons, digital PCR offers improved scope for high-order multiplexing relative to conventional quantitative PCR. In a standard multiplex PCR, mismatched transcript levels can lead to competitive inhibition of reactions involving less abundant targets, which is typically addressed by adjusting primer concentrations so that the amplification of abundant targets is primer limited. Such fine-tuning may not be practical in single-cell surveys, if transcript levels vary widely on a cell-by-cell basis, and is obviated in the digital assay. A second benefit arises from the concentration of template molecules because of reaction partitioning, which ameliorates the impact of primer–dimer side reactions. On the readout side, the digital assay lends itself to bar-coding schemes, whereby distinct probe color combinations are assigned to each target [13].

5.4 Conclusion

If cross-sectional analysis of cell populations at the transcriptional network level were to become routine, the impact on developmental studies could be profound. In the near term, PCR-based methods cannot be expected to yield single-cell expression data with the speed and economy of flow cytometry. This must be set against the consideration that transcription factor studies provide data bearing directly on the internal decision-making machinery of the cell. In a small-scale survey we could easily resolve two subpopulations within a progenitor type, the CMP, which has until recently been considered homogeneous. Here we were able to focus the analysis based on recent findings from the hematopoiesis literature. In principle, however, the heterogeneity in PU.1 levels within the CMP compartment could have been detected in a "blind" single-cell survey. The scale of survey

required to detect network state diversity will depend on several factors, including (1) the relative frequencies of divergent subsets, (2) the magnitude and sharpness of the expression differences, and (3) the extent to which such differences are correlated across transcripts and surface markers analyzed in the survey. If the case of PU.1 expression in the CMP is representative, indications of heterogeneity should emerge after looking at a few tens of cells, and surveys at the 100- to 1,000-cell level may offer significant insight into population substructure.

We have shown that it is possible to extend the sensitivity of quantitative RT-PCR to permit profiling of transcription factor expression within individual cells. This opens the door to sophisticated regulatory network analysis on even the rarest developmental progenitors. The dynamic range of the chip assay is suited to measuring the gamut of expression levels for regulatory genes, whether working from single-cell samples or from higher numbers of cells prepared at appropriately scaled concentration. By combining flow cytometry and digital RT-PCR, we can put gene-expression measurements on an absolute, copy-number-per-cell basis. The attainment of this "gold standard" should facilitate the spread of public databases cataloguing cell-type-specific expression data. Our assay can also support the progressive refinement of the taxonomies underlying such resources through the single-cell survey approach, helping to uncover diversity at the level of the cell's most delicate apparatus, the transcriptional regulatory network.

5.5 Materials and Methods

5.5.1 Microfluidic Digital PCR Chip

The single-cell measurements reported here were made using the Digital Array chip (Fluidigm, South San Francisco, CA). This single-use device supports the simultaneous analysis of 12 samples. Within each sample panel, fluid is distributed into parallel, dead-end channels under pneumatic pressure. After the load step, a comb valve with teeth at right angles to these channels is actuated, deflecting an elastomeric membrane down to partition the panel into 1200 isolated reaction chambers. The chip is then thermocycled, carrying out a total of 14,400 PCRs at once. A microarray scanner is used to image the chip at the end point of PCR. If a panel holds $\ll$1200 copies of template at the start of the PCR, the copy number can be read out accurately just by counting positive reactions. At higher DNA titers, a significant fraction of the reaction chambers capture more than one copy of template, and there is no longer a simple correspondence between positive reactions and individual template molecules. However, unless a panel is at or near saturation, template abundance can still be calculated with acceptable precision (see Digital PCR Response Characteristic, below). The quantitative dynamic range of the Digital Array is therefore about three logs: from a single copy to on the order of a thousand copies. This should be sufficient for single-cell quantification of all but the most abundant mRNA species [24].

5.5.2 Synthetic Standards

PU.1 and GAPDH RNA runoff transcripts were made for use in evaluating the RT efficiency and PCR amplification efficiency of our assays. The transcripts were designed to flank the amplicon regions of the TaqMan assays by at least 100 bases on each side, so that the secondary structure context seen by the reverse transcriptase would be similar to that in

lysate-based reactions. PCR products incorporating a T7 RNA polymerase promoter were used as template for the runoff reactions, which were done with the MEGAscript T7 kit (Ambion, Austin, TX). The concentration of the purified RNA was measured by UV absorbance spectroscopy, and the percentage of full-length template was estimated with a capillary electrophoresis system (Experion; Bio-Rad, Hercules, CA).

The PCRs used to make templates for runoff transcription were based on Mouse GAPDH DECAtemplate and Mouse Thymus PCR-Ready cDNA (Ambion). The PCR primers were as follows (T7 promoter tails underlined): for PU.1, 5'-TAATACGACTCACTATAGGGAGACTGACCCACGACCGTCCAGT-3' (forward) and 5'-TTGTCCTTGTCCACCCACCA-3' (reverse); for GAPDH, 5'-TAATACGACTCACTATAGGGAGCCCATCACCATCTTCC-3' (forward) and 5'-CTGTAGCCGTATTCATTGTC-3' (reverse).

5.5.3 TaqMan Assay Design

All RT-PCR data reported here were obtained by using duplex PU.1/GAPDH TaqMan assays. Primers and probes were designed with commercial software (Beacon Designer; Premier Biosoft, Palo Alto, CA), accepting the default T_m criteria for TaqMan assay design, which are based on a standard 60 °C annealing/extension step during the PCR. Primers were chosen so that the amplicon range was free of predicted secondary structure, as this is thought to impede efficient reverse transcription. To minimize background signal from genomic template, the PU.1 assay was designed so that the forward primer straddled an exon splice site. Assays were validated empirically using conventional quantitative PCR standard curve analysis with runoff transcript as template. Primers were at 100 nM concentration and probes at 50 nM concentration in all of the reported experiments. Oligonucleotides were

synthesized by Integrated DNA Technologies (Coralville, IA). The oligonucleotides used in the TaqMan assays were as follows: for PU.1, 5'-CATAGCGATCACTACTGGGATTTC-3' (forward primer), 5'-GGTTCTCAGGGAAGTTCTCAAA-3' (reverse/RT primer), and 5'-CGCACACCATGTCCACAACAACGA-3' (Cy5-labeled probe); for GAPDH, 5'-CCAATGTGTCCGTCGTGGATC-3' (forward primer), 5'-GCTTCACCACCTTCTTGATGTC-3' (reverse/RT primer), and 5'-CGTGCCGCCTGGAGAAACCTGCC-3' (FAM-labeled probe).

5.5.4 RT Efficiency Measurements

For on-chip standard curve assays, equimolar mixtures of PU.1 and GAPDH runoff transcript were added to RT-PCR buffer and the same digital RT-PCR protocol used on the cell lysates (described below) was executed on the samples. Three identical on-chip standard curve experiments were run, with each chip bearing four sets of three samples, at nominal template concentrations of 12.5, 25, 50, and 100 copies per microliter. All samples were derived from the same master mix; each individual sample was reverse transcribed in a separate tube. Data were recovered from 35 of the 36 panels in these chips.

5.5.5 Cell Isolation and Staining

A bone marrow cell suspension was prepared from five 8- to 12-week-old C57BL/6 mice. The suspension was filtered through a nylon membrane and contaminating red cells were lysed with ACK. The isolate was enriched for c-kit-positive early progenitor cells by immunomagnetic separation with anti-c-kit MACS beads (Miltenyi Biotec Auburn, CA). The cells were next stained for other surface markers by using the following fluorescent antibodies: CD34 FITC, flk2 phycoerythrin, Lineage phycoerythrin-Cy5 (a mixture of antibodies including CD3, CD4, CD5, CD8, B220, Mac1, Gr1, and Ter119), Sca-1 Cy5.5-

phycoerythrin, FcGr allophycocyanin, c-kit allophycocyanin-Cy7, and IL7Ra biotin. All antibodies were from Ebiosciences (San Diego, CA), except CD34 FITC (Pharmingen, San Diego, CA) and IL7Ra biotin (ILW's laboratory). The cells were then stained with streptavidin QD605 (Quantum Dot, Hayward, CA) to tag the IL7Ra antibodies and resuspended in PBS plus 2% FCS, with propidium iodide added to mark apoptotic cells.

5.5.6 Cell Sorting and Lysis

Cells were sorted to 0.2 mL sample tubes in 12-tube strips by using the FACSAria cell sorter (BD Biosciences, San Jose, CA). Doublets and dead or apoptotic cells were excluded based on forward scatter/side scatter and propidium iodide staining. All cells were sorted using Lineage$^-$ and c-kit$^+$ gates; additional sort criteria used to fractionate the cells into specific progenitor subsets were as indicated in figure 5.3. Individual cells were dispensed into 10 μL aliquots of RT-PCR buffer. The buffer components included a commercial RT-PCR mix (Platinum One-Step Reaction Buffer; Invitrogen, Carlsbad, CA), an RNase inhibitor (Ambion SUPERase-In), and 0.15% Tween 20 detergent. The latter was included as a surfactant to prevent nucleic acids binding the PDMS walls of the Digital Array during the PCR assay. No special cell lysis reagents were added. In tests, the efficiency and reproducibility of cDNA recovery was at least as good using direct hypotonic/detergent lysis in the RT-PCR buffer as obtained using chaotropic lysis with subsequent RNA purification.

5.5.7 Reverse Transcription

Reverse transcription reactions were done at 55 °C for 15 minutes, and followed by a 5 minute, 70 °C step to heat-denature the reverse transcriptase. Completed reactions were stored at -20 °C for later PCR analysis. The RT step was carried out in a 96-well block thermocycler. Three microliters of 5× primer–probe mix was added to each frozen lysate,

after which the samples were spun down and transferred to the preheated thermocycler block. As a precaution to minimize primer–dimer extension by the reverse transcriptase, the samples were warmed to 55 °C before adding 2 μL aliquots of enzyme to the reactions. MMLV RT/*Taq* polymerase enzyme blend (CellsDirect SuperScript III/Platinum *Taq*; Invitrogen) was diluted in RT-PCR buffer to stabilize the enzyme; the final reaction concentration was as directed by the manufacturer.

5.5.8 cDNA Quantitation

Digital Array chips mounted on 75 × 50 mm glass slides were primed for use by filling the control layer with osmolyte (35% PEG 3350). For each assay, 12 stored reverse transcription reactions were thawed, drawn into gel tips, and loaded into a chip under 15 psi pneumatic pressure. The load was performed in a cold room at 4 °C and took ~30 minutes. The sample load step was controlled manually with a 12-port manifold fed from a house air supply and connected to the gel tips by Tygon tubing with custom-made hose adaptors. After the load, the chip was transferred to a flat-block thermocycler; paraffin oil was used to improve thermal contact between the block and the glass-slide base. Samples were partitioned by applying 27.5 psi pneumatic pressure to the control layer comb valve via a gel tip filled with osmolyte solution. The PCR profile included a 3 minute, 95 °C hot start to activate the *Taq*, followed by 40 cycles of a two-step program: 15 seconds at 95 °C (denaturation) and 60 seconds at 60 °C (annealing and extension). After PCR, chips were imaged with an ArrayWoRx microarray scanner (Applied Precision, Issaquah, WA), adapted to accept a chip carrier. Scans were done at 13 μm resolution by using FAM and Cy5 filter sets. We wrote our own software to process the PCR end-point images and compute the template concentrations in each panel. The loaded sample volume in the chip, 7.5 μL (manufacturer's

data), represents half the volume of the reverse-transcribed lysate. All of the single-cell cDNA copy number data reported here was derived by multiplying the calculated template concentration in copies per microliter by the total lysate reaction volume, 15 μL.

5.5.9 Data Analysis

Normality tests were done with XLSTAT (Addinsoft, New York, NY). The test input consisted of the reported cDNA copy number for each cell in the set (normal test), or the log of the copy number (lognormal test). We wrote software to perform expression data set comparisons based on the K-S routines given in Numerical Recipes in C [134]. When used to compare two data sets, the algorithm calculates the maximum absolute distance between their respective cumulative distributions, and computes from this measure the significance of the null hypothesis that both data sets came from the same underlying distribution. The analysis does not involve any assumptions about the character of the underlying distributions involved.

5.5.10 Digital PCR Response Characteristic

If template molecules are randomly distributed within n compartments, the probability of any given molecule being trapped in any given compartment is $1/n$. Hence, the probability of a given compartment being empty when there are x template molecules in the sample is $(1 - 1/n)^x$. The expected number of non-empty compartments, y, is therefore as follows:

$$y = n \cdot [1 - (1 - 1/n)^x].$$

Consequently, a readout of y positive compartments gives the following estimate for x:

$$x = \log(1 - y/n) \,/\, \log(1 - 1/n).$$

If the number of positive reactions is small compared to the number of compartments, $x \approx y$. The response curve is therefore close to linear at low template concentrations. The statistical uncertainty in the estimated number of input molecules increases as the fraction of occupied compartments approaches unity. For a Digital Array panel with 1200 compartments, this error remains small even at an input of 4000 molecules (CV ≈ 5%, by Monte Carlo simulation). However, the shallowness of the response curve above 1000 input molecules implies increased sensitivity to uncertainty in positive/negative calls.

Chapter 6

TRANSCRIPTIONAL INSTABILITY IS NOT A UNIVERSAL ATTRIBUTE OF AGING*

Luigi A. Warren, Derrick J. Rossi, Geoffrey R. Schiebinger,

Stuart K. Kim, Irving L. Weissman, and Stephen R. Quake

6.1 Summary

It has been proposed that cumulating somatic mutations contribute to the aging process by disrupting the transcriptional networks which regulate cell structure and function. Experimental support for this model emerged from a recent study of cardiomyocytes which showed a dramatic increase in the transcriptional heterogeneity of these long-lived post-mitotic cells with age. To determine if regulatory instability is a hallmark of aging in renewing tissues, we evaluated gene-expression noise in four hematopoietic cell types: stem cells, granulocytes, and naïve B and T cells. We used flow cytometry to purify phenotypically equivalent cells from young and old mice, and applied multiplexed qRT-PCR to measure the copy number of six different mRNA transcripts in 324 individual cells. There was a trend to higher transcript levels in cells isolated from old animals, but no significant increase in transcriptional heterogeneity with age was found in the surveyed populations. Flow-cytometric analysis of membrane-protein expression also indicated that cell-to-cell variability

---

* This chapter has been accepted for publication in Aging Cell. LAW and DJR contributed equally to this work. The references for this chapter appear in the bibliography.

was unaffected by age. We conclude that large-scale regulatory destabilization is not a universal concomitant of aging, and may be of significance as an aging mechanism primarily in non-renewing tissues.

6.2 Introduction

For years, theoreticians were divided on whether aging results from a regulated developmental program, analogous to growth and sexual maturation, or constitutes an essentially passive, wear-and-tear process. Arguments grounded in evolutionary theory have now largely settled this debate in favor of the wear-and-tear model. The idea that natural selection favors "planned obsolescence," to prevent the aged from competing for resources with their own offspring, appears untenable on close examination, at least in the general case [135, 136]. However, as even robust animals have a limited half-life in the wild state, owing to accident, disease and predation, selection pressure for mutations whose benefits accrue in old age is weak, and ultimately falls below countervailing, entropic forces such as genetic drift. In addition, mutations which bring early-life benefits along with late-life deficits tend to accumulate, the costs being discounted by the attrition curve. Hopes for the discovery of a cellular or endocrine "death clock" have faded with the recognition that aging is not a programmed process, and it now seems likely that a multiplicity of factors contributes to the gradual loss of fitness we call aging. If aging has many causes, then the problem for aging research is to identify and characterize the most important drivers of decline at the different levels of physiology: cellular, tissue, organ, and systemic. For the most part, this project remains a work in progress.

Within the cell, the fundamental mechanism of homeostasis is the network which regulates the coordinated expression of genes underpinning cellular structure and function. The

connectivity of this network is encoded in the sequence and spatial relationship of regulatory elements dispersed through the genome; its activity is mediated by diffusive protein and RNA factors. It is reasonable to ask if this complex governor is vulnerable to age-related decline, either due to intrinsic instability in the chemical circuits, or as a result of cumulative damage to the genome. Relevant to the latter possibility, it has recently been shown that mammalian somatic genomes typically incur dozens of multi-megabase rearrangements over the course of a lifetime [137-139]. This has motivated the hypothesis that chromosomal instability produces major disturbances in gene expression with age, by altering the relationships between genes and distal regulatory elements, and perhaps also by disrupting the large-scale chromatin architecture [137, 140]. If so, the rearrangement-triggered dysregulation events often seen in oncogenesis may represent catastrophic outliers of a more general process underlying aging. Destabilized gene regulation, then, could be the missing link between cumulating DNA damage and age-related loss of cellular function.

While the regulatory instability hypothesis is conceptually attractive, its evaluation presents technical challenges. Standard mRNA assays work with samples equivalent to hundreds or thousands of cells, and the aggregate expression data they yield necessarily obscures the signature of transcriptional heterogeneity or "noise" predicted by the model. Transcriptional instability can only be evaluated by quantifying gene expression in single cells, to see how the variation between cells depends on age. Support for the hypothesis has emerged from a recent study which measured transcript levels in individual cardiomyocytes isolated from the hearts of young and old mice [48]. This work revealed an across-the-board increase in the cell-to-cell variability of transcript levels with age, affecting both tissue-specific and housekeeping genes. A direct link between increased transcriptional noise and genomic instability was not established, but a similar effect was seen in a cell line following exposure

to genotoxic stress. These findings are compatible with the possibility that destabilized gene expression is a central mechanism of aging. It remains to be determined if the regulatory instability detected in cardiomyocytes is a general attribute of aging and, in particular, whether it has a role in the functional decline of renewing tissues such as the blood. The cellular composition of whole tissues changes with age [141-143], hindering appraisal of cell-intrinsic expression noise unless phenotypically equivalent cells can be isolated from young and old animals. A refined taxonomy of blood cell types has been established based on cell-surface markers, allowing specific populations to be purified to near-homogeneity by flow cytometry. Here we describe a study conducted on four different hematopoietic cell types which provides evidence that regulatory homeostasis is maintained with age in the cells of renewing tissues.

6.3 Results

We performed single-cell mRNA profiling on four hematopoietic populations isolated from young and old mice: hematopoietic stem cells (HSCs) [117, 122, 144] (figure 6.1), granulocytes [145] (figure 6.2), naïve B-2 B cells [146, 147] (figure 6.3), and naïve CD8+ T cells [148] (figure 6.4). Individual cells were sorted into lysis buffer and analyzed using a two-round qRT-PCR strategy [89, 90]. A total of 324 cells were evaluated, comprising 34–47 cells of each cell type within each age cohort. Using synthetic RNA standards as a reference, we measured the copy number of six medium-to-high abundance transcripts in each cell: ActB, B2M, Rpl5, Rpl19, CD45 and H2K (figure 6.5).

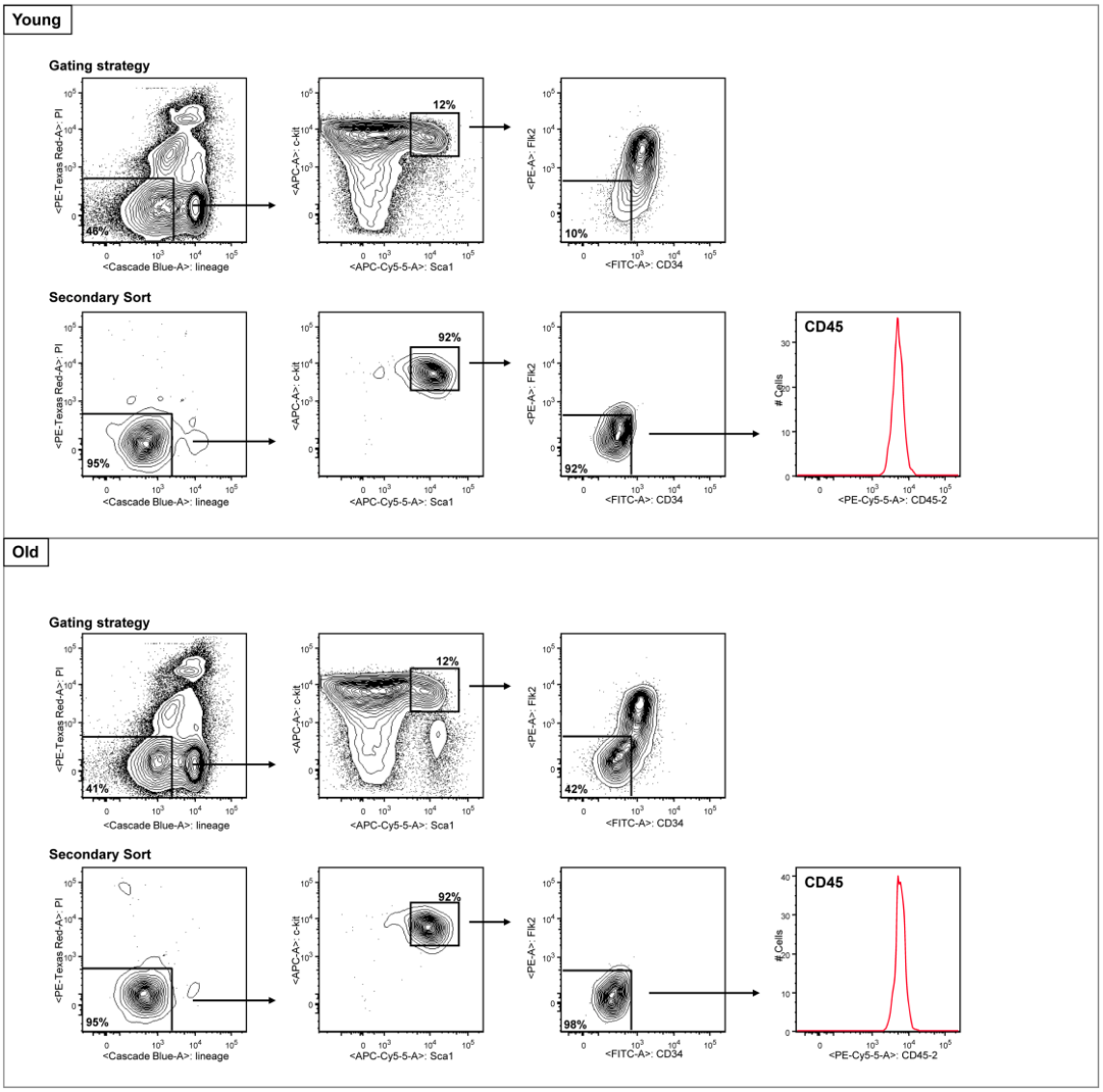

Figure 6.1. HSC sort strategy. Flow cytometric profiles showing gating strategy for purification of HSCs for representative young (top panels) and old (lower panels) mice. Cells were pregated through FSC-A versus SSC, and FSC-A versus FSC-W to exclude doublets (not shown). Primary and secondary sort data are shown, along with the protein expression histogram for CD45 from the final gate.

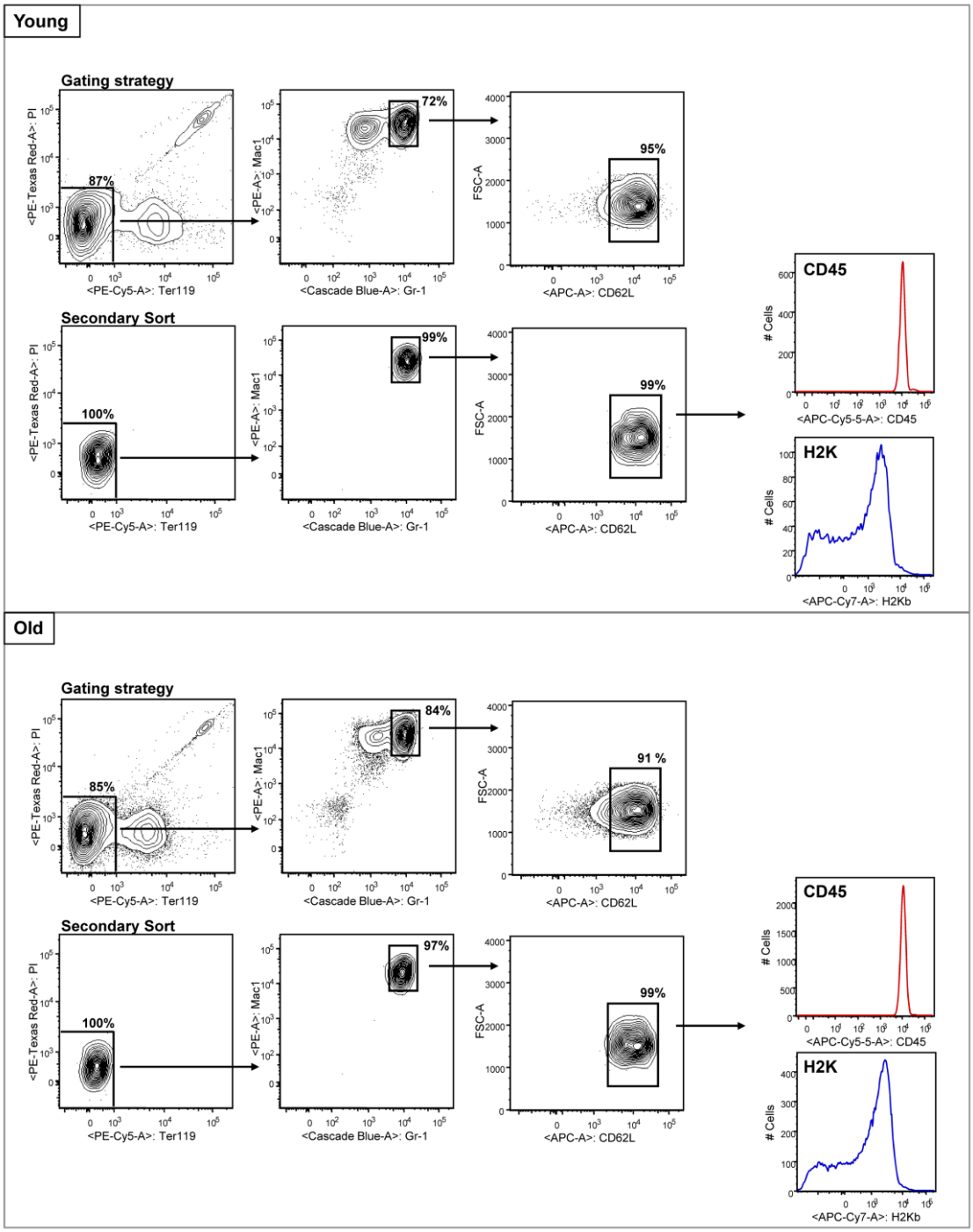

Figure 6.2. Granulocyte sort strategy. Flow cytometric profiles showing gating strategy for purification of granulocytes for representative young (top panels) and old (lower panels) mice. Cells were pregated through FSC-A versus SSC, and FSC-A versus FSC-W to exclude doublets (not shown). Primary and secondary sort data are shown, along with protein expression histograms for CD45 and H2K from the final gate.

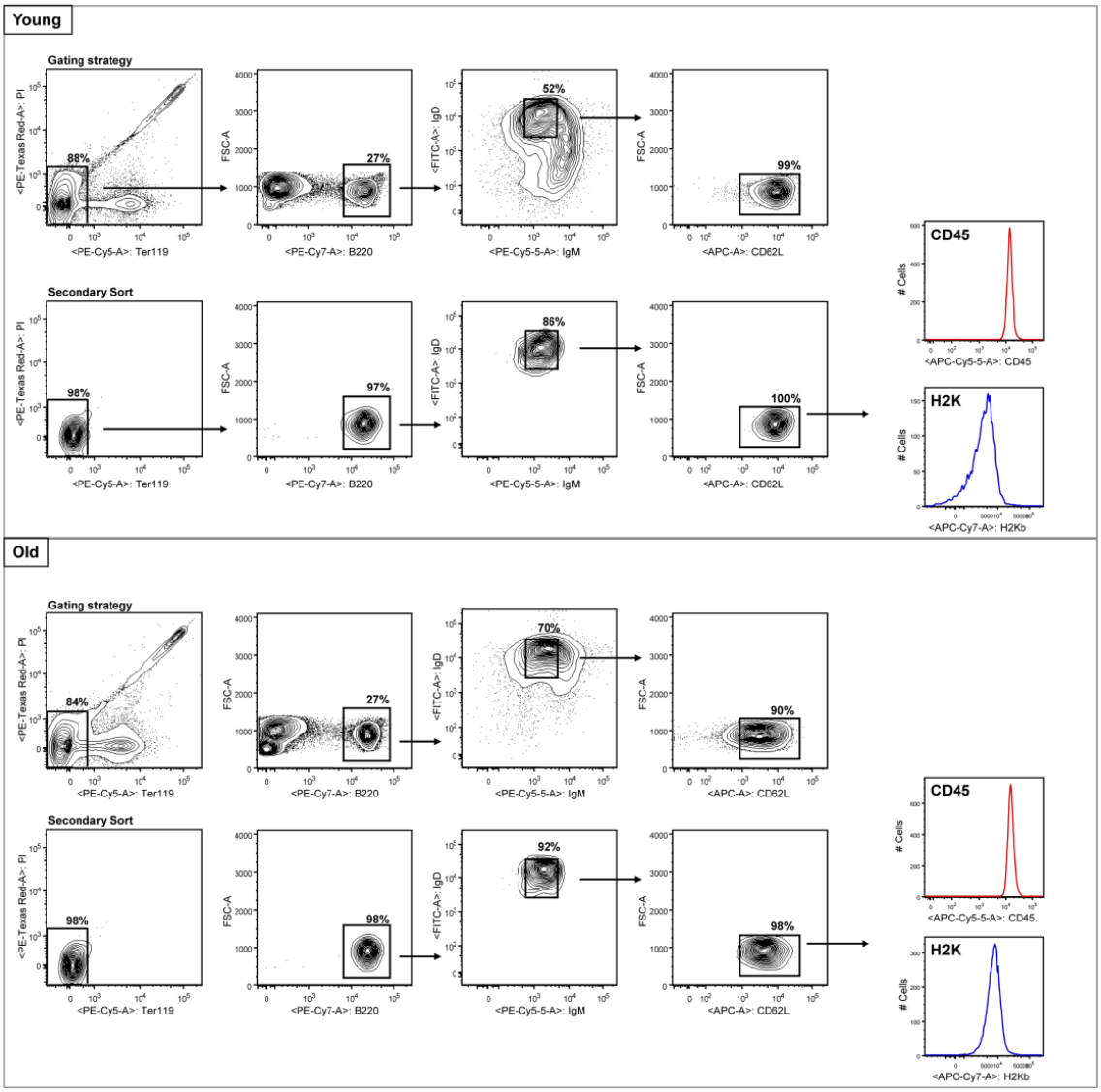

Figure 6.3. B-cell sort strategy. Flow cytometric profiles showing gating strategy for purification of naïve B-2 B cells for representative young (top panels) and old (lower panels) mice. Cells were pregated through FSC-A versus SSC, and FSC-A versus FSC-W to exclude doublets (not shown). Primary and secondary sort data are shown, along with protein expression histograms for CD45 and H2K from the final gate.

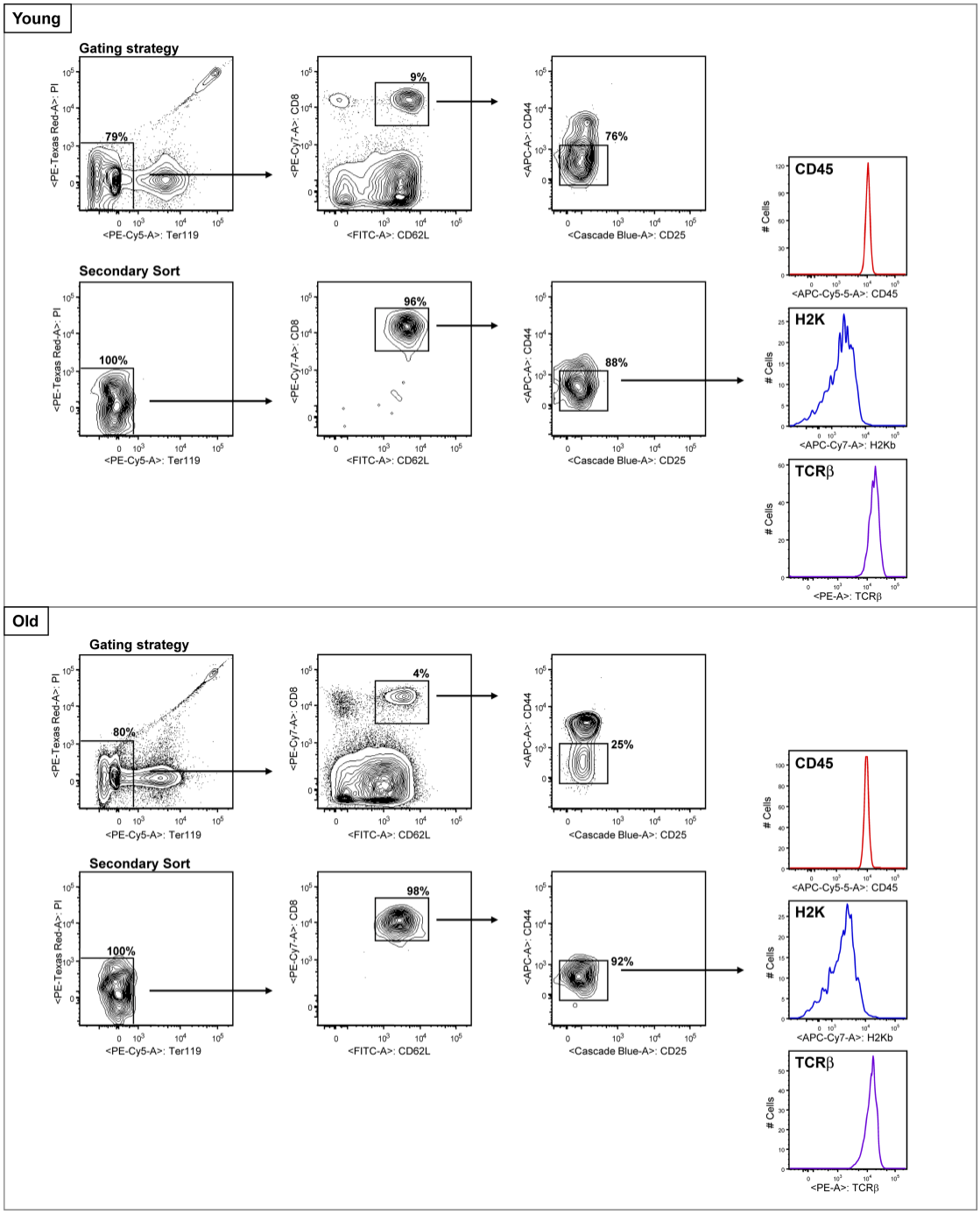

Figure 6.4. T-cell sort strategy. Flow cytometric profiles showing gating strategy for purification of naïve CD8 T cells for representative young (top panels) and old (lower panels) mice. Cells were pregated through FSC-A versus SSC, and FSC-A versus FSC-W to exclude doublets (not shown). Primary and secondary sort data are shown, along with protein expression histograms for CD45, H2K and TCRβ from the final gate.

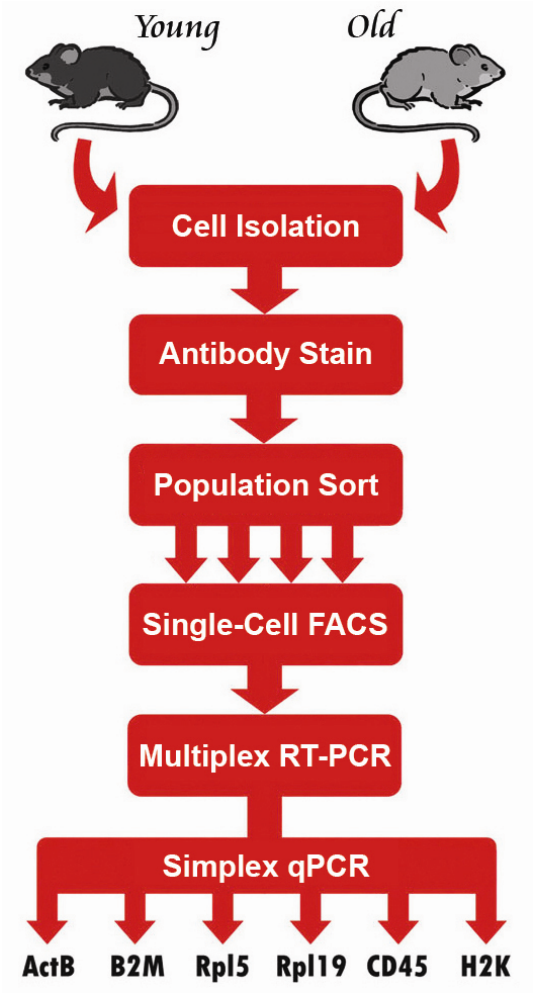

Figure 6.5. Experimental method. Cells were recovered from peripheral blood and bone marrow and stained with dye-conjugated antibodies. HSCs, granulocytes, naïve B cells, and naïve T cells were purified by FACS. In a secondary sort, individual cells from each isolate were dispensed to RT-PCR buffer, where they underwent hypotonic/detergent lysis. For transcript analysis, primers and an RT/*Taq* enzyme blend were added to the lysates, which were then subjected to multiplex, coupled RT-PCR. The PCR step was limited to 15 cycles in this "preamplification" round to prevent inhibition by primer-dimer reactions. Aliquots of amplified cDNA were taken forward to independent SYBR Green qPCRs to quantify the six target transcripts; first-round products and primers were diluted 100-fold going into this round. Quadruplicate RNA standards-based reactions were processed in parallel with each eight-tube strip of lysates. Ct values from cell-based reactions were translated into mRNA copy numbers by reference to the standards reactions using the ΔCt method.

Gene expression measurements were organized into 48 data sets, based on cell type, age cohort, and mRNA target (figure 6.6). The qPCR readouts from the cell-based reactions were generally well above the background signals detected in No Template and No RT control reactions (table 6.1). Interestingly, we found a trend to higher transcript levels in cells from old animals, particularly evident in HSCs and T cells (figure 6.7). The shift is apparent in median as well as average expression and is therefore not driven by high outliers, so there is no reason to suppose that it signals an increase in transcriptional noise.

Table 6.1. NTC and No RT controls

Control	ActB	B2M	Rpl5	Rpl19	CD45	H2K
NTC	1.4	0.3	3.2	4.7	0.0	0.9
No RT	0.0	0.0	3.8	3.2	0.0	0.0

Background readings from NTC and No RT control reactions, expressed in equivalent RNA copies. NTC values are averaged from 8 individual reactions. No-RT data are from a standard-curve analysis on an 8-point cell-concentration ramp, spanning 1 to 128 cells per well. The NTCs were processed identically to lysate-based reactions; for the No RT controls, Platinum *Taq* polymerase (Invitrogen) was substituted for the RT/*Taq* blend in the RT/preamplification round.

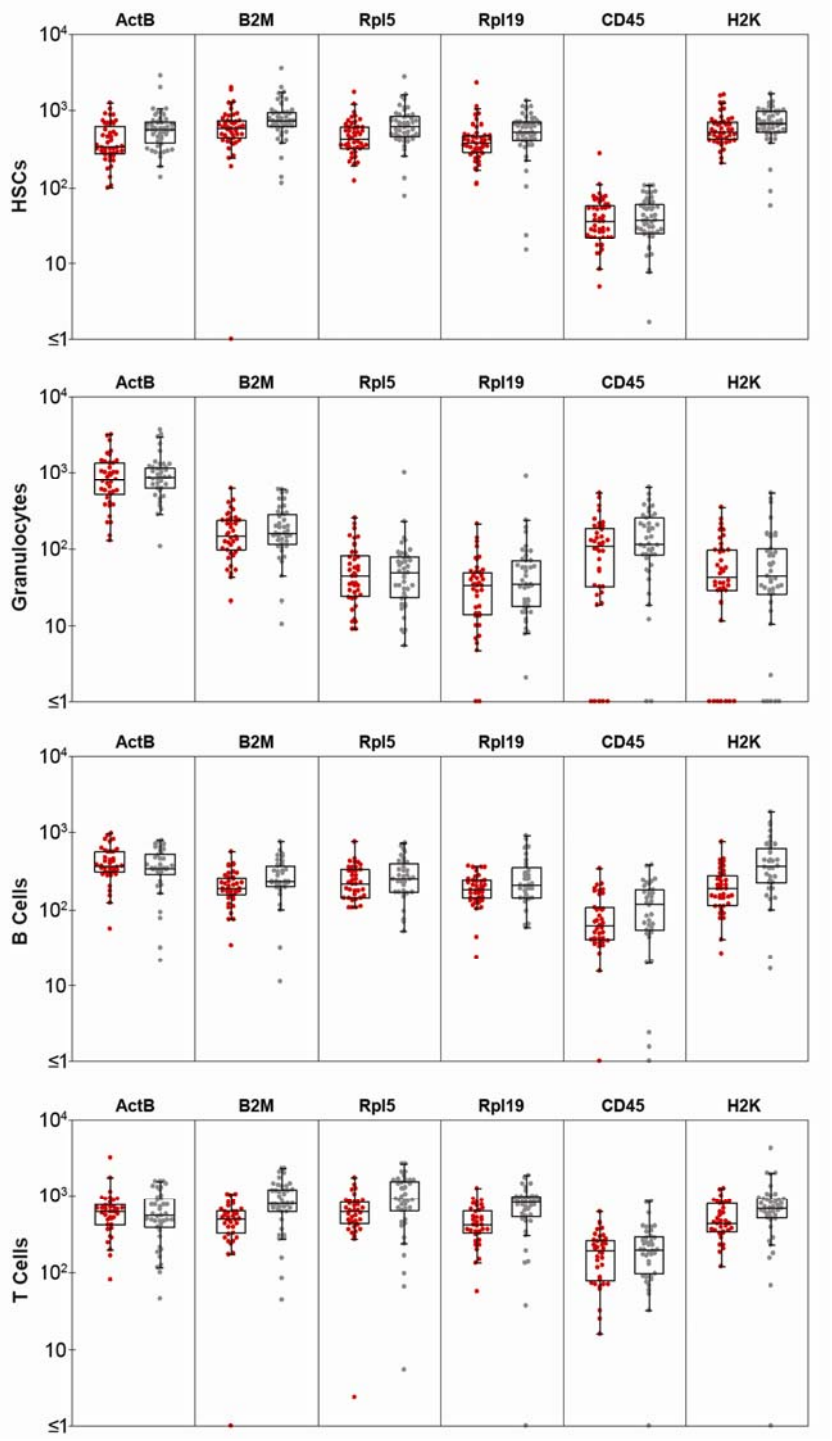

Figure 6.6. RNA expression data. Single-cell transcript copy number by cell type, gene, and age cohort. Young-cohort data are shown in red and old-cohort data are shown in grey within each scattergram pair. Superimposed boxplots show the median and the second and third quartiles; whiskers delimit non-outlier points, where an "outlier" is a value >1.5×IQR outside the middle quartiles.

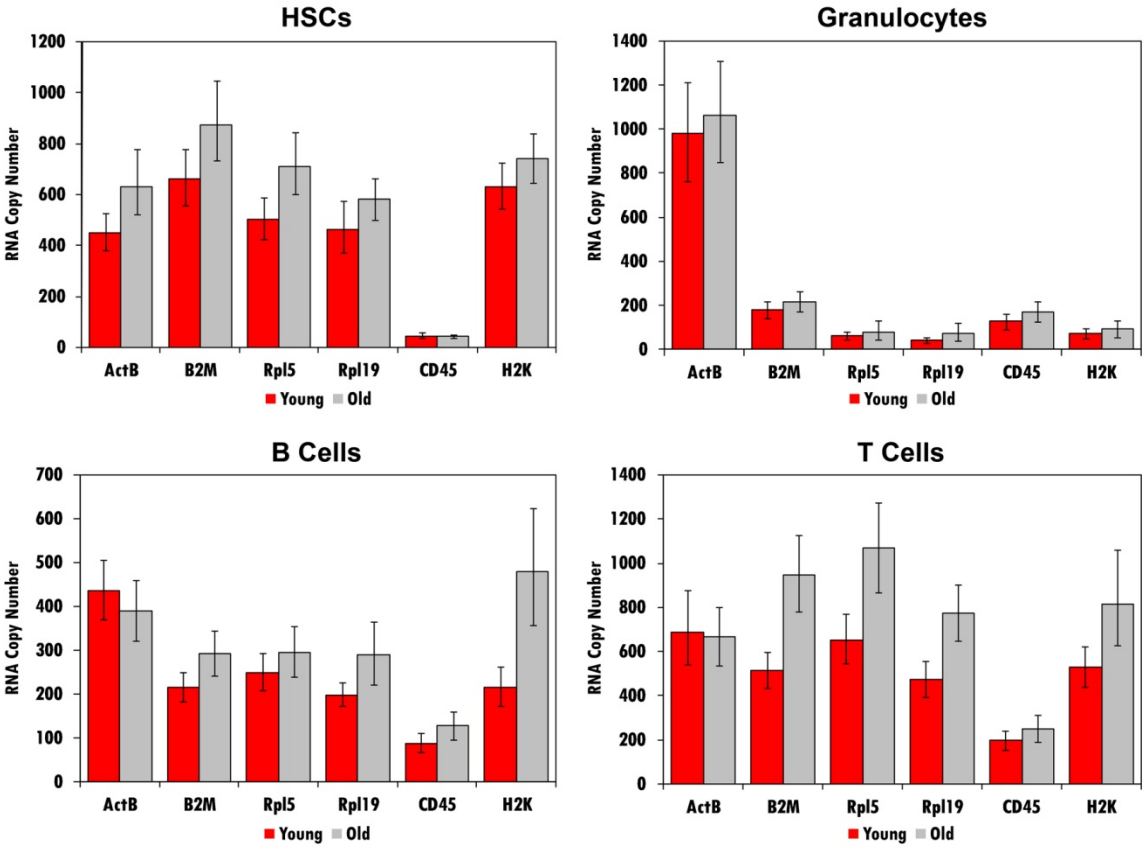

Figure 6.7. Gene-expression profiles. Expression profiles for the four cell populations analyzed in the study, based on the single-cell averages for each data set. Error bars delimit the 95% confidence interval on the mean, estimated by bootstrap resampling.

The coefficient of variation (CV) was computed for the transcript copy number values in each data set (figure 6.8). The median CV was 0.63 for the young-cohort data sets and 0.69 for the old-cohort data sets. The lowest cell-to-cell variation measured (CV = 0.43) was still well above the intrareplicate variation observed in RNA standards-based reactions (figure 6.9). Transcript copy number distributions are typically longtailed and hence violate the assumption of normality underlying most standard statistical tests [36], so we used the method of bootstrap resampling to put confidence bounds on the CV values [149]. The confidence intervals were wide in some cases, reflecting sensitivity to outliers. Bootstrap resampling was also applied to compute the significance level of the increased-noise hypothesis for each mRNA species, using three relative measures of dispersion: CV, geometric standard deviation (GSD), and the interquartile range (IQR) of median-normalized expression (figure 6.10). None of the P values fell below 0.05 for the HSCs and granulocytes, and the average P value was ~0.5 in both these populations. Thus, no age-dependent increase in transcriptional noise was detected in these cell types. The P value tables for the B and T cells suggest a modest trend to increased transcriptional heterogeneity in old-cohort lymphocytes, but $P < 0.05$ significance was attained in only 3 of 36 cases.

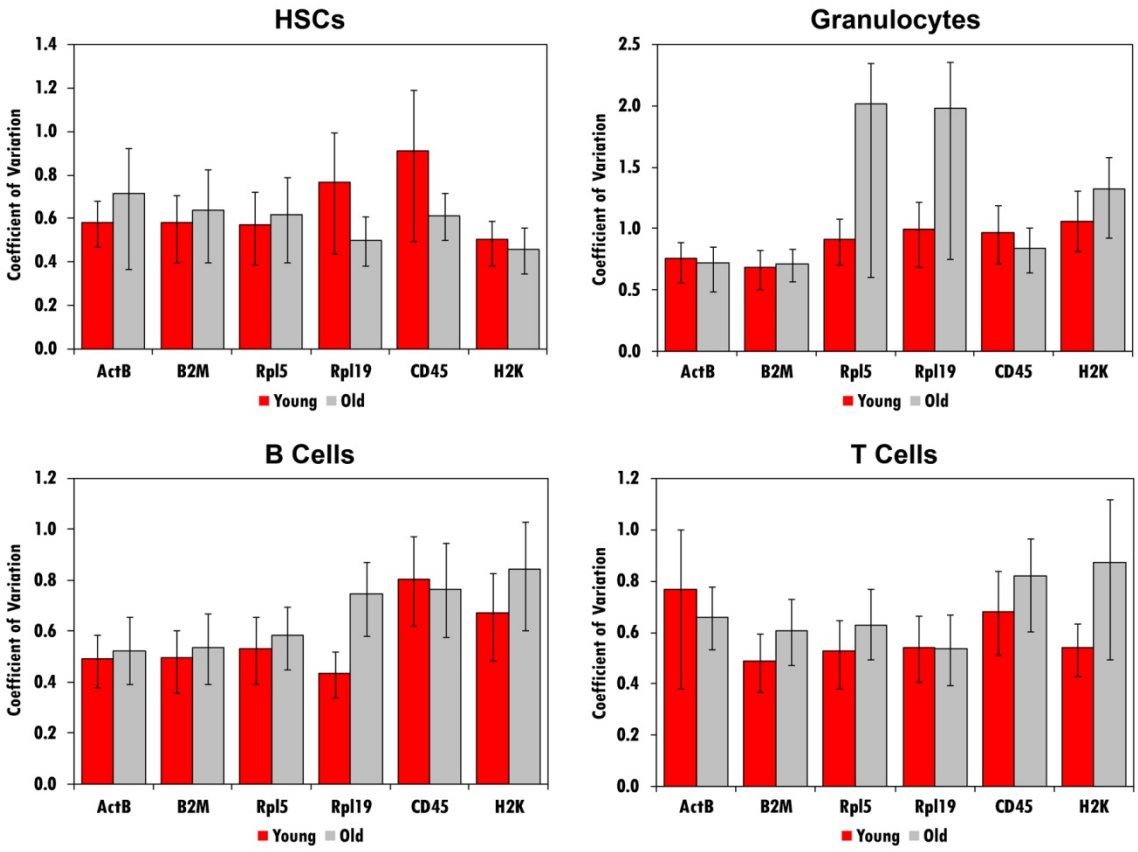

Figure 6.8. Cell-to-cell variability. Coefficients of variation for the RNA copy number measured in single-cell replicates, by cell type, gene and age cohort. Error bars delimit the 95% confidence intervals for the statistics, estimated by bootstrap resampling.

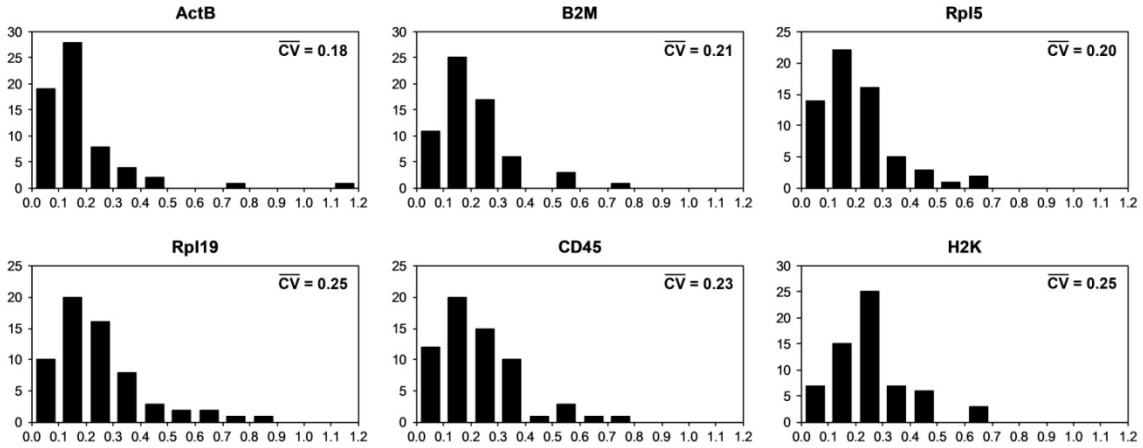

Figure 6.9. Technical noise in RNA quantitation. Histograms show the readout variability within the quadruplicate RNA standards processed alongside lysate-based reactions in the single-cell survey, using data from 63 qPCR runs. The CV metric is based on relative copy number, computed by the ΔCt method. The technical noise in the copy number values for the lysate-based reactions will reflect inherent well-to-well variability, as manifested in the standards replicate CVs, plus a smaller, orthogonal error contribution due to the statistical uncertainty in the interpolation of a nominal 1000-copy reference Ct from quadruplicate standards. For example, if the intrareplicate technical variation is normally distributed with a CV of 0.22, the expected copy number error in the data pooled from multiple qPCR runs is $\sqrt{[0.22^2+(0.22/\sqrt{4})^2]} = 0.25$.

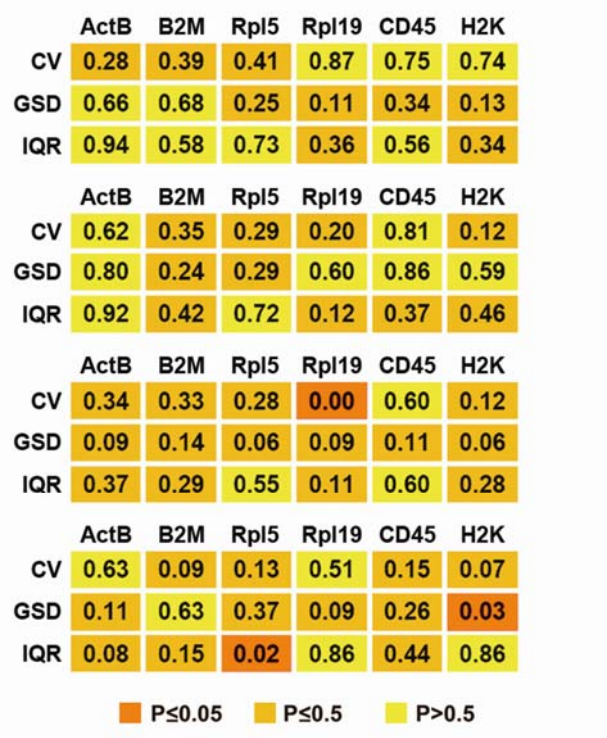

Figure 6.10. Bootstrap resampling analysis. Significance level of the hypothesis that transcriptional noise is increased in old animals, estimated by bootstrap resampling using three metrics of variability: coefficient of variation (CV), geometric standard deviation (GSD), and interquartile range (IQR).

Although the genes for the ribosomal subunit proteins Rpl5 and Rpl19 lie on different chromosomes, microarray analysis has shown that they are tightly coregulated [150]; we were interested to see if this coupling would be affected by age. The levels of these transcripts were strongly correlated when data for all cell types were aggregated (figure 6.11). The correlations within specific populations were generally weaker, but this was still the most consistently correlated pair of genes (figure 6.12). Pearson coefficients for the Rpl5-Rpl19 correlation were actually higher in the old cohort for the aggregated data (0.85 versus 0.80), and for three of the four specific cell types, implying that there was no transcriptional decoupling of these genes with age.

To determine if the observed transcriptional stability with age was reflected at the protein level, we used FACS to analyze cell-surface expression of CD45 in all cell types, H2K in granulocytes and lymphocytes, and TCRβ in T cells (figure 6.13). The sort criteria used to purify the populations of interest did not involve gating on these markers, permitting an unbiased assessment of the expression distribution in each cell type. No trend to increased variation in protein expression in the aged cohort was apparent, providing further evidence for the age-dependent maintenance of both transcriptional and translational networks.

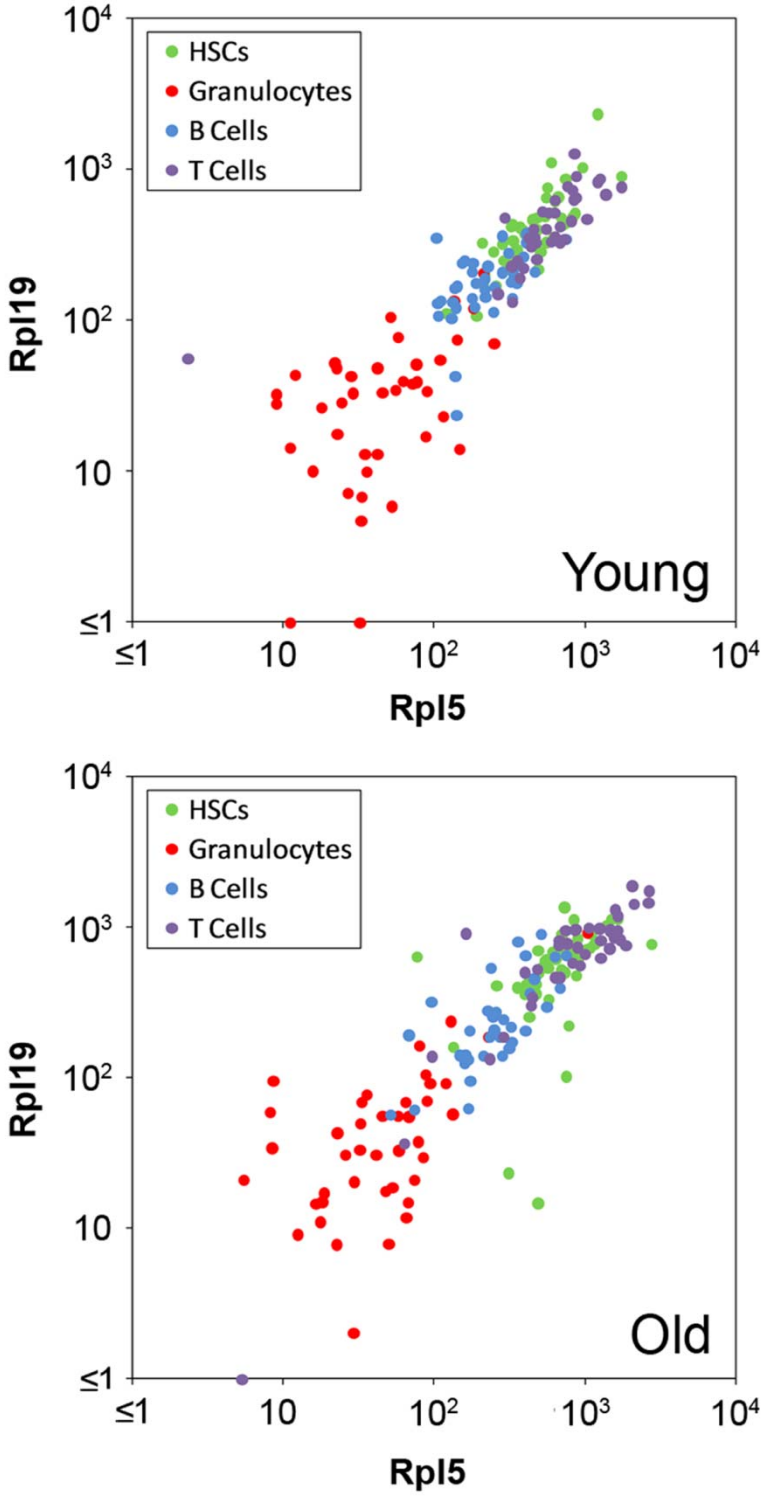

Figure 6.11. Rpl5-Rpl19 correlation data. 2D scatterplots of single-cell copy-number data for the coregulated ribosomal subunit genes Rpl5 and Rpl19.

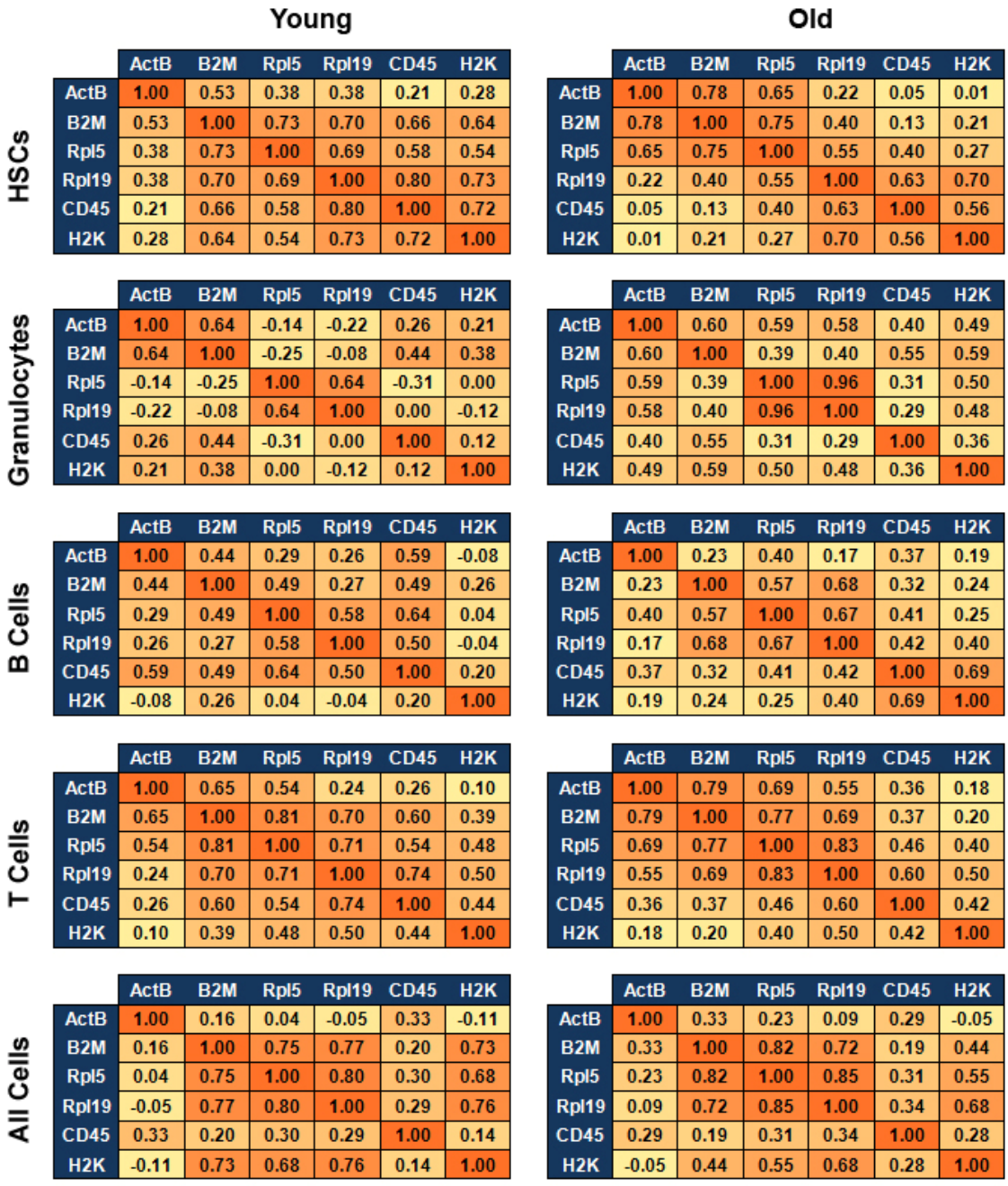

Figure 6.12. Transcript correlations. Pearson correlation coefficients for the expression of each pair of genes based on the single-cell RNA copy number data from the survey.

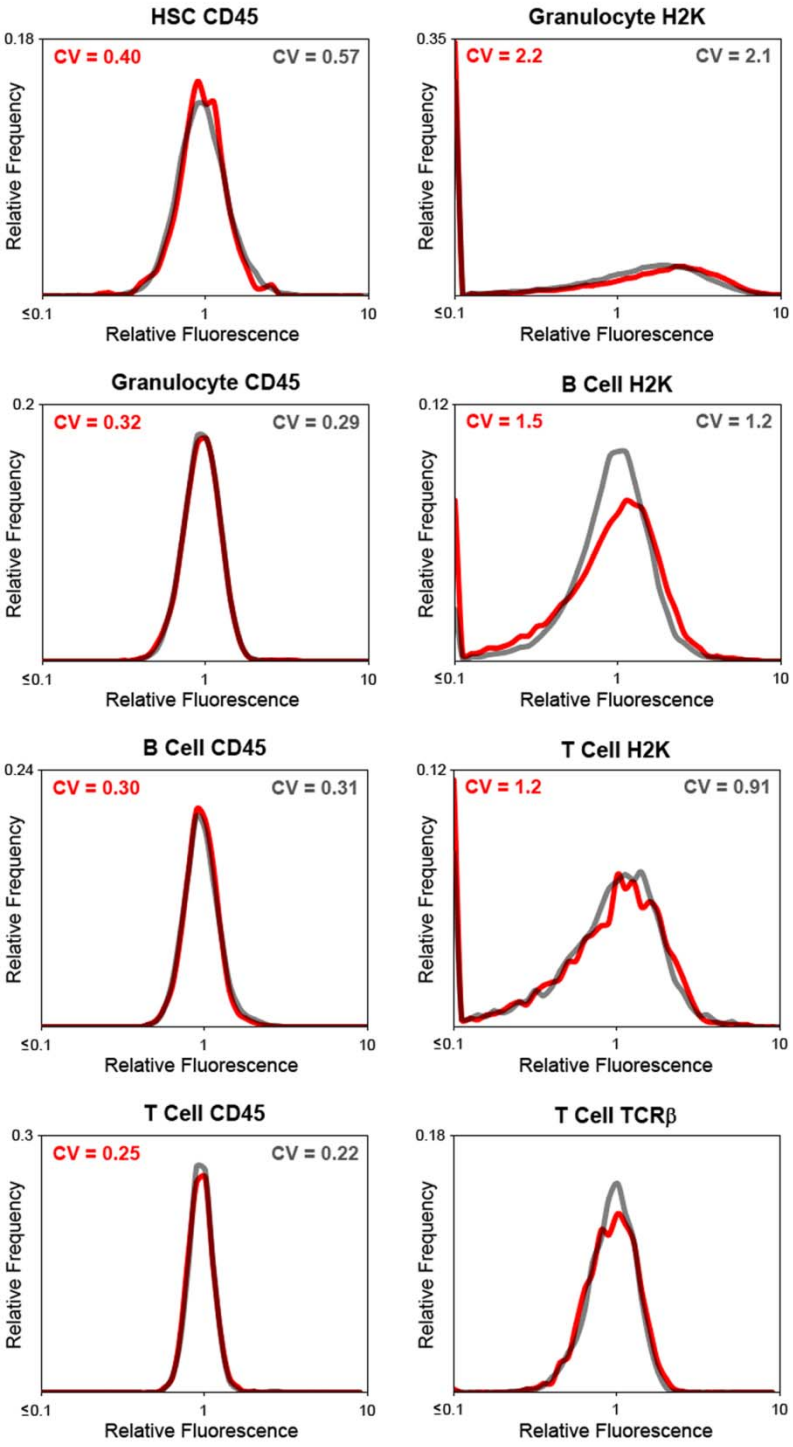

Figure 6.13. Protein expression analysis. Surface-protein expression histograms based on flow cytometry data from the population sorts. Young-cohort data are shown in red and old-cohort data in grey. H2K expression was bimodal in the cell types evaluated, with the histograms showing a secondary peak of $H2K^-$ cells; the CV metrics for this target are based on the fluorescence intensity distribution in the $H2K^+$ fraction.

6.4 Discussion

Our analyses revealed no marked tendency to destabilized gene expression with age at either the mRNA or protein level. This finding stands in contrast to the strong noise signature reported in cardiomyocytes [48]. The number of cells assayed from each population was similar to the total sample size in the cardiomyocyte study, so it is unlikely that the difference is a matter of statistical power. The lymphocyte populations showed signs of increased heterogeneity with age, but it is by no means clear that this reflects transcriptional instability. Higher cell-to-cell variability was manifested in Rpl5 and Rpl19 in these subsets, yet the abundance of the two transcripts showed no decorrelation with age. This tends to exclude mutations or epigenetic changes involving the loci for these genes as the source for the increased variability. Noise ramifying through the regulatory network could affect both genes without leading to decoupling by affecting a common regulator, but the observations are also compatible with changes in the internal population structure of the naïve B and T cell compartments, unrelated to cell-intrinsic transcriptional noise.

If genomic instability causes age-related transcriptional destabilization, then the discordance between our results and the cardiomyocyte data could reflect disparate mutation rates among somatic lineages. Studies conducted in mice using a knock-in reporter for mutations have measured differences in the burden of chromosomal rearrangements in several whole tissues, and these data show that heart tissue incurs almost twice as many mutations with age as the spleen, which is rich in B lymphocytes [137]. In this regard, it may be significant that the white cells of the blood are especially radiosensitive owing to acute apoptotic responses to DNA damage, presumably a safeguard against neoplastic changes in these proliferative

lineages [151-153]. It could be that hematopoietic cells escape the worst effects of genomic instability because damaged cells are rigorously purged from the population.

A potentially important difference between the cell types we surveyed and cardiomyocytes is the post-mitotic lifetime of the cells. Granulocyte and naïve B and T cell populations in the peripheral blood are continuously renewed from the stem-cell pool in the bone marrow. The turnover rate of granulocytes is especially rapid—perhaps less than a day [154]. With respect to the HSCs, there is an order of magnitude expansion of the stem cell pool in mice between maturity and old age [155, 156], implying that the average post-mitotic age of the cells we examined may be no more than a few months. In contrast, the tissues of the heart show little turnover [157, 158], which implies that cardiomyocytes probably have post-mitotic ages similar to the chronological age of the animals from which they are recovered. Since at least some DNA damage repair and apoptotic response mechanisms are linked to cell cycle progression, cells with long post-mitotic lifetimes may be particularly vulnerable to the accrual of genomic damage leading to transcriptional dysregulation. It is also possible that age-related transcriptional noise is a sign of chemical instability in the regulatory circuits, rather than a secondary consequence of changes at the DNA level. Our data suggest that the regulatory logic is inherently quite stable over the course of a lifetime, but it is conceivable that cell division provides a "reset" which counters the effects of drift and stochastic perturbations in the network. If so, destabilized gene expression may be largely a phenomenon of long-term post-mitotic cells.

Finally, it remains possible that the elevated cell-to-cell variability detected in aged cardiomyocytes is symptomatic of tissue heterogeneity rather than cell-intrinsic transcriptional noise, in which case the stringent phenotypic matching attainable with FACS

could explain the absence of such a signature in our results. A full resolution on the question of age-related transcriptional instability will require additional studies integrating data on post-mitotic lifetime, accumulated DNA damage and gene expression noise in disparate cell types, using methods which ensure, insofar as possible, the phenotypic identity of cells isolated from young and old animals. In conclusion, while our findings do not invalidate the noise hypothesis, they do place limits on its generality, frame questions about the mechanistic basis of the effect reported in cardiomyocytes, and underscore the need for further research before transcriptional instability enters the canon of accepted aging mechanisms.

6.5 Experimental Procedures

6.5.1 Mice

All the mice used in this study were C57BL/6. Animals were obtained from the National Institute of Aging (NIA, Bethesda, MD), and then maintained at the Stanford University Laboratory Animal Facility (SULAF). The ages of the mice in the young and old cohorts were 2–3 months and 23–25 months, respectively.

6.5.2 Cell Purification

Peripheral blood samples were taken from three mice in each age cohort, and diluted in cold PBS supplemented with 10 mM EDTA. Red cells were lysed using ACK lysis buffer (150 mM NH_4Cl, 10 mM $KHCO_3$, 0.1 mM EDTA, pH 7.2), and the remaining cells were stained with fluorescence-conjugated monoclonal antibodies. The antibodies used were Ter119•Cy5PE, CD8•Cy7PE, TCRβ•PE, B220•Cy7PE, CD45.2•APCCy5.5, IgM•PECy5.5, IgD•FITC, streptavidin•APCCy7 (e-Bioscience, San Diego, CA), $H2K^b$•biotin (Pharmingen, San Diego, CA), and CD62L•APC, Mac1•PE, GR-1•Alexa405, CD62L•Alexa488,

CD44•APC, CD25•Alexa405 (all prepared in the Weissman lab). To recover HSCs, whole bone marrow cells from three mice in each age cohort were enriched by positive selection using CD117-conjugated magnetic beads (Miltenyi, Germany). Enriched cells were stained with antibodies to Sca1 (Pharmingen), c-kit (clone 2B8, Pharmingen), CD34 (Pharmingen), lineage (e-Bioscience), and flk2 (e-Bioscience). Cells were sorted on a FACSAria (Becton Dickinson, San Jose, CA). The subsets evaluated were gated as follows: HSCs (Lin^- $c\text{-}kit^+Sca^+flk2^-CD34^-$), granulocytes ($Ter119^-Mac1^+GR\text{-}1^+CD62L^+$), naïve B-2 B cells ($Ter119^-B220^+IgD^+IgM^{lo}CD62L^+$), and naïve CD8+ T cells ($Ter119^-CD8^+CD62L^+CD44^{lo}CD25^-$). Cells were kept on ice during the experiments whenever possible.

6.5.3 Single-Cell Sort

10 μL aliquots of cell lysis buffer were dispensed to 0.2 mL PCR tubes in 8-tube strips. The solution comprised RT-PCR buffer (CellsDirect 2X Reaction Mix, Invitrogen, Carlsbad, CA), RNase inhibitor (SUPERase-In, Ambion, Austin, TX), and nuclease-free water (RT-PCR Grade Water, Ambion). Tween 20 detergent (Sigma Chemical, St. Louis, MO) was added at a final concentration of 0.1% to ensure rapid cell lysis. Lysis buffer strips were arrayed in 96-well plate holders and kept at -20 °C until needed. Plates were warmed to 4 °C prior to the FACS session, and then frozen down to -20 °C as soon as cells had been sorted into lysis buffer.

6.5.4 Reverse Transcription and Preamplification

In the RT/preamplification phase of the transcript analysis, two 8-tube strips of cell lysates and one 8-tube strip of RNA standards were processed at a time. A 5 μL aliquot of multiplex primer mix was added to each frozen sample, and the tubes were briefly spun down in a centrifuge. The strips were then transferred to a preheated thermocycler block;

after giving the samples time to warm up, 5 μL aliquots of diluted RT/Taq blend (CellsDirect Superscript III/Platinum *Taq*, Invitrogen) were pipetted into each reaction. The RT/Taq blend was diluted in RT-PCR buffer to prevent denaturation; the final enzyme concentration was as directed by the manufacturer. The RT-PCR thermal profile comprised a 15 minute, 55 °C RT incubation followed by a 3 minute, 95 °C hot start and 15 cycles of PCR amplification (15 second, 95 °C denaturation step; 60 second, 60 °C annealing/extension step). Reactions were moved to a cold block immediately the PCR completed, and 5 μL aliquots of each reaction were diluted in 200 μL TE (pH 8.0). Dilutions were prepared in two 12-tube strips, each corresponding to one strip of cell-based reactions plus four standards-based reactions. Strips were stored at -20 °C until analysis.

6.5.5 Quantitative PCR

Each 12-tube strip from the RT/preamplification round was analyzed in a single run using a Chromo4 qPCR machine (Bio-Rad, Hercules, CA). Simplex reactions were set up in six rows of a 96-well block. Each 20 μL reaction comprised 10 μL of qPCR reaction mix (SYBR GreenER qPCR Supermix, Invitrogen), 2 μL of primers, and 8 μL of diluted first-round product. The PCR profile comprised a 15 minute, 95 °C hot start followed by 40 cycles of amplification (15 second, 95 °C denaturation step; 60 second, 60 °C annealing/extension step). A melt-curve analysis was included to detect secondary or non-specific product formation.

6.5.6 Primer Design

Identical PCR primers were used in the multiplexed RT/preamplification round and the simplex qPCR round. The reverse primers functioned as gene-specific RT primers during cDNA synthesis. Primers were at 100 nM final concentration in all reactions. Primers were

designed with Primer3 (MIT); primer sets were also evaluated in silico using NetPrimer (Premier Biosoft, Palo Alto, CA) and FastPCR (Institute of Biotechnology, University of Helsinki, Finland). One of the primers in each pair straddled an exon boundary, except in the case of the ActB assay, where the primers bracketed a splice junction. To maximize RT efficiency, RNA folding prediction software (Beacon Designer, Premier Biosoft) was used to target the assays to regions of mRNA free of secondary structure. Primers were checked for high priming efficiency (85%–100%) by qRT-PCR standard-curve analysis using RNA standards as template. Melt-curve analysis was used to disqualify primers with high primer-dimer potential. Primer sequences are given in table 6.2. Primers were synthesized by Integrated DNA Technologies (Coralville, IA).

Table 6.2. Transcript analysis primers

Target	GenBank ID	Forward Primer	Reverse Primer
ActB	NM_007393	CAGCTTCTTTGCAGCTCCTT	GCAGCGATATCGTCATCCA
B2M	NM_009735	CGGTGACCCTGGTCTTTCT	GAATTTGAGGGGTTTTCTGGA
Rpl5	NM_016980	GGCGAGAGGGTAAAACTGAC	TCATCCTATATTTGGGTGTGTT
Rpl19	NM_009078	AGAAGATTGACCGCCATATGTA	GGATGCGCTTGTTTTTGAAC
CD45	NM_011210	GCTGAATACCAGAGACTTCCTT	GCTCATCTCCAGTTCATGCTT
H2K	AY989882	ACTATGCTCTGGCTCCAGG	GGGTCATGAACCATCACTTTAC

Primer sets used in RT/preamplification step and SYBR Green qPCR analysis.

6.5.7 RNA Standards

RNA quantitation standards were generated from PCR-product templates with the MEGAscript T7 runoff transcription kit (Ambion) and purified with the MEGAclear kit (Ambion). The primers used to make DNA templates are given in table 6.3. PCRs were templated with Mouse Thymus PCR-Ready cDNA (Ambion). RNA was quantitated by UV absorbance spectroscopy. Transcript purity and length were checked with a capillary electrophoresis system (Experion, Bio-Rad). Lysis buffer was spiked with an equimolar mixture of RNA standards and 10 μL aliquots were dispensed to 8-tube strips, each tube receiving approximately 1000 copies of each of the six target transcripts. The standards strips were stored at -20 °C until needed.

Table 6.3. Runoff-transcription template primers

Target	GenBank ID	Forward Primer	Reverse Primer
ActB	NM_007393	CCGCGAGCACAGCTTCTTTG	AGGAAGAGGATGCGGCAGTG
B2M	NM_009735	CTACTCGGCGCTTCAGTCG	CACAGGGTTGGGGGTGAGAA
Rpl5	NM_016980	CTCTGCAGGTCTGCGTGGAG	TCAGCAGCCCTTTCCTGAGC
Rpl19	NM_009078	CGCTGCGGGAAAAAGAAGGT	TGGTCTCCTCCTCCTTGGACA
CD45	NM_011210	AGCATGGAGGAAGGCACTCG	TGCTTTCCTTCGCCCCAGTA
H2K	AY989882	CCCTGGGCTTCTACCCTGCT	TCACGCTAGAGAATGAGGGTC

Primer sets used to generate PCR product templates for RNA runoff transcription. Forward primers incorporated a 5' T7 promoter tail (5'-TAATACGACTCACTATAGGG-3').

6.5.8 Data Analysis

Threshold cycle (Ct) readings obtained in qPCR reactions were translated to RNA copy numbers by reference to parallel reactions on RNA standards. First, a 1000-copy reference Ct was interpolated from the quadruplicate standards Ct values, assuming an average 1000 template copies per reaction and a nominal PCR efficiency of 0.95. The transcript copy number for lysate-based reactions was computed using the formula $N = 1000 \cdot 1.95^{\Delta Ct}$, where $\Delta Ct = Ct_{ref} - Ct_{sample}$. The single-cell sorts were ~60% efficient in delivering cells into the lysis buffer, negative wells being distinguished by low genomic background signals in Rpl5 and Rpl19 assays and negligible amplification in the other four assays. Samples which gave an ActB readout below 20 copies were excluded from the analysis. For each age cohort, cells from three different animals contributed approximately equally to the expression data. Confidence intervals for CV metrics and P values for the age-related noise hypothesis were estimated by bootstrap resampling using Resampling Stats for Excel (Resampling Stats, Arlington, VA). Expression data sets were resampled with replacement 10,000 times. Confidence bounds were established by taking the 2.5th and 97.5th percentile values for the CVs calculated on the resampled data. P values correspond to the fraction of resampled data sets which gave lower variability metrics for old-cohort data. Copy number readouts of zero were rounded up to 1 copy for GSD calculations; IQR was evaluated after normalizing expression values to the data set medians. Membrane-protein expression histograms are based on FACS analyses of samples taken from three different animals within each age cohort. Fluorescence values were normalized to the sample medians before the data were pooled. Each histogram represents data from at least 1405 individual cells.

Appendix

The Digital Array Response Curve

Luigi A. Warren Joshua A. Weinstein
Stephen R. Quake

Department of Bioengineering, Stanford University and HHMI

1 The Digital PCR Assay

DNA quantitation in the Digital Array is based on the partitioning of a TaqMan PCR reaction into an array of 765 compartments or wells. If there are only a few template molecules in the sample, most of the wells capture either one or no molecules, and the number of positive wells at the PCR end-point gives a count of the molecules in the sample, to a close approximation. If the number of molecules is not small compared to the number of wells, many wells capture more than one template copy, and the positive well count is significantly less than the number of molecules. Unless the array is fully saturated, template abundance can still be estimated based on the statistical relationship between the number of molecules and the expected number of positive wells. Here, we show how to compute this dose-response curve and put error bars on the readout.

2 Binomial Approximation

Exact calculation of the digital PCR response curve is mathematically non-trivial and computationally expensive. Before giving the deriving and arriving at an algorithm for the exact solution, we here derive an approximate solution which turns out to give quite accurate results for the case where the number of molecules is significantly smaller than the wells available. This simple formula allows the curve to be recomputed quickly if the total number of wells changes, for example because certain wells have to be excluded owing to chip defects. Consider the general case of m template molecules randomly distributed within n wells. The probability of any given molecule being trapped in any given well is $1/n$, so the probability, p, of a given well capturing at least one molecule is as follows:

$$p = 1 - \left(1 - \frac{1}{n}\right)^m \tag{1}$$

If we assume that the positive/negative status of every well represents the outcome of an independent trial with probability p of success, then the number of positive wells, k, is a binomial random variable with parameters (n, p) and expectation np. The relation between the expected value of k and the number of molecules in the array is therefore:

$$E(k) = n\left[1 - \left(1 - \frac{1}{n}\right)^m\right] \tag{2}$$

We are more interested in estimating m, the number of molecules, from k, the readout of positive wells. We can rearrange (2) to get such an estimate:

$$m = \frac{\log\left(1 - \frac{k}{n}\right)}{\log\left(1 - \frac{1}{n}\right)} \tag{3}$$

Although this equation gives us a useful estimator for m, it does not represent an exact solution for the expectation value for m given k, $E[m]$. In the first place, k is not a true binomial random variable, since the probability of any given well capturing at least one molecule depends on the events in the other wells. Also, while $E[m]$ is determined for m, the relation between k and $E[m]$ involves the prior probability distribution for m, $p(m)$.

3 Bayesian Logic and Statistical Measures

If we assume a uniform probability distribution for m over a finite range, 1 to N, then $p(m)$ is $1/N$ for all m within that range. Substituting gives us the following equality:

$$p(m|k) = \frac{p(k|m)/N}{\sum_{i=1}^{N} p(k|i)/N} = \frac{p(k|m)}{\sum_{i=1}^{N} p(k|i)} \tag{4}$$

Thus, given a table of $p(k|m)$ values, we can readily compute a table of $p(m|k)$ values: for every pair m and k, we divide $p(k|m)$ by the sum of $p(k|i)$ for $i = 1$ to N. This sum converges for large N, i.e. the result becomes independent of the choice of N. For any given k, $E[m]$ is the weighted average obtained by summing the product of each m value by the corresponding $p(m|k)$ entry. Confidence intervals on $E[m]$ can be derived by building a cumulative distribution function table from the $p(m|k)$ table. Another useful uncertainty metric, the coefficient of variance (CV), is calculated as follows:

$$CV = \frac{\sqrt{E[m^2] - E[m]^2}}{E[m]} \tag{5}$$

The section entitled "Analytic Solution" gives a MATLAB implementation of the response curve algorithm. The program output is a table which lists for each value of k the expectation value for m, the CV of the estimate, and lower and upper confidence bounds (LCB and UCB) on the 95% confidence interval. The estimate of m obtained using equation (3) is also included in the output (BA). The a sampling of these results is included in Table 1.

Figure 1 plots $E[m]$ against k from the computed table. The 95% confidence interval for the estimated copy number is also indicated. Note that the expectation value and upper confidence limit curves begin to plateau around $k \simeq 755$ owing to the arbitrary bound at $m = 4000$ used in the calculation.

4 Probability Mass Function

The exact, rigorous solution to the probability mass function - and an efficient implementation in a computer algorithm in MATLAB code - is given in "Analytic Solution" section. Therein, the derived closed form for the $p(k|m)$ distribution which is pre-requisite to the derivation of $p(m|k)$ is

$$p(k|m,N) = \frac{\Omega(k|m,N)}{\sum_{i=1}^{N} \Omega(i|m,N)}$$

The function $\Omega(k|m,N)$, that is the multiplicity of molecular assignment outcomes given that exactly k wells are occupied by m molecules out of N available wells is shown to be expressable in two distinct, however equivalent, forms:

$$\frac{N!}{(N-k)!} \sum_{j=1}^{k} \frac{(-1)^{j+k} j^m}{(k-j)!j!} = \frac{N!(N+\Delta)^m}{2\pi(N-k)!} \int_{-\pi}^{\pi} d\theta \frac{e^{im\theta}}{\prod_{l=1}^{k} ((N+\Delta)e^{i\theta} - l)} \tag{6}$$

Here, Δ is an arbitrary positive number, the choice of which does not have an effect on the theoretical outcome of the expression but which may affect its numerical stability when the expression is evaluated on a real machine with round-off error. The first of the expressions on the line above follows from the transformation of the problem into a linear inversion problem. The second expression follows from the first, but uses rudimentary complex analysis to transform the discrete math problem into one of continuous fields. This transformation is shown to be far more computationally tractable because of its avoidance of very large numbers, an obstacle evidenced by the appearance of j^m in the first's summand.

5 Technical Noise and Dynamic Noise

The response curve table shows that the statistical uncertainty in the digital PCR readout rises slowly as k increases, with the CV reaching 5% and the 95% confidence range with $\pm 10\%$ of the expectation value at $k = 715$, which corresponds to $m \simeq 2100$ copies. (The uncertainty metrics start to decrease around $k = 755$, reflecting the upper bound on m.) The estimate for m derived from the binomial approximation is close to the expectation value over this range: again, there is an upward trend in the difference between estimates with increasing k, but it remains below 0.5% at $k = 715$. In conclusion, the analysis shows that the 765-well Digital Array has a quantitative dynamic range of at least 1-2000 copies, with an intrinsic statistical uncertainty in the copy number readout of $3 - 5\%$ over this range. Non-statistical factors, particularly uncertainty in the well calls, may significantly reduce measurement precision for some assays – especially at the high end of the readout range where the response curve is steep. For any specific assay, a true estimate of precision should therefore include an evaluation of well intensity histograms and/or replicate measurements on standards.

6 Analytic Solution

We present here an exact solution to the general problem of the response curve, complete with its conversion to a practicable solution using complex analysis. The end result is presented in short form at the end of this section under the title "Implementation in an Algorithm".

6.1 $p(k|m)$ is Expressable as a Slowly Convergent Series of Finite Length N

For *at most* n wells to fill, and exactly m molecules to fill them, there are n^m ways of filling them when we do so without regard for what number, or which wells in particular, are empty. Once we move further into concerning ourselves with only those outcomes for which exactly k wells have at least 1 molecule, we must define the multiplicities $\Omega(k|m,n)$, which we will define as the number of distinguishable outcomes, with each molecule being assigned one well, for which, given n available wells, exactly k are occupied. Following from above ...

$$n^m = \sum_{i=1}^{n} \left(\begin{array}{c} n \\ i \end{array} \right) \Omega(k = i|m,n)$$

In matrix form, then, for some arbitrary number of cases of n from 1 to (capital) N ...

$$\begin{pmatrix} 1^m \\ 2^m \\ \vdots \\ N^m \end{pmatrix} = \begin{pmatrix} \binom{1}{1} & 0 & \cdots & 0 \\ \vdots & & & \vdots \\ \binom{N-1}{1} & \binom{N-1}{2} & \ddots & 0 \\ \binom{N}{1} & \binom{N}{2} & \cdots & \binom{N}{N} \end{pmatrix} \times \begin{pmatrix} \Omega(k=1|m,n=1) \\ \Omega(k=2|m,n=2) \\ \vdots \\ \Omega(k=n|m,n=N) \end{pmatrix}$$

So a lower-triangular matrix of rank N defines the N interrelations. Let us label the above $N \times N$ matrix $\tilde{\mathbf{M}}$. Because the matrix is non-singular and invertible ...

$$\begin{pmatrix} \Omega(k=1|m,n=1) \\ \Omega(k=2|m,n=2) \\ \vdots \\ \Omega(k=n|m,n=N) \end{pmatrix} = \tilde{\mathbf{M}}^{-1} \begin{pmatrix} 1^m \\ 2^m \\ \vdots \\ N^m \end{pmatrix}$$

However, as it turns out, the inversion of $\tilde{\mathbf{M}}$ by Gauss-Jordan Elimination is relatively simple. It can be shown that for the i^{th} row and j^{th} column,

$$\tilde{\mathbf{M}}_{ij}{}^{-1} = \tilde{\mathbf{M}}_{ij}(-1)^{i+j}$$

However, we're not done yet, because each element of the Ω vector is presently restricted to its own "scope", that is, it sees only n wells and finds all the possibilities as a function of that number n. Therefore, we must *transform* this basis into that in which the operator accounts for an arbitrary number of wells, N. This transformation will take the form of a simple diagonal matrix defining the number of ways we can *choose* the scope defined in each entry of the vector, given the N wells available to choose from. This will give us the expression ...

$$\begin{pmatrix} \Omega(k=1|m,N) \\ \Omega(k=2|m,N) \\ \vdots \\ \Omega(k=n|m,N) \end{pmatrix} = \begin{pmatrix} \binom{N}{1} & 0 & 0 \\ 0 & \ddots & 0 \\ 0 & 0 & \binom{N}{N} \end{pmatrix} \begin{pmatrix} \Omega(k=1|m,n=1) \\ \Omega(k=2|m,n=2) \\ \vdots \\ \Omega(k=n|m,n=N) \end{pmatrix}$$

$$= \begin{pmatrix} \binom{N}{1} & 0 & 0 \\ 0 & \ddots & 0 \\ 0 & 0 & \binom{N}{N} \end{pmatrix}$$

$$\times \begin{pmatrix} \binom{1}{1}(-1)^{1+1} & 0 & \cdots & 0 \\ \vdots & & \ddots & 0 \\ \binom{N-1}{1}(-1)^{N+1-1} & \binom{N-1}{2}(-1)^{N+1} & \ddots & 0 \\ \binom{N}{1}(-1)^{N+1} & \binom{N}{2}(-1)^{N+2} & \cdots & \binom{N}{N}(-1)^{N+N} \end{pmatrix} \begin{pmatrix} 1^m \\ 2^m \\ \vdots \\ N^m \end{pmatrix}$$

The closed form of this solution is then

$$\Omega(k|m,N) = \frac{N!}{(N-k)!}\sum_{j=1}^{k}\frac{(-1)^{j+k}j^m}{(k-j)!j!} \tag{7}$$

while the sought-after probability $p(k|m,N)$ is then

$$p(k|m,N) = \frac{\Omega(k|m,N)}{\sum_i \Omega(i|m,N)}$$

6.2 Complex Analysis May Be Used to Simplify the Computation

We begin with the previously derived expression for $\Omega(k|m,N)\ldots$

$$\frac{N!}{(N-k)!}\sum_{j=1}^{k}\frac{(-1)^{j+k}j^m}{(k-j)!j!}$$

and assert that there exists some function $f(j)$, where j may sit anywhere in the complex plane, there exists a countable set of poles at $f\,(j = q \in \{1\ldots k\})$ such that the function $f(j)$ has the following enumerated residues evaluated at these points:

$$Res_q\left(f(j)\right) = \frac{(-1)^{q+k}q^m}{(k-q)!q!}\ \forall\ q \in \{1\ldots k\}$$

If such a function exists, then by Cauchy's Integral Theorem, we can write the above sum as a continuous integral of the form

$$\Omega(k|m,N) = \frac{N!}{(N-k)!}\sum_{q=1}^{k}Res_q\left(f(j)\right) = \frac{N!}{2\pi i(N-k)!}\oint f(j)dj$$

Choosing a general function $f(j)$ with singularities at $j = q \in 1\ldots k$:

$$f(j) = \frac{(-1)^{j+k}j^m}{(k-j)!j!}\cdot\frac{g(j)}{\prod_{l=1}^{k}(j-l)}$$

we must then choose $g(j)$ as some other function with the property

$$\lim_{j\to q\in\{1\ldots k\}}\frac{g(j)}{\prod_{l=1}^{k}(j-l)} = \frac{1}{j-q}$$

in order to ensure that in fact the residues of f have the values we want. $g(j)$ is meanwhile analytic for all other $j \notin \{1\ldots k\}$. Then

$$\begin{aligned}
g(j=1) &= (-1)(-2)(-3)\ldots(1-k) = (k-1)!(-1)^{k-1}\\
g(j=2) &= (1)(-1)(-2)\ldots(2-k) = (k-2)!(1!)(-1)^{k-2}\\
&\vdots\\
g(j) &= (1)(2)\ldots(j-1)(k-j)(k-j-1)\ldots(2)(1)(-1)^{k-j}\\
&\vdots\\
g(j=k) &= (1)(2)\ldots(j-1)
\end{aligned}$$

From which we infer that for in the neighborhood of the integral values $j \in \{1 \dots k\}$

$$g(j) = (-1)^{k-j}(k-j)!(j-1)!$$

so

$$f(j) = \frac{(-1)^{j+k} j^m}{(k-j)!j!} \cdot \frac{(-1)^{k-j}(k-j)!(j-1)!}{\prod_{l=1}^{k}(j-l)} = \frac{j^{m-1}}{\prod_{l=1}^{k}(j-l)}$$

Notice that this form dispenses with the need for our defining $f(j)$ only in the neighborhood of integral values. In other words, if we would like to perform "analytic continuation" into non-integral values, no further work is needed. Now, going back to the original problem

$$\Omega(k|m,N) = \frac{N!}{2\pi i(N-k)!} \oint_S f(j)dj$$

where, in order for the integral to completely enclose the function's poles, the set $j \in \{1 \dots k\} \subset S$. We are then free to parametrize $j = (N+\Delta)e^{i\theta}$, since ranging θ from 0 to 2π (or similarly $-\pi$ to π) will effectively sweep out the desired closed curve, so long as Δ is positive. Performing this transformation of coordinates on the integral, we get the multiplicity of molecule-well pairings

$$\Omega(k|m,N) = \frac{N!(N+\Delta)^m}{2\pi(N-k)!} \int_{-\pi}^{\pi} d\theta \frac{e^{im\theta}}{\prod_{l=1}^{k}\left((N+\Delta)e^{i\theta}-l\right)} \tag{8}$$

6.3 Implementation in an Algorithm

Though the problem is now solved, the above integrand still oscillates dramatically for large m, making a direct evaluation of the integral difficult. However, we have now defined each $p(k|m,N)$ as a unique *field* over θ, with the fields $h = h(\theta,k)$ of consecutive k's having a very simple interrelation:

$$\frac{h(\theta,k)}{h(\theta,k-1)} = \frac{N-k+1}{(N+\Delta)e^{i\theta}-k} \tag{9}$$

with $\theta = [-\pi,\pi)$. We may initialize this recursion relation with

$$h(\theta,k=1) = \frac{e^{im\theta}}{(N+\Delta)e^{i\theta}-1}$$

where we have excluded the cancelling term, $N(N+\Delta)^m/2\pi$ which is independent of both θ and k. And so

$$p(k|m,N) = \frac{\int_{-\pi}^{\pi} d\theta \cdot h(\theta,k)}{\int_{-\pi}^{\pi} d\theta \sum_{l=1}^{N} h(\theta,l)} \tag{10}$$

Now we're ready to crunch the numbers on a desktop machine. The following MATLAB algorithm will output two matrices

`pkm_arr`

and

`pmk_arr`

The former will have rows whose index defines a given number of molecules m, its columns having indices which denote the number of positive wells k, and the corresponding element to the m^{th} row and k^{th} column will have the value of $p(k|m)$. Similarly, the latter's k^{th} row and m^{th} column will correspond to an entry whose value is $p(m|k)$.

```
clc; clear all;
N=765; %input
m_max=4000; %input

pkm_arr = zeros(m_max,N);
pmk_arr = pkm_arr';
%Set resolve to degree of fineness needed for integration: the contour will
%become a polygon of as many sides.
resolve = 1e4;

th_arr = linspace(-pi,pi,resolve);
th_arr = th_arr(1:(resolve-1));

%The number below needs only be greater than N. Varying it should not
%change the end result (as per the Cauchy Integral Theorem)
d = N+3;

for(m=1:m_max)
    m
    f=1; %initialize
    omega = [ ];
    for(k=1:N)
        if(m<k)
            break;
        end;
        a = (N-k+1)./(d*exp(i*th_arr)-k);
        f = f.*a;
        omega = [omega sum(f.*exp(i*m*th_arr))];
    end;
    omega = real(omega);
    pkm = omega/sum(omega);
    pkm = [pkm zeros(1,(N-length(pkm)))];
    pkm_arr(m,:) = pkm;
    clc;
end;

% assigning "significant digits" to the 6th decimal place
pkm_arr = abs((1e-6)*round(1e6 * pkm_arr));

for(count=1:N)
    count
    pmk_arr(count,:) = pkm_arr(:,count)/sum(pkm_arr(:,count));
    clc;
end;
```

This code can then be appended to calculate the relevant statistical measures discussed earlier:

```
vals = 1:4000;
```

```
cv = [];
ave = [];
lcb = [];
ucb = [];
ba = [];

for(count = 1:765);

    cv = [cv sqrt(abs(sum(pmk_arr(count,:).*(vals).^2)
      - (sum(pmk_arr(count,:).*(vals)))^2))/(sum(pmk_arr(count,:).*(vals)))]; % CV

    ave = [ave sum(pmk_arr(count,:).*vals)]; % E(m)

    ba = [ba (log(1 - (count/765))/log(1 - 1/765))]; % Binomial approximation

    cudf = [];

    for(count2 = 1:4000)
        cudf = [cudf sum(pmk_arr(count,(1:count2)))];
    end;

    indl = find(cudf>0.025);
    if(indl(1) == 1)
        l = indl(1);
    else
        l = indl(1)-1;
    end;

    indu = find(cudf<0.975);
    if(length(indu) == 0)
        u = l;
    elseif(indu(length(indu))==4000)
        u = indu(length(indu));
    else
        u = indu(length(indu))+1;
    end;

    lcb = [lcb l];
    ucb = [ucb u];

end;
```

k	BA	E(m)	CV	LCB	UCB
5	5.0	5.0	0.03	4	5
10	10.1	10.1	0.03	9	11
15	15.1	15.2	0.03	14	16
20	20.3	20.3	0.03	19	22
25	25.4	25.4	0.03	24	27
30	30.6	30.6	0.03	29	33
35	35.8	35.9	0.03	34	38
40	41.1	41.1	0.03	39	44
45	46.4	46.4	0.03	44	49
50	51.7	51.7	0.03	49	55
55	57.0	57.1	0.03	54	60
60	62.4	62.5	0.03	59	66
65	67.9	68.0	0.03	64	72
70	73.4	73.5	0.03	69	78
75	78.9	79.0	0.03	75	84
80	84.4	84.6	0.03	80	89
85	90.1	90.2	0.03	85	95
90	95.7	95.8	0.03	91	101
95	101.4	101.5	0.03	96	107
100	107.1	107.2	0.03	101	113
105	112.9	113.0	0.03	107	119
110	118.7	118.8	0.03	112	126
115	124.5	124.7	0.03	118	132
120	130.4	130.6	0.03	124	138
125	136.4	136.6	0.03	129	144
130	142.4	142.6	0.03	135	151
135	148.4	148.6	0.03	141	157
140	154.5	154.7	0.03	146	163
145	160.7	160.9	0.03	152	170
150	166.9	167.1	0.03	158	176
155	173.1	173.3	0.03	164	183
160	179.4	179.6	0.03	170	190
165	185.7	186.0	0.03	176	196
170	192.1	192.4	0.03	182	203
175	198.6	198.9	0.03	188	210
180	205.1	205.4	0.03	194	217
185	211.7	212.0	0.03	200	224
190	218.3	218.6	0.03	207	231
195	225.0	225.3	0.03	213	238
200	231.7	232.0	0.03	219	245
205	238.5	238.8	0.03	226	252
210	245.3	245.7	0.03	232	259
215	252.3	252.6	0.03	239	267
220	259.2	259.6	0.03	246	274
225	266.3	266.7	0.03	252	282
230	273.4	273.8	0.03	259	289
235	280.6	281.0	0.03	266	297
240	287.8	288.2	0.03	273	304
245	295.1	295.6	0.03	279	312
250	302.5	303.0	0.03	286	320
255	310.0	310.4	0.03	294	328
260	317.5	318.0	0.03	301	336
265	325.1	325.6	0.03	308	344
270	332.8	333.3	0.03	315	352
275	340.6	341.1	0.03	322	360
280	348.4	348.9	0.03	330	369
285	356.3	356.9	0.03	337	377
290	364.3	364.9	0.03	345	386
295	372.4	373.0	0.03	352	394
300	380.6	381.2	0.03	360	403
305	388.9	389.5	0.03	368	412
310	397.2	397.8	0.03	376	421
315	405.7	406.3	0.03	384	430
320	414.2	414.8	0.03	392	439
325	422.9	423.5	0.03	400	448
330	431.6	432.2	0.03	408	457
335	440.4	441.1	0.03	417	466
340	449.4	450.1	0.03	425	476
345	458.4	459.1	0.03	434	486
350	467.6	468.3	0.03	442	495
355	476.8	477.6	0.03	451	505
360	486.2	487.0	0.03	460	515
365	495.7	496.5	0.03	469	525
370	505.3	506.1	0.03	478	536
375	515.1	515.9	0.03	487	546
380	524.9	525.8	0.03	496	557
385	534.9	535.8	0.03	505	567
390	545.1	545.9	0.03	515	578
395	555.3	556.2	0.03	525	589
400	565.7	566.6	0.03	534	600
405	576.3	577.2	0.03	544	611
410	587.0	587.9	0.03	554	623
415	597.8	598.8	0.03	564	634
420	608.8	609.8	0.03	575	646
425	620.0	621.0	0.03	585	658
430	631.3	632.3	0.03	596	670
435	642.8	643.9	0.03	607	683
440	654.5	655.6	0.03	618	695
445	666.3	667.4	0.03	629	708
450	678.3	679.5	0.03	640	721
455	690.6	691.8	0.03	651	734
460	703.0	704.2	0.03	663	747
465	715.6	716.9	0.03	675	761
470	728.5	729.8	0.03	687	775
475	741.6	742.9	0.03	699	789
480	754.9	756.2	0.03	711	803
485	768.4	769.8	0.03	724	818
490	782.2	783.6	0.03	737	832
495	796.2	797.6	0.03	750	847
500	810.5	812.0	0.03	763	863
505	825.0	826.6	0.03	777	879
510	839.9	841.4	0.03	791	895
515	855.0	856.6	0.03	805	911
520	870.5	872.1	0.03	819	928
525	886.2	887.9	0.03	834	945
530	902.3	904.1	0.03	849	962
535	918.8	920.5	0.03	864	980
540	935.6	937.4	0.03	879	998
545	952.8	954.6	0.03	895	1017
550	970.3	972.3	0.03	912	1036
555	988.3	990.3	0.03	928	1055
560	1006.7	1008.8	0.03	945	1075
565	1025.6	1027.7	0.03	963	1096
570	1045.0	1047.1	0.03	980	1117
575	1064.8	1067.1	0.03	999	1139
580	1085.2	1087.5	0.03	1018	1161
585	1106.2	1108.5	0.03	1037	1184
590	1127.7	1130.1	0.03	1057	1207
595	1149.9	1152.4	0.03	1077	1232
600	1172.7	1175.3	0.03	1098	1257
605	1196.2	1198.9	0.03	1120	1282
610	1220.5	1223.3	0.03	1142	1309
615	1245.6	1248.4	0.03	1165	1337
620	1271.5	1274.4	0.04	1188	1365
625	1298.3	1301.4	0.04	1213	1395
630	1326.1	1329.3	0.04	1238	1425
635	1355.0	1358.3	0.04	1265	1457
640	1384.9	1388.4	0.04	1292	1491
645	1416.2	1419.8	0.04	1320	1525
650	1448.7	1452.5	0.04	1350	1561
655	1482.7	1486.6	0.04	1380	1599
660	1518.2	1522.4	0.04	1412	1639
665	1555.5	1559.9	0.04	1446	1681
670	1594.8	1599.3	0.04	1481	1725
675	1636.1	1640.9	0.04	1518	1771
680	1679.8	1684.9	0.04	1558	1821
685	1726.1	1731.6	0.04	1599	1873
690	1775.5	1781.2	0.04	1643	1929
695	1828.2	1834.4	0.04	1690	1990
700	1884.9	1891.5	0.04	1740	2055
705	1946.1	1953.2	0.04	1794	2125
710	2012.6	2020.4	0.04	1852	2202
715	2085.4	2094.0	0.05	1915	2287
720	2166.0	2175.4	0.05	1985	2382
725	2256.0	2266.6	0.05	2063	2489
730	2358.1	2370.1	0.05	2150	2612
735	2476.0	2489.9	0.05	2250	2755
740	2615.3	2632.0	0.05	2366	2928
745	2786.0	2806.5	0.06	2506	3144
750	3005.9	3033.1	0.06	2683	3433
755	3315.9	3350.3	0.07	2924	3829
760	3845.8	3703.7	0.05	3262	3986
765	N/A	3870.3	0.03	3573	3997

Figure 1. Statistical measures of a digital array with N=765 and $1 \leq m \leq 4000$

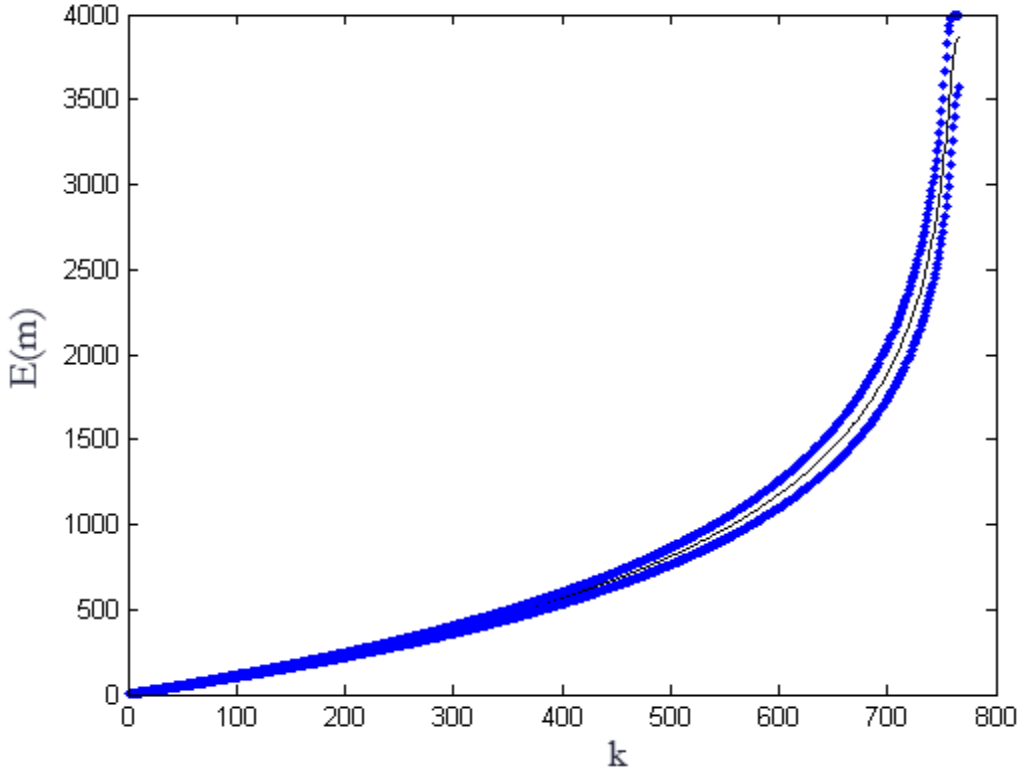

Figure 1. Molecule-number expectation bounded by 95% confidence interval

The above plot shows the expectation value, E(m) in black, bounded by the upper and lower bounds to the 95% confidence interval. These values apply to the scenario where N = 765, $1 \leq m \leq 4000$, and our a priori knowledge of m makes any value in this interval equally probable.

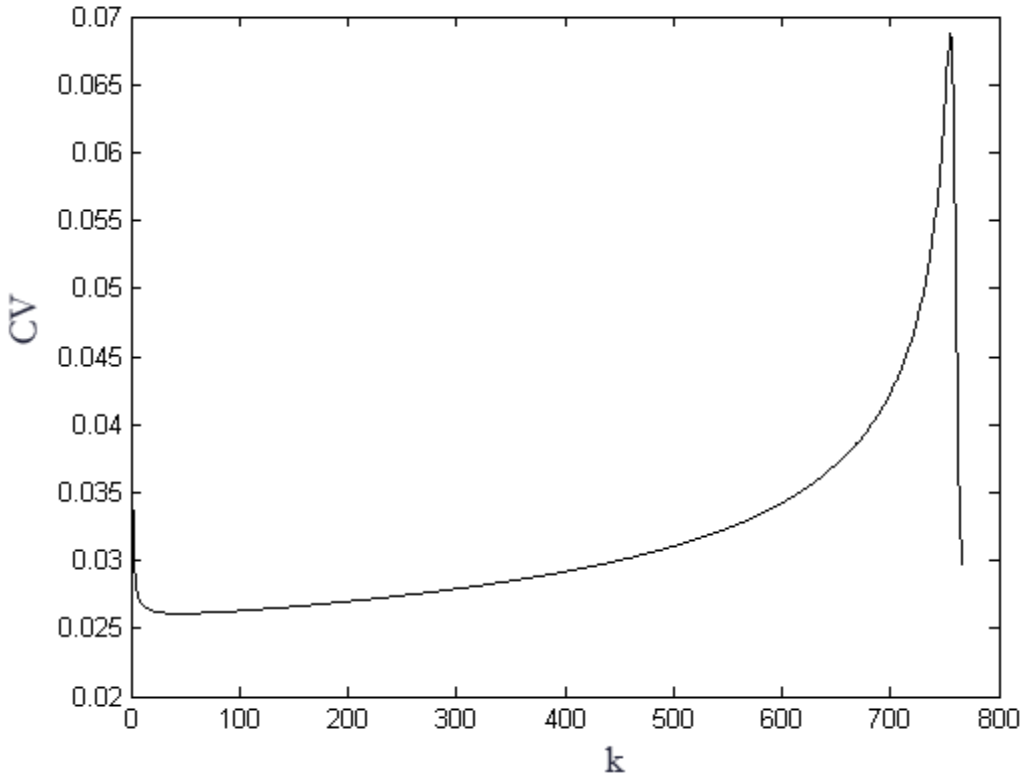

Figure 2. CV versus k

The above plot shows the coefficient of variance, or *CV*, in the same scenario as in figure 1. Its rise to a peak just before hitting the maximum occupancy of $k = 765$ corresponds to the widening of the confidence interval in figure 1 in that region. This increase in uncertainty is related to the increased likelihood that a given signal is due to multiple molecules occupying a well, instead of just one.

Bibliography

1. Eddy, S. R., Non-coding RNA genes and the modern RNA world. *Nat Rev Genet*, 2001. **2**(12): p. 919-929.

2. Mattick, J. S. and I. V. Makunin, Non-coding RNA. *Hum Mol Genet*, 2006. **15**(R1): p. 17-29.

3. Kapranov, P., J. Cheng, S. Dike, D. A. Nix, R. Duttagupta, A. T. Willingham, P. F. Stadler, et al., RNA maps reveal new RNA classes and a possible function for pervasive transcription. *Science*, 2007. **316**(5830): p. 1484-1488.

4. Elowitz, M. B., A. J. Levine, E. D. Siggia, and P. S. Swain, Stochastic gene expression in a single cell. *Science*, 2002. **297**(5584): p. 1183-1186.

5. Swain, P. S., M. B. Elowitz, and E. D. Siggia, Intrinsic and extrinsic contributions to stochasticity in gene expression. *PNAS*, 2002. **99**(20): p. 12795-12800.

6. Suel, G. M., R. P. Kulkarni, J. Dworkin, J. Garcia-Ojalvo, and M. B. Elowitz, Tunability and noise dependence in differentiation dynamics. *Science*, 2007. **315**(5819): p. 1716-1719.

7. Suel, G. M., J. Garcia-Ojalvo, L. M. Liberman, and M. B. Elowitz, An excitable gene regulatory circuit induces transient cellular differentiation. *Nature*, 2006. **440**(7083): p. 545-550.

8. Rosenfeld, N., J. W. Young, U. Alon, P. S. Swain, and M. B. Elowitz, Gene regulation at the single-cell level. *Science*, 2005. **307**(5717): p. 1962-1965.

9. Elowitz, M. B. and S. Leibler, A synthetic oscillatory network of transcriptional regulators. *Nature*, 2000. **403**(6767): p. 335-338.

10. Sprinzak, D. and M. B. Elowitz, Reconstruction of genetic circuits. *Nature*, 2005. **438**(7067): p. 443-448.

11. Cai, L., N. Friedman, and X. S. Xie, Stochastic protein expression in individual cells at the single molecule level. *Nature*, 2006. **440**(7082): p. 358-362.

12. Elf, J., G. W. Li, and X. S. Xie, Probing transcription factor dynamics at the single-molecule level in a living cell. *Science*, 2007. **316**(5828): p. 1191-1194.

13. Levsky, J. M., S. M. Shenoy, R. C. Pezo, and R. H. Singer, Single-cell gene expression profiling. *Science*, 2002. **297**(5582): p. 836-840.

14. Levsky, J. M. and R. H. Singer, Gene expression and the myth of the average cell. *Trends Cell Biol*, 2003. **13**(1): p. 4-6.

15. Raj, A., C. S. Peskin, D. Tranchina, D. Y. Vargas, and S. Tyagi, Stochastic mRNA Synthesis in Mammalian Cells. *PLoS Biology*, 2006. **4**(10): p. 1707-1719.

16. Niemeyer, C. M., M. Adler, and R. Wacker, Immuno-PCR: High sensitivity detection of proteins by nucleic acid amplification. *Trends Biotechnol*, 2005. **23**(4): p. 208-216.

17. Sano, T., C. L. Smith, and C. R. Cantor, Immuno-PCR: Very sensitive antigen detection by means of specific antibody-DNA conjugates. *Science*, 1992. **258**(5079): p. 120-122.

18. Hall, D. A., J. Ptacek, and M. Snyder, Protein microarray technology. *Mech Ageing Dev*, 2007. **128**(1): p. 161-167.

19. De Rosa, S. C., J. M. Brenchley, and M. Roederer, Beyond six colors: A new era in flow cytometry. *Nat Med*, 2003. **9**(1): p. 112-117.

20. De Rosa, S. C., L. A. Herzenberg, L. A. Herzenberg, and M. Roederer, 11-color, 13-parameter flow cytometry: Identification of human naive T cells by phenotype, function, and T-cell receptor diversity. *Nat Med*, 2001. **7**(2): p. 245-248.

21. Zamir, E., B. Geiger, N. Cohen, Z. Kam, and B. Z. Katz, Resolving and classifying haematopoietic bone-marrow cell populations by multi-dimensional analysis of flow-cytometry data. *Br J Haematol*, 2005. **129**(3): p. 420-431.

22. Back, J., D. Allman, S. Chan, and P. Kastner, Visualizing PU.1 activity during hematopoiesis. *Exp Hematol*, 2005. **33**(4): p. 395-402.

23. Nutt, S. L., D. Metcalf, A. D'Amico, M. Polli, and L. Wu, Dynamic regulation of PU.1 expression in multipotent hematopoietic progenitors. *J Exp Med*, 2005. **201**(2): p. 221-231.

24. Carter, M. G., A. A. Sharov, V. VanBuren, D. B. Dudekula, C. E. Carmack, C. Nelson, and M. S. Ko, Transcript copy number estimation using a mouse whole-genome oligonucleotide microarray. *Genome Biol*, 2005. **6**(7): p. R61.1-R61.12.

25. Zhang, L., W. Zhou, V. E. Velculescu, S. E. Kern, R. H. Hruban, S. R. Hamilton, B. Vogelstein, and K. W. Kinzler, Gene expression profiles in normal and cancer cells. *Science*, 1997. **276**(5316): p. 1268-1272.

26. Velculescu, V. E., S. L. Madden, L. Zhang, A. E. Lash, J. Yu, C. Rago, A. Lal, et al., Analysis of human transcriptomes. *Nat Genet*, 1999. **23**(4): p. 387-388.

27. Canales, R. D., Y. Luo, J. C. Willey, B. Austermiller, C. C. Barbacioru, C. Boysen, K. Hunkapiller, et al., Evaluation of DNA microarray results with quantitative gene expression platforms. *Nat Biotechnol*, 2006. **24**(9): p. 1115-1122.

28. Henegariu, O., N. A. Heerema, S. R. Dlouhy, G. H. Vance, and P. H. Vogt, Multiplex PCR: Critical parameters and step-by-step protocol. *Biotechniques*, 1997. **23**(3): p. 504-511.

29. Elnifro, E. M., A. M. Ashshi, R. J. Cooper, and P. E. Klapper, Multiplex PCR: Optimization and application in diagnostic virology. *Clin Microbiol Rev*, 2000. **13**(4): p. 559-570.

30. Eberwine, J., H. Yeh, K. Miyashiro, Y. Cao, S. Nair, R. Finnell, M. Zettel, and P. Coleman, Analysis of gene expression in single live neurons. *PNAS*, 1992. **89**(7): p. 3010-3014.

31. Brady, G., Expression profiling of single mammalian cells—small is beautiful. *Yeast*, 2000. **17**(3): p. 211-217.

32. Todd, R. and D. H. Margolin, Challenges of single-cell diagnostics: Analysis of gene expression. *Trends Mol Med*, 2002. **8**(6): p. 254-257.

33. Tremain, N., J. Korkko, D. Ibberson, G. C. Kopen, C. DiGirolamo, and D. G. Phinney, MicroSAGE analysis of 2,353 expressed genes in a single cell-derived colony of undifferentiated human mesenchymal stem cells reveals mRNAs of multiple cell lineages. *Stem Cells*, 2001. **19**(5): p. 408-418.

34. Nygaard, V. and E. Hovig, Options available for profiling small samples: a review of sample amplification technology when combined with microarray profiling. *Nucleic Acids Res*, 2006. **34**(3): p. 996-1014.

35. Dixon, A. K., P. J. Richardson, K. Lee, N. P. Carter, and T. C. Freeman, Expression profiling of single cells using 3 prime end amplification (TPEA) PCR. *Nucleic Acids Res*, 1998. **26**(19): p. 4426-4431.

36. Bengtsson, M., A. Stahlberg, P. Rorsman, and M. Kubista, Gene expression profiling in single cells from the pancreatic islets of Langerhans reveals lognormal distribution of mRNA levels. *Genome Res.*, 2005. **15**(10): p. 1388-1392.

37. Brandt, S., S. Kloska, T. Altmann, and J. Kehr, Using array hybridization to monitor gene expression at the single cell level. *J Exp Bot*, 2002. **53**(379): p. 2315-2323.

38. Cornelison, D. D. and B. J. Wold, Single-cell analysis of regulatory gene expression in quiescent and activated mouse skeletal muscle satellite cells. *Dev Biol*, 1997. **191**(2): p. 270-283.

39. Chow, N., C. Cox, L. M. Callahan, J. M. Weimer, L. Guo, and P. D. Coleman, Expression profiles of multiple genes in single neurons of Alzheimer's disease. *PNAS*, 1998. **95**(16): p. 9620-9625.

40. Ziegler, B. L., R. Muller, M. Valtieri, C. P. Lamping, C. A. Thomas, M. Gabbianelli, C. Giesert, et al., Unicellular-unilineage erythropoietic cultures: molecular analysis of regulatory gene expression at sibling cell level. *Blood*, 1999. **93**(10): p. 3355-3368.

41. Theilgaard-Monch, K., J. Cowland, and N. Borregaard, Profiling of gene expression in individual hematopoietic cells by global mRNA amplification and slot blot analysis. *J Immunol Methods*, 2001. **252**(1-2): p. 175-189.

42. Han, S. H., B. A. McCool, D. Murchison, S. S. Nahm, A. R. Parrish, and W. H. Griffith, Single-cell RT-PCR detects shifts in mRNA expression profiles of basal forebrain neurons during aging. *Brain Res Mol Brain Res*, 2002. **98**(1-2): p. 67-80.

43. Chiang, M. K. and D. A. Melton, Single-cell transcript analysis of pancreas development. *Dev Cell*, 2003. **4**(3): p. 383-393.

44. Hartmann, C. H. and C. A. Klein, Gene expression profiling of single cells on large-scale oligonucleotide arrays. *Nucleic Acids Res.*, 2006. **34**(21):e143.

45. Jensen, K. B. and F. M. Watt, Single-cell expression profiling of human epidermal stem and transit-amplifying cells: Lrig1 is a regulator of stem cell quiescence. *PNAS*, 2006. **103**(32): p. 11958-11963.

46. Kurimoto, K., Y. Yabuta, Y. Ohinata, Y. Ono, K. D. Uno, R. G. Yamada, H. R. Ueda, and M. Saitou, An improved single-cell cDNA amplification method for efficient high-density oligonucleotide microarray analysis. *Nucleic Acids Res.*, 2006. **34**(5):e42.

47. Tang, F., P. Hajkova, S. C. Barton, K. Lao, and M. A. Surani, MicroRNA expression profiling of single whole embryonic stem cells. *Nucleic Acids Res*, 2006. **34**(2):e9.

48. Bahar, R., C. H. Hartmann, K. A. Rodriguez, A. D. Denny, R. A. Busuttil, M. E. Dolle, R. B. Calder, et al., Increased cell-to-cell variation in gene expression in ageing mouse heart. *Nature*, 2006. **441**(7096): p. 1011-1014.

49. Gaynor, E. M., M. L. Mirsky, and H. A. Lewin, Use of flow cytometry and RT-PCR for detecting gene expression by single cells. *Biotechniques*, 1996. **21**(2): p. 286-291.

50. Miyamoto, T., H. Iwasaki, B. Reizis, M. Ye, T. Graf, I. L. Weissman, and K. Akashi, Myeloid or lymphoid promiscuity as a critical step in hematopoietic lineage commitment. *Dev Cell*, 2002. **3**(1): p. 137-147.

51. Warren, L., D. Bryder, I. L. Weissman, and S. R. Quake, Transcription factor profiling in individual hematopoietic progenitors by digital RT-PCR. *PNAS*, 2006. **103**(47): p. 17807-17812.

52. Marcus, J. S., W. F. Anderson, and S. R. Quake, Microfluidic single-cell mRNA isolation and analysis. *Anal Chem*, 2006. **78**(9): p. 3084-3089.

53. King, K. R., S. Wang, D. Irimia, A. Jayaraman, M. Toner, and M. L. Yarmush, A high-throughput microfluidic real-time gene expression living cell array. *Lab Chip*, 2007. **7**(1): p. 77-85.

54. Auroux, P. A., Y. Koc, A. Demello, A. Manz, and P. J. Day, Miniaturised nucleic acid analysis. *Lab Chip*, 2004. **4**(6): p. 534-546.

55. DeMello, A. J., Microfluidics: DNA amplification moves on. *Nature*, 2003. **422**(6927): p. 28-29.

56. Fu, A. Y., C. Spence, A. Scherer, F. H. Arnold, and S. R. Quake, A microfabricated fluorescence-activated cell sorter. *Nat Biotechnol*, 1999. **17**(11): p. 1109-1111.

57. Hashimoto, M., P. C. Chen, M. W. Mitchell, D. E. Nikitopoulos, S. A. Soper, and M. C. Murphy, Rapid PCR in a continuous flow device. *Lab Chip*, 2004. **4**(6): p. 638-645.

58. Kalinina, O., I. Lebedeva, J. Brown, and J. Silver, Nanoliter scale PCR with TaqMan detection. *Nucleic Acids Res*, 1997. **25**(10): p. 1999-2004.

59. Liu, J., M. Enzelberger, and S. Quake, A nanoliter rotary device for polymerase chain reaction. *Electrophoresis*, 2002. **23**(10): p. 1531-1536.

60. Obeid, P. J., T. K. Christopoulos, H. J. Crabtree, and C. J. Backhouse, Microfabricated device for DNA and RNA amplification by continuous-flow polymerase chain reaction and reverse transcription-polymerase chain reaction with cycle number selection. *Anal Chem*, 2003. **75**(2): p. 288-295.

61. Thorsen, T., S. J. Maerkl, and S. R. Quake, Microfluidic large-scale integration. *Science*, 2002. **298**(5593): p. 580-584.

62. Waters, L. C., S. C. Jacobson, N. Kroutchinina, J. Khandurina, R. S. Foote, and J. M. Ramsey, Microchip device for cell lysis, multiplex PCR amplification, and electrophoretic sizing. *Anal Chem*, 1998. **70**(1): p. 158-162.

63. Khademhosseini, A., R. Langer, J. Borenstein, and J. P. Vacanti, Microscale technologies for tissue engineering and biology. *PNAS*, 2006. **103**(8): p. 2480-2487.

64. Hartshorn, C., A. Anshelevich, and L. J. Wangh, Rapid, single-tube method for quantitative preparation and analysis of RNA and DNA in samples as small as one cell. *BMC Biotechnol*, 2005. **5**(2): p. 1-13.

65. Klebe, R. J., G. M. Grant, A. M. Grant, M. A. Garcia, T. A. Giambernardi, and G. P. Taylor, RT-PCR without RNA isolation. *Biotechniques*, 1996. **21**(6): p. 1094-1100.

66. Wagatsuma, A., H. Sadamoto, T. Kitahashi, K. Lukowiak, A. Urano, and E. Ito, Determination of the exact copy numbers of particular mRNAs in a single cell by quantitative real-time RT-PCR. *J Exp Biol*, 2005. **208**(Pt 12): p. 2389-2398.

67. Tang, F., P. Hajkova, S. C. Barton, D. O'Carroll, C. Lee, K. Lao, and M. A. Surani, 220-plex microRNA expression profile of a single cell. *Nat. Protocols*, 2006. **1**(3): p. 1154-1159.

68. Osawa, M., G. Egawa, S. S. Mak, M. Moriyama, R. Freter, S. Yonetani, F. Beermann, and S. Nishikawa, Molecular characterization of melanocyte stem cells in their niche. *Development*, 2005. **132**(24): p. 5589-5599.

69. Jena, P. K., A. H. Liu, D. S. Smith, and L. J. Wysocki, Amplification of genes, single transcripts and cDNA libraries from one cell and direct sequence analysis of amplified products derived from one molecule. *J Immunol Methods*, 1996. **190**(2): p. 199-213.

70. Yan, L., G. Kaczorowski, and M. Kohler, One-tube protocol for single-cell reverse transcriptase-polymerase chain reaction. *Analytical Biochemistry*, 2002. **304**(2): p. 267-270.

71. Eberwine, J., Amplification of mRNA populations using aRNA generated from immobilized oligo(dT)-T7 primed cDNA. *Biotechniques*, 1996. **20**(4): p. 584-591.

72. O'Dell, D. M., R. Raghupathi, P. B. Crino, B. Morrison, 3rd, J. H. Eberwine, and T. K. McIntosh, Amplification of mRNAs from single, fixed, TUNEL-positive cells. *Biotechniques*, 1998. **25**(4): p. 566-8, 570.

73. Brady, G. and N. N. Iscove, Construction of cDNA libraries from single cells. *Methods Enzymol*, 1993. **225**: p. 611-623.

74. Dixon, A. K., P. J. Richardson, R. D. Pinnock, and K. Lee, Gene-expression analysis at the single-cell level. *Trends Pharmacol Sci*, 2000. **21**(2): p. 65-70.

75. Iscove, N. N., M. Barbara, M. Gu, M. Gibson, C. Modi, and N. Winegarden, Representation is faithfully preserved in global cDNA amplified exponentially from sub-picogram quantities of mRNA. *Nat Biotechnol*, 2002. **20**(9): p. 940-943.

76. Klein, C. A., S. Seidl, K. Petat-Dutter, S. Offner, J. B. Geigl, O. Schmidt-Kittler, N. Wendler, et al., Combined transcriptome and genome analysis of single micrometastatic cells. *Nat Biotechnol*, 2002. **20**(4): p. 387-392.

77. Peixoto, A., C. Evaristo, I. Munitic, M. Monteiro, A. Charbit, B. Rocha, and H. Veiga-Fernandes, CD8 single-cell gene coexpression reveals three different effector types present at distinct phases of the immune response. *J. Exp. Med.*, 2007: p. 1193-1205.

78. Bustin, S. A., Absolute quantification of mRNA using real-time reverse transcription polymerase chain reaction assays. *J Mol Endocrinol*, 2000. **25**(2): p. 169-193.

79. Bustin, S. A., Quantification of mRNA using real-time reverse transcription PCR (RT-PCR): trends and problems. *J Mol Endocrinol*, 2002. **29**(1): p. 23-39.

80. Dheda, K., J. F. Huggett, J. S. Chang, L. U. Kim, S. A. Bustin, M. A. Johnson, G. A. Rook, and A. Zumla, The implications of using an inappropriate reference gene for real-time reverse transcription PCR data normalization. *Analytical Biochemistry*, 2005. **344**(1): p. 141-143.

81. Huggett, J., K. Dheda, S. Bustin, and A. Zumla, Real-time RT-PCR normalisation: Strategies and considerations. *Genes Immun*, 2005. **6**(4): p. 279-284.

82. Tricarico, C., P. Pinzani, S. Bianchi, M. Paglierani, V. Distante, M. Pazzagli, S. A. Bustin, and C. Orlando, Quantitative real-time reverse transcription polymerase chain reaction: normalization to rRNA or single housekeeping genes is inappropriate for human tissue biopsies. *Analytical Biochemistry*, 2002. **309**(2): p. 293-300.

83. Vandesompele, J., K. De Preter, F. Pattyn, B. Poppe, N. Van Roy, A. De Paepe, and F. Speleman, Accurate normalization of real-time quantitative RT-PCR data by geometric averaging of multiple internal control genes. *Genome Biol*, 2002. **3**(7): p. R31.1-R31.11.

84. Dheda, K., J. F. Huggett, S. A. Bustin, M. A. Johnson, G. Rook, and A. Zumla, Validation of housekeeping genes for normalizing RNA expression in real-time PCR. *Biotechniques*, 2004. **37**(1): p. 112-4, 116, 118-9.

85. Vogelstein, B. and K. W. Kinzler, Digital PCR. *PNAS*, 1999. **96**(16): p. 9236-9241.

86. Stahlberg, A., J. Hakansson, X. Xian, H. Semb, and M. Kubista, Properties of the reverse transcription reaction in mRNA quantification. *Clin Chem*, 2004. **50**(3): p. 509-515.

87. Stahlberg, A., M. Kubista, and M. Pfaffl, Comparison of reverse transcriptases in gene expression analysis. *Clin Chem*, 2004. **50**(9): p. 1678-1680.

88. Phillips, J. K. and J. Lipski, Single-cell RT-PCR as a tool to study gene expression in central and peripheral autonomic neurones. *Auton Neurosci*, 2000. **86**(1-2): p. 1-12.

89. Peixoto, A., M. Monteiro, B. Rocha, and H. Veiga-Fernandes, Quantification of multiple gene expression in individual cells. *Genome Res*, 2004. **14**(10A): p. 1938-1947.

90. Stanley, K. K. and E. Szewczuk, Multiplexed tandem PCR: gene profiling from small amounts of RNA using SYBR Green detection. *Nucleic Acids Res*, 2005. **33**(20):e180.

91. Cossman, J., Gene expression analysis of single neoplastic cells and the pathogenesis of Hodgkin's lymphoma. *J Histochem Cytochem*, 2001. **49**(6): p. 799-800.

92. Bustin, S., *A-Z of Quantitative PCR*. 2004. La Jolla, CA: International University Line.

93. Ross, J., mRNA stability in mammalian cells. *Microbiol Rev*, 1995. **59**(3): p. 423-450.

94. Stiles, C. D., K. L. Lee, and F. T. Kenney, Differential degradation of messenger RNAs in mammalian cells. *PNAS*, 1976. **73**(8): p. 2634-2638.

95. Yang, E., E. van Nimwegen, M. Zavolan, N. Rajewsky, M. Schroeder, M. Magnasco, and J. E. Darnell, Jr, Decay rates of human mRNAs: Correlation with functional characteristics and sequence attributes. *Genome Res.*, 2003. **13**(8): p. 1863-1872.

96. Halford, S. E. and J. F. Marko, How do site-specific DNA-binding proteins find their targets? *Nucleic Acids Res*, 2004. **32**(10): p. 3040-3052.

97. Zhang, Z., P. M. Harrison, Y. Liu, and M. Gerstein, Millions of years of evolution preserved: a comprehensive catalog of the processed pseudogenes in the human genome. *Genome Res*, 2003. **13**(12): p. 2541-2558.

98. Hurteau, G. J. and S. D. Spivack, mRNA-specific reverse transcription-polymerase chain reaction from human tissue extracts. *Analytical Biochemistry*, 2002. **307**(2): p. 304-315.

99. Malboeuf, C. M., S. J. Isaacs, N. H. Tran, and B. Kim, Thermal effects on reverse transcription: improvement of accuracy and processivity in cDNA synthesis. *Biotechniques*, 2001. **30**(5): p. 1074-8, 1080, 1082, passim.

100. Harrison, G. P., M. S. Mayo, E. Hunter, and A. M. Lever, Pausing of reverse transcriptase on retroviral RNA templates is influenced by secondary structures both 5' and 3' of the catalytic site. *Nucleic Acids Res*, 1998. **26**(14): p. 3433-3442.

101. Liss, B., Improved quantitative real-time RT-PCR for expression profiling of individual cells. *Nucleic Acids Res*, 2002. **30**(17):e89.

102. Chumakov, K. M., Reverse transcriptase can inhibit PCR and stimulate primer-dimer formation. *PCR Methods Appl*, 1994. **4**(1): p. 62-64.

103. Peters, I. R., C. R. Helps, E. J. Hall, and M. J. Day, Real-time RT-PCR: Considerations for efficient and sensitive assay design. *J Immunol Methods*, 2004. **286**(1-2): p. 203-217.

104. Chandler, D. P., C. A. Wagnon, and H. Bolton, Jr., Reverse transcriptase (RT) inhibition of PCR at low concentrations of template and its implications for quantitative RT-PCR. *Appl Environ Microbiol*, 1998. **64**(2): p. 669-677.

105. Sellner, L. N., R. J. Coelen, and J. S. Mackenzie, Reverse transcriptase inhibits Taq polymerase activity. *Nucleic Acids Res*, 1992. **20**(7): p. 1487-1490.

106. Suslov, O. and D. A. Steindler, PCR inhibition by reverse transcriptase leads to an overestimation of amplification efficiency. *Nucleic Acids Res.*, 2005. **33**(20):e181.

107. Fehlmann, C., R. Krapf, and M. Solioz, Reverse transcriptase can block polymerase chain reaction. *Clin Chem*, 1993. **39**(2): p. 368-369.

108. Kojima, T., Y. Takei, M. Ohtsuka, Y. Kawarasaki, T. Yamane, and H. Nakano, PCR amplification from single DNA molecules on magnetic beads in emulsion: application for high-throughput screening of transcription factor targets. *Nucleic Acids Res*, 2005. **33**(17):e150.

109. Williams, R., S. G. Peisajovich, O. J. Miller, S. Magdassi, D. S. Tawfik, and A. D. Griffiths, Amplification of complex gene libraries by emulsion PCR. *Nat Methods*, 2006. **3**(7): p. 545-550.

110. Quake, S. R. and A. Scherer, From micro- to nanofabrication with soft materials. *Science*, 2000. **290**(5496): p. 1536-1540.

111. Unger, M. A., H. P. Chou, T. Thorsen, A. Scherer, and S. R. Quake, Monolithic microfabricated valves and pumps by multilayer soft lithography. *Science*, 2000. **288**(5463): p. 113-116.

112. Marras, S. A. E., F. R. Kramer, and S. Tyagi, Efficiencies of fluorescence resonance energy transfer and contact-mediated quenching in oligonucleotide probes. *Nucleic Acids Res.*, 2002. **30**(21):e122.

113. *SuperScript III Reverse Transcriptase*, Invitrogen Product Note.

114. *Taq DNA Polymerases (Native, Recombinant & Platinum) and Platinum Taq Antibody*, Invitrogen Product Note.

115. Revilla-i-Domingo, R. and E. H. Davidson, Developmental gene network analysis. *Int J Dev Biol*, 2003. **47**(7-8): p. 695-703.

116. Gilman, A. and A. P. Arkin, Genetic "code": Representations and dynamical models of genetic components and networks. *Annu Rev Genomics Hum Genet*, 2002. **3**: p. 341-369.

117. Adolfsson, J., O. J. Borge, D. Bryder, K. Theilgaard-Monch, I. Astrand-Grundstrom, E. Sitnicka, Y. Sasaki, and S. E. Jacobsen, Upregulation of Flt3 expression within the bone marrow Lin(-)Sca1(+)c-kit(+) stem cell compartment is accompanied by loss of self-renewal capacity. *Immunity*, 2001. **15**(4): p. 659-669.

118. Akashi, K., D. Traver, T. Miyamoto, and I. L. Weissman, A clonogenic common myeloid progenitor that gives rise to all myeloid lineages. *Nature*, 2000. **404**(6774): p. 193-197.

119. Kondo, M., I. L. Weissman, and K. Akashi, Identification of clonogenic common lymphoid progenitors in mouse bone marrow. *Cell*, 1997. **91**(5): p. 661-672.

120. Nakauchi, H., Isolation and characterization of the hematopoietic stem cell. *Rinsho Ketsueki*, 1995. **36**(5): p. 400-405.

121. Suda, J., T. Suda, and M. Ogawa, Analysis of differentiation of mouse hemopoietic stem cells in culture by sequential replating of paired progenitors. *Blood*, 1984. **64**(2): p. 393-399.

122. Christensen, J. L. and I. L. Weissman, Flk-2 is a marker in hematopoietic stem cell differentiation: a simple method to isolate long-term stem cells. *PNAS*, 2001. **98**(25): p. 14541-14546.

123. Karsunky, H., M. Merad, A. Cozzio, I. L. Weissman, and M. G. Manz, Flt3 ligand regulates dendritic cell development from Flt3+ lymphoid and myeloid-committed progenitors to Flt3+ dendritic cells in vivo. *J Exp Med*, 2003. **198**(2): p. 305-313.

124. Nerlov, C. and T. Graf, PU.1 induces myeloid lineage commitment in multipotent hematopoietic progenitors. *Genes Dev.*, 1998. **12**(15): p. 2403-2412.

125. Laiosa, C. V., M. Stadtfeld, and T. Graf, Determinants of lymphoid-myeloid lineage diversification. *Annu Rev Immunol*, 2006. **24**: p. 705-738.

126. Dahl, R. and M. C. Simon, The importance of PU.1 concentration in hematopoietic lineage commitment and maturation. *Blood Cells, Molecules, and Diseases*, 2003. **31**(2): p. 229-233.

127. Rothenberg, E. V. and M. K. Anderson, Elements of transcription factor network design for T-lineage specification. *Dev Biol*, 2002. **246**(1): p. 29-44.

128. Akashi, K., X. He, J. Chen, H. Iwasaki, C. Niu, B. Steenhard, J. Zhang, J. Haug, and L. Li, Transcriptional accessibility for genes of multiple tissues and hematopoietic lineages is hierarchically controlled during early hematopoiesis. *Blood*, 2003. **101**(2): p. 383-389.

129. Enver, T., C. M. Heyworth, and T. M. Dexter, Do stem cells play dice? *Blood*, 1998. **92**(2): p. 348-351.

130. Kondo, M., A. J. Wagers, M. G. Manz, S. S. Prohaska, D. C. Scherer, G. F. Beilhack, J. A. Shizuru, and I. L. Weissman, Biology of hematopoietic stem cells and progenitors: implications for clinical application. *Annu Rev Immunol*, 2003. **21**: p. 759-806.

131. Bustin, S. A., V. Benes, T. Nolan, and M. W. Pfaffl, Quantitative real-time RT-PCR—a perspective. *J Mol Endocrinol*, 2005. **34**(3): p. 597-601.

132. Koch, A. L., The logarithm in biology: Mechanisms generating the log-normal distribution exactly. *J Theor Biol*, 1966. **12**(2): p. 276-290.

133. Cantor, A. B. and S. H. Orkin, Hematopoietic development: A balancing act. *Curr Opin Genet Dev*, 2001. **11**(5): p. 513-519.

134. Press, W. H., B. P. Flannery, S. A. Teukolsky, and W. T. Vetterling, *Numerical Recipes in C*. 2nd ed. 1992. Cambridge, UK: Cambridge University Press.

135. Kirkwood, T. B., Understanding the odd science of aging. *Cell*, 2005. **120**(4): p. 437-447.

136. Kirkwood, T. B. and S. N. Austad, Why do we age? *Nature*, 2000. **408**(6809): p. 233-238.

137. Dolle, M. E. T. and J. Vijg, Genome dynamics in aging mice. *Genome Res.*, 2002. **12**(11): p. 1732-1738.

138. Dolle, M. E., H. Giese, C. L. Hopkins, H. J. Martus, J. M. Hausdorff, and J. Vijg, Rapid accumulation of genome rearrangements in liver but not in brain of old mice. *Nat Genet*, 1997. **17**(4): p. 431-434.

139. Dolle, M. E., W. K. Snyder, J. A. Gossen, P. H. Lohman, and J. Vijg, Distinct spectra of somatic mutations accumulated with age in mouse heart and small intestine. *PNAS*, 2000. **97**(15): p. 8403-8408.

140. Vijg, J., *Aging of the Genome*. 2007. New York, NY: Oxford University Press.

141. Miller, R. A., The aging immune system: primer and prospectus. *Science*, 1996. **273**(5271): p. 70-74.

142. Montecino-Rodriguez, E. and K. Dorshkind, Evolving patterns of lymphopoiesis from embryogenesis through senescence. *Immunity*, 2006. **24**(6): p. 659-662.

143. Allman, D. and J. P. Miller, B cell development and receptor diversity during aging. *Current Opinion in Immunology*, 2005. **17**(5): p. 463-467.

144. Osawa, M., K. Hanada, H. Hamada, and H. Nakauchi, Long-term lymphohematopoietic reconstitution by a single CD34-low/negative hematopoietic stem cell. *Science*, 1996. **273**(5272): p. 242-245.

145. Lewinsohn, D. M., R. F. Bargatze, and E. C. Butcher, Leukocyte-endothelial cell recognition: Evidence of a common molecular mechanism shared by neutrophils, lymphocytes, and other leukocytes. *J Immunol*, 1987. **138**(12): p. 4313-4321.

146. Hayakawa, K., R. R. Hardy, D. R. Parks, and L. A. Herzenberg, The "Ly-1 B" cell subpopulation in normal immunodefective, and autoimmune mice. *J Exp Med*, 1983. **157**(1): p. 202-218.

147. Black, S. J., W. van der Loo, M. R. Loken, and L. A. Herzenberg, Expression of IgD by murine lymphocytes. Loss of surface IgD indicates maturation of memory B cells. *J Exp Med*, 1978. **147**(4): p. 984-996.

148. Barrat, F., H. Haegel, A. Louise, S. Vincent-Naulleau, H. J. Boulouis, T. Neway, R. Ceredig, and C. Pilet, Quantitative and qualitative changes in CD44 and MEL-14

expression by T cells in C57BL/6 mice during aging. *Res Immunol*, 1995. **146**(1): p. 23-34.

149. Simon, J. L. and P. Bruce, The new biostatistics of resampling. *MD Comput*, 1995. **12**(2): p. 115-121, 141.

150. Stuart, J. M., E. Segal, D. Koller, and S. K. Kim, A gene-coexpression network for global discovery of conserved genetic modules. *Science*, 2003. **302**(5643): p. 249-255.

151. Strober, S. and I. L. Weissman, Immunosuppresive and tolerogenic effects of whole-body, total lymphoid, and regional irradiation, in *The Current Status of Modern Therapy*. 1981, MTP Press. p. 19-53.

152. Roos, W. P. and B. Kaina, DNA damage-induced cell death by apoptosis. *Trends Mol Med*, 2006. **12**(9): p. 440-450.

153. Verheij, M. and H. Bartelink, Radiation-induced apoptosis. *Cell Tissue Res*, 2000. **301**(1): p. 133-142.

154. Galbraith, P. R., L. S. Valberg, and M. Brown, Patterns of granulocyte kinetics in health, infection and in carcinoma. *Blood*, 1965. **25**: p. 683-692.

155. Rossi, D. J., D. Bryder, and I. L. Weissman, Hematopoietic stem cell aging: Mechanism and consequence. *Exp Gerontol*, 2007: p. 385-390.

156. Rossi, D. J., D. Bryder, J. M. Zahn, H. Ahlenius, R. Sonu, A. J. Wagers, and I. L. Weissman, Cell intrinsic alterations underlie hematopoietic stem cell aging. *PNAS*, 2005. **102**(26): p. 9194-9199.

157. Edwards, J. L. and R. E. Klein, Cell renewal in adult mouse tissues. *Am J Pathol*, 1961. **38**: p. 437-453.

158. Hinrichs, H. R., R. O. Petersen, and R. Baserga, Incorporation of thymidine into DNA of mouse organs. *Arch Pathol*, 1964. **78**: p. 245-253.